AD-A169 168 AEROSOL AND HUMIDITY STRUCTURE BENEATH MARITIME STRATUS CLOUDS: 1981 DATA(U) NAVAL OCEAN SYSTEMS CENTER SAN DIEGO CA V R NOONKESTER 03 MAY 82 NOSC/TR-783 1/2

UNCLASSIFIED F/G 4/2 NL

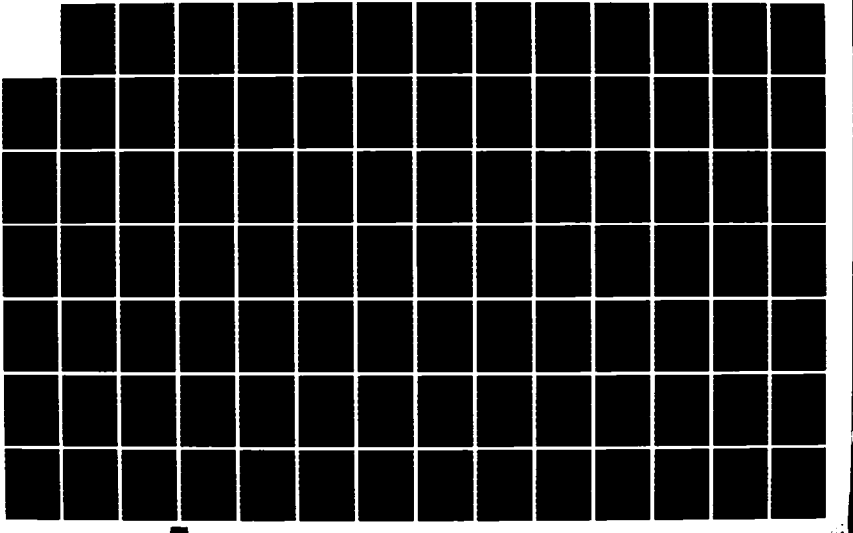

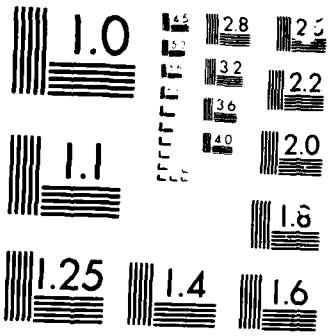
1.0
1.1
1.25
1.4
1.6
1.8
2.0
2.2
2.8
3.2
3.6
4.0

NOSC TR 783

NOSC TR 783

Technical Report 783

AEROSOL AND HUMIDITY STRUCTURE BENEATH MARITIME STRATUS CLOUDS: 1981 DATA

VR Noonkester

3 May 1982

Approved for public release; distribution unlimited

NOSC

NAVAL OCEAN SYSTEMS CENTER
San Diego, California 92152

UNCLASSIFIED

SECURITY CLASSIFICATION OF THIS PAGE (When Data Entered)

REPORT DOCUMENTATION PAGE

READ INSTRUCTIONS BEFORE COMPLETING FORM

1. REPORT NUMBER: NOSC Technical Report 783 (TR 783)

2. GOVT ACCESSION NO.:

3. RECIPIENT'S CATALOG NUMBER:

4. TITLE (and Subtitle): Aerosol and Humidity Structure Beneath Maritime Stratus Clouds: 1981 Data

5. TYPE OF REPORT & PERIOD COVERED: Data analysis, May 1981 – May 1982

6. PERFORMING ORG. REPORT NUMBER:

7. AUTHOR(s): VR Noonkester

8. CONTRACT OR GRANT NUMBER(s):

9. PERFORMING ORGANIZATION NAME AND ADDRESS: Naval Ocean Systems Center, San Diego, CA 92152

10. PROGRAM ELEMENT, PROJECT, TASK AREA & WORK UNIT NUMBERS: program element 61153N, project WR03302, task WR0330200 work unit 532-MP04

11. CONTROLLING OFFICE NAME AND ADDRESS: Naval Air Systems Command

12. REPORT DATE: 3 May 1982

13. NUMBER OF PAGES: 128

14. MONITORING AGENCY NAME & ADDRESS (if different from Controlling Office):

15. SECURITY CLASS. (of this report): Unclassified

15a. DECLASSIFICATION DOWNGRADING SCHEDULE:

16. DISTRIBUTION STATEMENT (of this Report): Approved for public release; distribution unlimited

17. DISTRIBUTION STATEMENT (of the abstract entered in Block 20, if different from Report):

18. SUPPLEMENTARY NOTES:

19. KEY WORDS (Continue on reverse side if necessary and identify by block number):

Aerosols
Electro-optics
Marine atmospheres
Meteorological data
Stratus clouds - maritime

20. ABSTRACT (Continue on reverse side if necessary and identify by block number):

Navy electro-optical systems will operate beneath decks of maritime stratus clouds. Radiation supporting the EO systems will be attenuated by aerosols and water vapor. Methods and models are needed to specify the concentrations and vertical gradients as a function of atmospheric parameters easily and routinely measured. A measurement program designed by the author was described in a previous publication. This report presents data acquired southwest of San Diego.

(cont)

DD FORM 1 JAN 73 1473 EDITION OF 1 NOV 65 IS OBSOLETE

UNCLASSIFIED

SECURITY CLASSIFICATION OF THIS PAGE (When Data Entered)

Distinct differences in the aerosol spectra at all elevations relative to cloud base height suggest that the May and August data respectively represent marine and continental aerosols. Significant data characteristics are outlined.

Contents

1.0 INTRODUCTION

Navy electro-optical (EO) systems will be expected to operate efficiently beneath extensive decks of maritime stratus clouds. The optical radiation supporting the EO systems will be attenuated along slant transmission paths beneath the stratus decks by aerosols and water vapor of generally unknown concentrations and vertical gradients. The Navy needs methods/models to specify the aerosol and water vapor concentrations and vertical gradients as a function of atmospheric parameters easily and routinely measured to support EO systems.

Existing knowledge on aerosols and humidity below maritime stratus cloud decks was reviewed by Noonkester (1981a). A measurement program using the NOSC airborne platform was designed according to findings of the review and the NOSC sensor capabilities and is described by Noonkester (1981b). This report presents data acquired during May and August 1981 in stratus-cloud layers southwest of San Diego. Distinct differences in the aerosol spectra at all elevations relative to cloud base height suggest that the May and August data respectively represent marine and continental aerosols. Significant data characteristics are outlined.

2.0 SENSORS

The parameters measured by the NOSC airborne sensors were:

- Elevation, Z
  - Radar altimeter: BONZAR Inc. Mark-10X
  - Pressure altimeter: Rosemount altitude/air speed transducer, model 542K

- Aerosols spectrum, n(r)
  - PMS ASSP-100 spectrometer (0.23 μm $\leq$ r $\leq$ 14.7 μm)
  - PMS OAP-200 spectrometer (14.2 μm $\leq$ r $\leq$ 150 μm)

- Temperature, T
  - HP Quartz thermometer, model 2801A

- Dew Point, T_d
  - EG&G, model 137-C3

- Sea Surface Temperature, T_{IR}
  - Barnes PRT-5 infrared sensor ($9.5 < \lambda < 11.5\mu m$)

Measurements of T, T_d, T_{IR} and z were made every 4 s. A complete aerosol spectrum was obtained every 8 s. The relative humidity f was calculated from T and T_d.

The error of the radar altimeter was less than the pressure altimeter error below about 38m. Prior to making horizontal flight measurements the pressure altitude was set equal to the radar altitude along a low-level run. After this setting, the pressure altitude, accurate to about ±2m up to 700m, was used for elevation measurements.

The surface wind speed and direction were estimated from ocean surface conditions just before horizontal runs were made.

3.0 MEASUREMENT TECHNIQUE

3.1 Measurement Levels

A slow descent through an extensive stratus cloud deck was made to estimate the elevation of the cloud top Z_t and cloud base Z_c. Two-minute horizontal runs were then made near the following elevations: Z_o (low-level, near surface), 0.2 Z_c, $Z_c/2$, Z_c-80m, Z_c-60m, Z_c-40m, Z_c-20m, Z_c, Z_c+20m, Z_c+40m, $(Z_c+Z_t)/2$ (mid cloud), Z_t-40m, Z_t and Z_t+40m. The runs were made at all elevations into and with the estimated surface wind flow.

3.2 Data Filtering by Elevation Span

The maximum and minimum standard deviations of the elevation Z were respectively 9.3 and 1.6m and the average standard deviation was 4.7m. All data were accepted along a horizontal run if they were within ±7m of the

average elevation. Thus, most data were included within this range along each run.

4.0 GENERAL DATA TABULATION

Table 1 gives the relative geographic position of the stratus clouds measurements, the surface wind conditions, the number of horizontal runs and the time span of the measurements. Figure 1 shows the elevation of each horizontal run, Z_c and Z_t for each of the eight days given in Table 1. The Z_c's ranged from 352m to 1090m and Z_t-Z_c ranged from 131m to 470m. (The method of obtaining Z_c is given in Section 5.) The unequal distribution of the measurements above and below Z_c was created by either poor estimates of Z_c (used to specify measurement elevations) during the initial descent through the stratus deck or temporal changes in Z_c. Drizzle was not observed below the clouds on any day.

5.0 VERTICAL TEMPERATURE AND HUMIDITY PROFILES

Figure 2 (a through h) presents T(z) and f(z) for the eight stratus decks examined.

5.1 Temperature Profiles

Distinct changes in the vertical lapse rate of temperature were found near the estimated cloud base heights. The elevation of this change in lapse rate is defined to be the cloud base height Z_c. Z_c must represent the elevation above which the latent heat of condensation is sufficient to reduce the lapse rate of temperature from a "near" dry to a "near" moist adiabatic rate. This change in lapse rate is clearly shown in Figures 2a and 2h.

A superadiabatic lapse rate of temperature was measured immediately below Z_c on 5 stratus cloud decks. The cause of this has not yet been determined. If large cloud droplets were carried by turbulence to the sub-cloud region and were collected on the temperature probe, the temperature sensor would show a lower temperature than the true air temperature because the droplet temperature would approximate the (cooler) cloud air temperature and the water on the

Table 1. General data on stratus measurements.

Date 1981	Location (Polar, from San Diego) Range nm	Radial deg.∇	Wind* v m s^{-1}	θ	Number of Levels	Time (PST) From	To
May							
14	60	225	3	W	13	0818	0905
28	60	225	-	WNW	15	0811	0856
29	60	225	-	WNW	14	0610	0654
Aug							
11	50	225	3	WNW	16	0803	0856
13	80	215	3	MW	14	0826	0912
14	110	260	3	NW	14	0825	0905
17	80	225	6	NW	15	0816	0901
18	70	215	5	NW	16	0814	0904

* Estimated from airborne platform at low elevation

∇ Degrees from true north clockwise

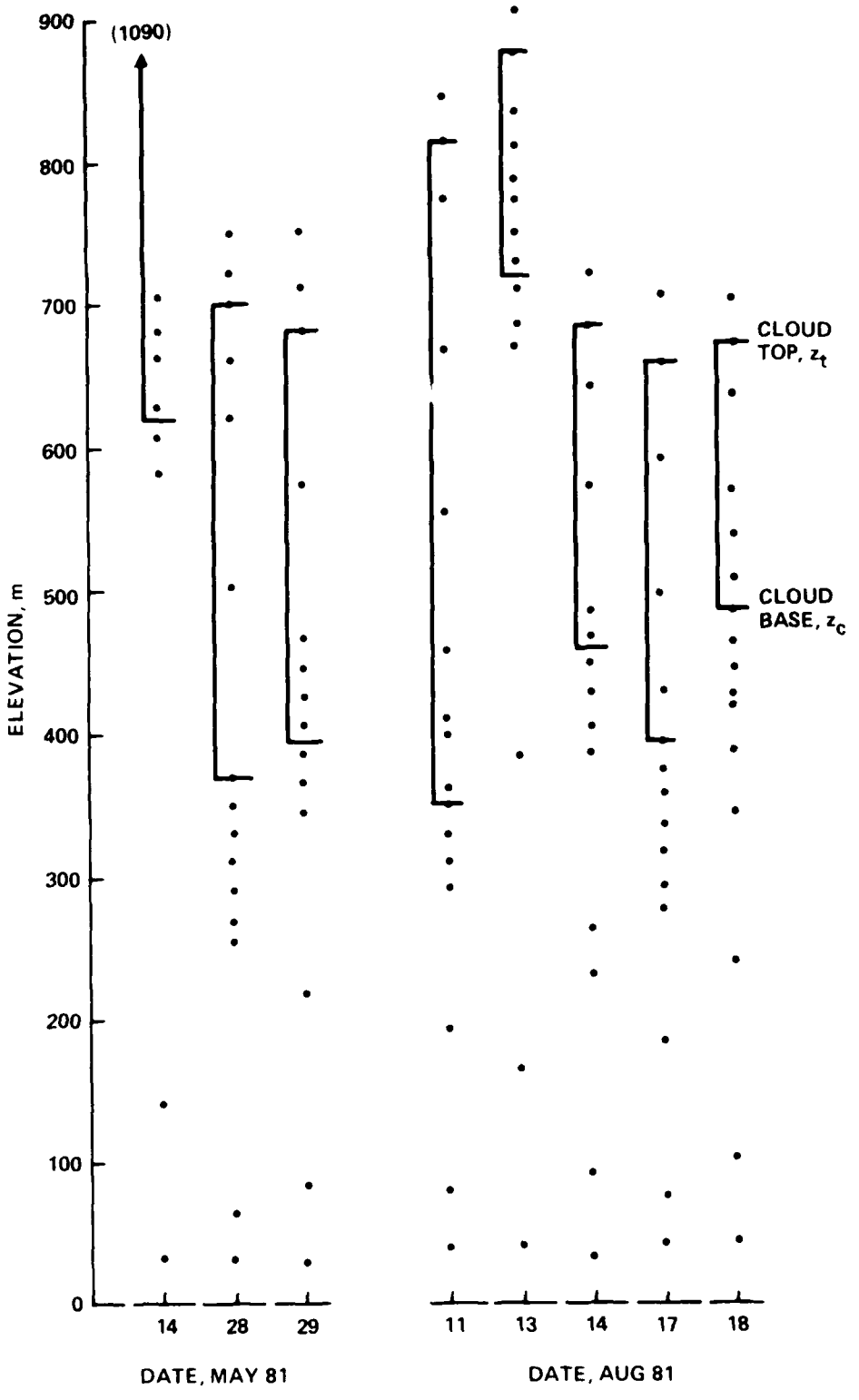

Figure 1. Elevation of horizontal runs by NOSC airborne sensor system and region of cloud deck for each day of measurement.

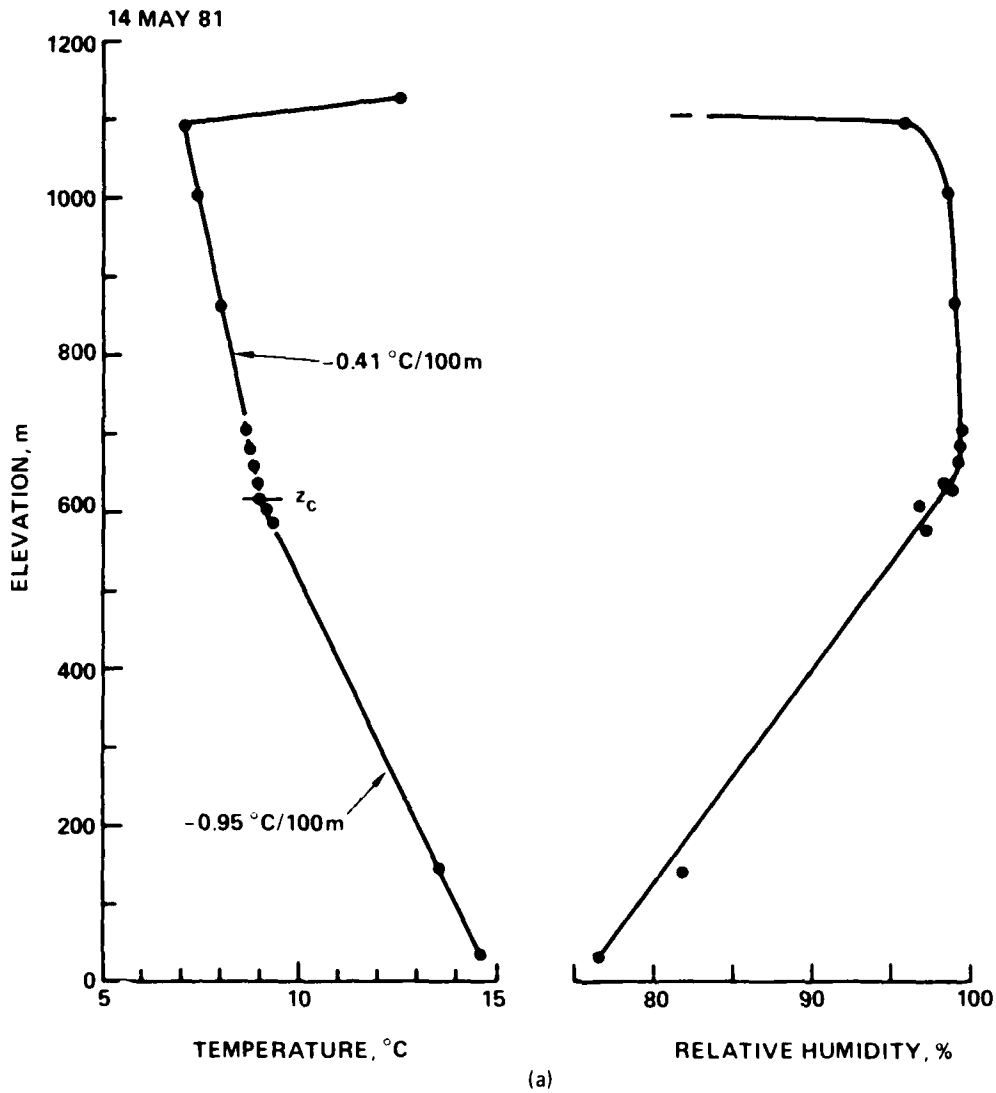

Figure 2. Vertical profile of temperature and relative humidity for each day of measurement.

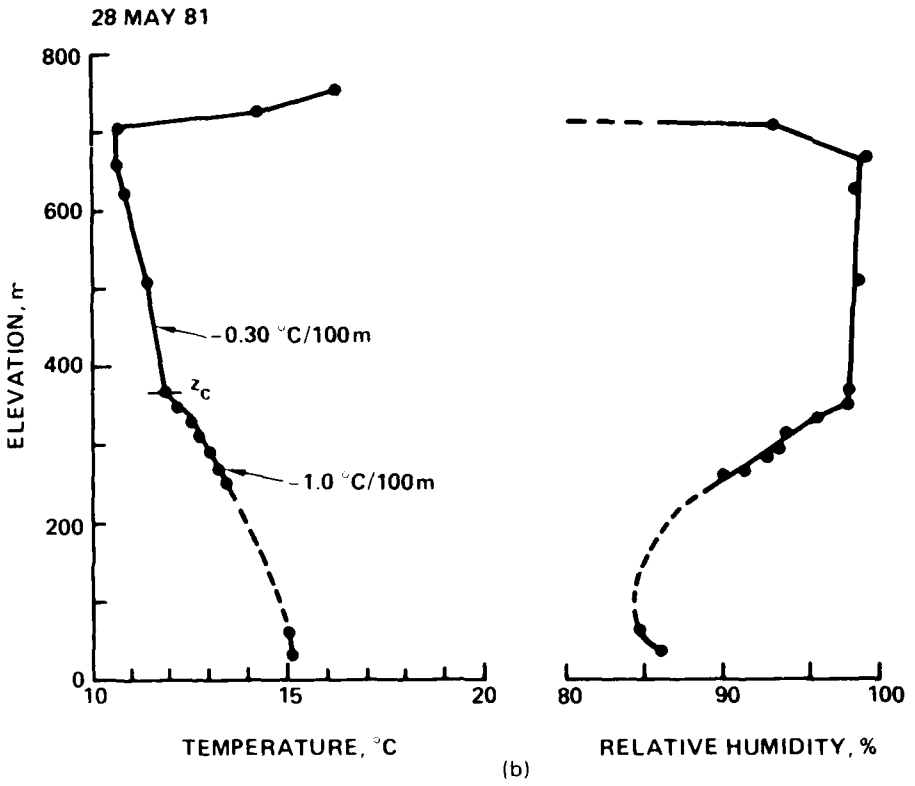

(b)

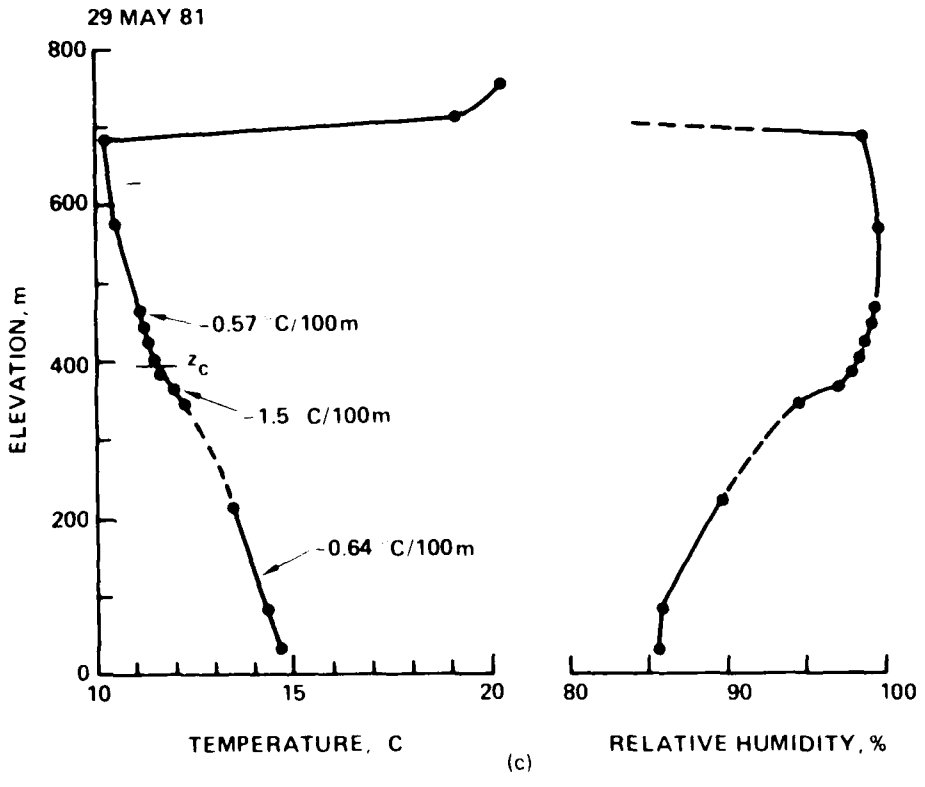

(c)

Figure 2. Continued.

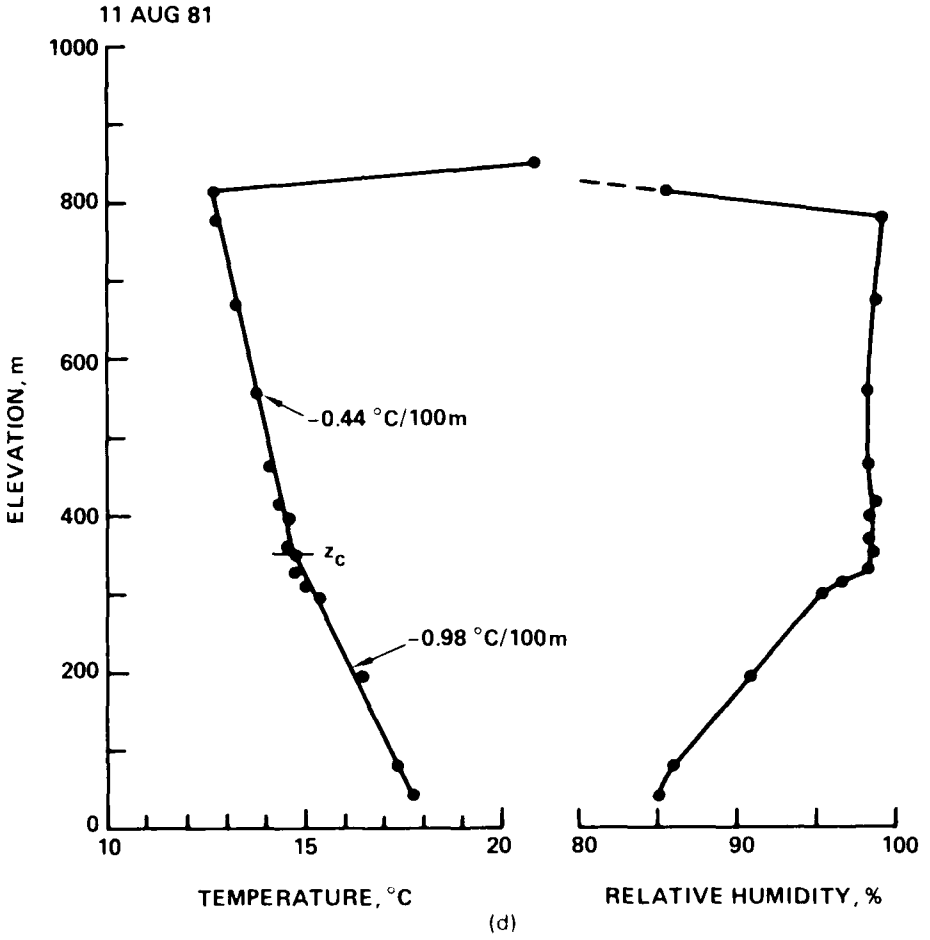

Figure 2. Continued.

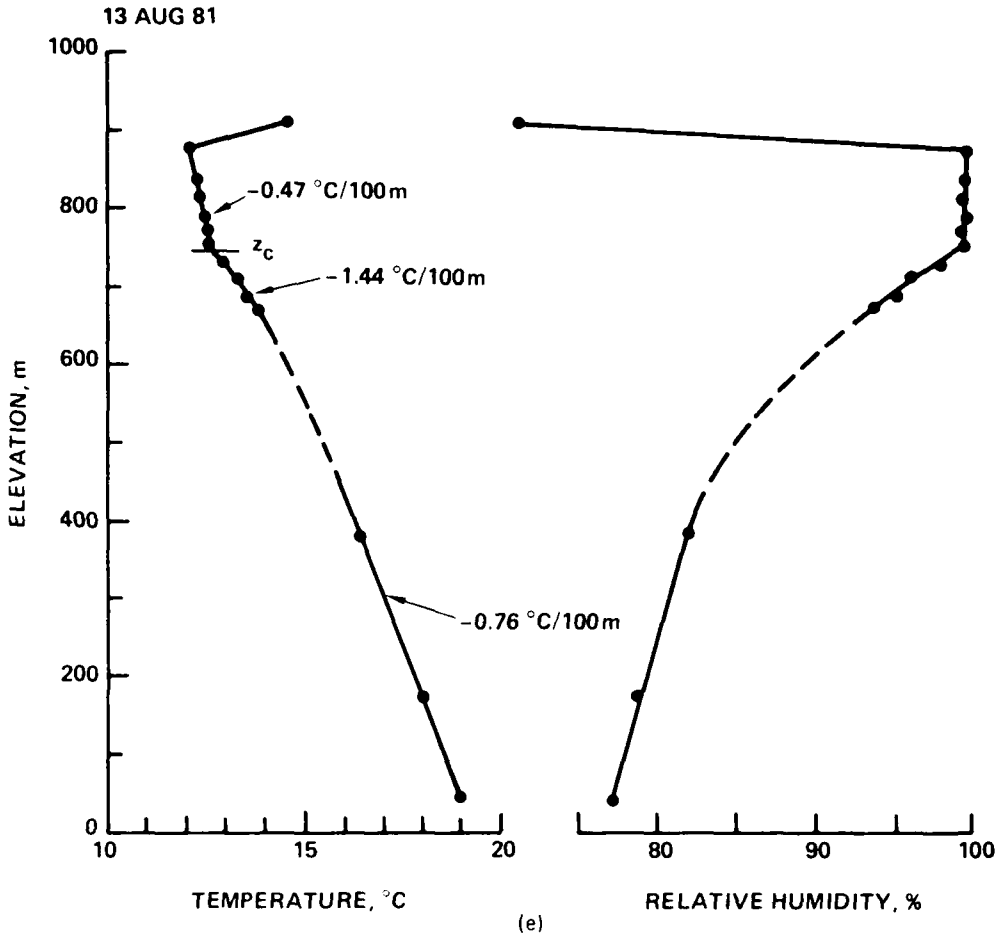

(e)

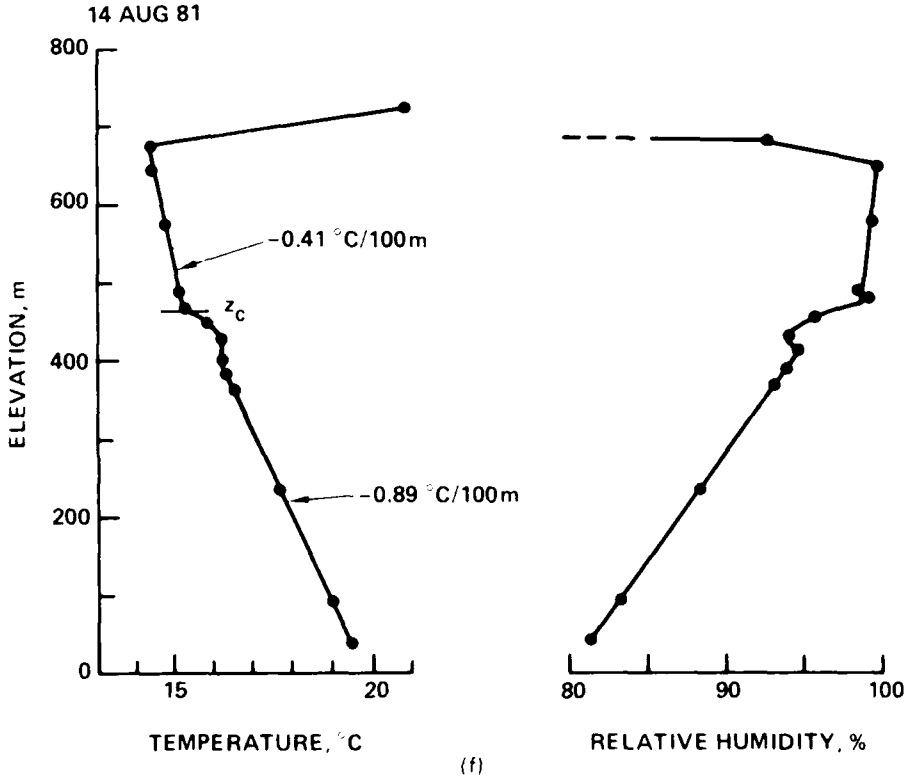

(f)

Figure 2. Continued.

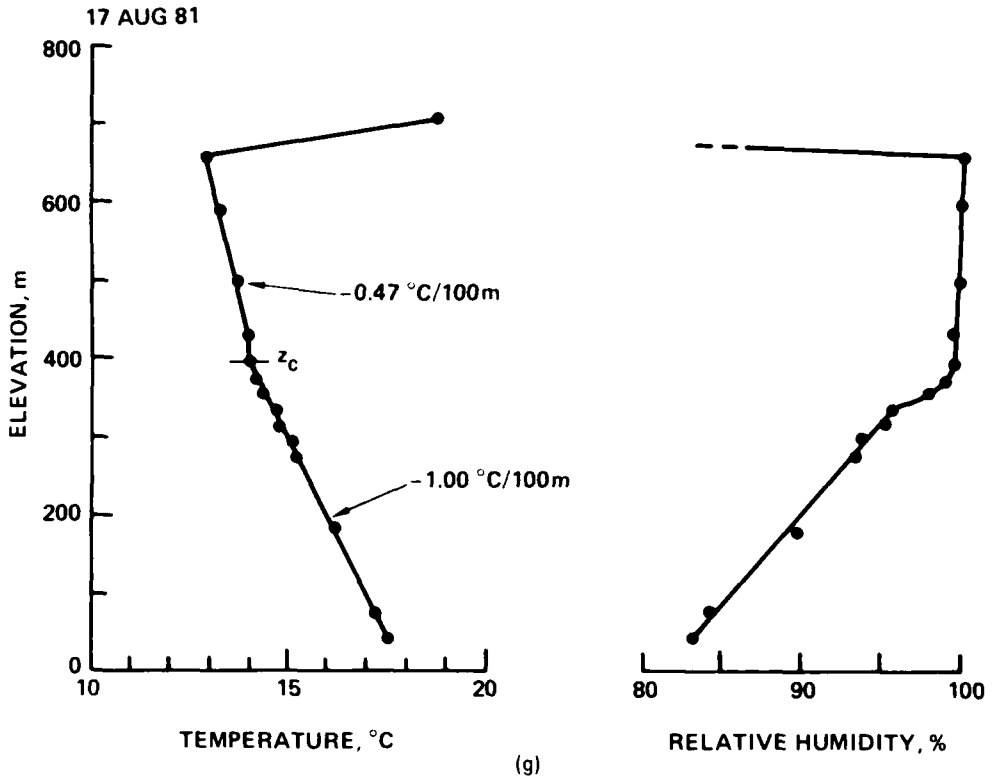

(g)

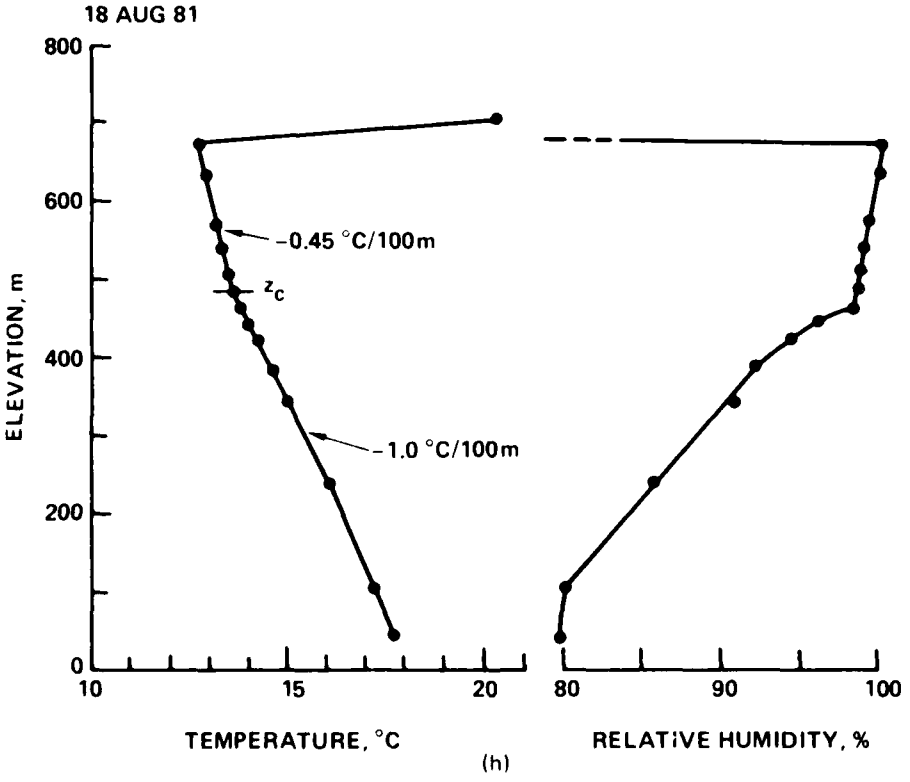

(h)

Figure 2. Continued.

probe would cool the probe by evaporation. However, if the true temperature below Z_c were greater, a large discontinuity in temperature at Z_c would exist. Any explanation for the presence of the superadiabatic region immediately below Z_c on 5 cloud decks must permit its absence on the remaining 3 cloud decks.

Cloud top data were taken along horizontal runs when the pilot attempted to fly in the small cloud top billows about 50 percent of the time. Detailed measurements near Z_t were not attempted.

5.2 Humidity Profiles

The relative humidity f was calculated from the temperature and dew point. The error in f increases with f and is >±5% near 99%. Because of the excessive errors, f cannot be used for regions in or near the cloud. The observed f's rarely exceeded 100% in the cloud. Trends in f have not been examined.

The observed vertical gradients of f beneath Z_c varied considerably from the expected gradient for a dry adiabatic change. These variabilities from a dry adiabatic change are unexplained, although turbulence is suspected. Sensor errors are not likely to create these variations.

5.3 Sea-Surface and Cloud-Top IR Temperatures

The average sea surface temperature (SST) was obtained along the low-level horizontal run using the downward looking Barne's PRT-5 infrared sensor. These SST's are given in Figure 2 (a through h) (the sensor was inoperative on 14 May 81). The average cloud-top temperature was obtained in a similar manner for the run immediately above Z_t.

6.0 AEROSOL SPECTRA

Measurements of the number n of aerosols in a volume of one cm^3 for a band width of one micron centered at a specific radius r_i were made every eight seconds during each two-minute horizontal run. A complete spectrum n(r)

consisted of 47 $n(r_i)$'s from $n(r_i = 0.3\ \mu m)$ to $n(r_i = 150\ \mu m)$. An average $n(r_i)$ in each radius band was obtained by averaging each $n(r_i)$ observed during each two-minute period, if found within ±7m of the average elevation. The mean deviations of the $n(r_i)$ values above (+MD) and below (-MD) the average were also determined. These spectra were both tabulated and plotted by computer.

Parameters calculated from the three spectra of each horizontal run included (1) the cumulative distribution of the number of particles where N is defined to be the total number, (2) the total liquid water content W, (3) the total cross sectional area A, (4) the mean radius $\bar{r}$ and (5) the extinction coefficient k_e for wave lengths of 0.53, 1.06, 3.75 and 10.59μm. The aerosols were considered to be spherical water droplets.

Figure 3 (parts a through h) shows the average n(r) for each horizontal run as a continuous line. The vertical lines connect the +MD and -MD values at selected r_i's. Some -MD values approximately equal the average value. When this occurs the lower part of the line terminates near the average, or because of occasional graphing inaccuracies, just above the average.

Figure 3 (parts a through h) and the printout of the spectra containing the derived parameters have considerable information on the aerosol structure in a maritime stratus-cloud layer. Graphic presentations of the data have been constructed to depict various stratus-layer characteristics. These presentations are displayed in this report and some preliminary results are briefly given.

7.0 VERTICAL PROFILES OF $n(r_i)$

Figure 4 (a through h) presents $n(r_i)$ as a function of elevation for selected r_i's, depicts Z_c and Z_t and indicates the measurement levels. All $n(r_i)$'s were taken from horizontal runs except the data on 14 May (Fig. 4a) when slow descent data were used because of the small number of horizontal runs made below Z_c. All other data in this report were taken from horizontal runs.

One approach to develop a model specifying n(r) as a function of elevation is to obtain an n-degree polynomial equation closely approximating n(r) at selected elevations using average $n(r_i)$'s from several data sets. An elevation dependent model for n(r) could then be obtained by specifying the polynomial coefficients as a function of $Z-Z_c$. This approach was initiated by Noonkester (1981b) for data taken on horizontal runs on 14 May 81.

Another method would utilize average $n(r_i)$'s from several days' data at a number of elevations and obtain an n-degree polynomial equation for $n(r_i)$ having $Z-Z_c$ as the independent variable. The extent these approaches will be pursued has not been determined.

A few characteristics gleaned from Figure 4 are:

- $n(r_i)$'s do not increase appreciably until $Z-Z_c \tilde{>} -100m$.
- $n(r_i)$'s increase rapidly from about $Z-Z_c \tilde{=} 50m$ to Z_c.
- The vertical variation of the $n(r_i)$'s below Z_c does not appear to have a pattern.
- Changes in $n(r_i)$ above Z_c are different for the May and August data. For small r_i, the $n(r_i)$'s decrease and converge to the same value near Z_t, but at greater values for the August data.
- Almost all $n(r_i)$'s decrease rapidly above Z_t. Some stratus cases show an increase in $n(r_i)$ for $r_i = 0.3\mu m$ above Z_t.

8.0 AEROSOL STRUCTURE NEAR AND IN CLOUD

Figure 5 (a through h) shows the vertical variation of W, $W(\Gamma_a)$ (moist adiabatic), N and $\bar{r}$ for all days. The modal radius r_m and $n(r_m)$ are given for the May days. (The August data have no modes in n(r).) The data points are at the flight levels. The data in Figure 5 are summarized in later sections.

8.1 Cloud Base Height as Reference

The following common features are found near the cloud base Z_c:

- a distinct change in the lapse rate of temperature,
- a rapid increase in $n(r_i)$,
- formation of a mode in n(r) near r = 3μm for the May data, and
- a rapid increase in N for the August data without the formation of a mode.

These features may be expected when f approaches and exceeds an f of 1. The third feature is expected for marine aerosols (Neiburger and Chien, 1960). The last feature appears to indicate the presence of a large number of condensation nuclei, an indication of continental aerosols. Determination of aerosol conditions relative to Z_c should reveal features common to the saturation or condensation level. No other elevation appears to be a reasonable reference height. Elevations relative to Z_c are defined to be Z^* ($Z^* = Z-Z_c$). Because the variations of some parameters near Z_t are functions of cloud thickness, Z_t could not be used as a reference elevation.

Figure 6 shows the vertical distribution of the measurement elevations for each day relative to Z^*. Using data at these levels, values of several parameters were determined by interpolation for Z^*'s of -40, -20, 0, +20, +40, +60, +80, +100, +120, +160 and 200m for each day. Then average values for the days in May and August were computed for these eleven levels, called prime levels.

8.2 Average Structure Near Cloud Base

Figure 7 shows the average vertical variation of W, N, $\bar{r}$ and r_m in the range $-40 \leq Z^* \leq 200$m for the May and August data.

The May and August data clearly represent different conditions. The large value of N for the August data suggests the presence of continental aerosols. The value of N for the May data agrees with values previously found in marine clouds. The formation of the mode in the May data at Z_c near an r of 3μm and the steady increase of the mode with elevation are also characteristics of marine clouds. $\bar{r}$ increases with elevation above Z_c less rapidly in the August data. In the May data, $\bar{r}$ and r_m increase with elevation above Z_c at the same rate. Thus $\bar{r}$ is controlled by the large concentration of aerosols in the mode during May. W increases with elevation above Z_c at about the same rate during both months although W is 0.03 and 0.07 gm m^{-3} at Z_c respectively for May and August. The average W at Z_c for both months (equal weights) is 0.05 gm m^{-3}, a value found for data taken near San Nicolas Island in a convective layer with thin broken stratus (Noonkester, 1981c).

8.3 Air Mass Source

An examination of surface pressure synoptic maps (provided by J. Rosenthal and T. Battalino of PMTC, Pt. Mugu, CA) at 0400 PST on 13, 14, 27, 28 and 29 May 81 and on 10-14 and 16-18 August 81 suggests the presence of a marine air source at the measurement site during the May days and continental or mixed air source during the August days. Average surface pressure maps will be constructed for the western U.S. coastal region separately for the May and August days to better estimate the air flow and air mass source region.

8.4 Parameters at Selected Elevations

Tables 2 and 3 contain values of various parameters at the surface, Z_c, Z_c+100m, Z_t and immediately above Z_t.

Differences in the average W and $\bar{r}$ at the surface for the May and August data may be characteristic of marine and continental aerosols. The average W is 3.8 times greater and the average $\bar{r}$ is 1.7 times greater in May than in August. This indicates the presence of a greater number of large particles in May. A greater number of small aerosols would be expected in August if the air source is continental.

Table 2. Data taken along low-level horizontal runs by airborne sensors beneath stratus clouds.

Date 1981	Z m	T °C	T_{IR} °C	f %	N cm^{-3}	W $gm\ m^{-3}$	$\bar{r}$ µm
May							
14	32	14.7	--	77	148	9.3×10^{-5}	0.35
28	32	15.1	17.6	86	19	1.2×10^{-4}	0.81
29	28	14.6	18.3	86	20	8.7×10^{-4}	0.86
Ave.	31	14.8	18.0	83	62	3.6×10^{-4}	0.67
Aug							
11	40	17.8	22.3	85	61	3.9×10^{-5}	0.33
13	41	19.0	19.7	77	54	2.2×10^{-5}	0.35
14	39	19.5	20.2	81	62	3.9×10^{-5}	0.39
17	44	17.5	19.1	83	125	2.4×10^{-4}	0.46
18	43	17.7	20.6	80	117	1.3×10^{-4}	0.40
Ave.	41	18.3	20.4	81	84	9.4×10^{-5}	0.39

Table 3. Data taken along horizontal runs in and near stratus clouds.

Date 1981	Cloud Base					100m Above Cloud Base					Cloud Top		Above Z_t		
	Z_c m	T °C	N cm^{-3}	W $gm\ m^{-3}$	$\bar{r}$ µm	$\Delta T/\Delta Z$ °C $(100m)^{-1}$	N cm^{-3}	W $gm\ m^{-3}$	W_Γ* $gm\ m^{-3}$	$\bar{r}$ µm	Z_t m	$Z_t - Z_c$ m	T °C	$Z - Z_t$ m	T_{IR} °C
May															
14	620	9.1	203	0.02	2.2	-0.41	193	0.12	0.23	3.5	1090	470	7.1	32	7.4
28	369	11.8	260	0.04	2.8	-0.30	305	0.10	0.28	4.7	701	332	10.7	23	11.2
29	395	11.6	275	0.02	1.6	-0.57	310	0.23	0.22	3.8	684	289	10.3	27	10.5
Ave.	461	10.8	246	0.03	2.2	-0.43	269	0.15	0.24	4.0	825	364	9.4	27	9.7
Aug															
11	352	14.8	640	0.10	2.4	-0.44	680	0.18	0.28	3.2	814	462	12.7	31	12.5
13	745	12.7	680	0.07	2.2	-0.47	680	0.25	0.27	3.8	876	131	12.1	33	12.2
14	460	15.4	700	0.04	1.3	-0.41	670	0.15	0.26	2.4	679	219	14.5	45	14.8
17	396	14.0	620	0.09	2.1	-0.47	610	0.23	0.30	3.3	660	264	12.9	48	13.1
18	488	13.5	680	0.06	1.5	-0.45	685	0.24	0.25	2.8	673	185	12.7	32	12.8
Ave.	488	14.1	664	0.07	1.9	-0.45	665	0.21	0.27	3.1	740	252	13.0	38	13.1

*Liquid water assuming $\Delta T/\Delta Z$ is moist adiabatic and w = 0 at cloud base.

The negative air-sea surface temperature difference is large in the May data and moderate in the August data. The IR temperature is considered to be representative because the average T_{IR} above Z_c is only 0.3°C and 0.1°C greater than the average cloud top temperature respectively for May and August. T_{IR} above Z_c would be expected to be slightly greater than T_{Z_t} because some IR received by the IR probe would emanate from regions just below Z_t where T is slightly greater than T_{Z_t}. The values of T-SST are apparently real.

9.0 AVERAGE VERTICAL VARIATION OF n(r)

A graphical method was devised to derive n(r) at the eleven prime levels for the May and August days and is described in the following sections.

9.1 Isopleths of Normalized $n(r_i)$

All $n(r_i)$ values for r_i = 0.3, ..., 13μm were normalized by N and multiplied by 100 to obtain the parameter $[n(r_i)/N]100$ (Slingo and Brown, 1980) having units of μm^{-1} at measurement elevations above Z_c-100m for each day. Isopleths of this parameter $n'(r_i)$ were constructed in a (r_i,Z) cartesian coordinate system. Figure 8 (a through h) shows these isopleth patterns for each day in the region r_i = 2, ..., 13μm. (Similar figures for r_i = 0.3, ..., 2μm are not shown.) A spectrum can be reconstructed for any elevation by selecting representative $n'(r_i)$'s and multiplying by 0.01N where N is representative of that elevation.

Values of $n'(r_i)$ were extracted from the isopleth patterns of $n'(r_i)$ at the prime levels for each day at 24 selected r_i's in the range $0.4\mu m \leq r_i \leq 13m$. An average $n'(r_i)$ was computed for each selected r_i separately for the May and August data at each prime level. The isopleth pattern of the average $n'(r_i)$'s was constructed for the May and August data as shown in Figure 9 (a and b) for $2\mu m \leq r_i \leq 13\mu m$.

Isopleth patterns of $n'(r_i)$ for May and August in Figure 9 have distinctly different patterns. The presence of maximum values extending from 3μm at

Z^* = 0 to 6.5μm at Z^* = 200m in the May data is a glaring feature not present in the August data. Placement of this line of maximum in the May isopleths to a similar position in the August isopleths provides a reference line separating common and uncommon factors. Isopleths to the right of this line have a similar slope indicating that $n(r_i)$ in this region increase with elevation at about the same rate for both months. Isopleth values to the left of this line decrease in value with elevation in the May data indicating the decrease in the number of aerosols with $r<r_m$. Isopleths of $n'(r_i)$ to the left of this line in the August data spread and approach a common value of about $15\mu m^{-1}$ at Z^* = 200m.

9.2 Average Spectra Near Cloud Base

The average $n'(r_i)$ values at the prime levels used to construct Figure 9 were used to construct the average n(r) for May and August at the prime levels. An average n(r) at the surface for May and August was also constructed (the minor elevation differences of the low-level data runs were ignored). The average N at the surface and at each prime elevation were used in this construction.

Figure 10 (a through l) presents the average n(r) at the surface and at each prime elevation. Because the average Z_c for May and August are approximately the same, the average n(r) at the surface essentially represents a Z^* of -475m. Most differences in these n(r)'s have been discussed. However, additional important differences are revealed in Figure 10 in the n(r) changes from the surface to Z^* = -20m. For $r < 0.9$ μm, n(r) is greater for August than for May at the surface. This cross-over r increases to 3.6μm at Z^* = -40m. At $Z^* \geq$ -20m, n(r) for August is essentially greater at all r.

If the humidity increased steadily from the surface to Z_c as expected in a well-mixed layer, f should be a function of Z^* only. Thus, the n(r)'s in Figure 10 would represent specific values of f for $Z^* \lesssim 0$.

The rate of increase of n(r) with elevation is greater at all r for the August data from the surface to Z_c. If f is assumed to be the same at each Z^* for the May and August data, then dr/df for May and August are different.

Differences in the chemical characteristics of the nuclei could cause the difference. A chemical difference (effectively more hygroscopic) and a larger number of condensation nuclei during August could cause the difference in n(r) at all elevations. The aerosols for May and August are apparently from different source regions.

10.0 LIQUID WATER CONTENT

The vertical profile of liquid water content is often used to characterize stratus clouds. The liquid water content was determined for the average n(r) and the ±MD n(r)'s by numerical evaluation of

$$W = \frac{4}{3}\pi\rho \int_{r_1}^{r_2} r^3\, n(r)dr$$

where r_1 is 0.23 μm, r_2 is 150 μm and ρ is the density of water.

10.1 Profiles of W

The vertical profiles of W are shown in Figure 11 (a through h) for each day. These data show a more complete profile of W and provide ranges (±MD) of W in marine stratus clouds not previously available. Some significant features revealed in Figure 11 include: (1) a large increase in W from the surface up to regions near the cloud top; (2) the maximum W in the cloud increases with cloud thickness; (3) the largest MD's are near Z_t and immediately beneath Z_c; (4) most +MD's are greater than -MD's above Z_t and below Z_c; (5) the greatest ranges of W from +MD to -MD are observed immediately below Z_c in many profiles and (6) the profiles are considerably more similar near Z_c than near Z_t. Feature (1) is expected. Features (2) and (6) indicate that a model of n(r) near Z_t will be a function of cloud thickness. Features (3), (4) and (5) provide information on the turbulent mixing processes across Z_c and Z_t affecting n(r). Some analyses of relationships between $\bar{r}$, N and W in progress suggest that the turbulent mixing process is inhomogeneous.

10.2 Profiles of Average W

Profiles of the average W for the May and August data are shown in Figure 12a. The profiles are significantly different. Although W for August is less than for May near the surface, W for August increases at a greater rate from the surface to Z^* = 60m. The W's for these months are equal at Z^* = -150m. The greater increase of W with elevation below Z^* = 60m for August is additional evidence that aerosols present in August respond differently to increases in humidity.

Figure 12a contains regression equations of W as a function of Z^* for various elevation spans. The correlation coefficients between W's specified by these least-square regression equations and the observed W's are 1.00. W increases exponentially with elevation below Z^* = -60m and linearly above Z_c. The cusp in $W(Z^*)$ at Z_c in the May data is considered to be caused by unusual variations in the small data set of three days.

Figure 12b shows an average $W(Z^*)$ for the months of May and August and shows the least-square regression equations for various elevation spans. (An equal weight was given for the May days and the August days in determining the average.) $W(Z^*)$ is exponential below Z^* = -60m and linear above.

The abrupt changes in $\Delta T/\Delta Z$ at Z_c (see Fig. 2) are undoubtedly caused by the release of appreciable latent heat commencing at Z_c and continuing to near Z_t in saturated air parcels having an average positive rise rate. The sudden release of latent heat at Z_c for rising air parcels suggests that $\Delta W/\Delta Z$ would increase rapidly at Z_c. The data indicate only a small increase in $\Delta W/\Delta Z$ near Z_c in apparent contradiction to the abrupt changes in $\Delta T/\Delta Z$. Turbulence, undoubtedly present near Z_c would transport large aerosols from above Z_c to below Z_c and mask the increase in W caused by condensation. Large values of W_{+MD} below Z_c suggest the presence of large aerosols below Z_c possibly carried by turbulence. Profiles of $W(Z^*)$ shown in Figure 12 are considered to be steady-state profiles representing a balance between condensation and turbulent transport.

11.0 REFERENCES

Neiburger, M. and C. W. Chien, 1960: Computations of the growth of cloud drops by condensation using an electronic digital computer. Physics of Precipitation, Monograph No. 5, Amer. Geophys. Union, 191-209.

Noonkester, V. R. 1981a: Aerosol and Humidity Structure Beneath Maritime Stratus Clouds: A Review of Theory, Models and Observations, NOSC TN 1070, October 1981.

Noonkester, V. R. 1981b: Aerosol and Humidity Structure Beneath Maritime Stratus Clouds: A Preliminary Data Report, NOSC TN 1085, December 1981.

Noonkester, V. R. 1981c: Aerosol size spectra in a convective marine layer with stratus: Results of airborne measurements near San Nicolas Island, J. Appl. Meteor., v. 20, no. 9, p 1076-1080, September.

Slingo, A. and R. Brown, 1980: High resolution radiative and microphysical observations of nocturnal stratocumulus, Preprints, Eighth International Conf. on Cloud Physics, Am. Meteor. Society, Boston, Mass.

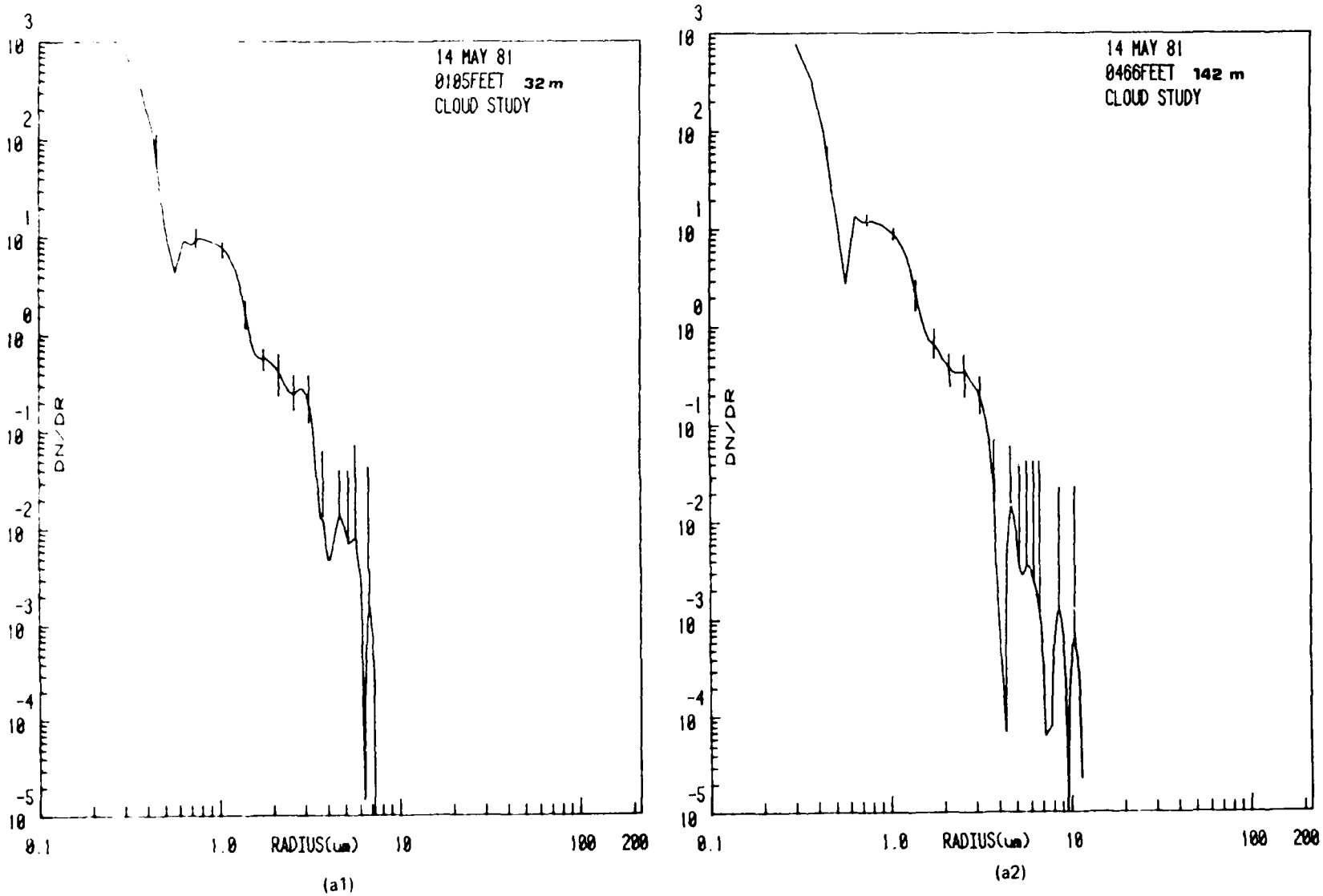

Figure 3. Aerosol spectra (DN/DR or n(r), $cm^{-3}\ \mu m^{-1}$) for each horizontal run. The continuous line is the average spectra. The vertical lines at selected radii connect the mean deviations of the spectra above and below the average. Plotting errors have terminated some vertical lines above or below the average. Parts of the average DN/DR and the vertical lines are shown in regions when DN/DR $\lesssim 10^{-5}\ cm^{-3}\ \mu m^{-1}$.

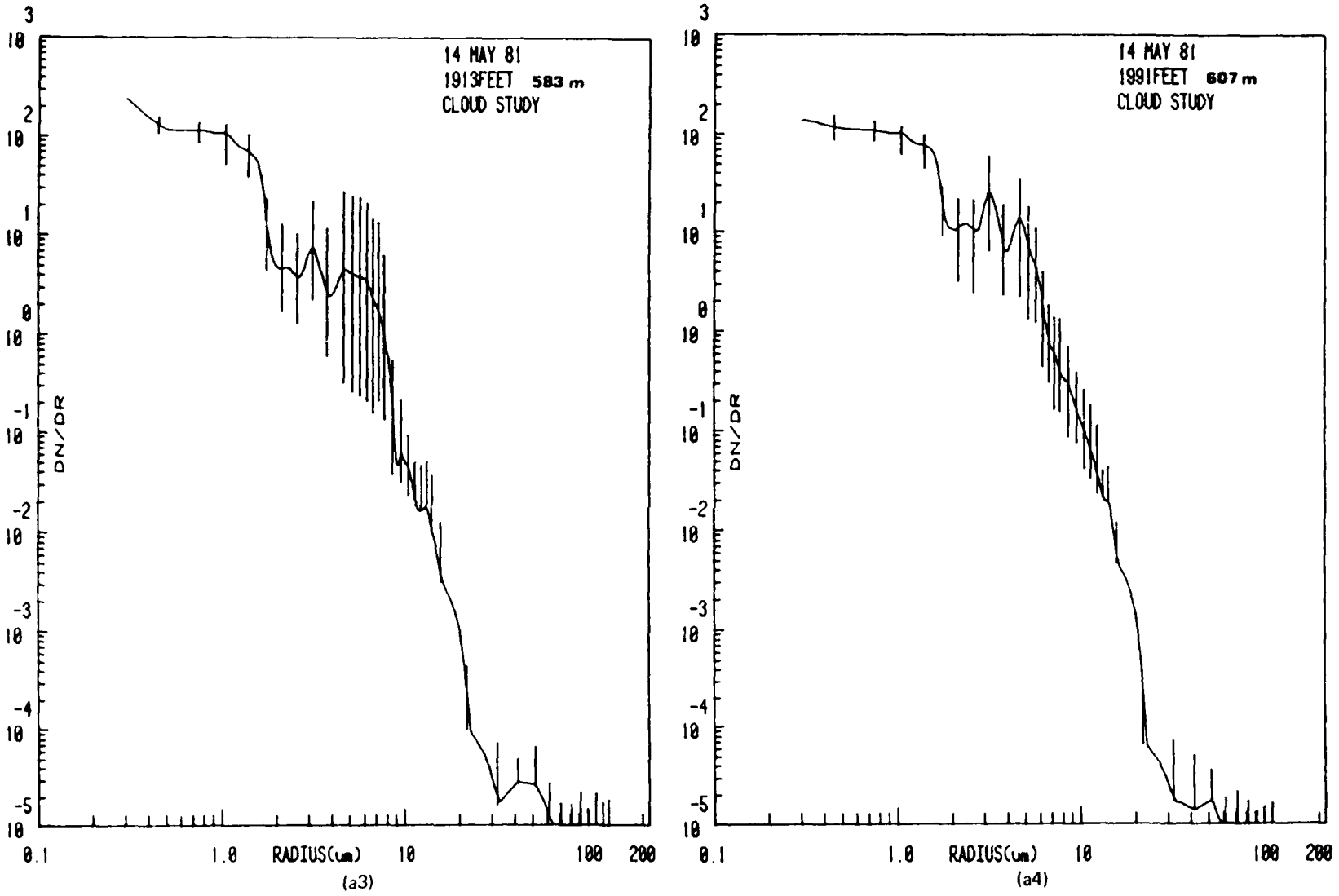

Figure 3. Continued.

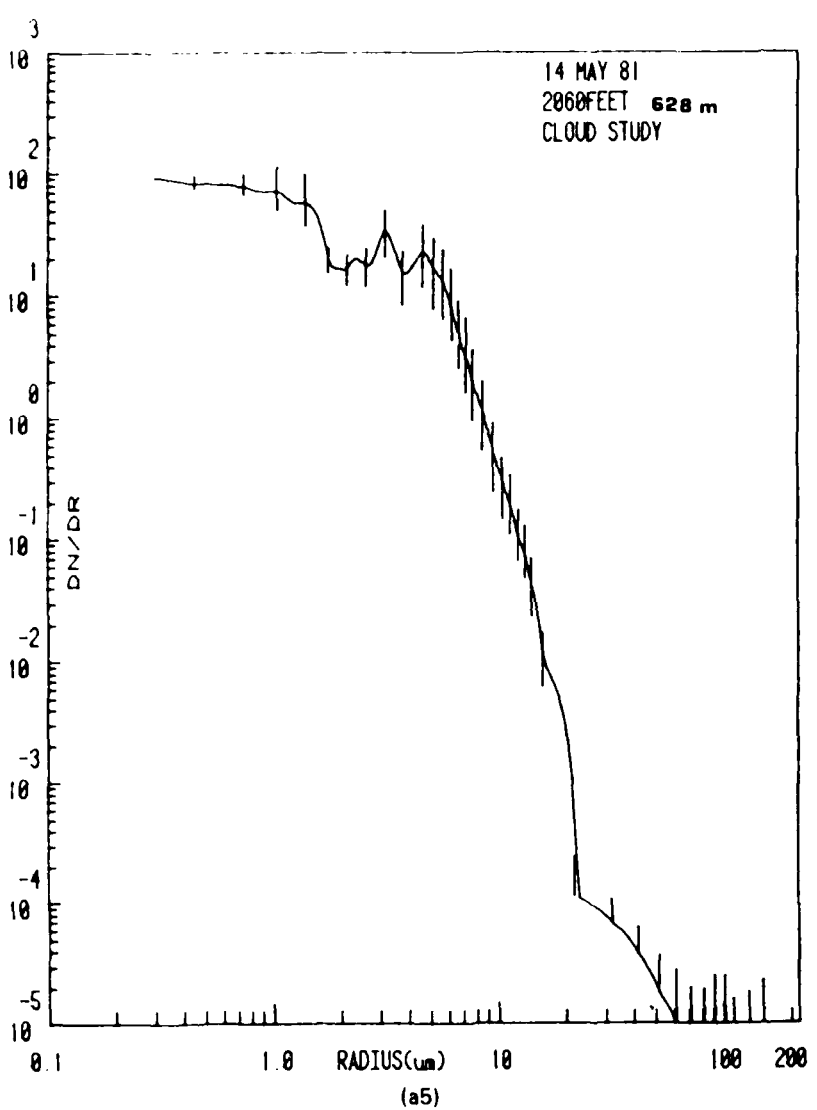

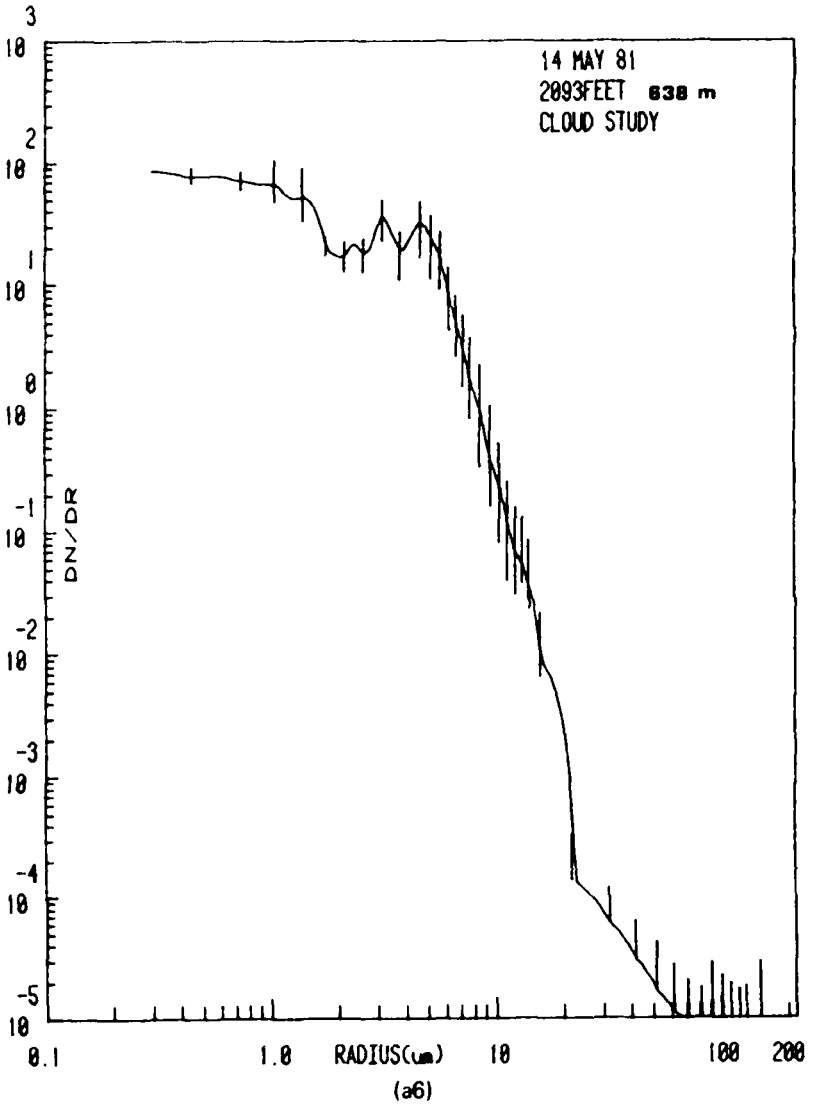

Figure 3. Continued.

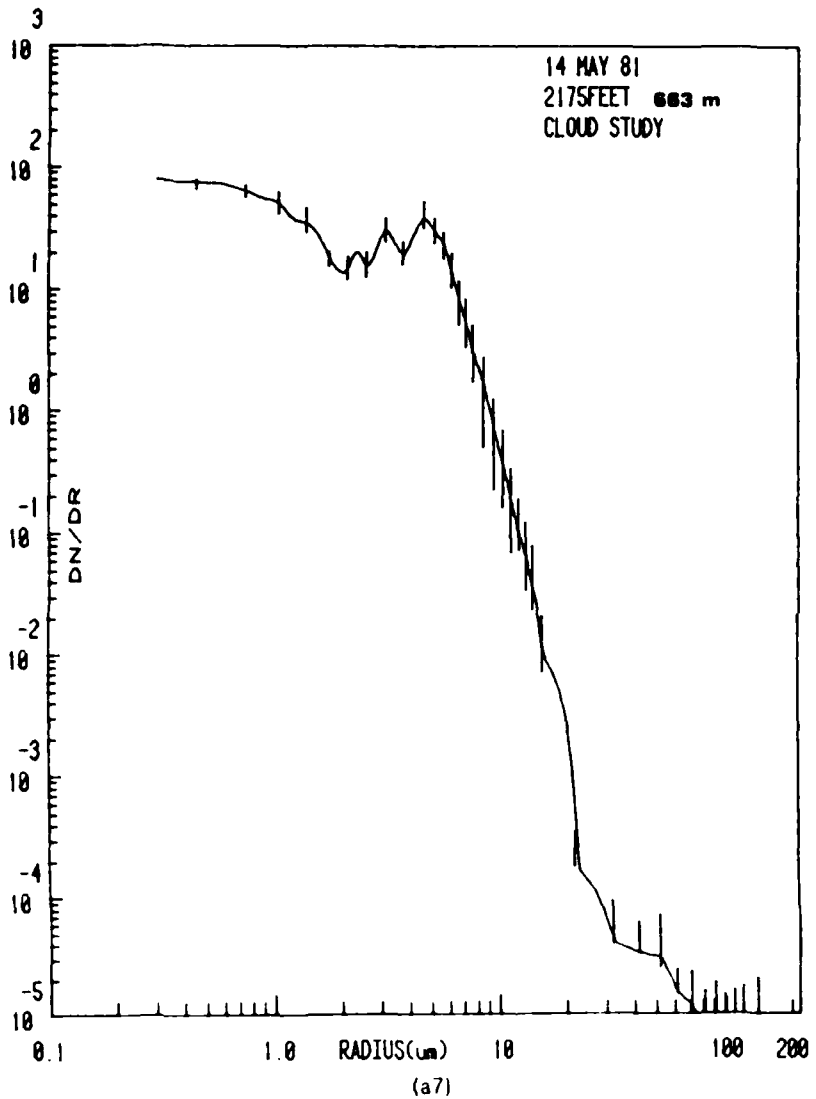

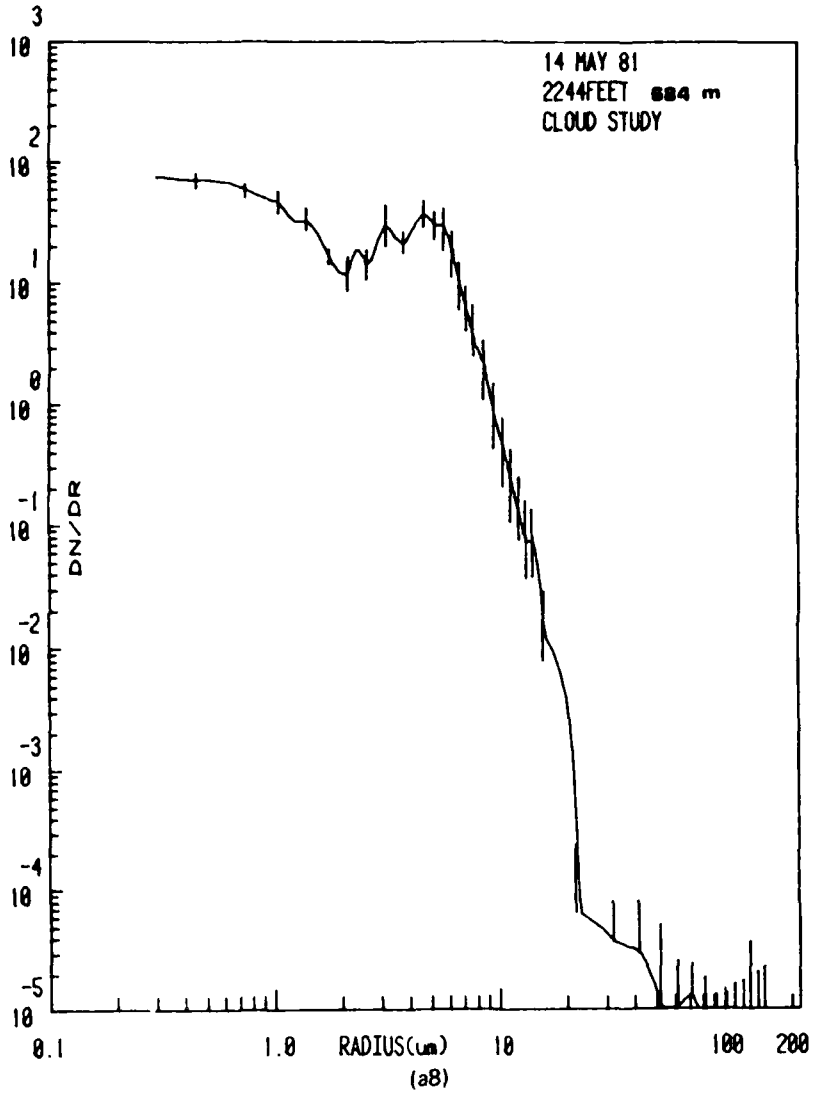

Figure 3. Continued.

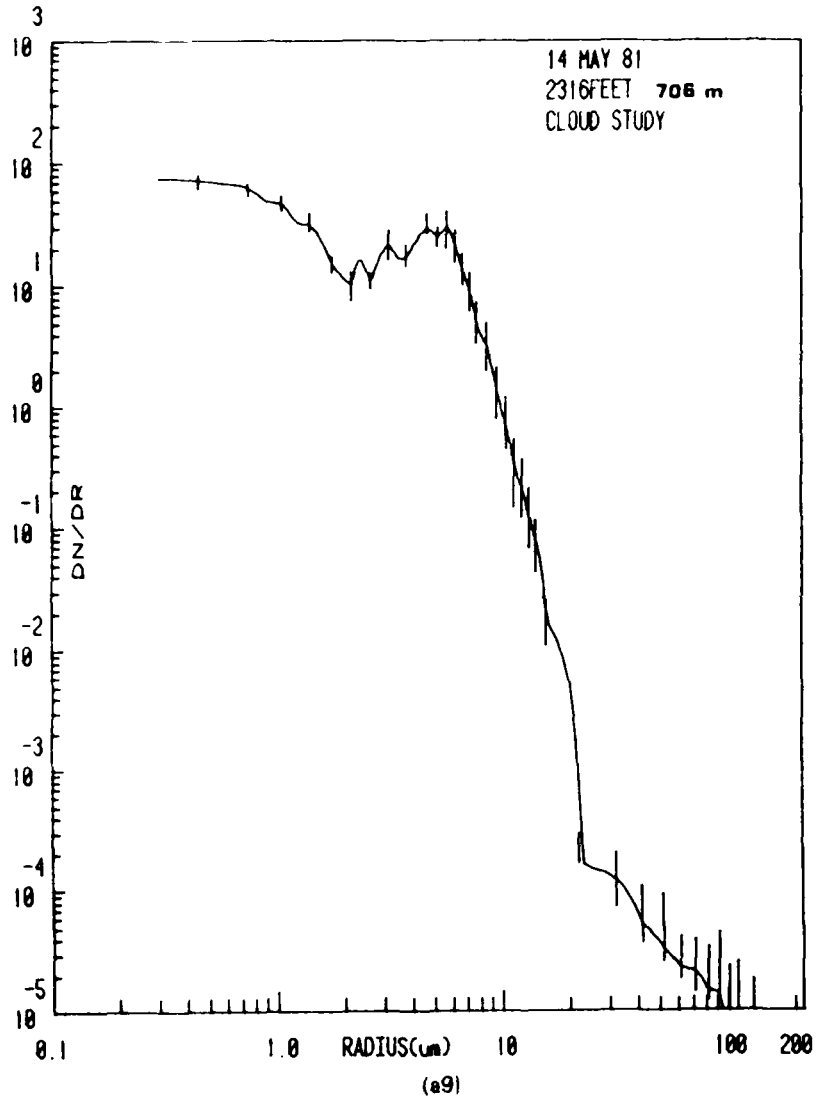

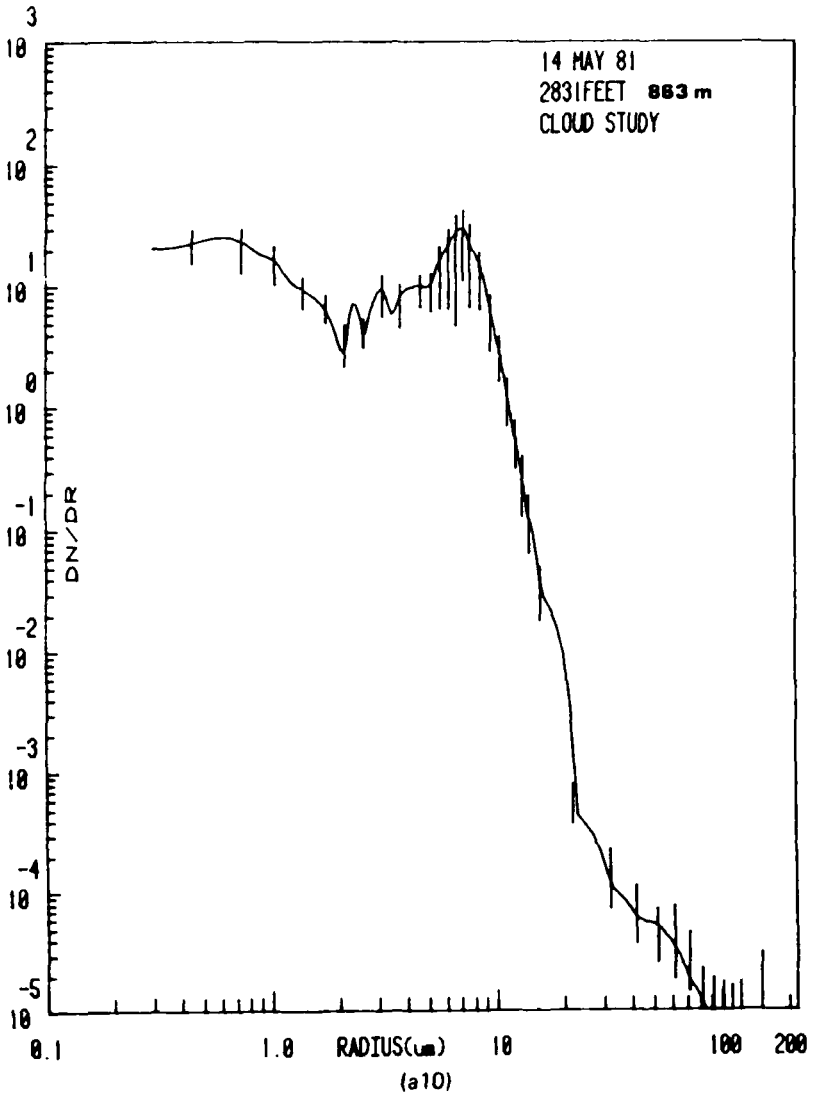

Figure 3. Continued.

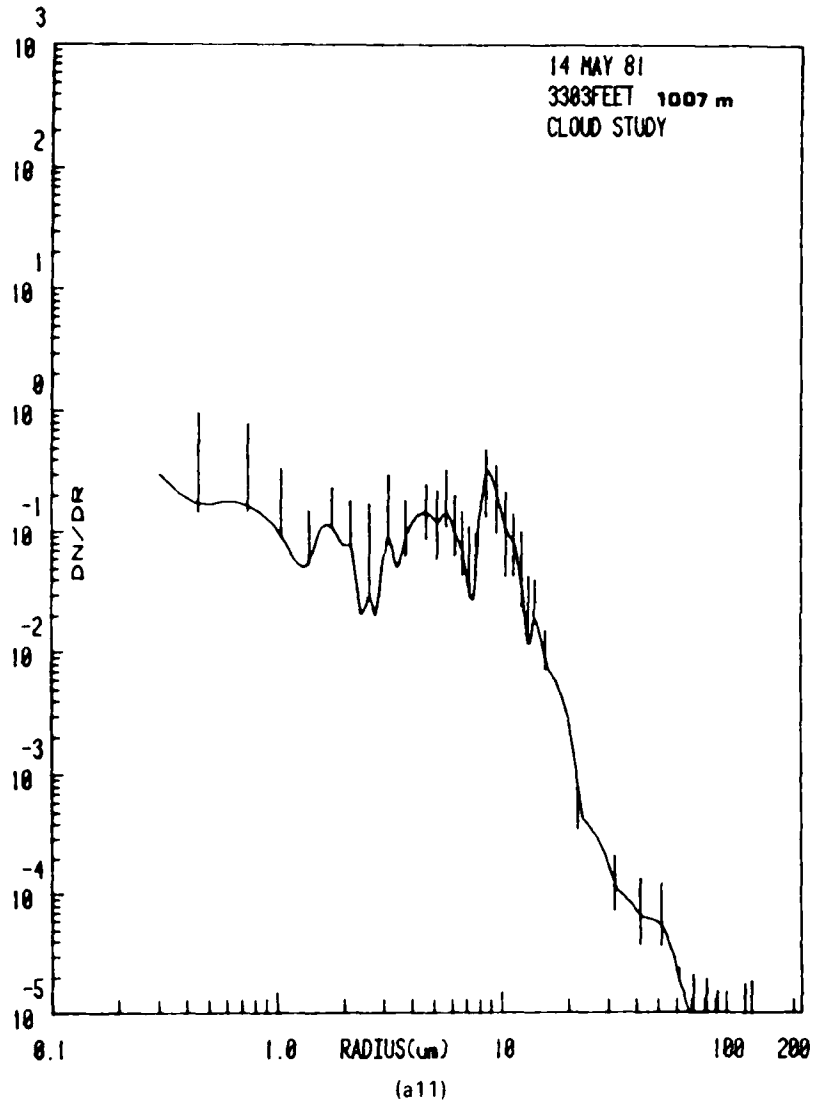

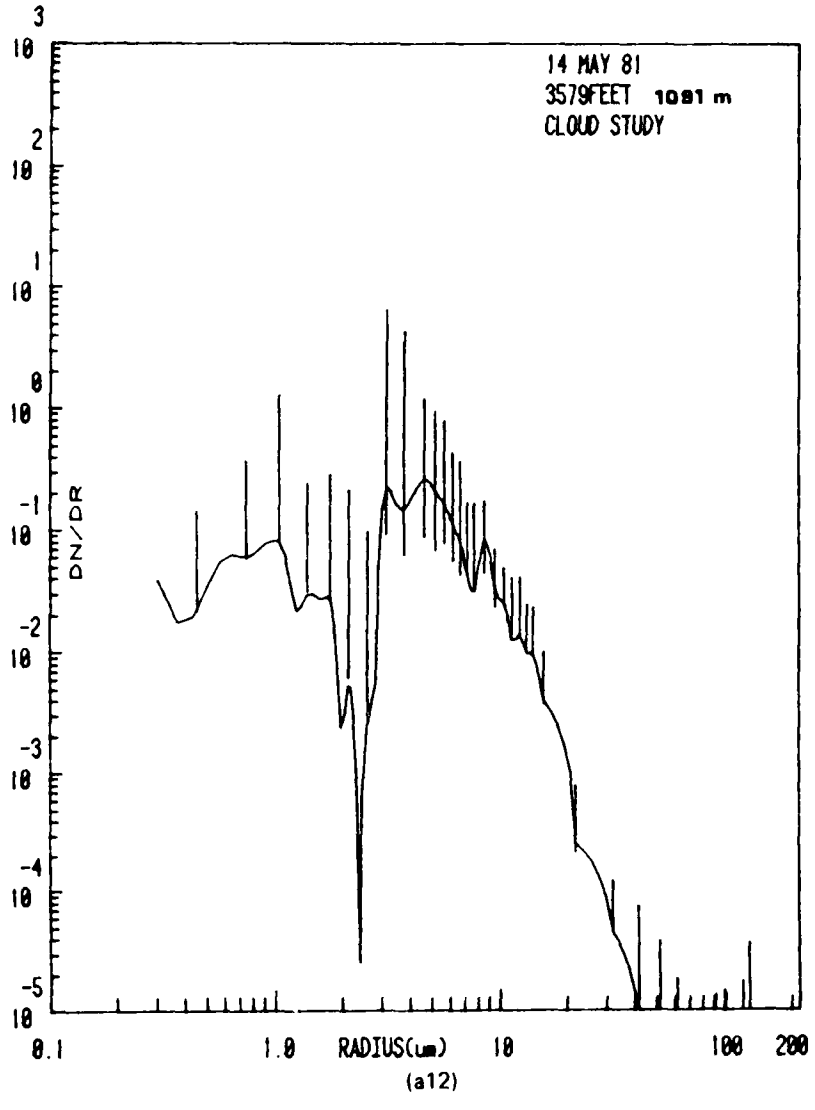

Figure 3. Continued.

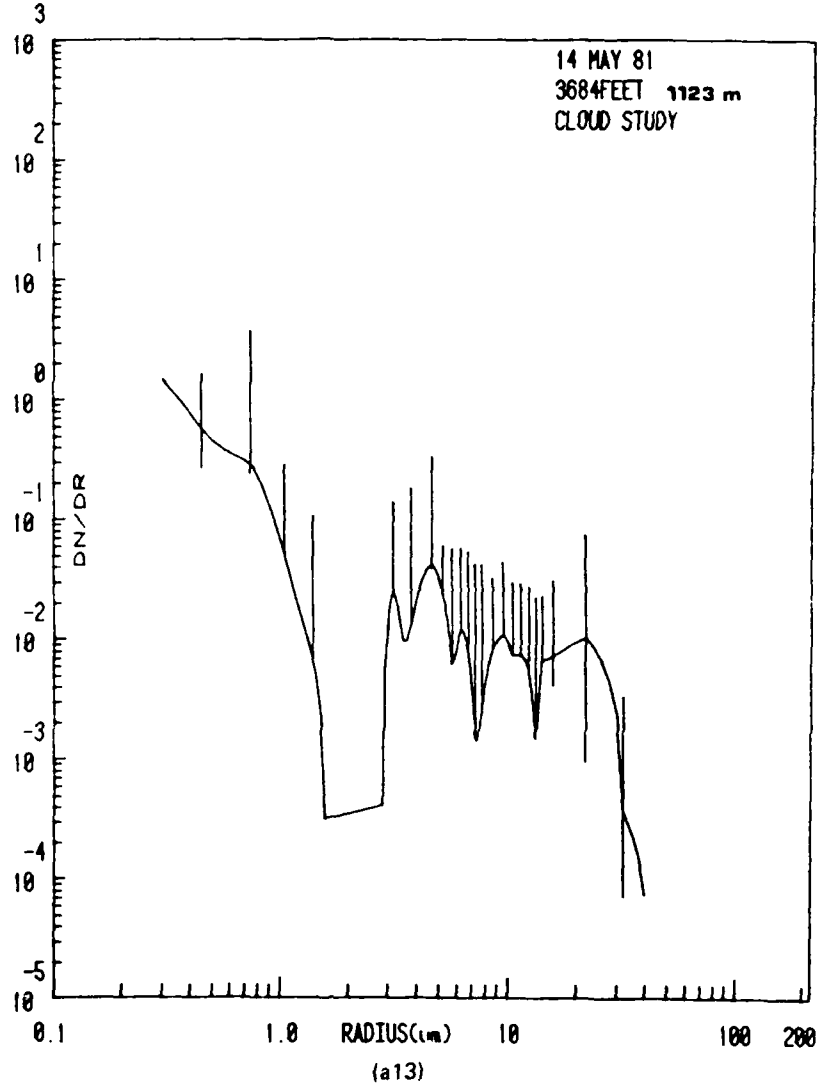

Figure 3. Continued.

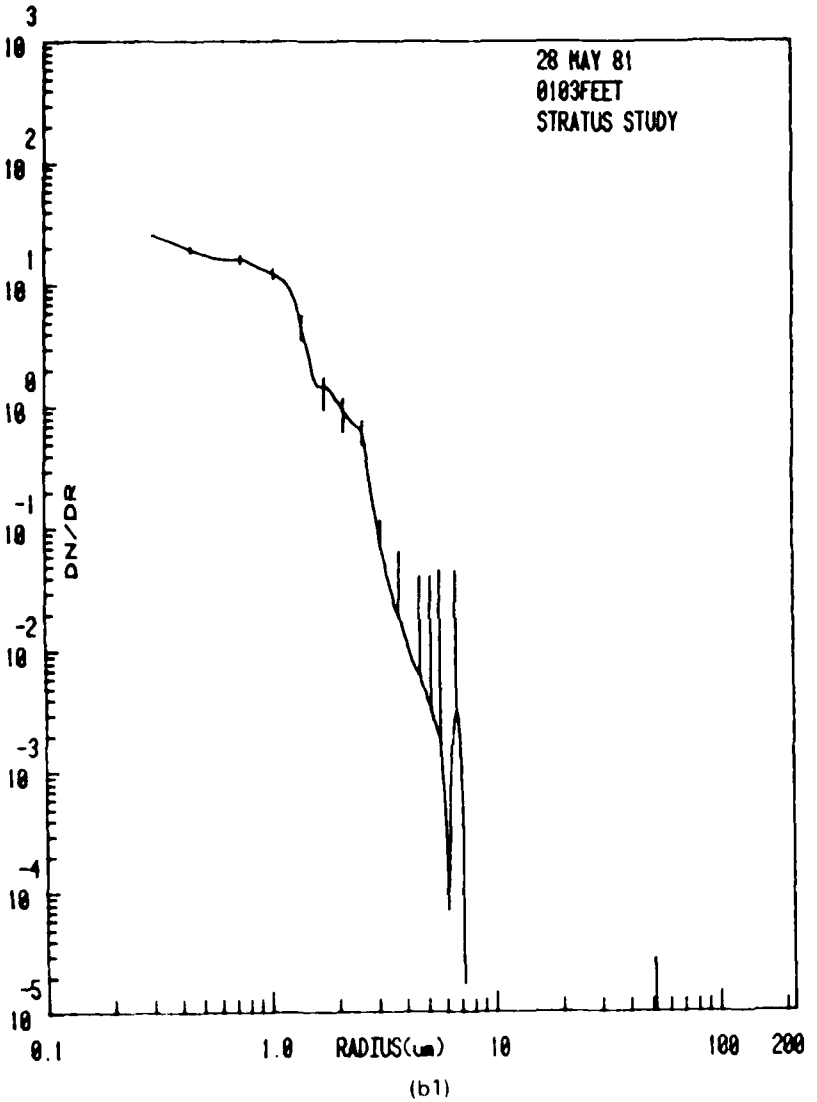

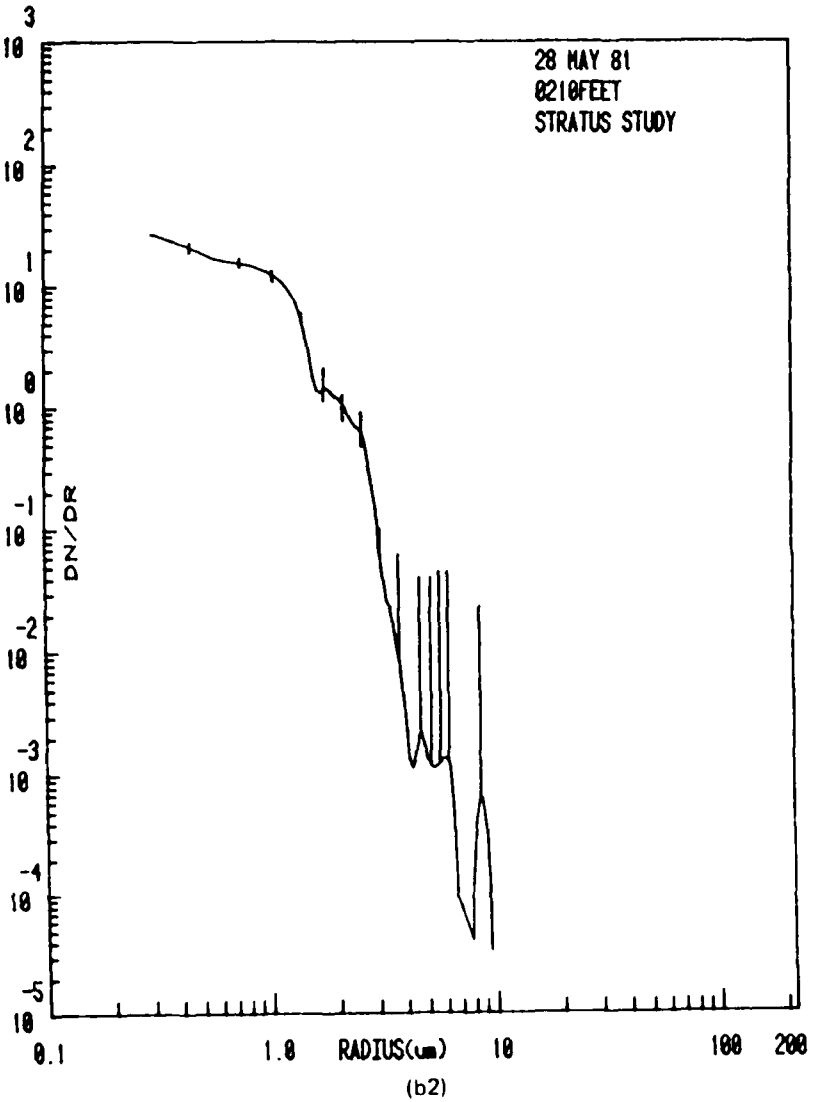

Figure 3. Continued.

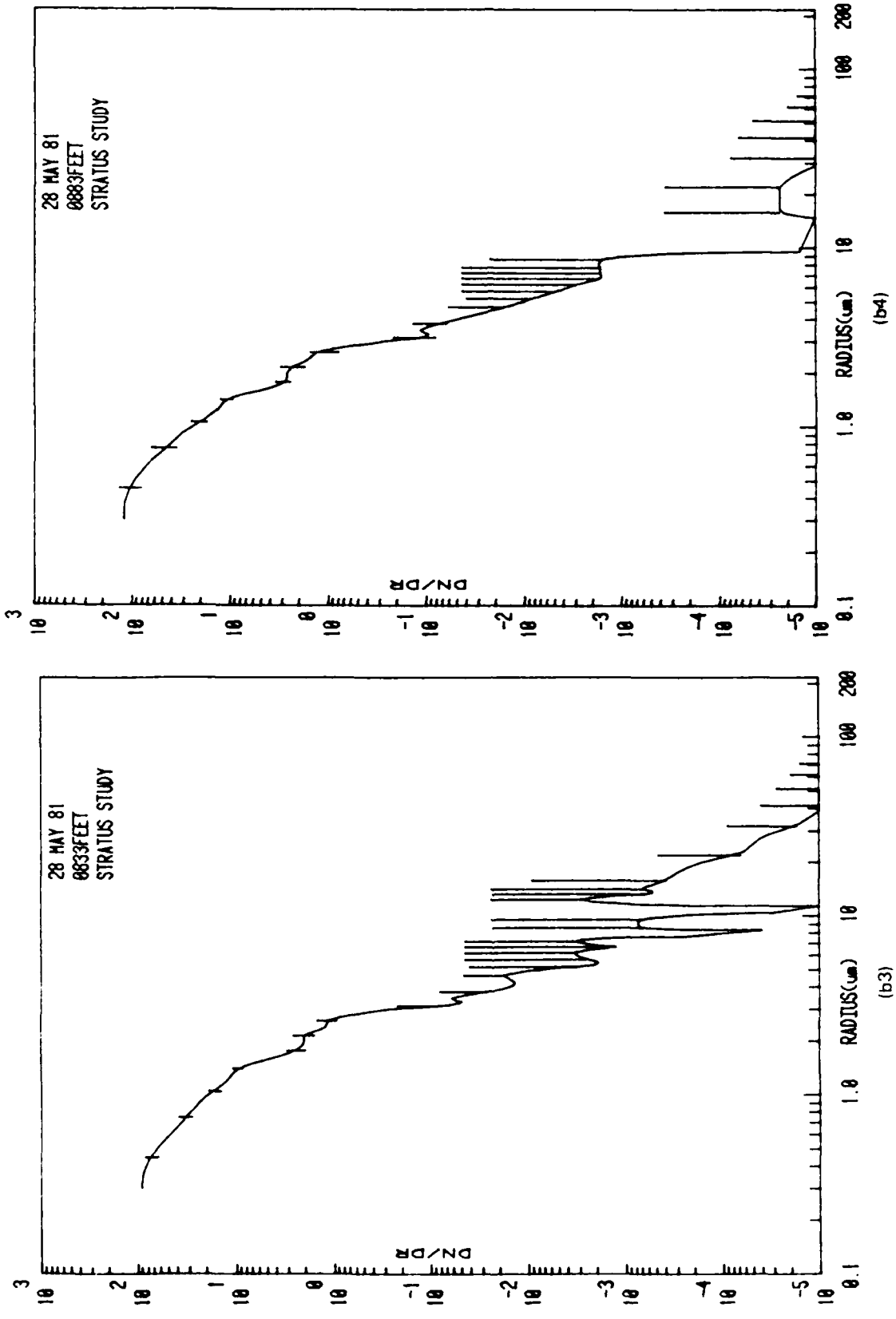

Figure 3. Continued.

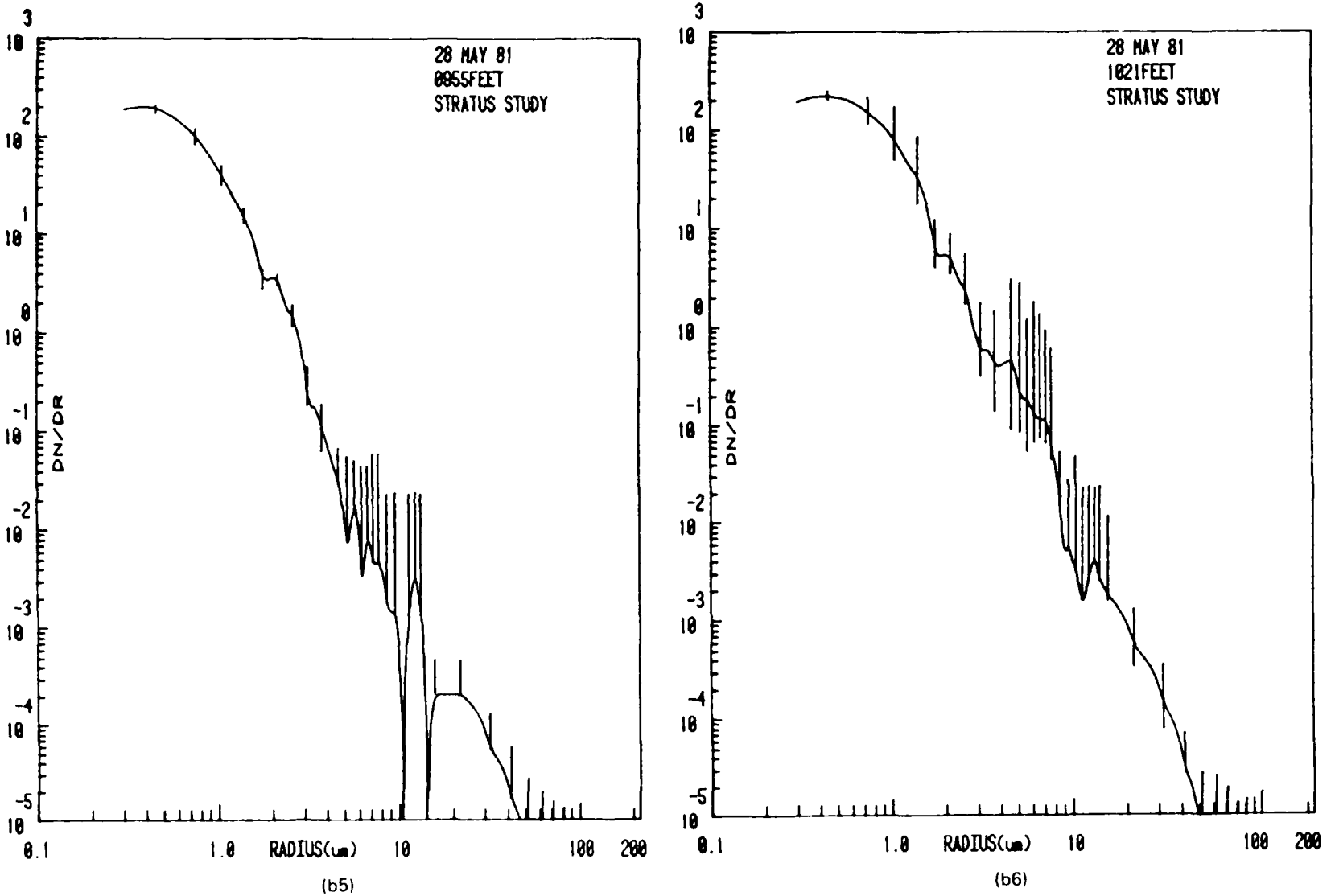

Figure 3. Continued.

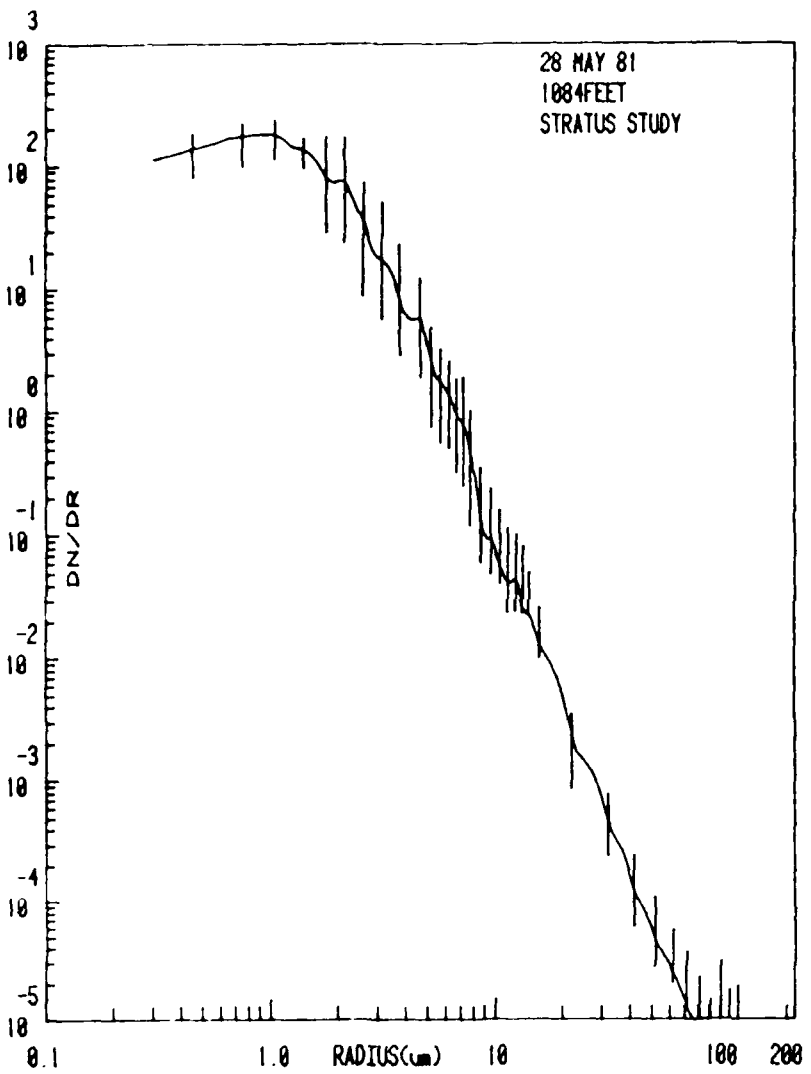

(b7)

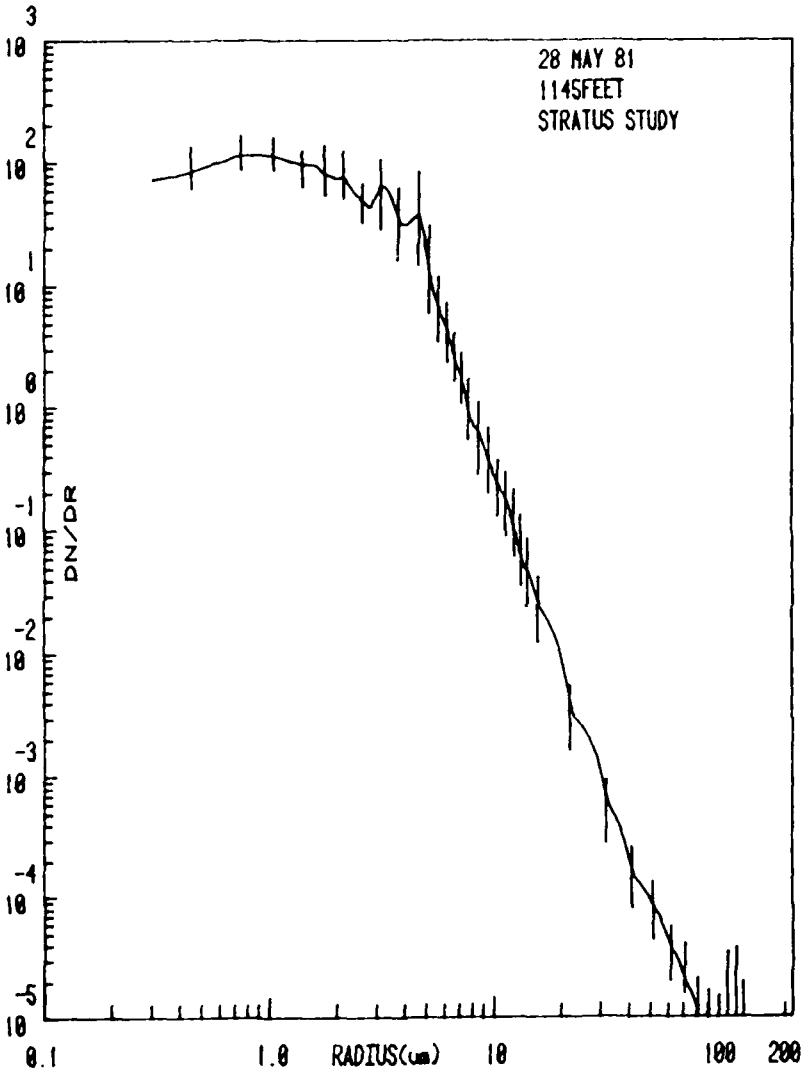

(b8)

Figure 3. Continued.

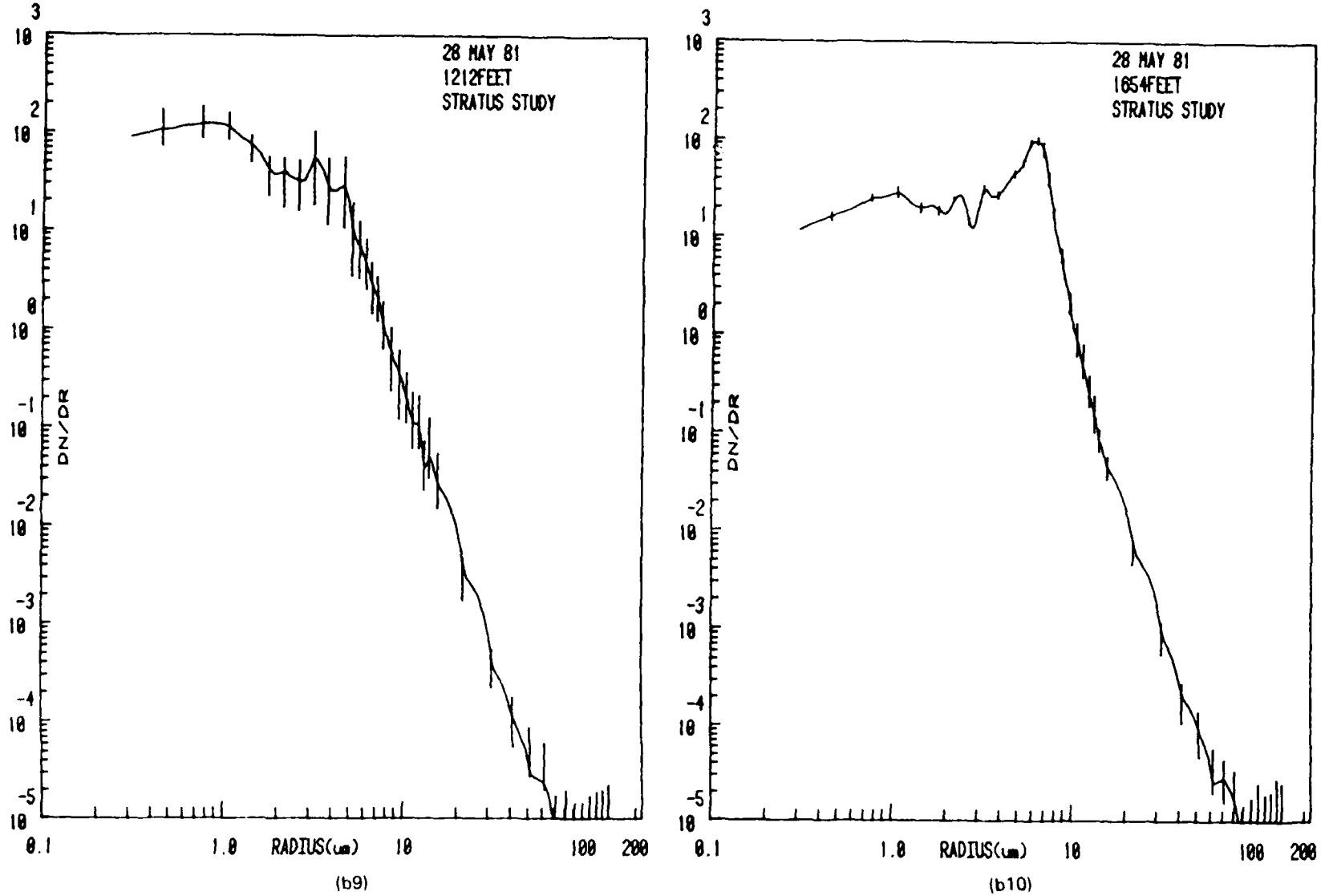

Figure 3. Continued.

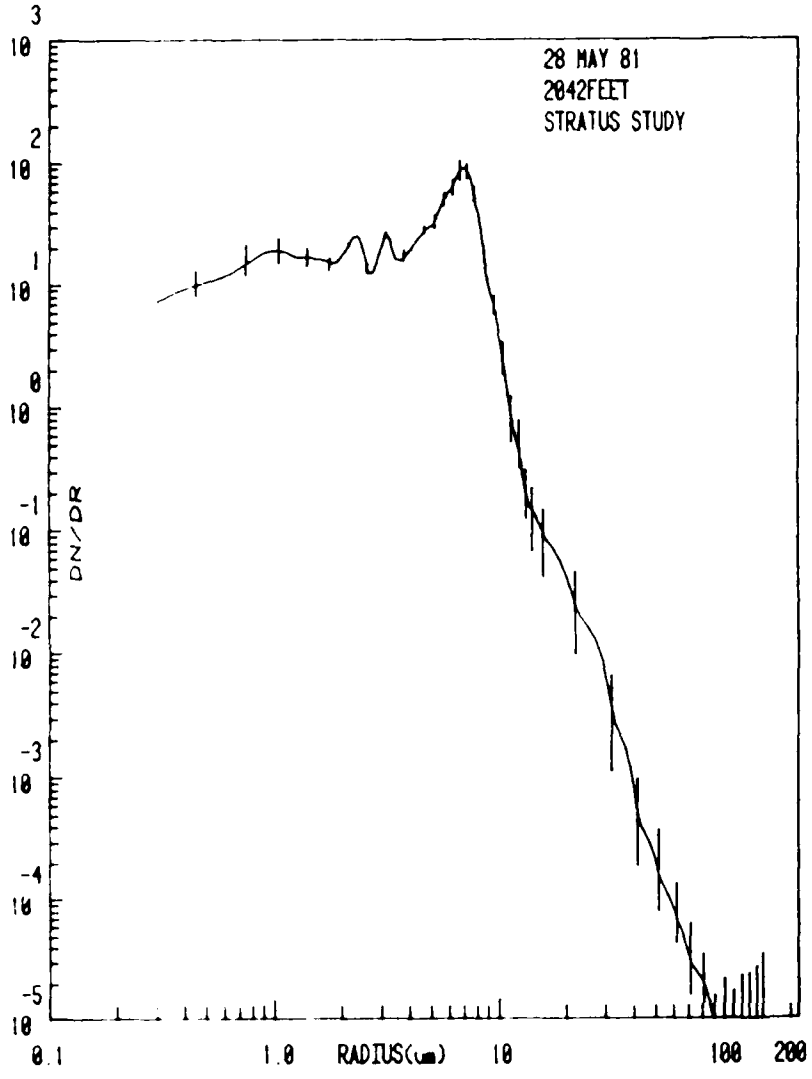

(b11)

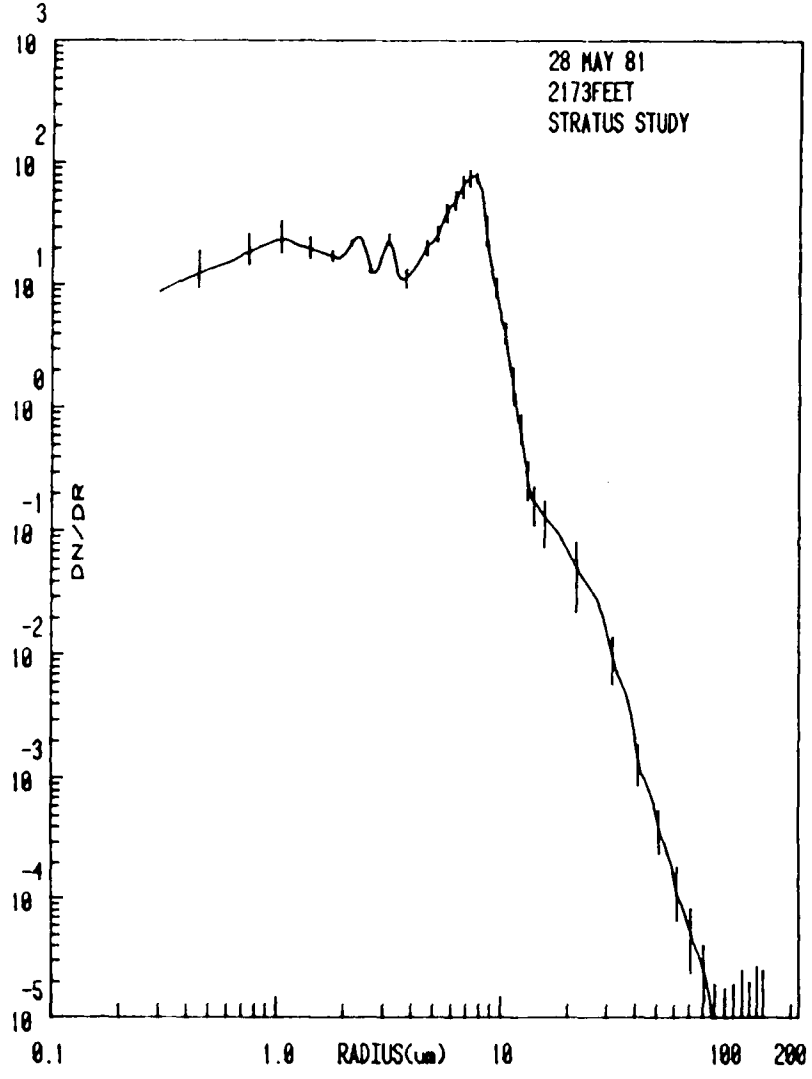

(b12)

Figure 3. Continued.

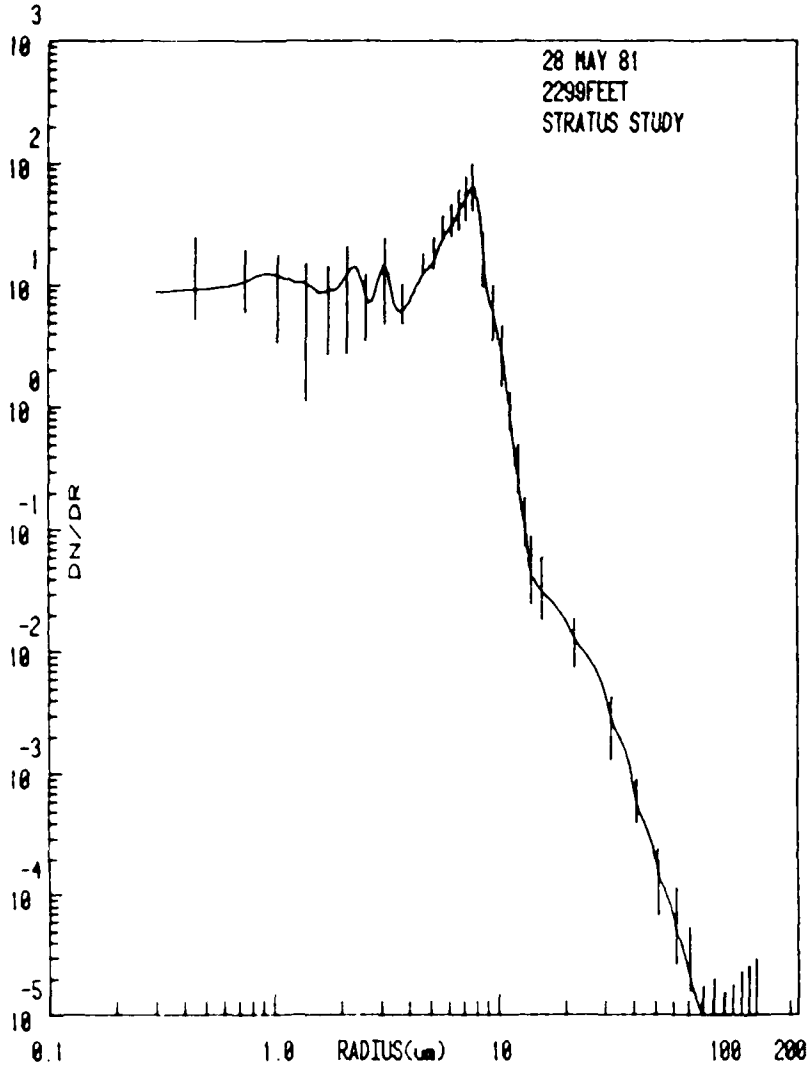

(b13)

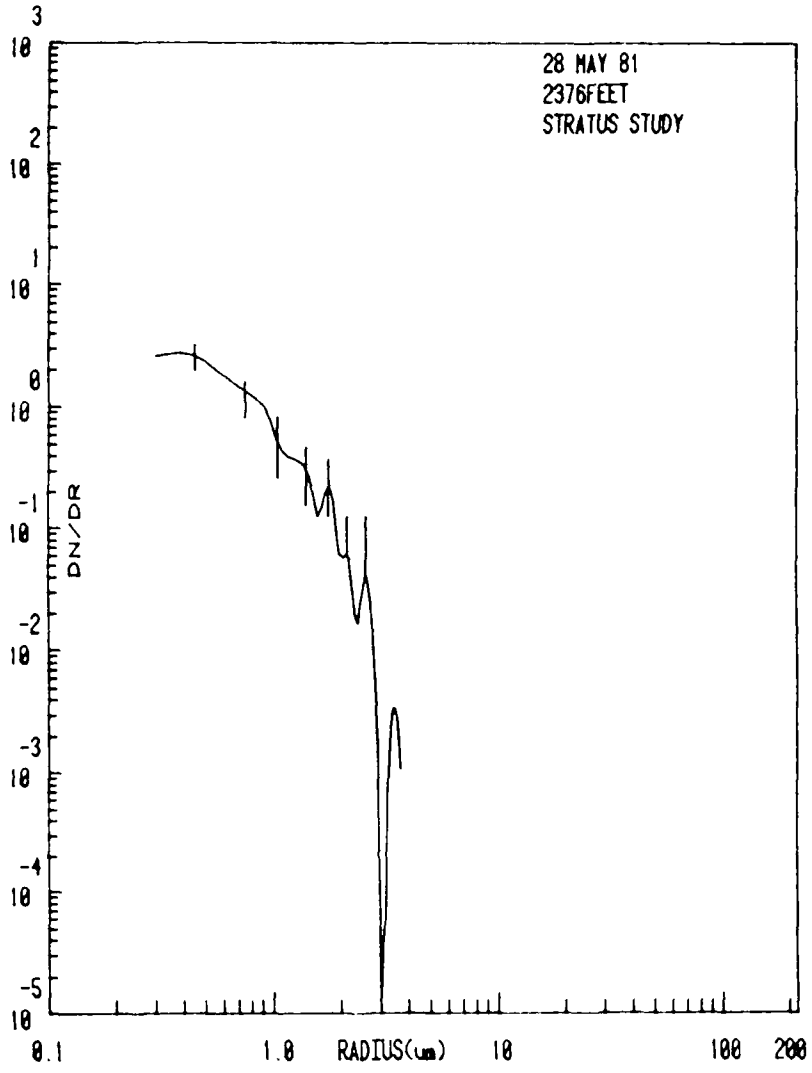

(b14)

Figure 3. Continued.

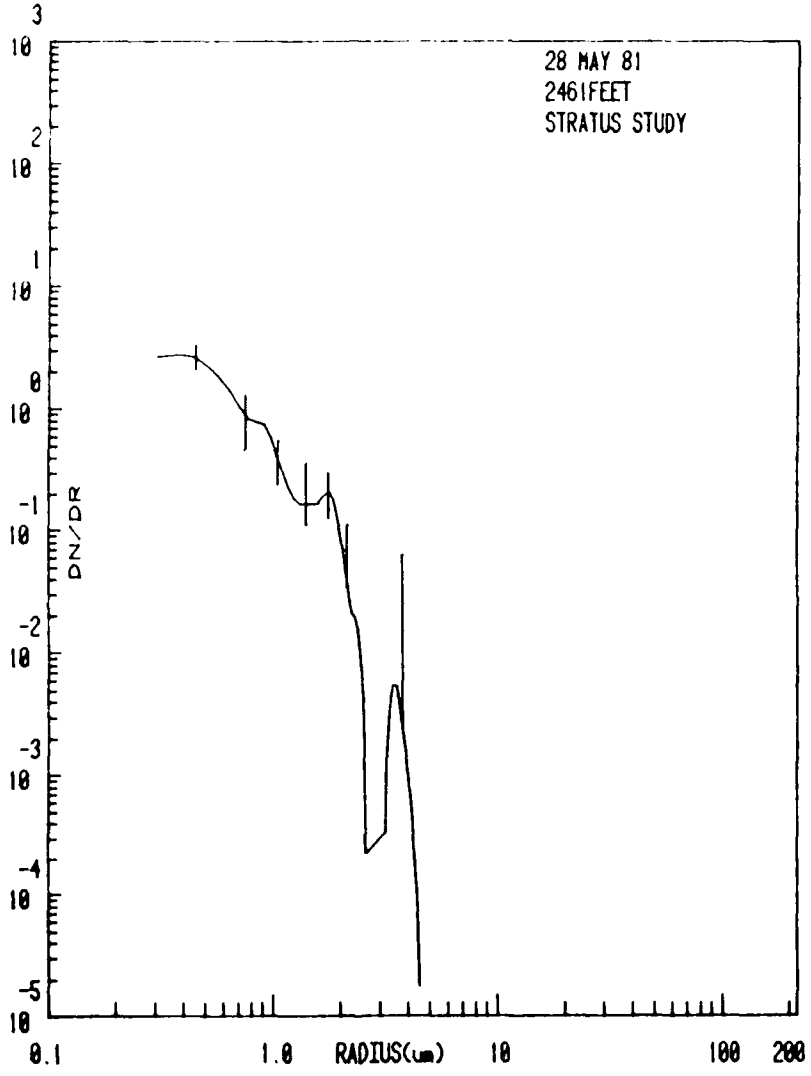

Figure 3b. Continued

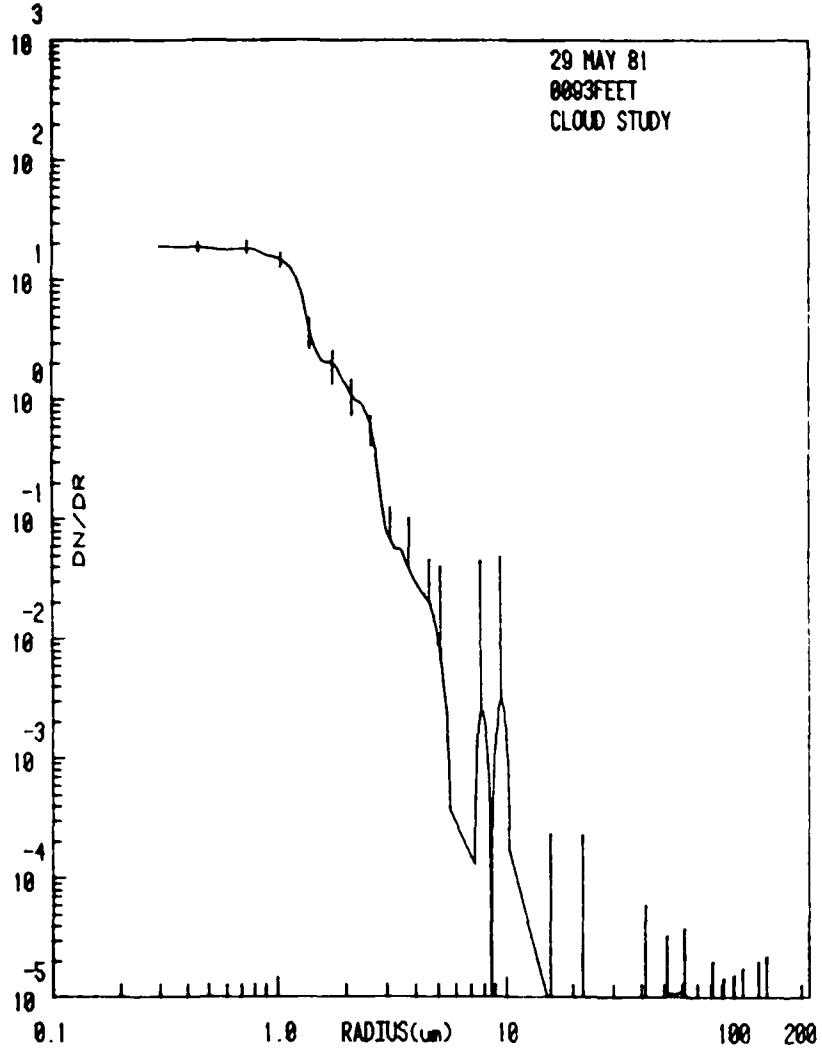

(c1)

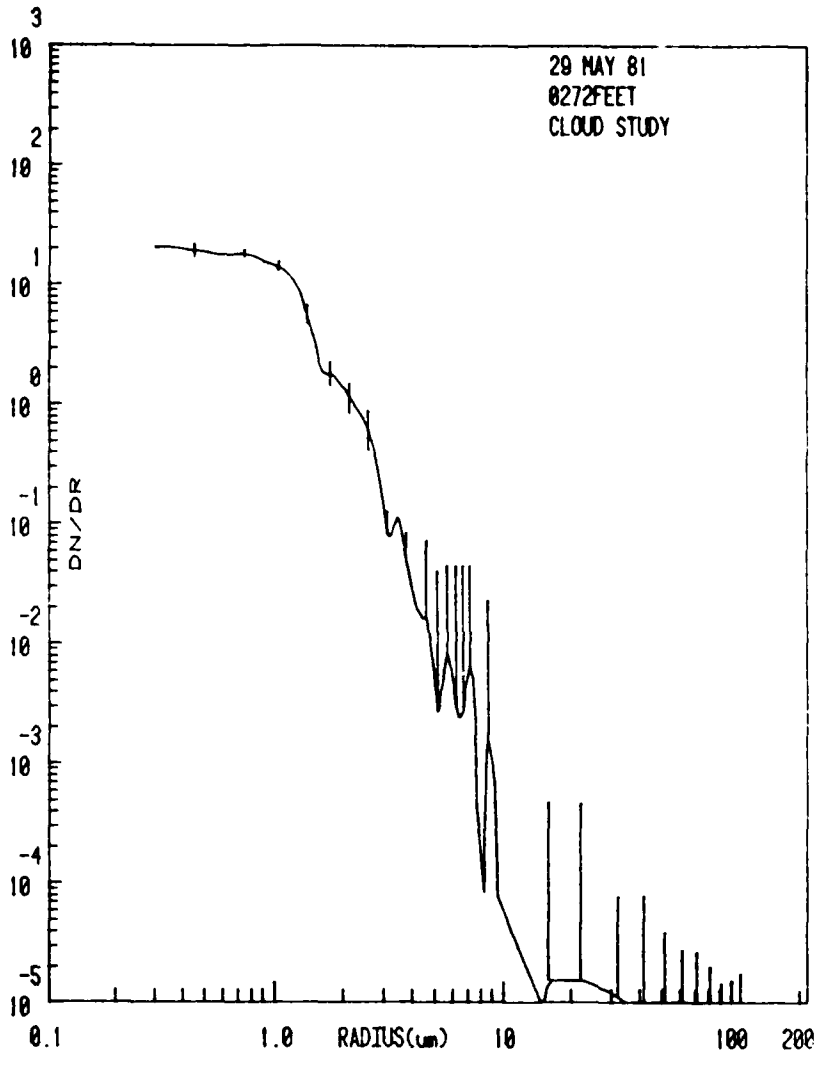

(c2)

Figure 3. Continued.

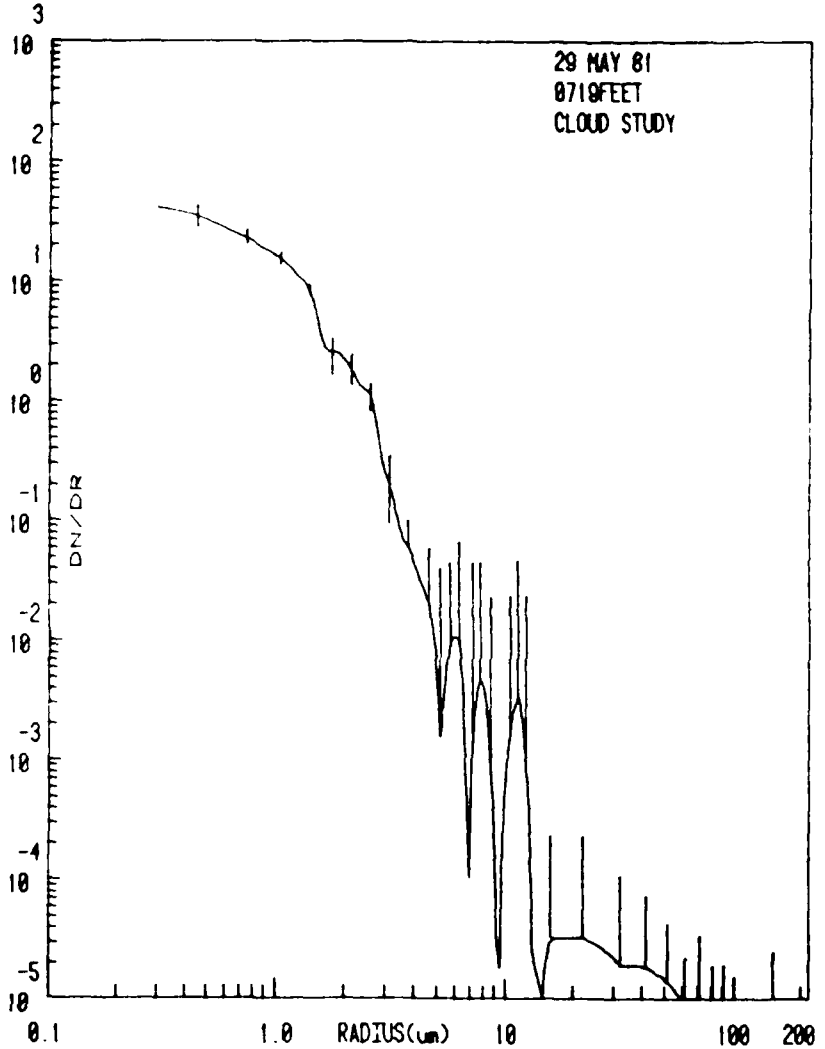

(c3)

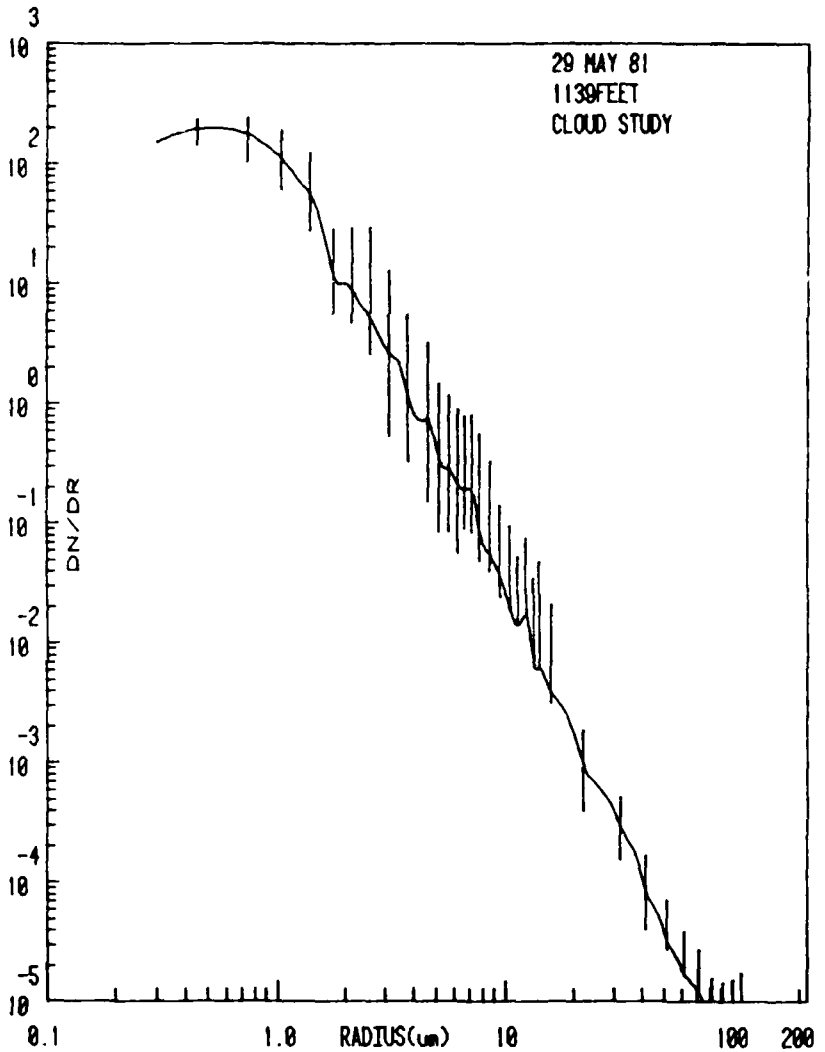

(c4)

Figure 3. Continued.

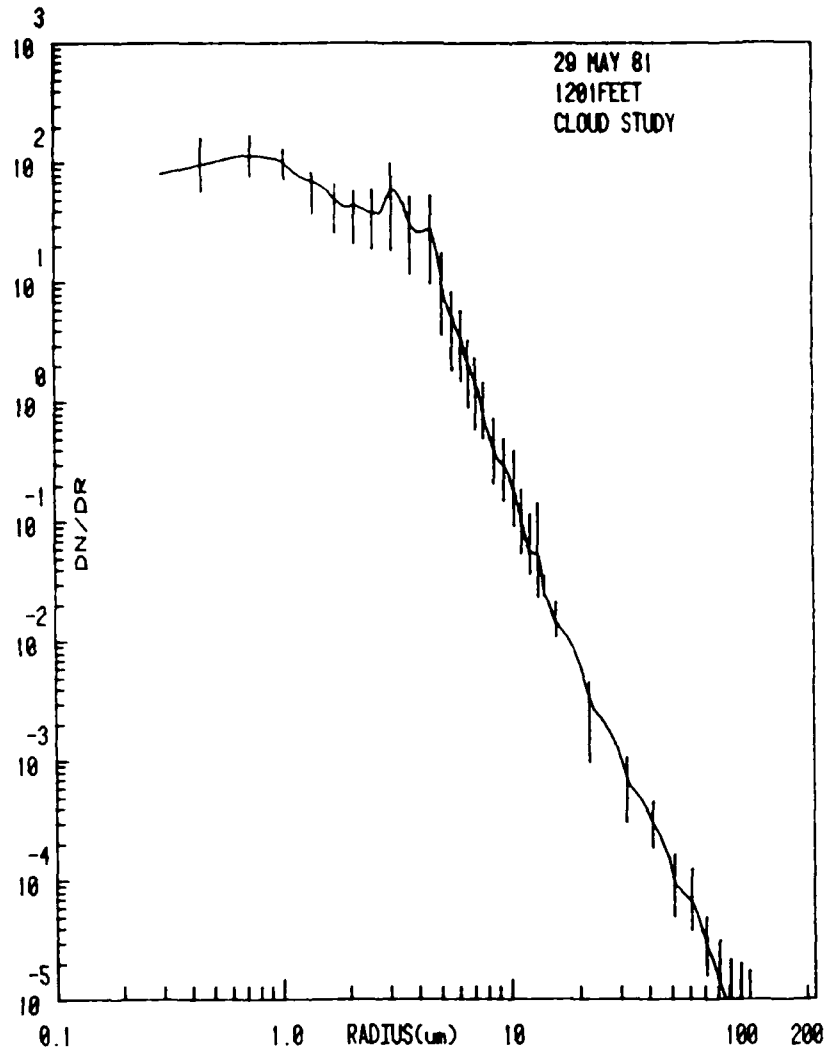

(c5)

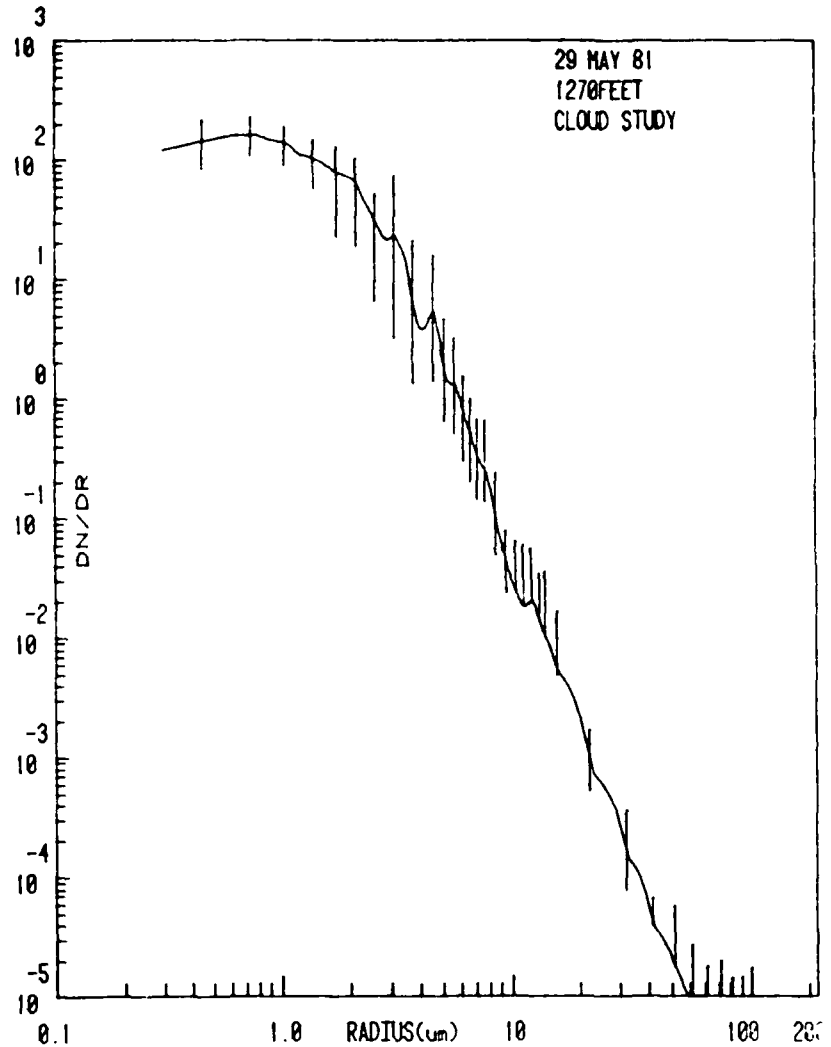

(c6)

Figure 3. Continued.

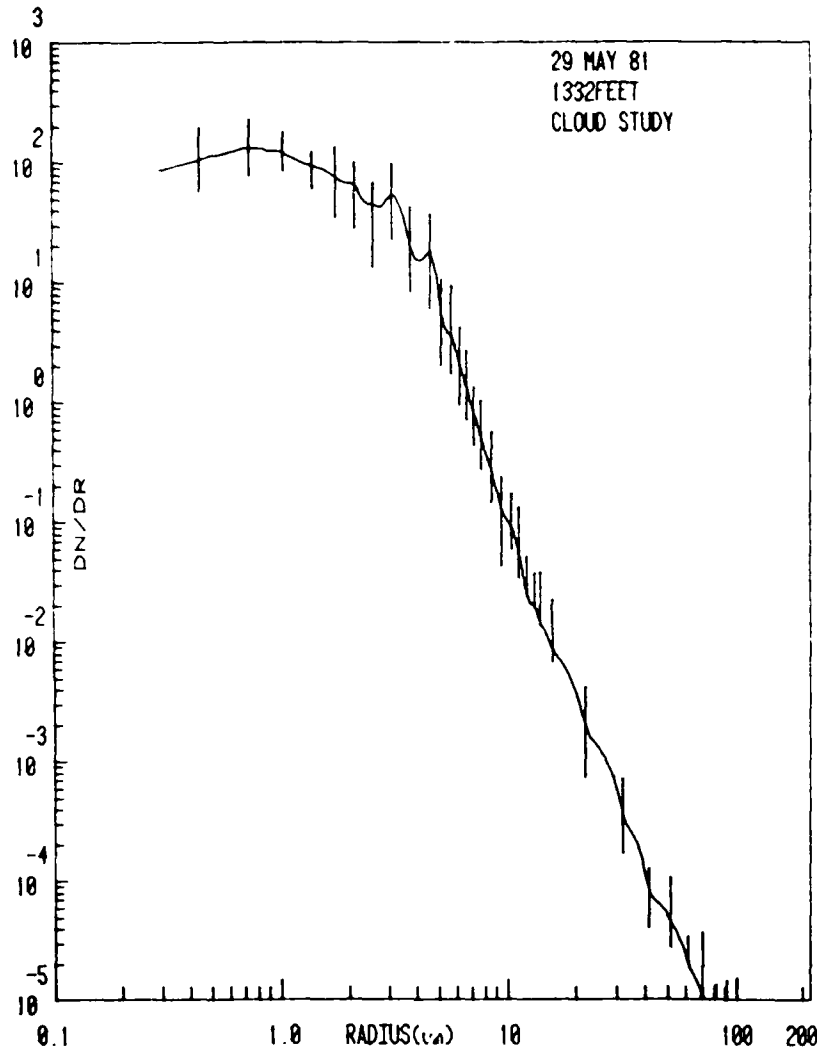

(c7)

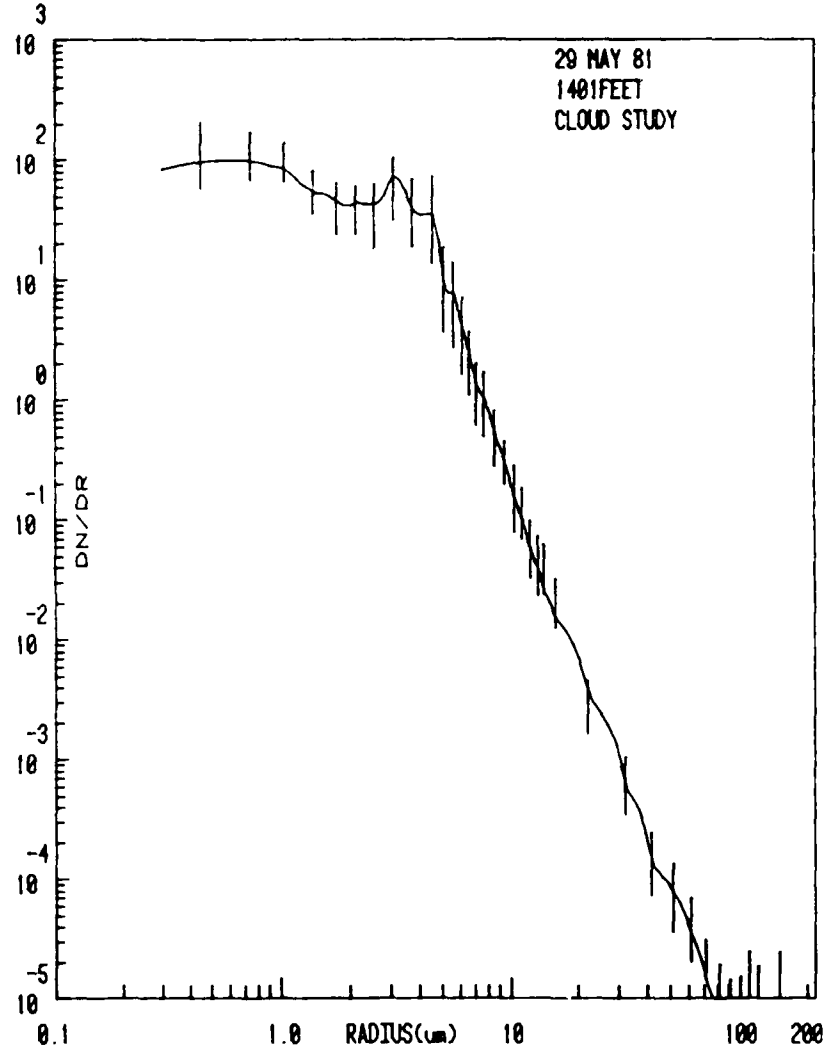

(c8)

Figure 3. Continued.

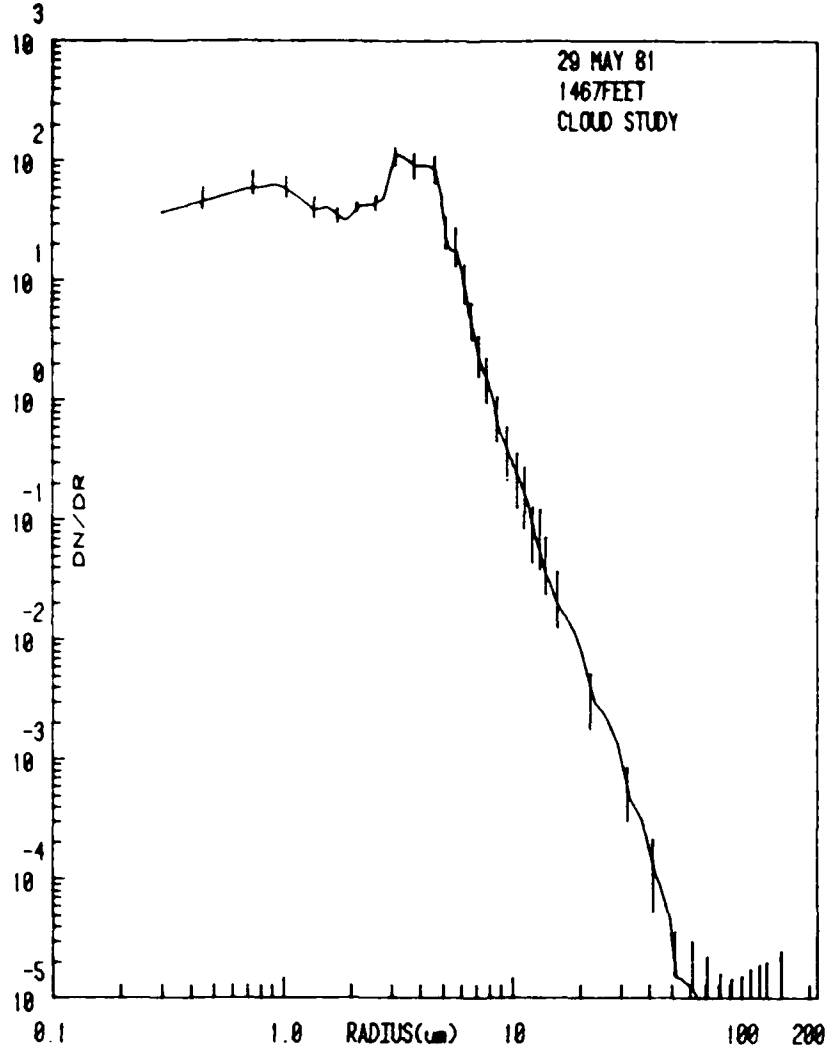

(c9)

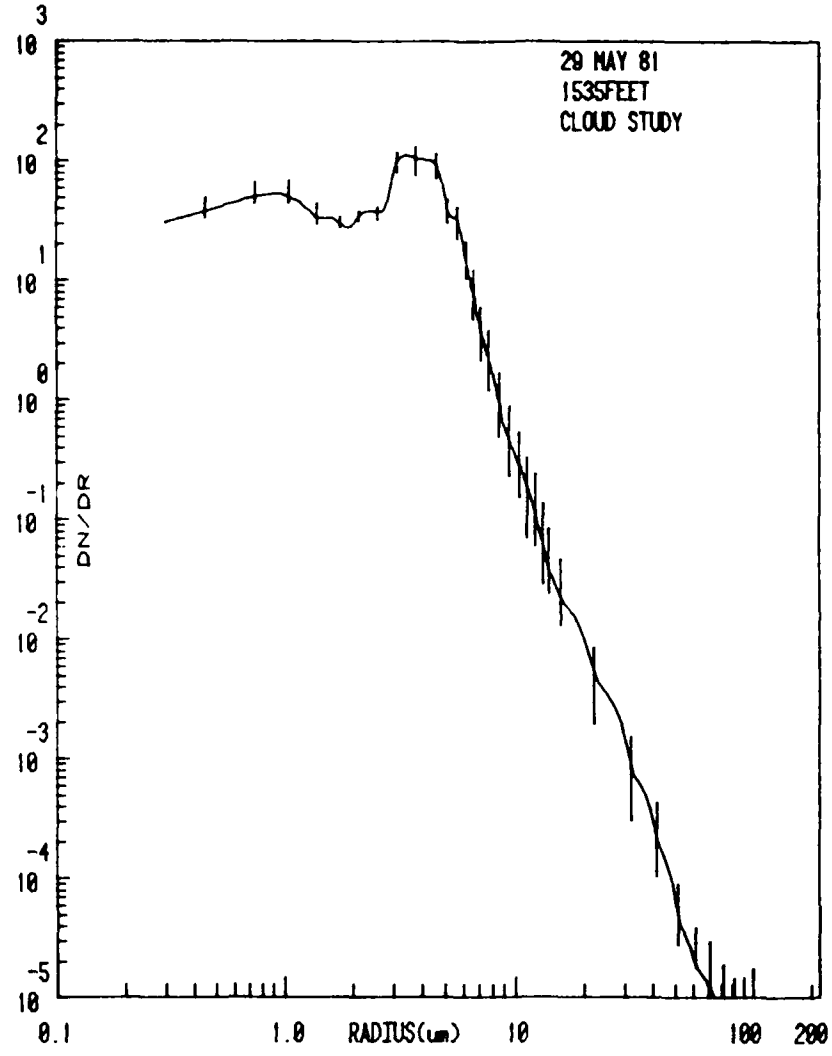

(c10)

Figure 3. Continued.

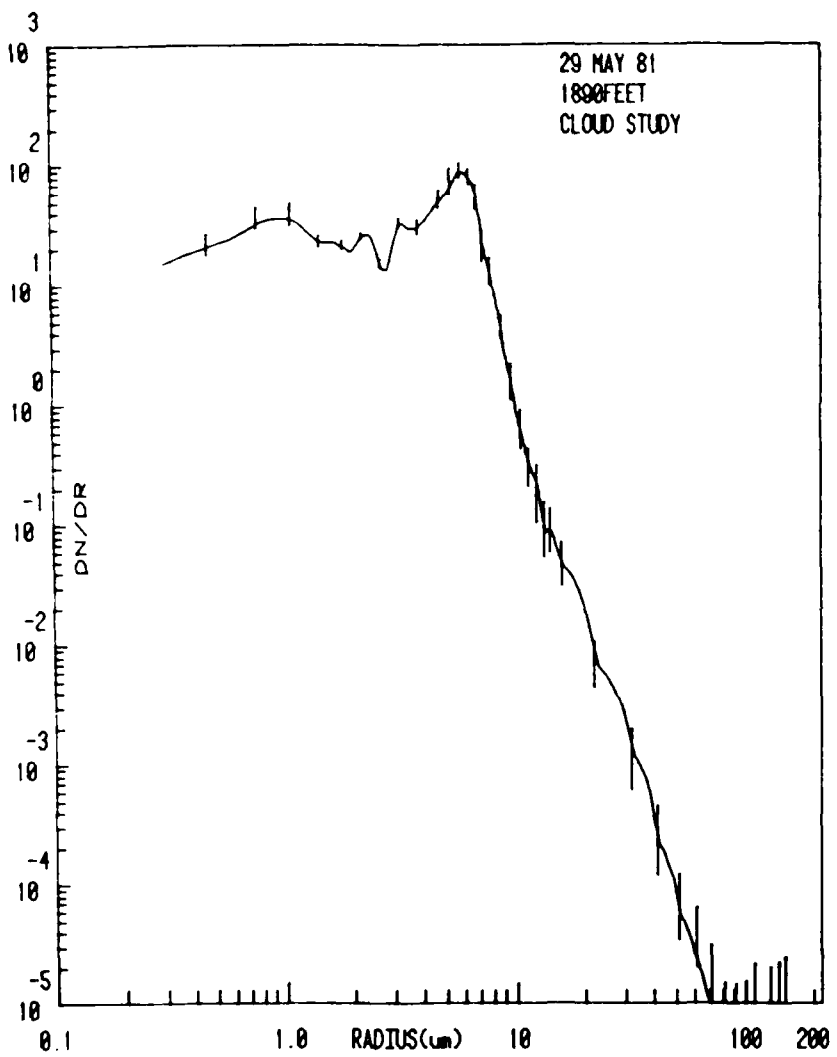

(c11)

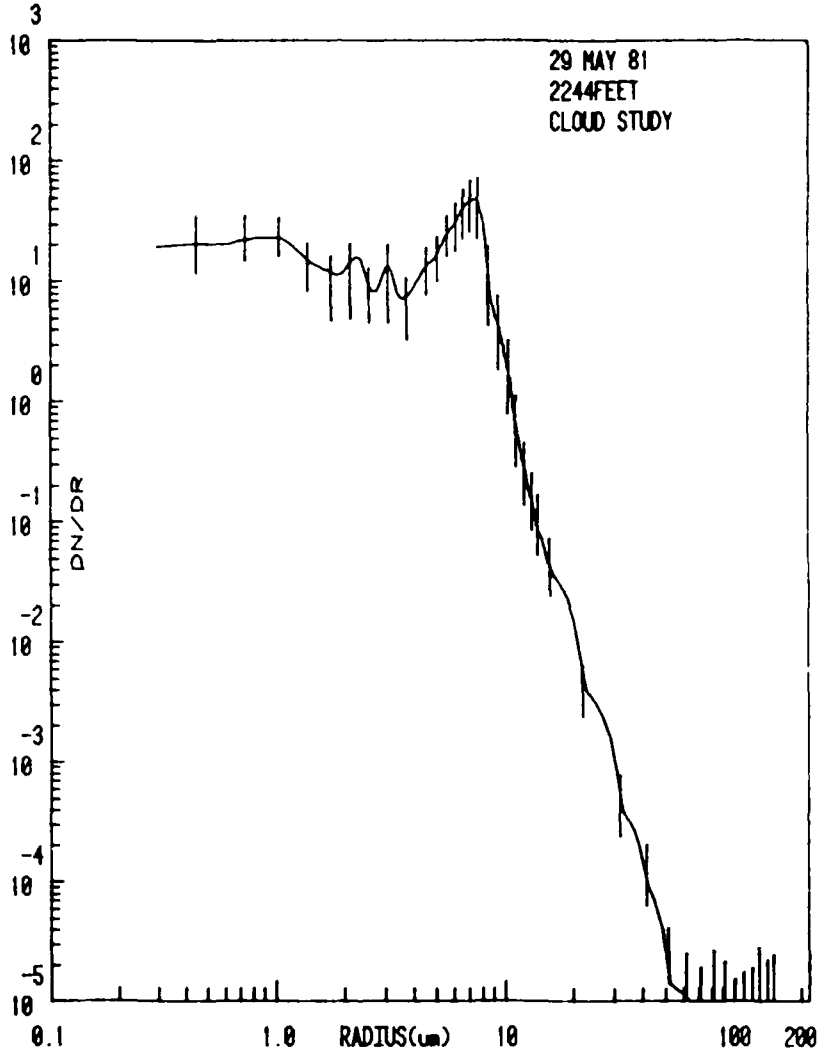

(c12)

Figure 3. Continued.

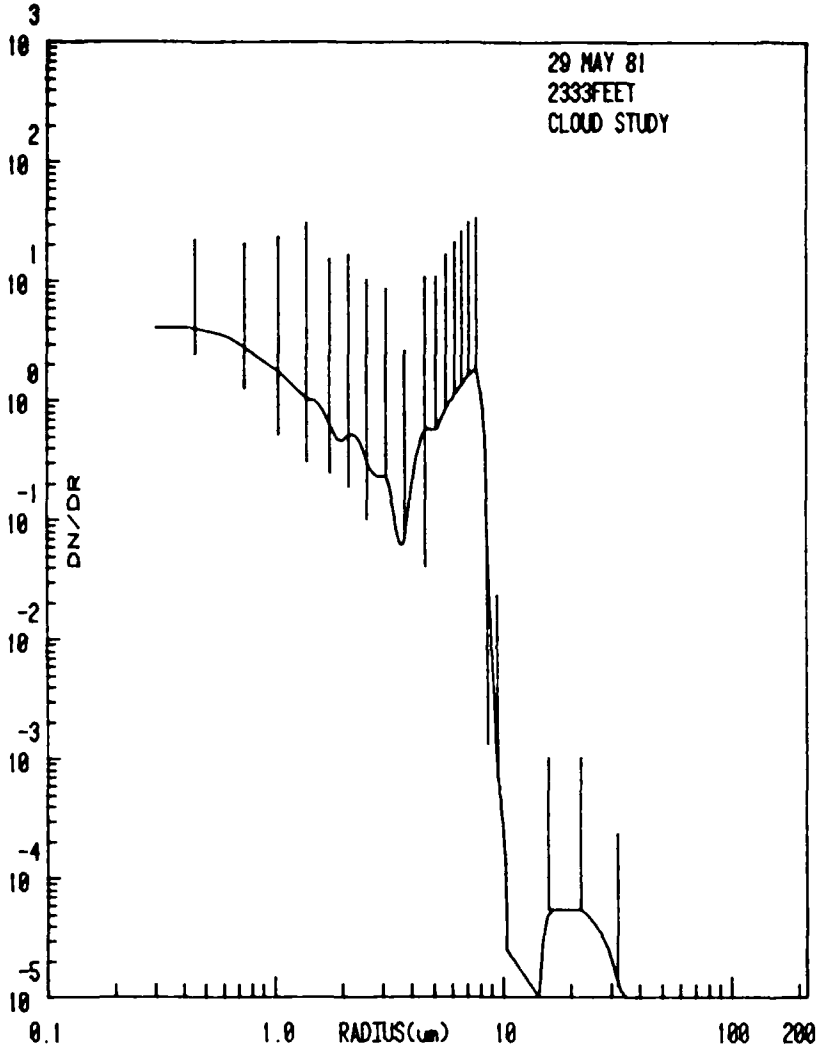

(c13)

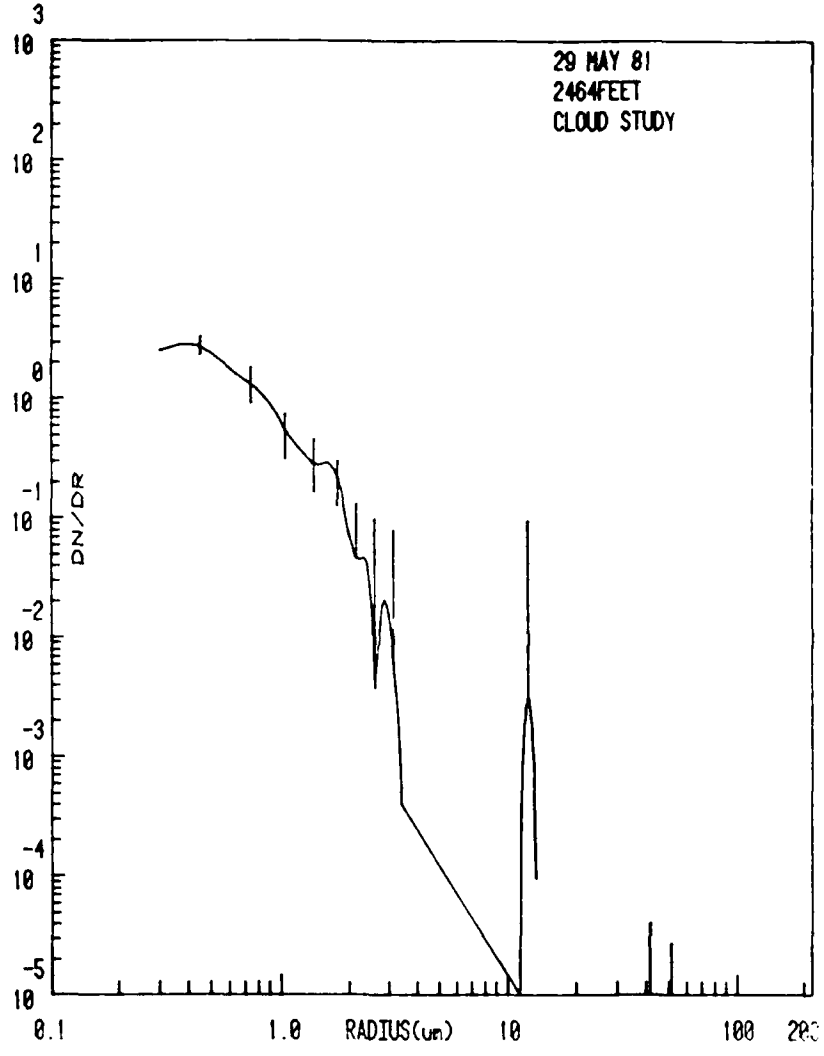

(c14)

Figure 3. Continued.

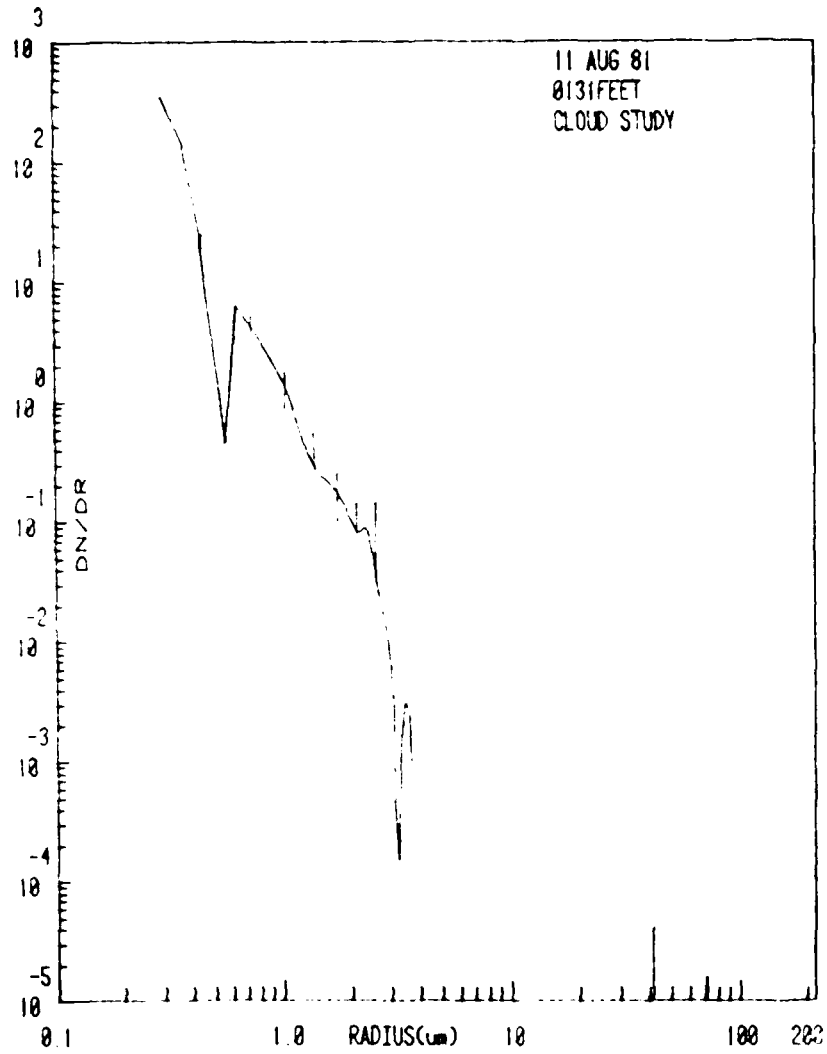

(d1)

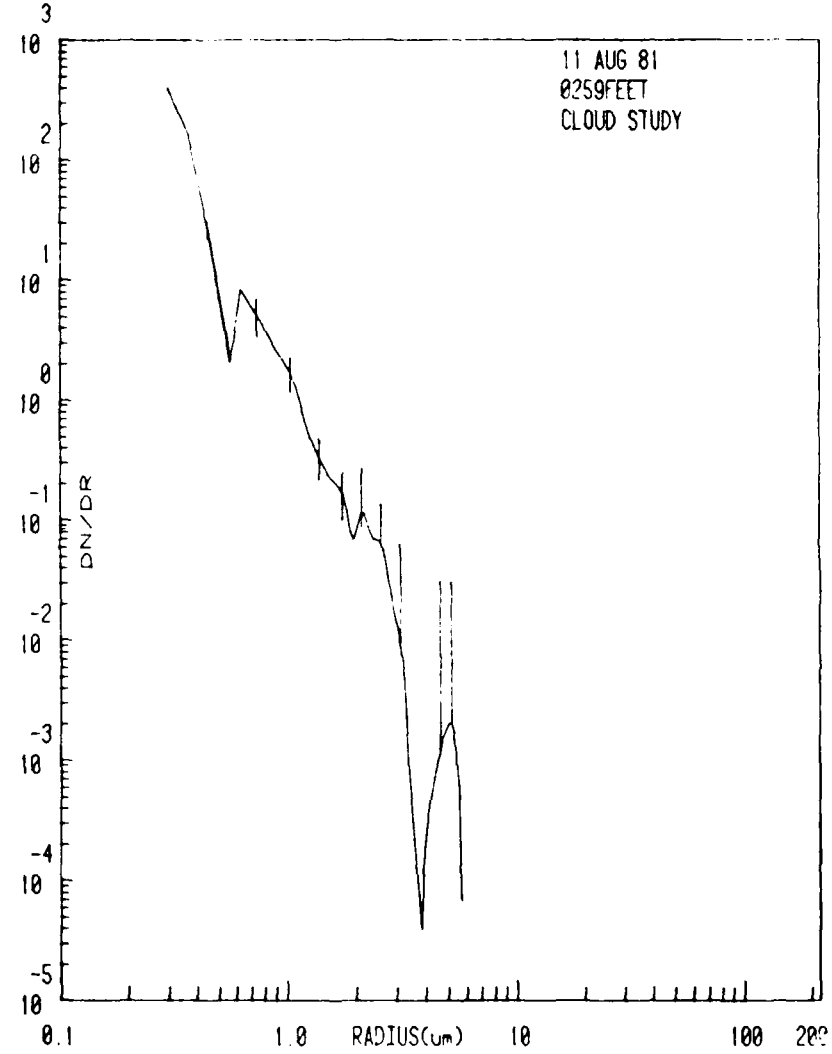

(d2)

Figure 3. Continued.

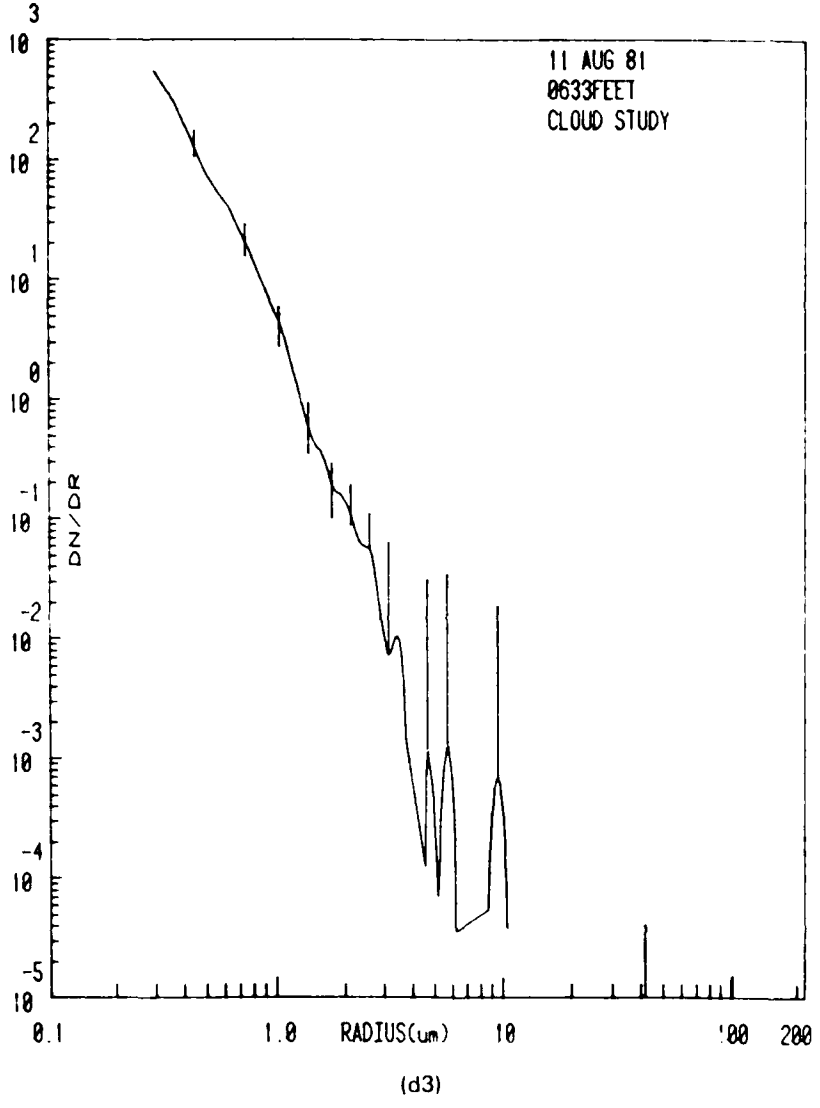

(d3)

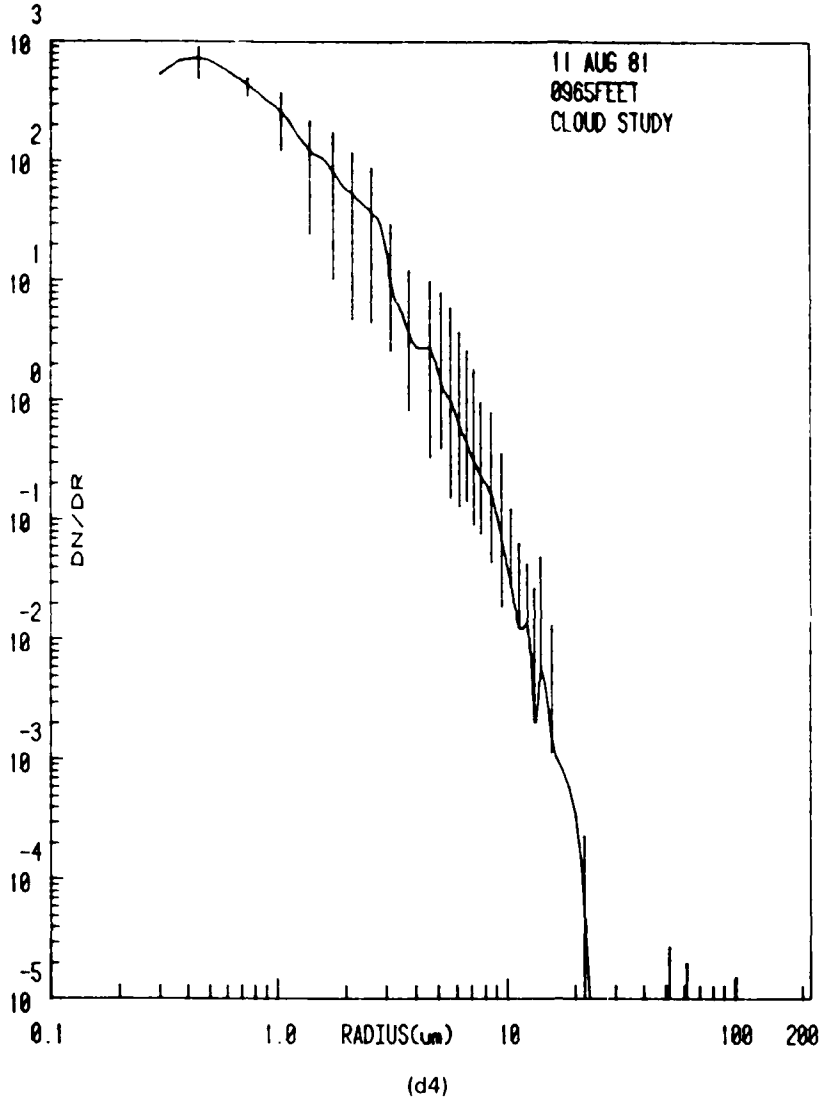

(d4)

Figure 3. Continued.

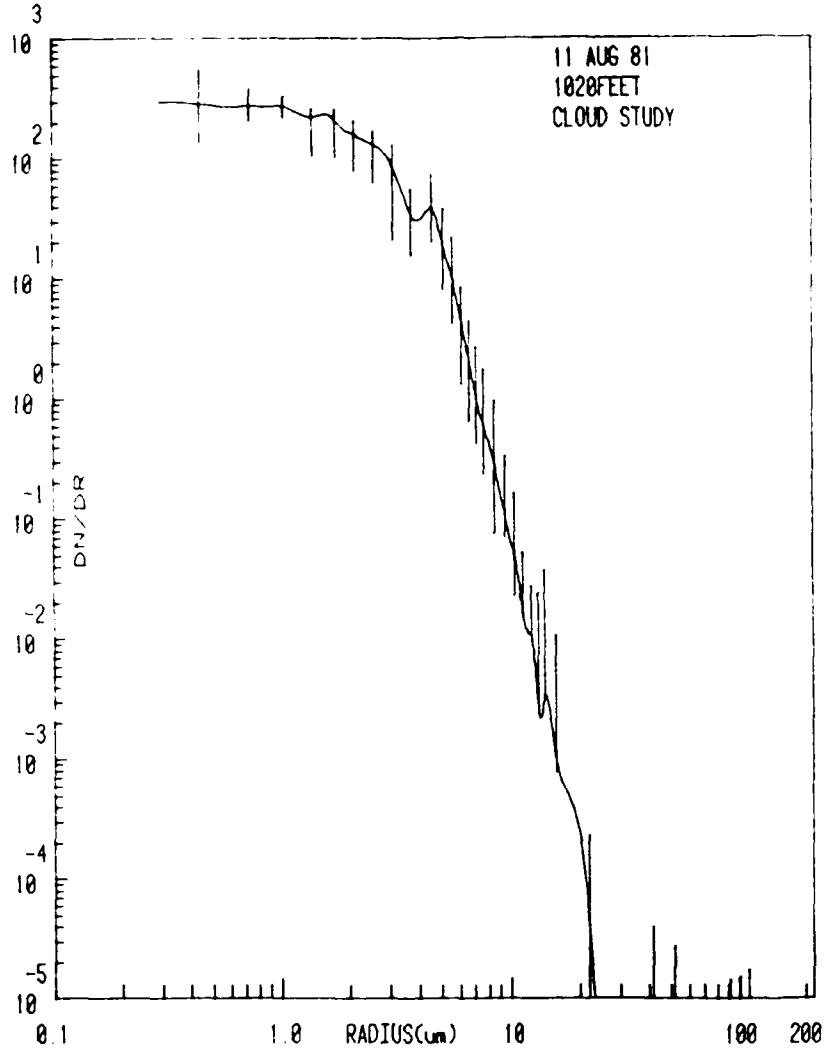

(d5)

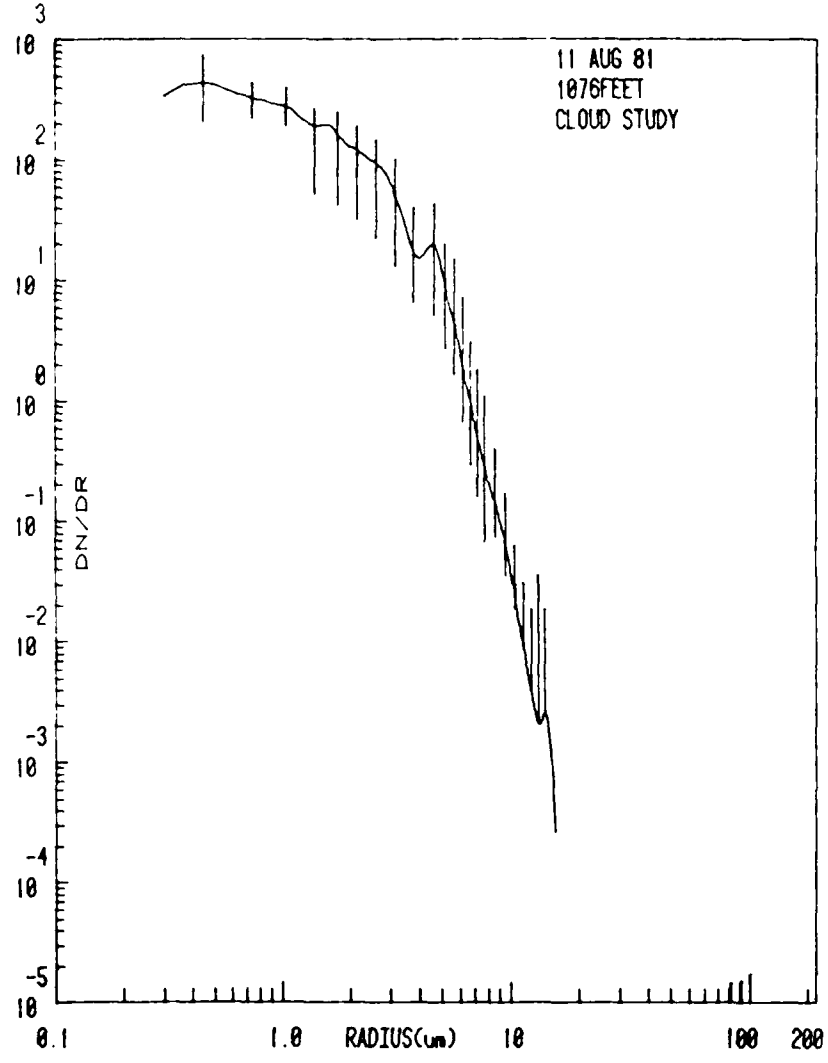

(d6)

Figure 3. Continued.

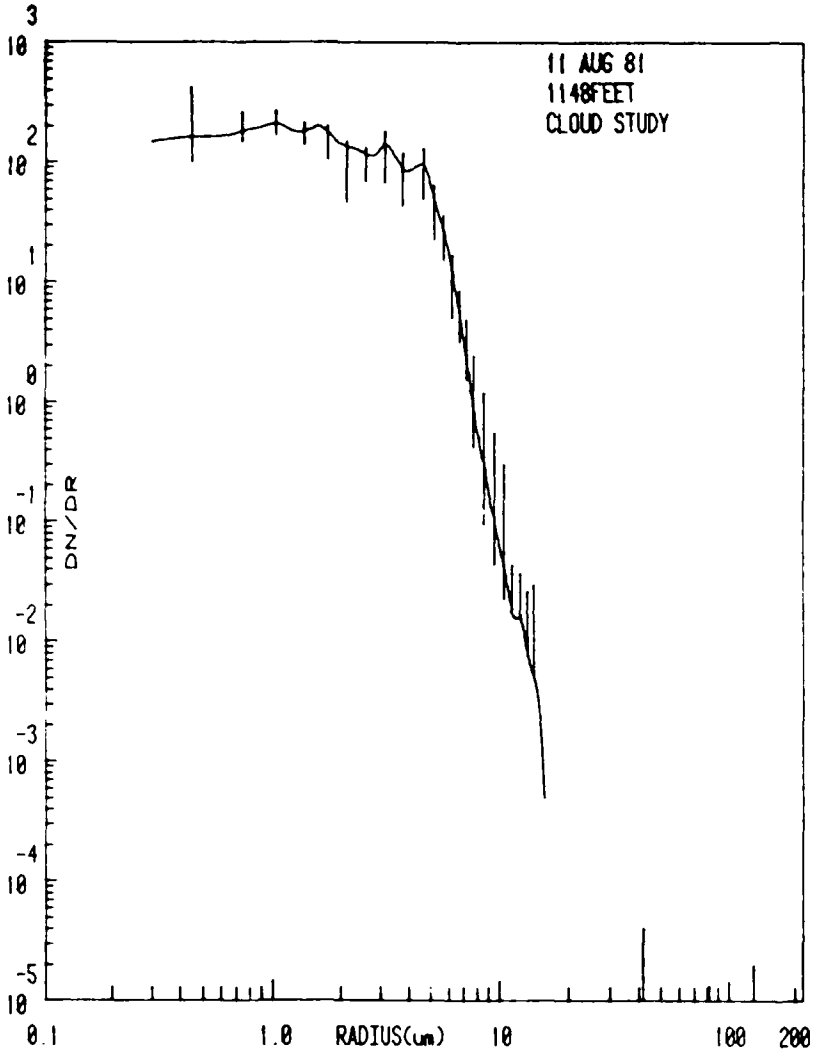

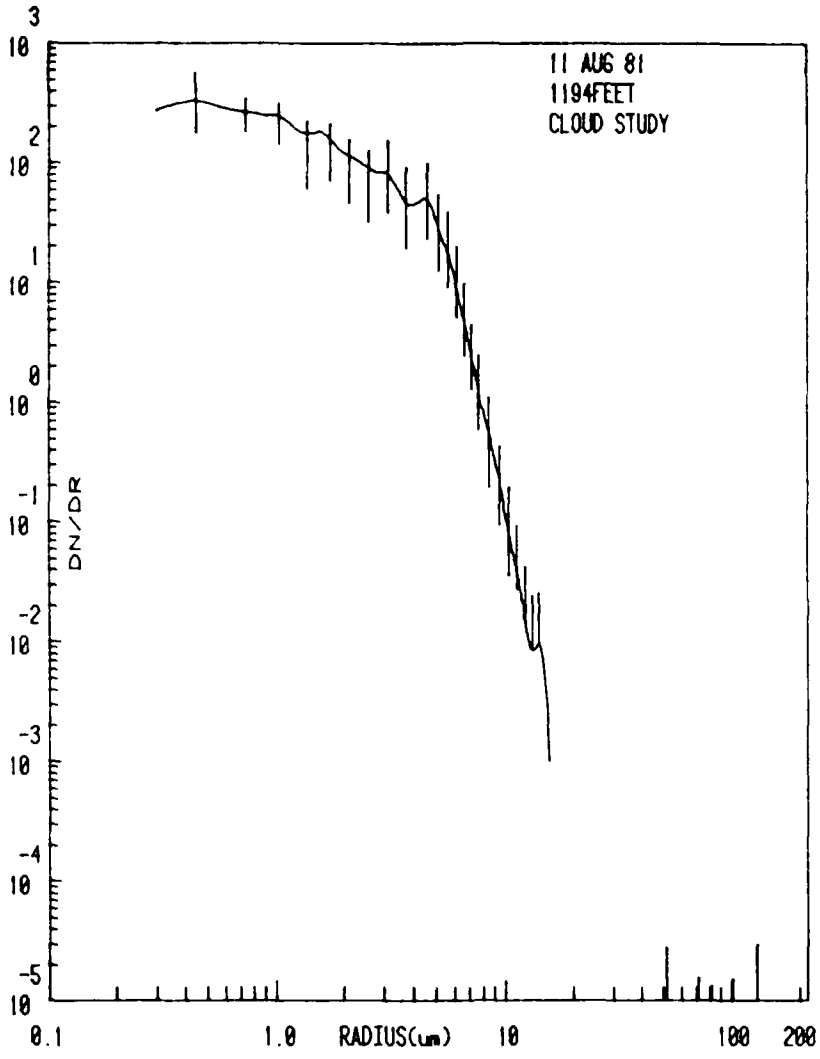

Figure 3. Continued.

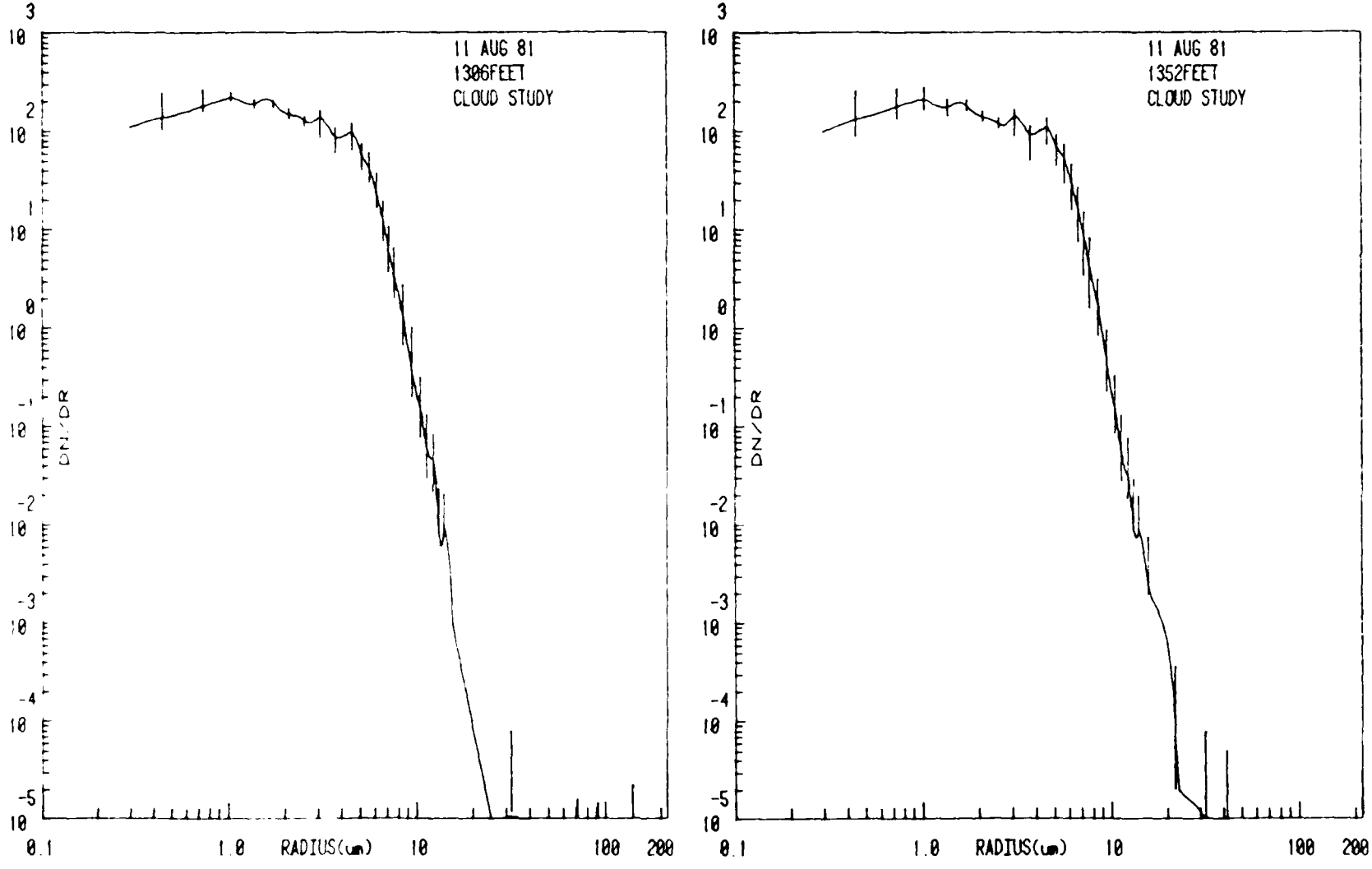

Figure 3 Continued.

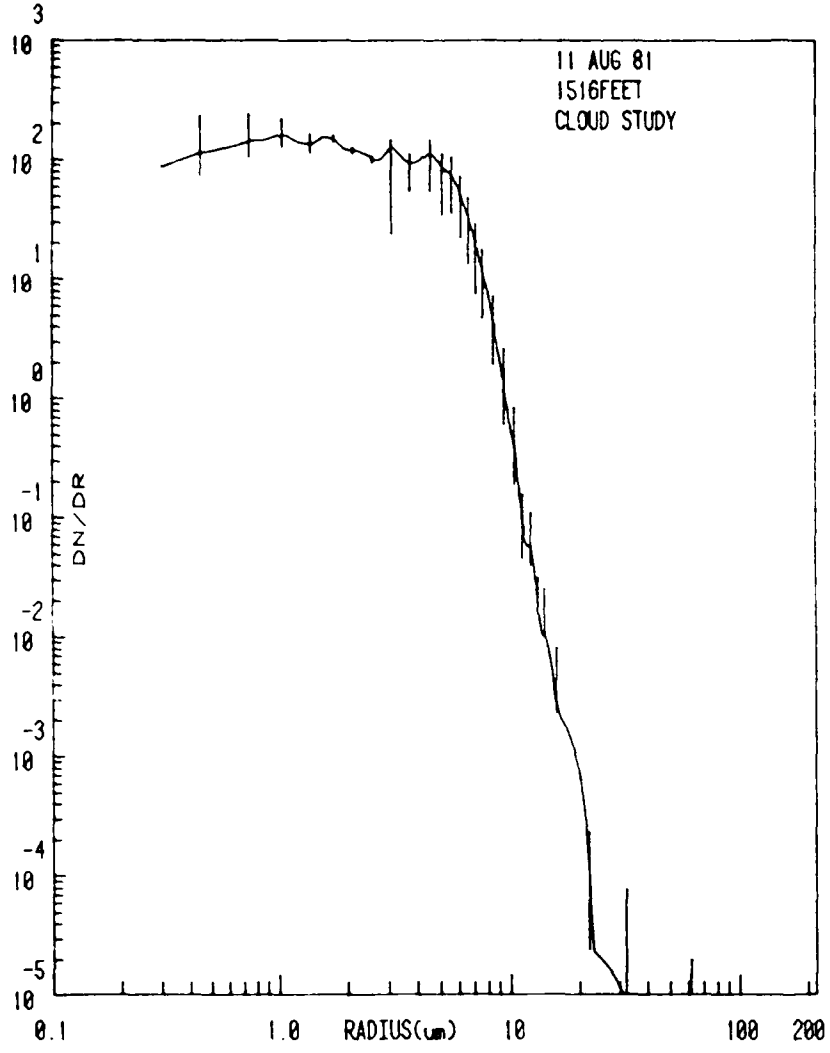

(d11)

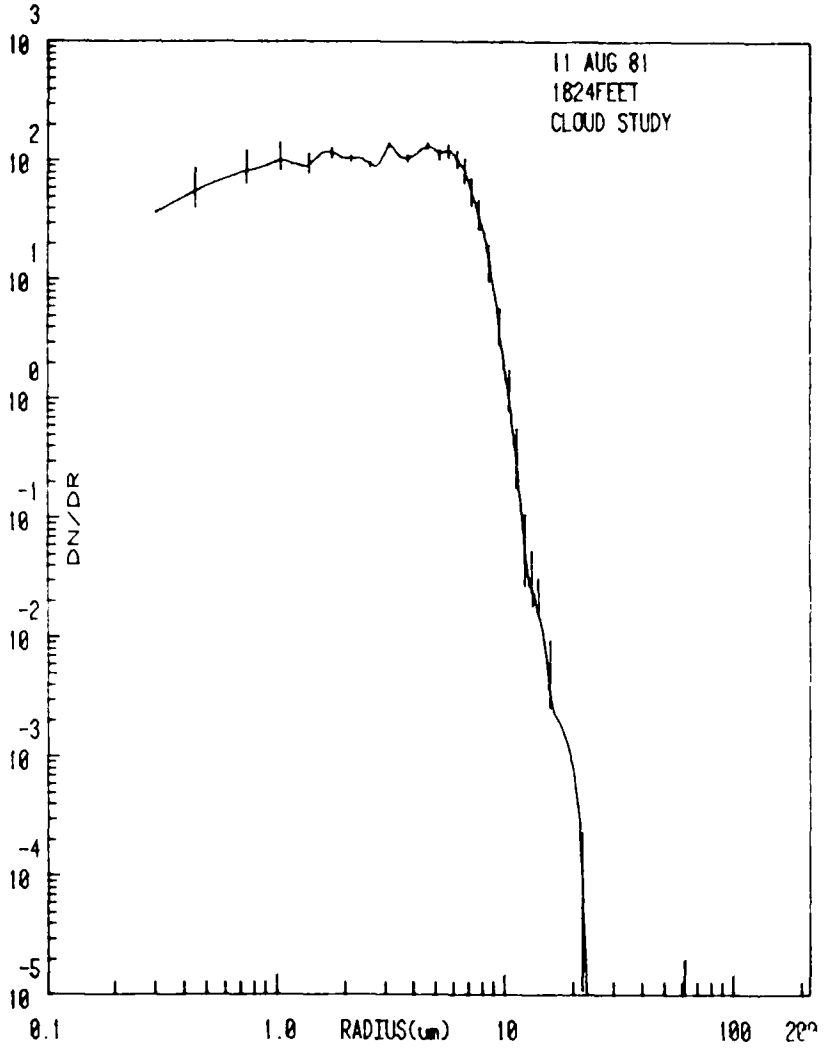

(d12)

Figure 3. Continued.

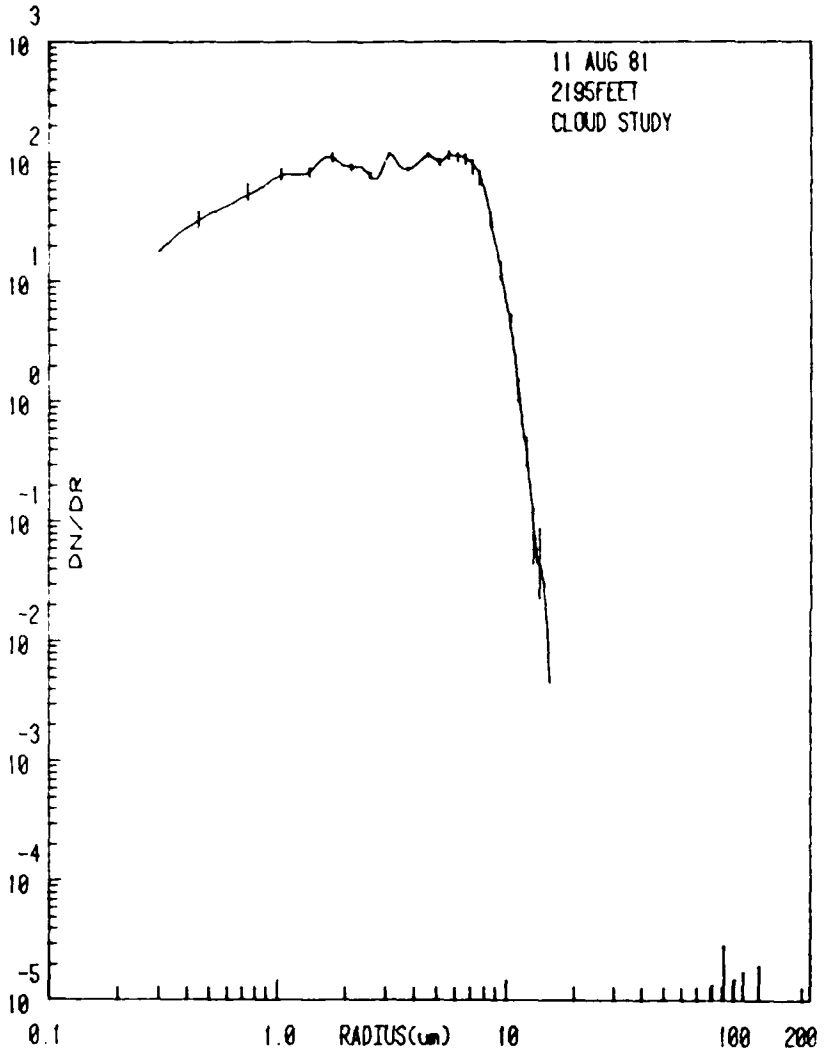

(d13)

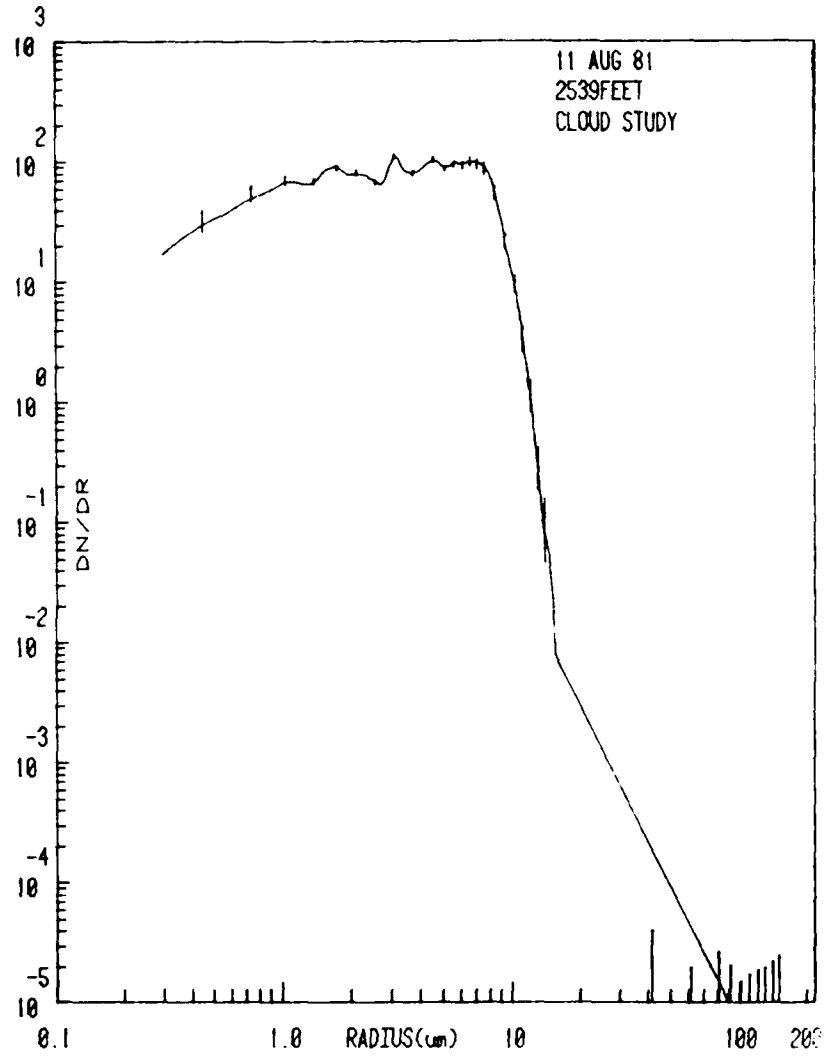

(d14)

Figure 3. Continued.

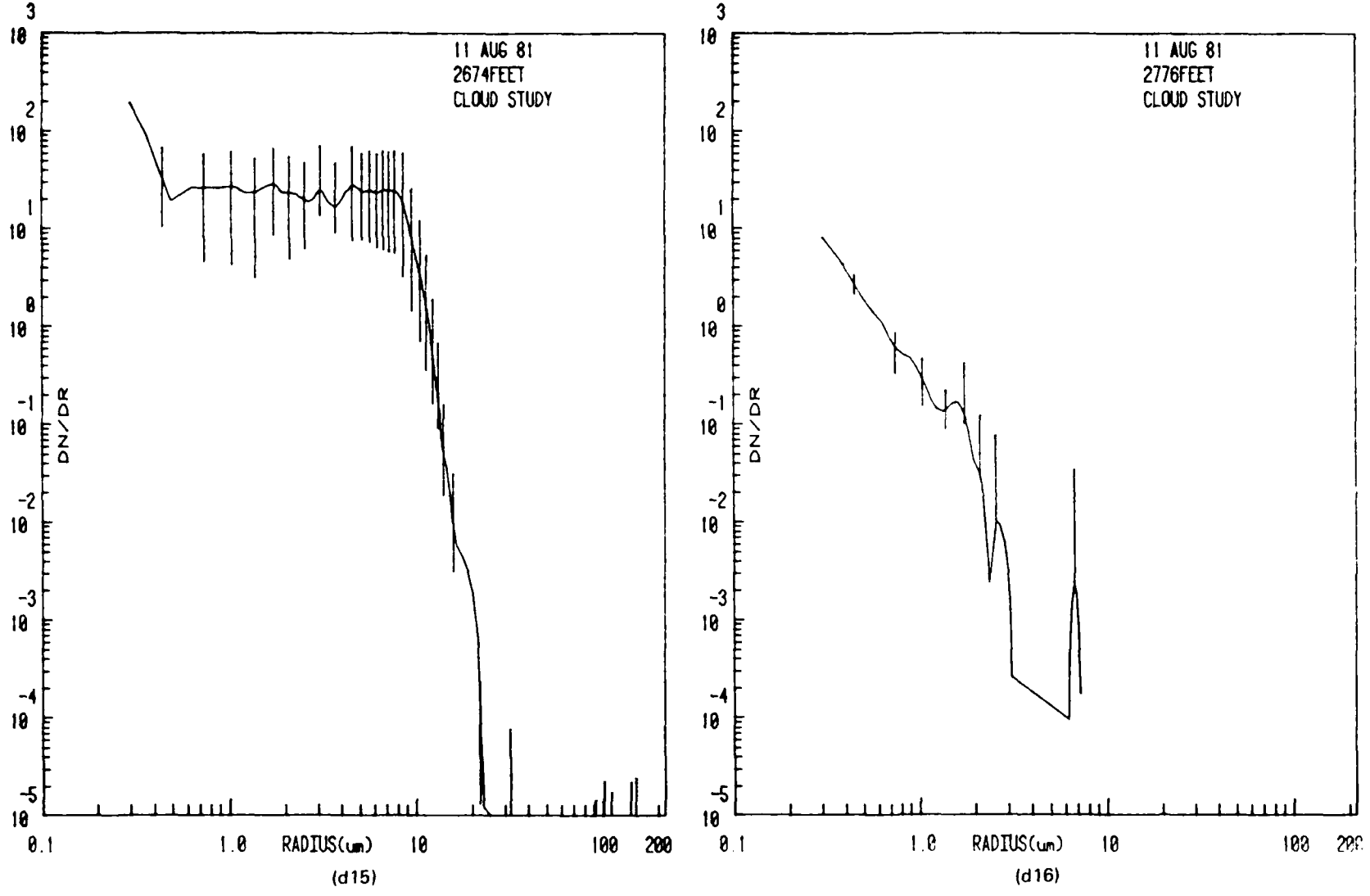

Figure 3. Continued.

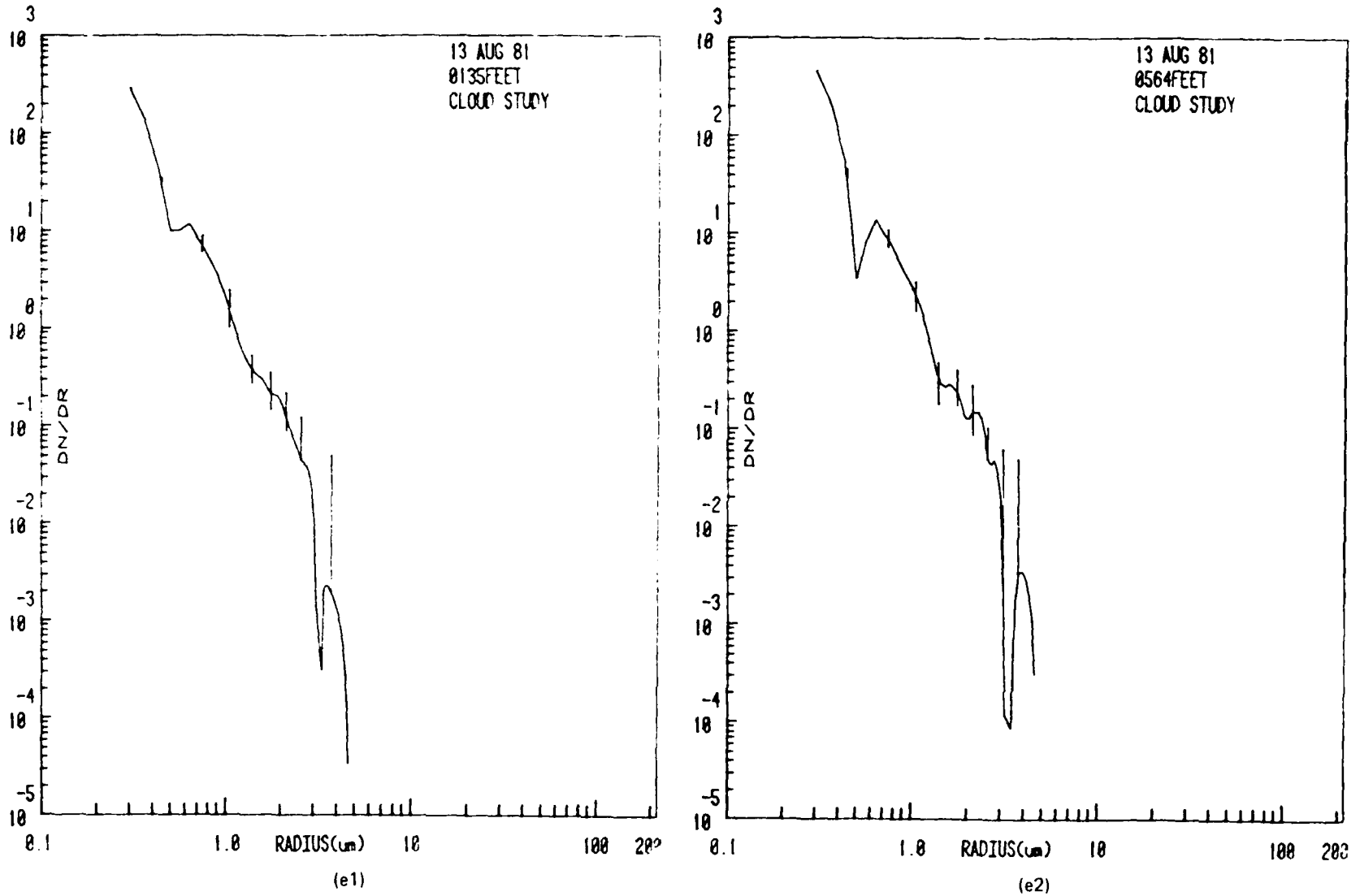

Figure 3. Continued.

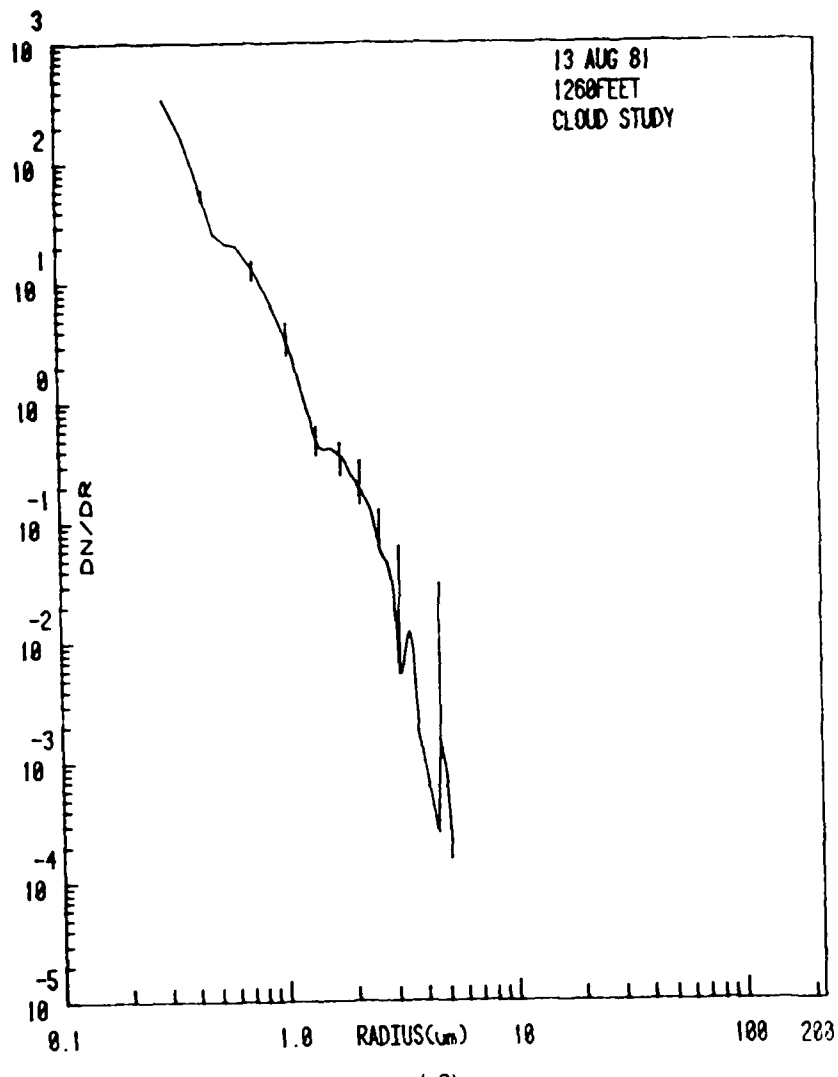

(e3)

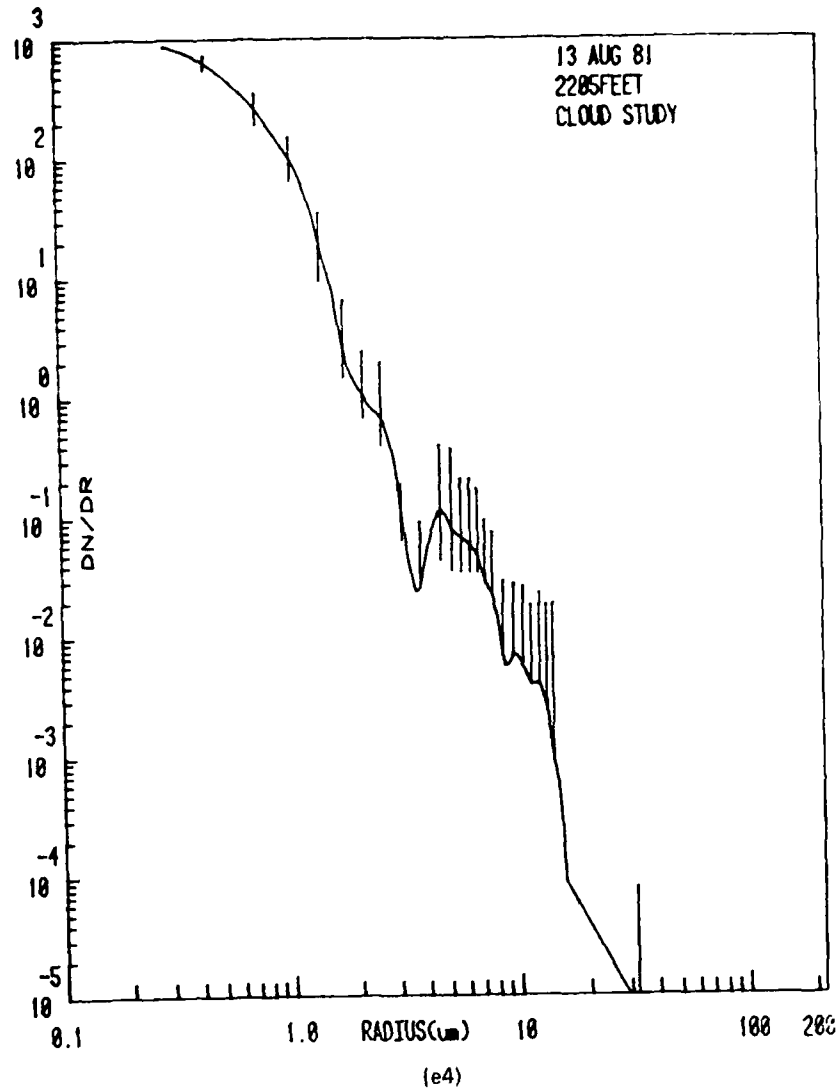

(e4)

Figure 3. Continued.

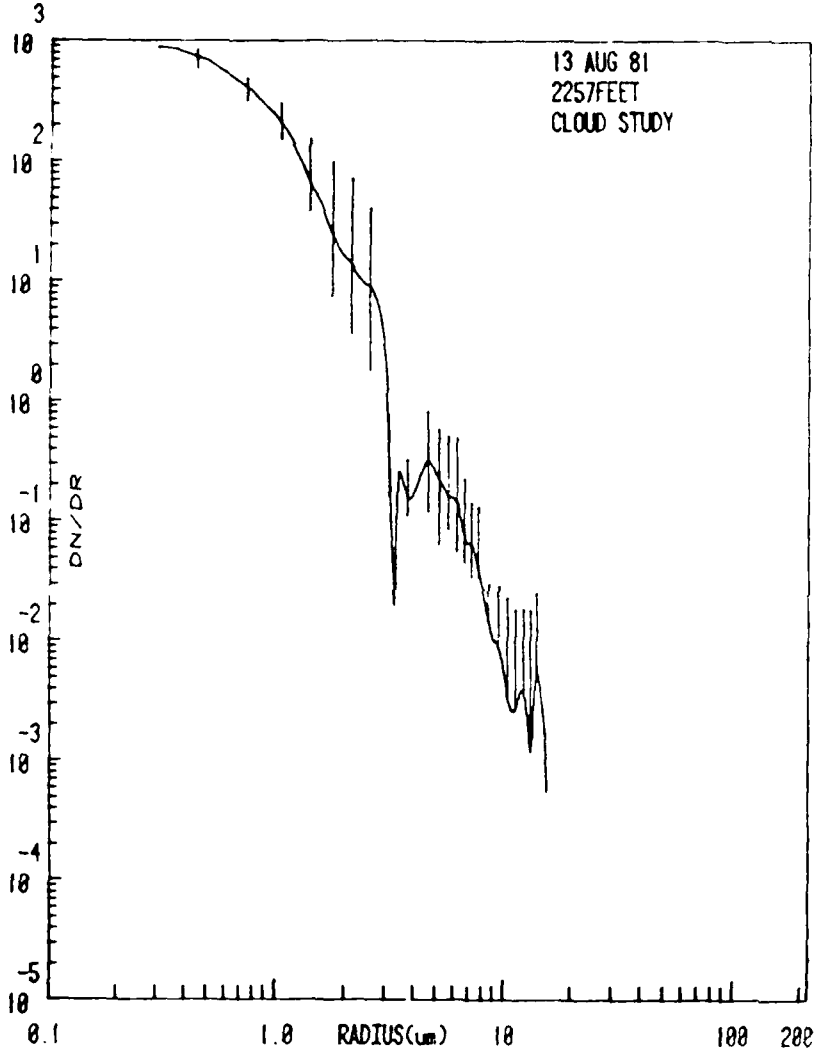

(e5)

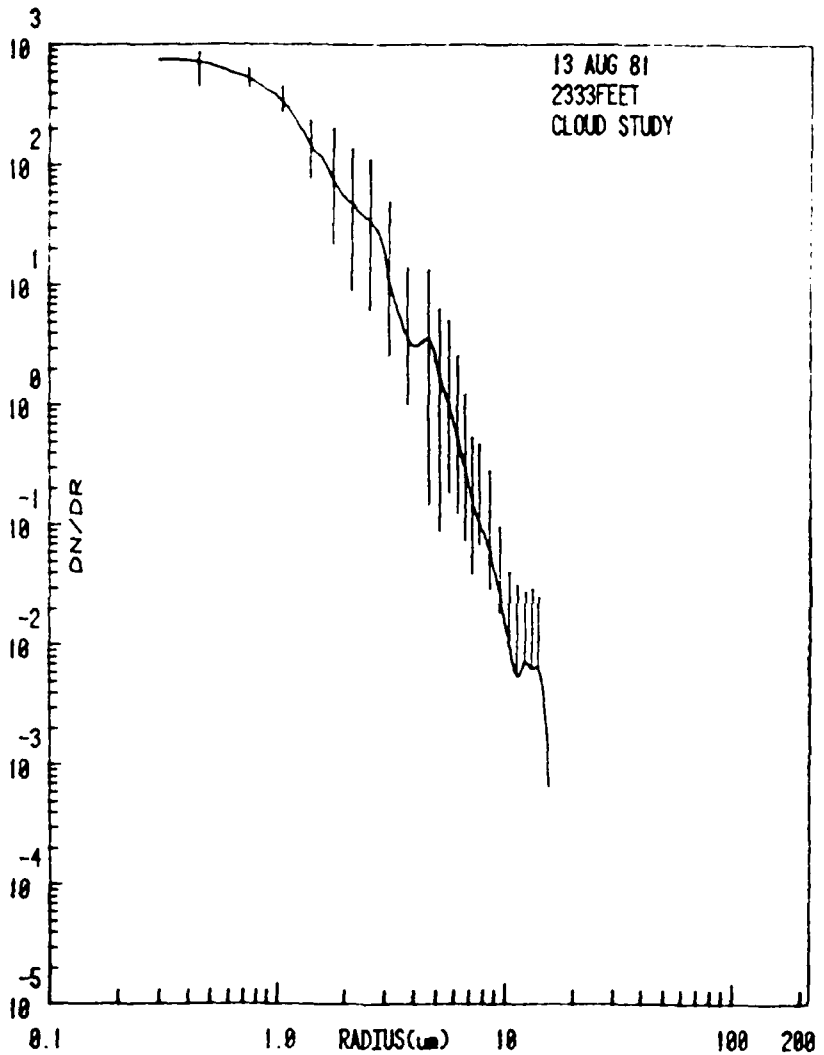

(e6)

Figure 3. Continued.

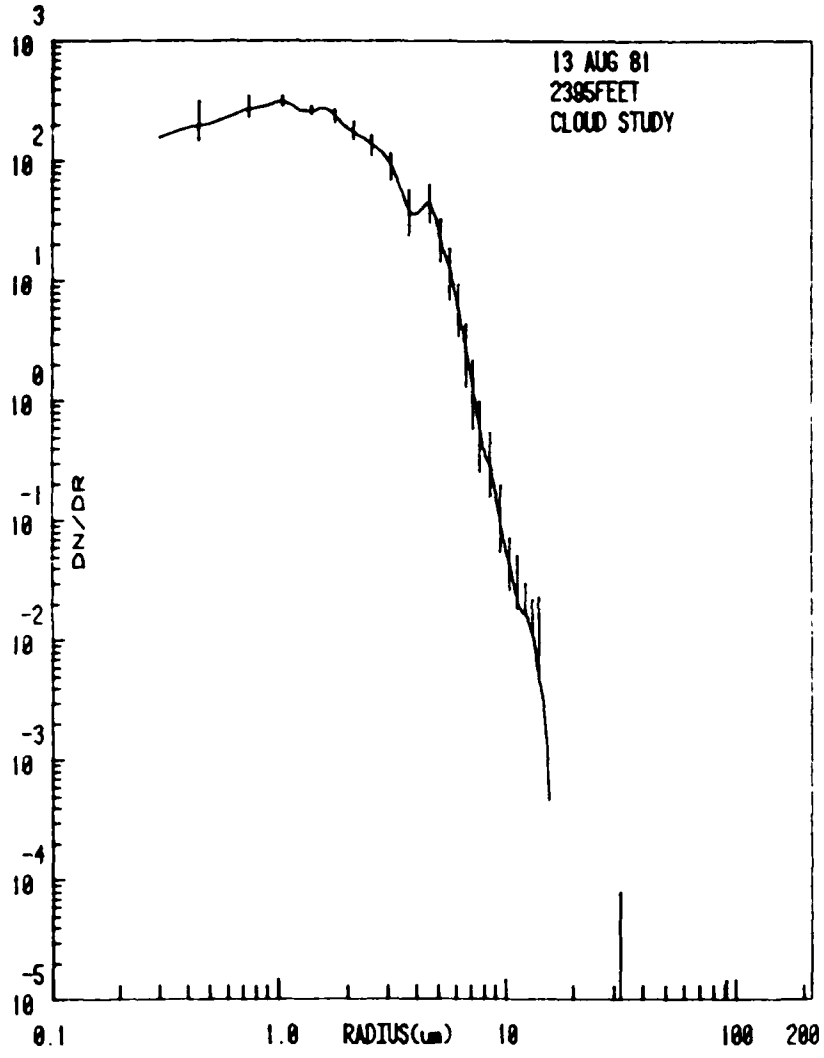

(e7)

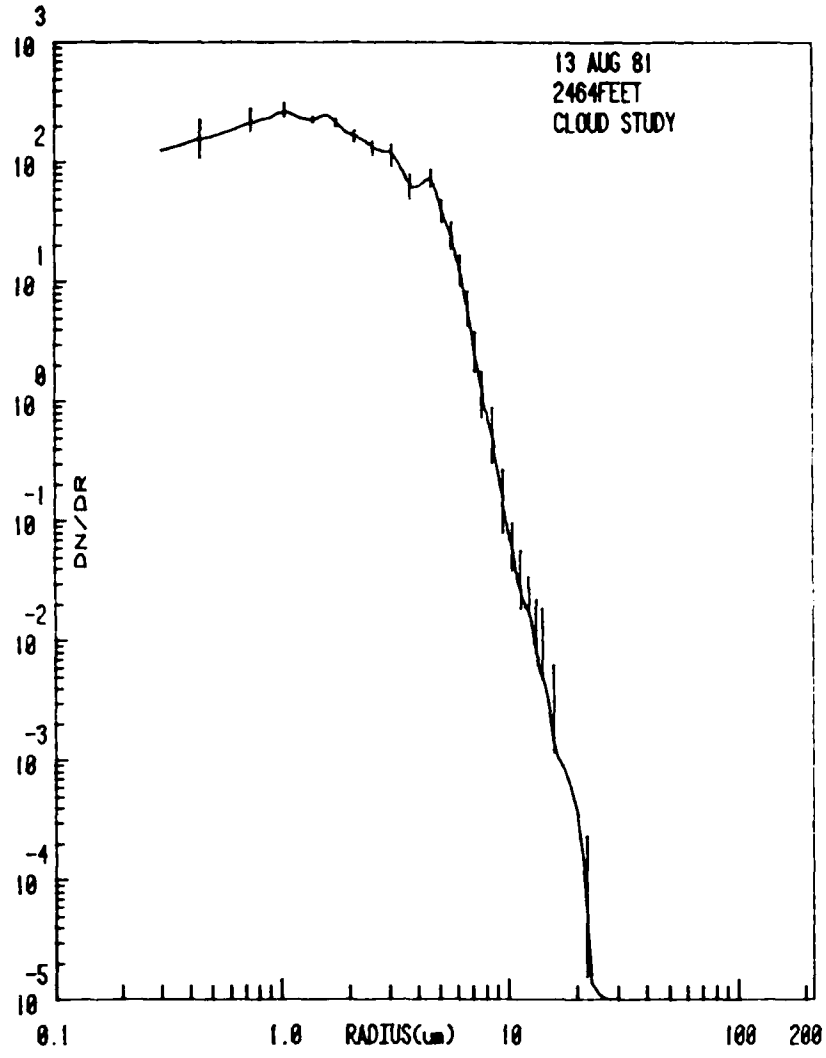

(e8)

Figure 3. Continued.

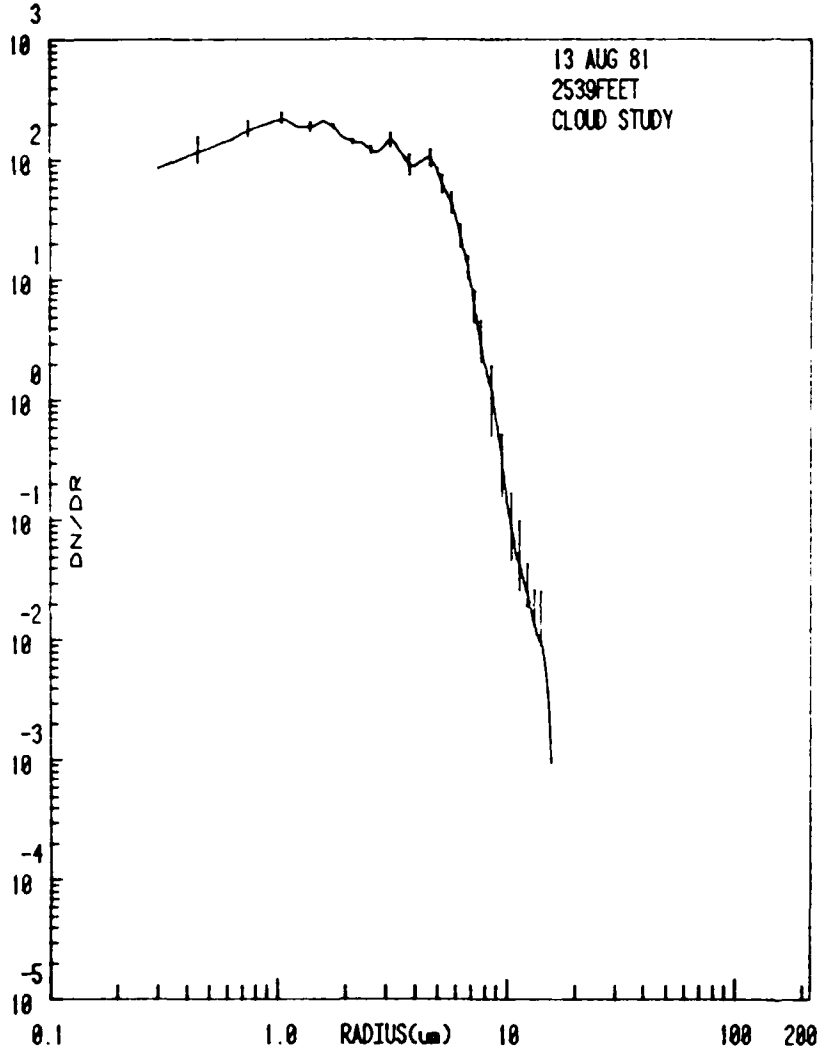

(e9)

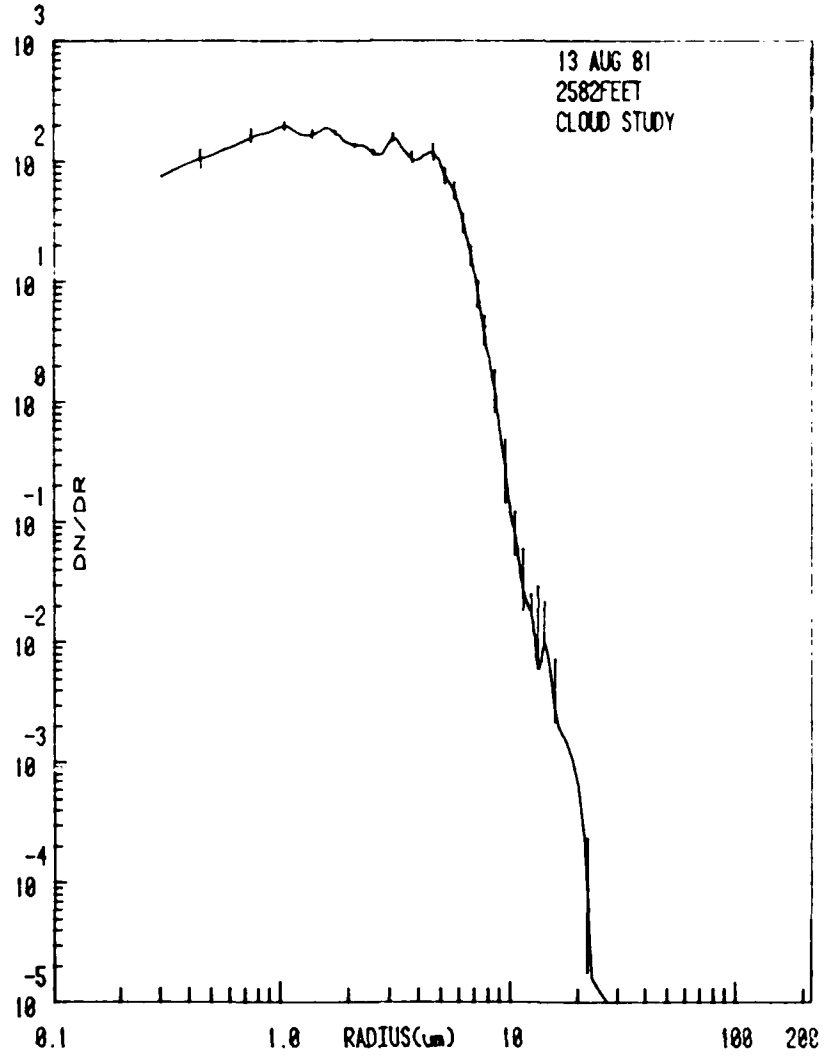

(e10)

Figure 3. Continued.

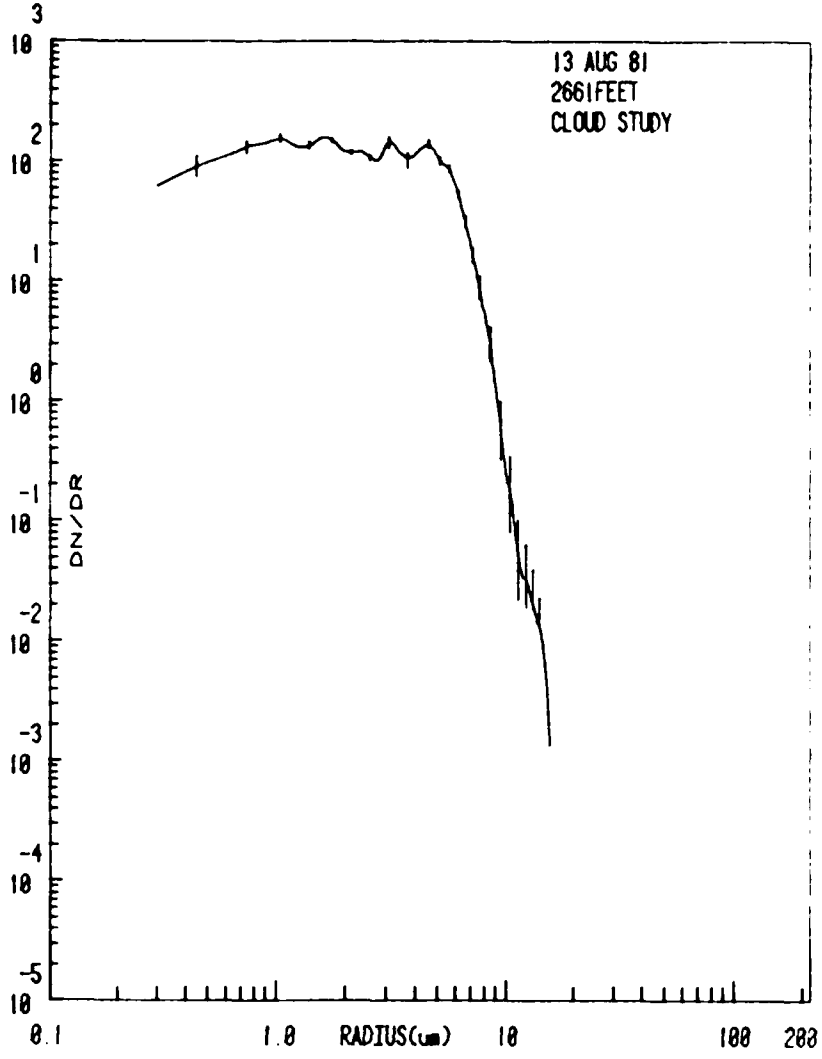

(e11)

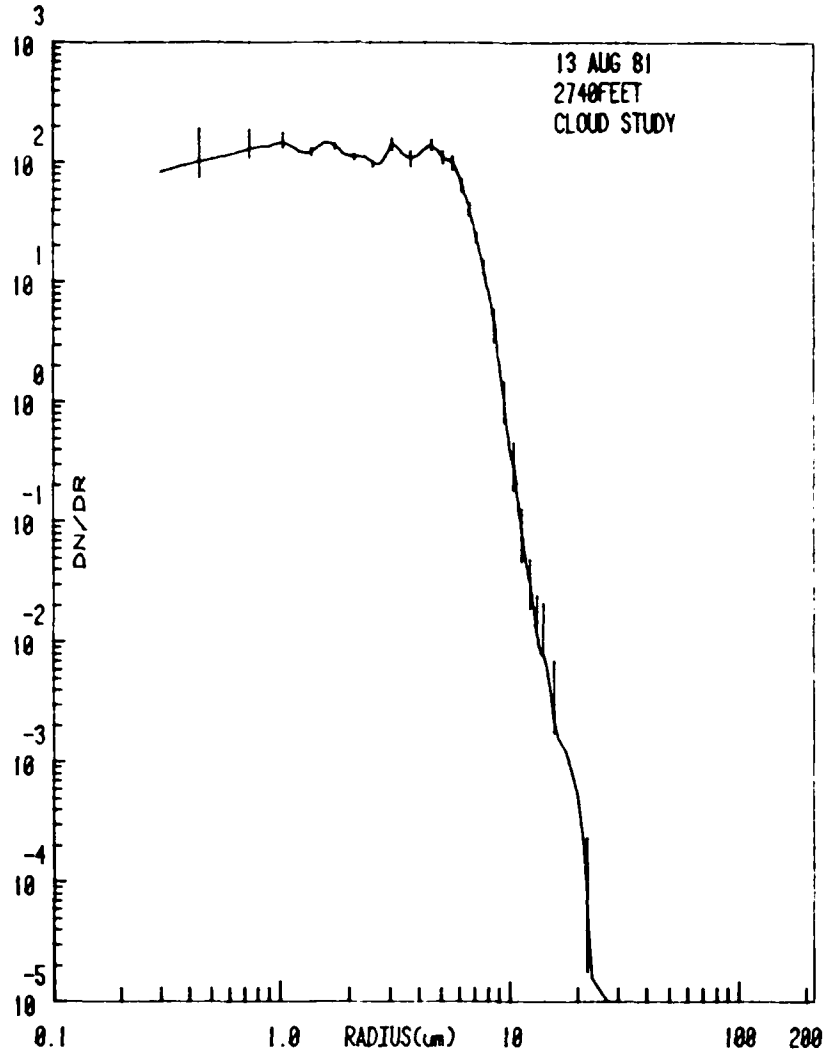

(e12)

Figure 3. Continued.

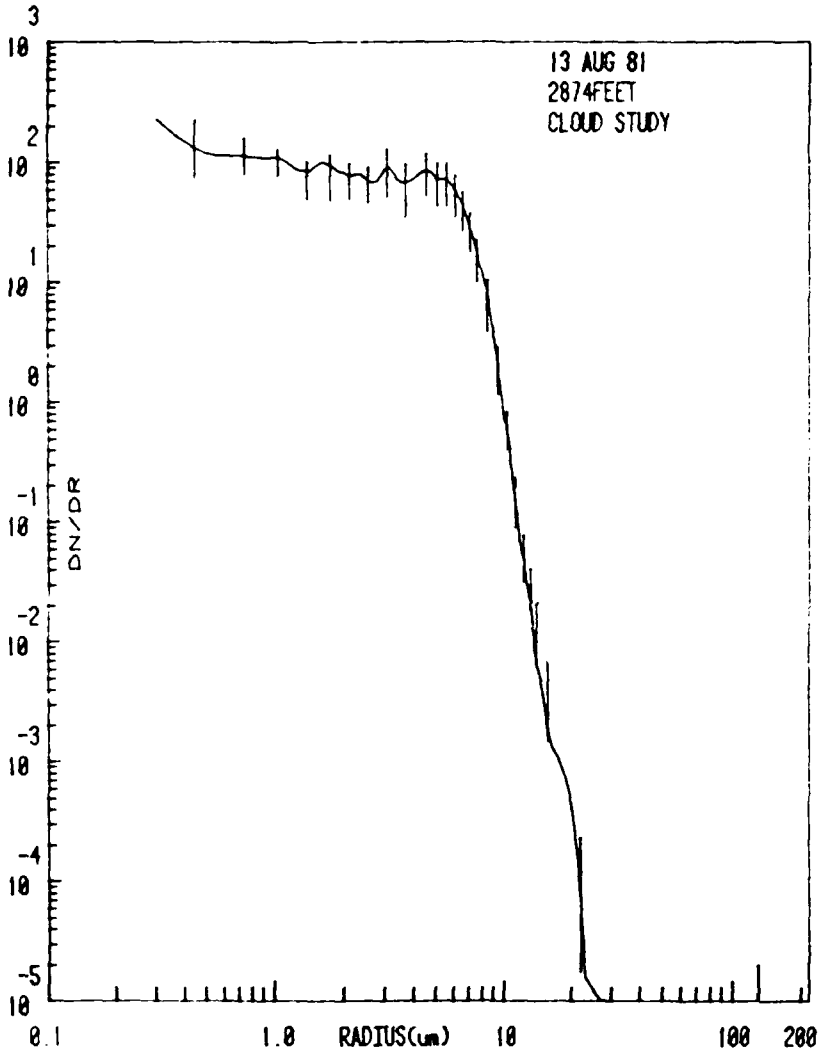

(e13)

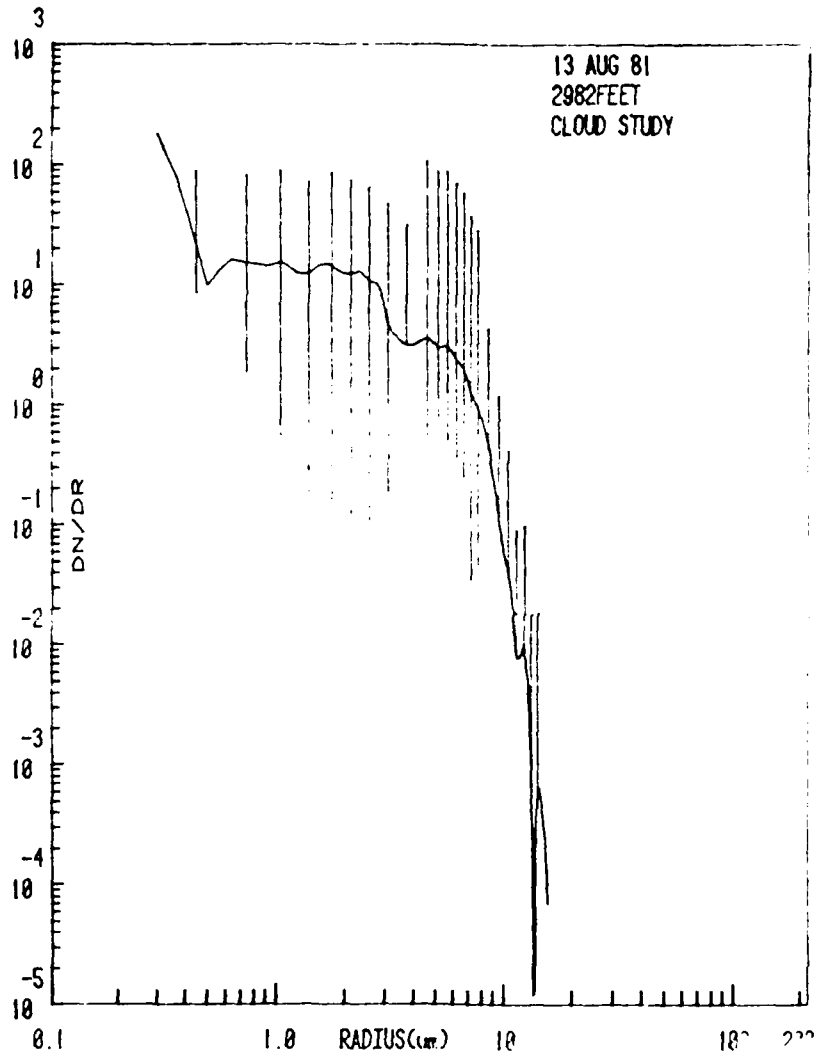

(e14)

Figure 3. Continued.

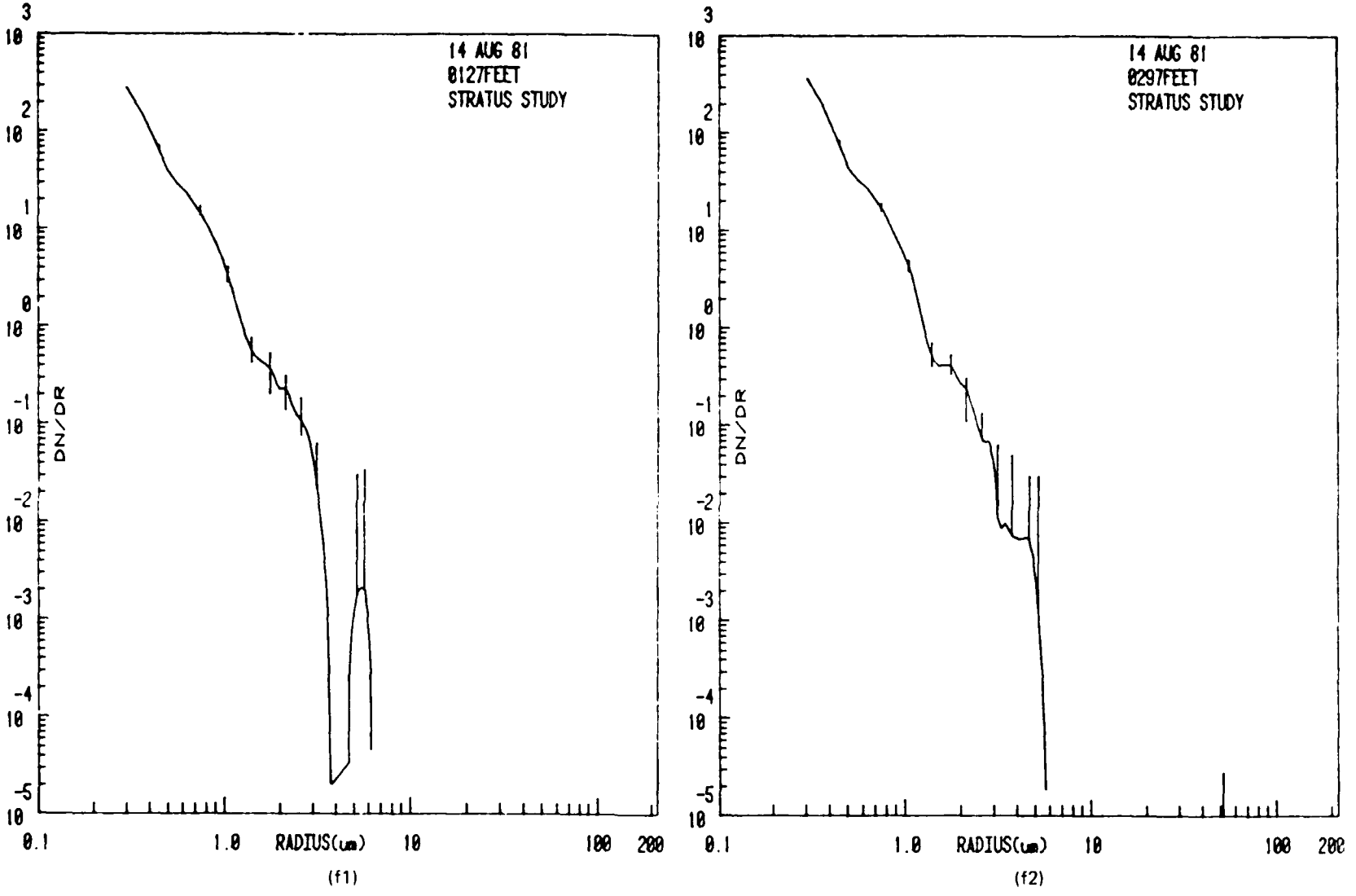

Figure 3. Continued.

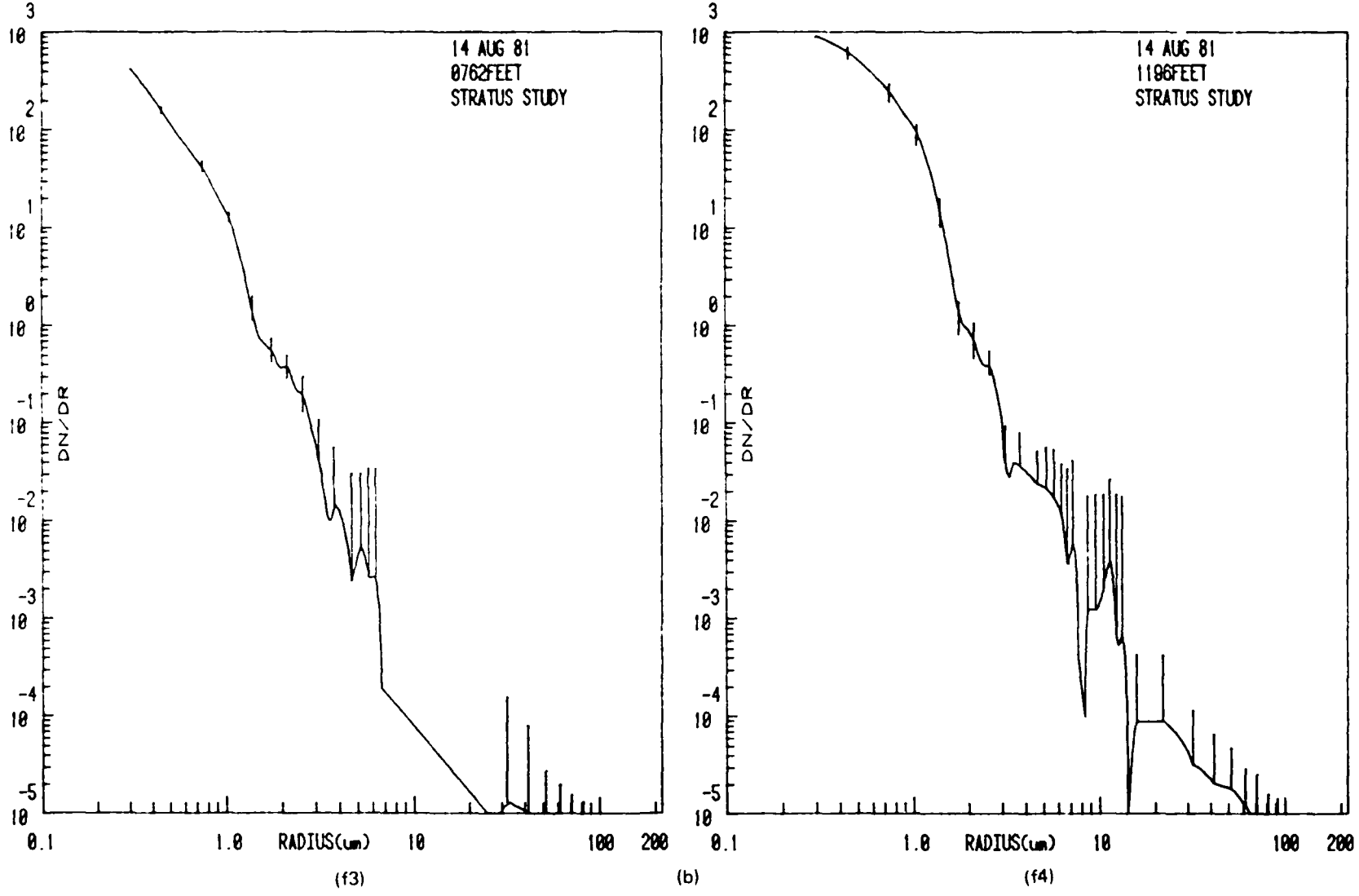

Figure 3. Continued.

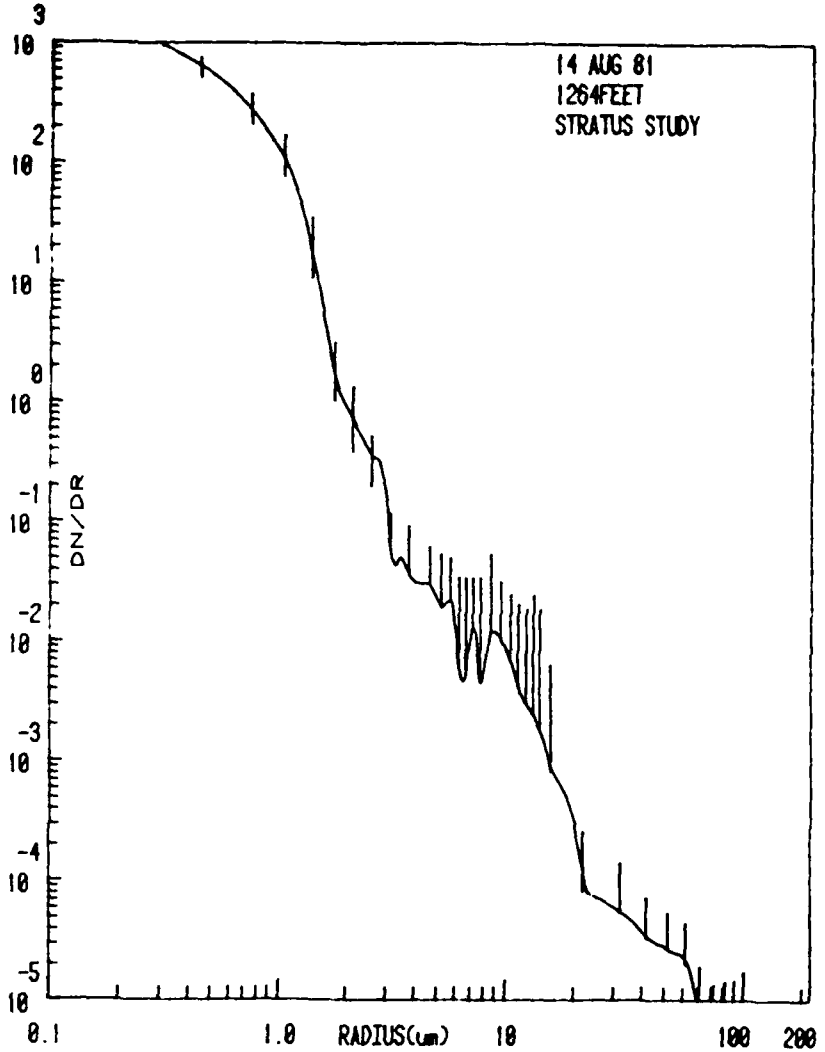

(f5)

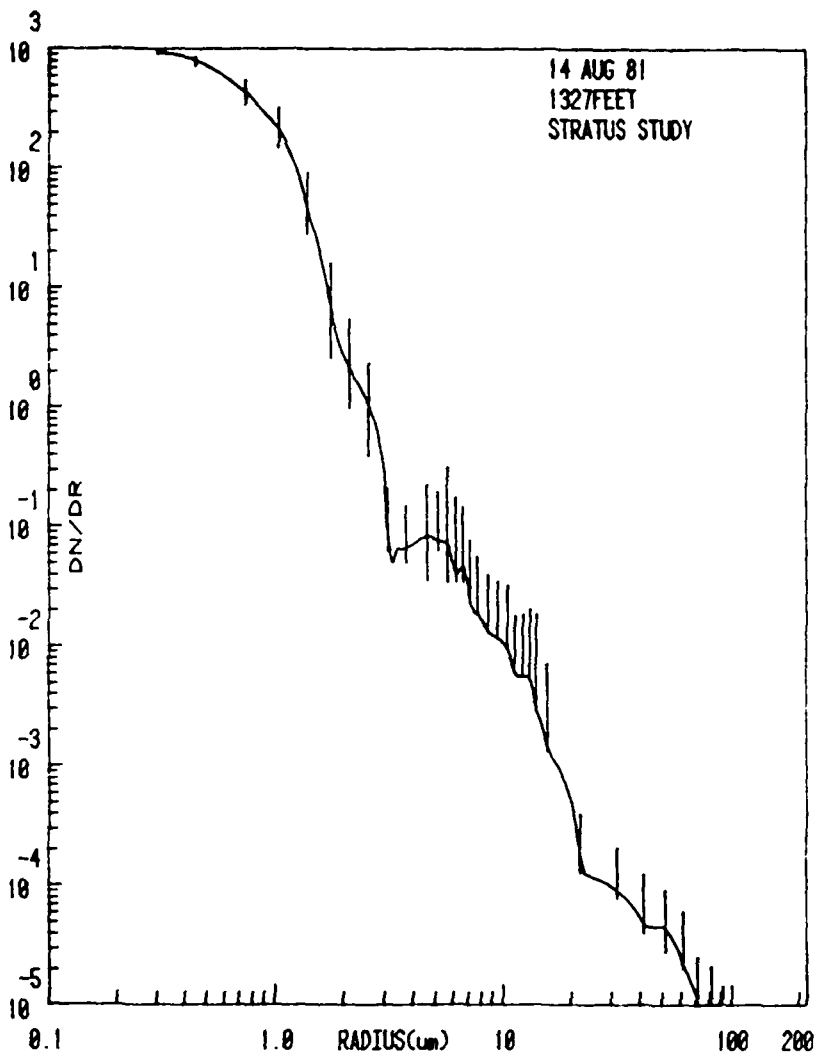

(f6)

Figure 3. Continued.

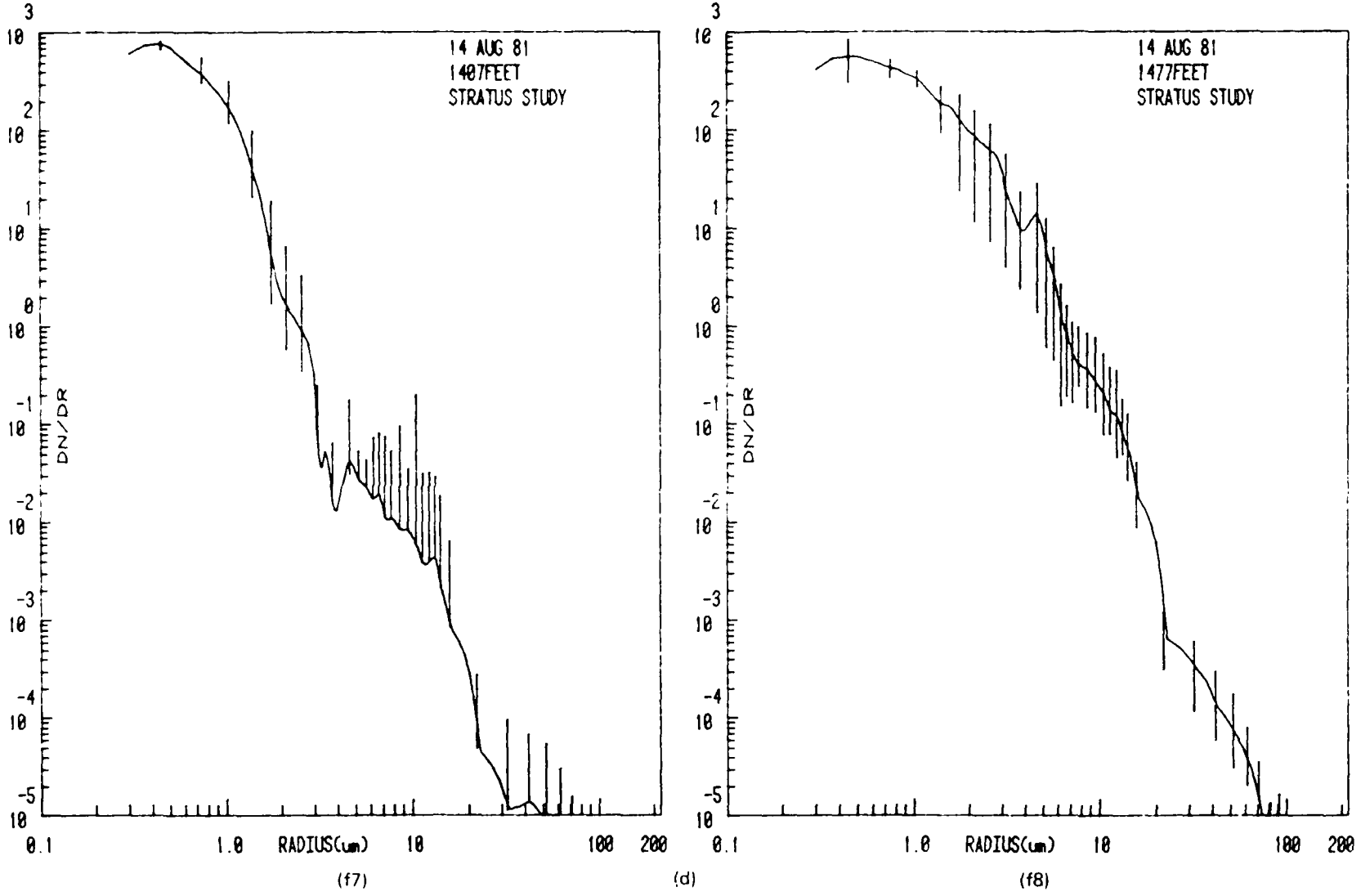

Figure 3. Continued.

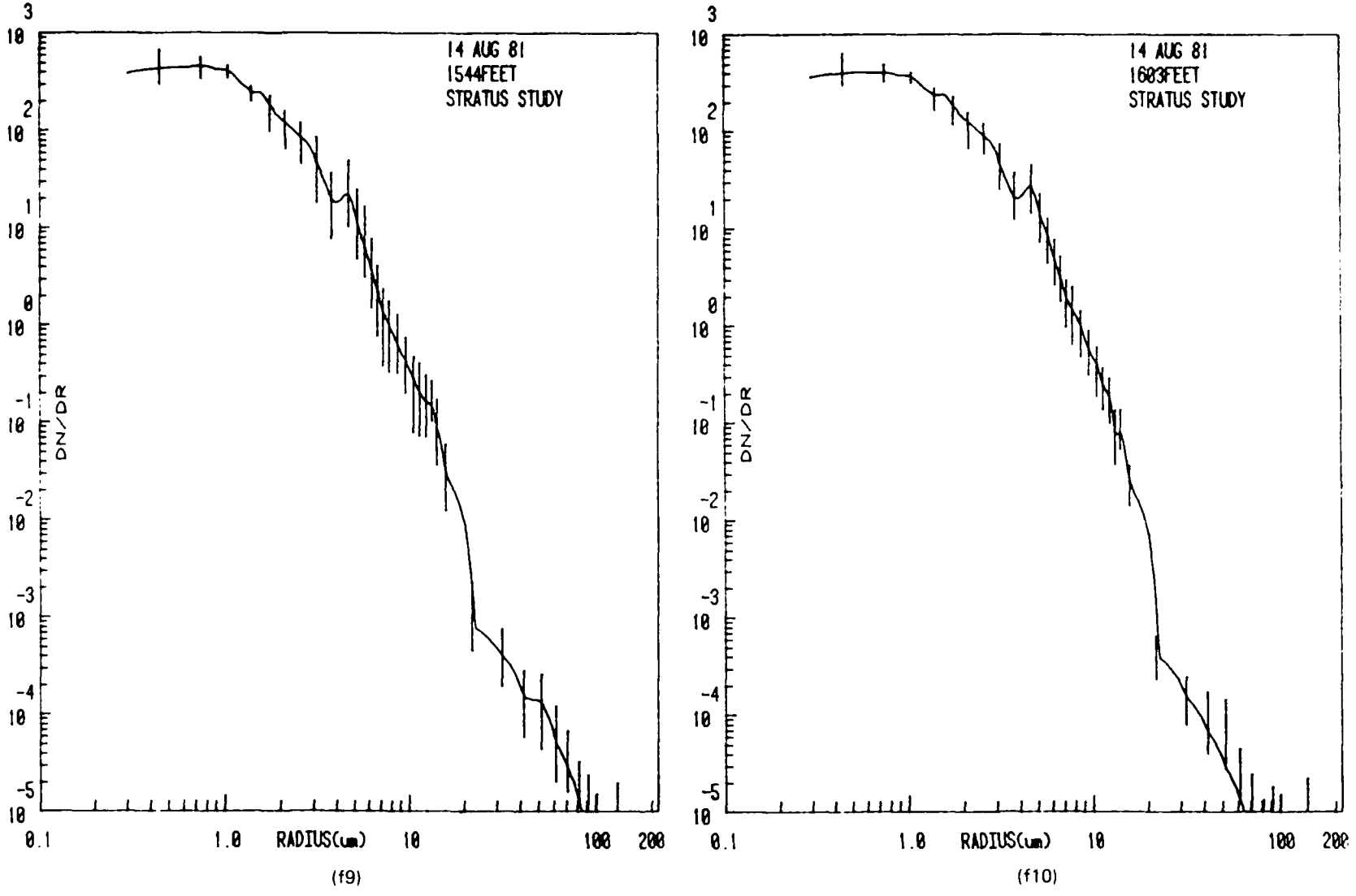

Figure 3. Continued.

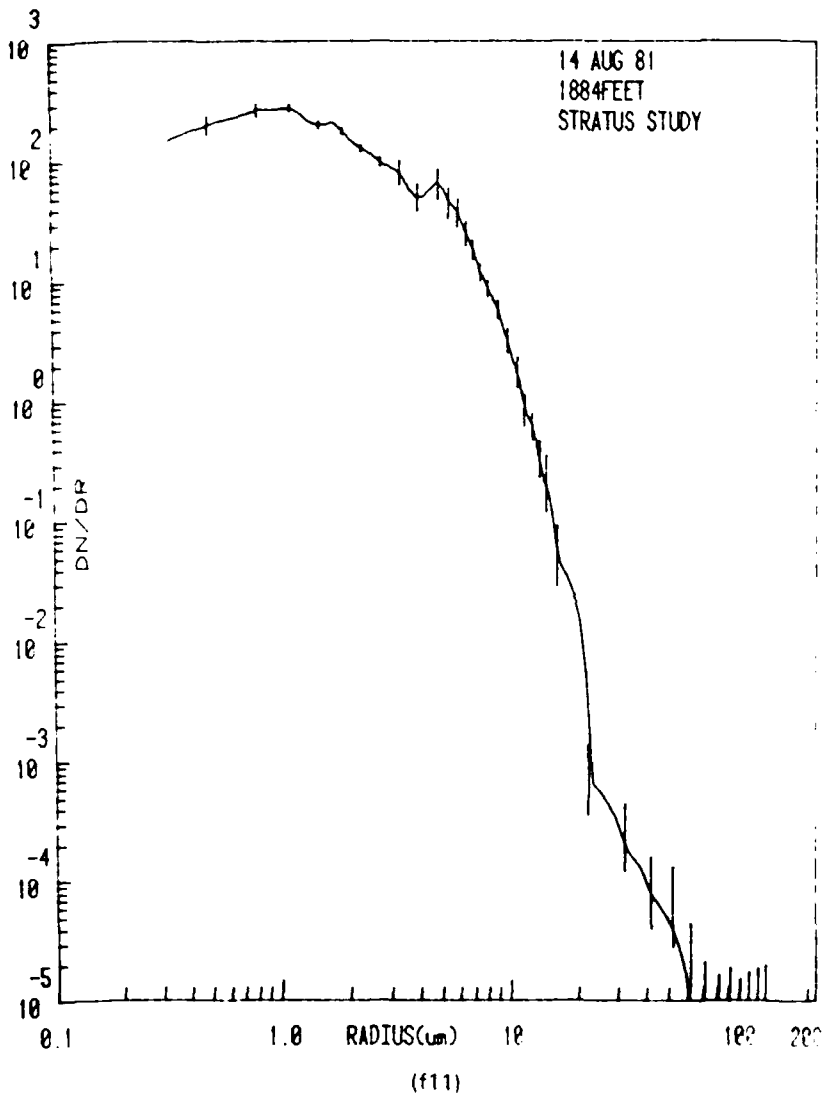

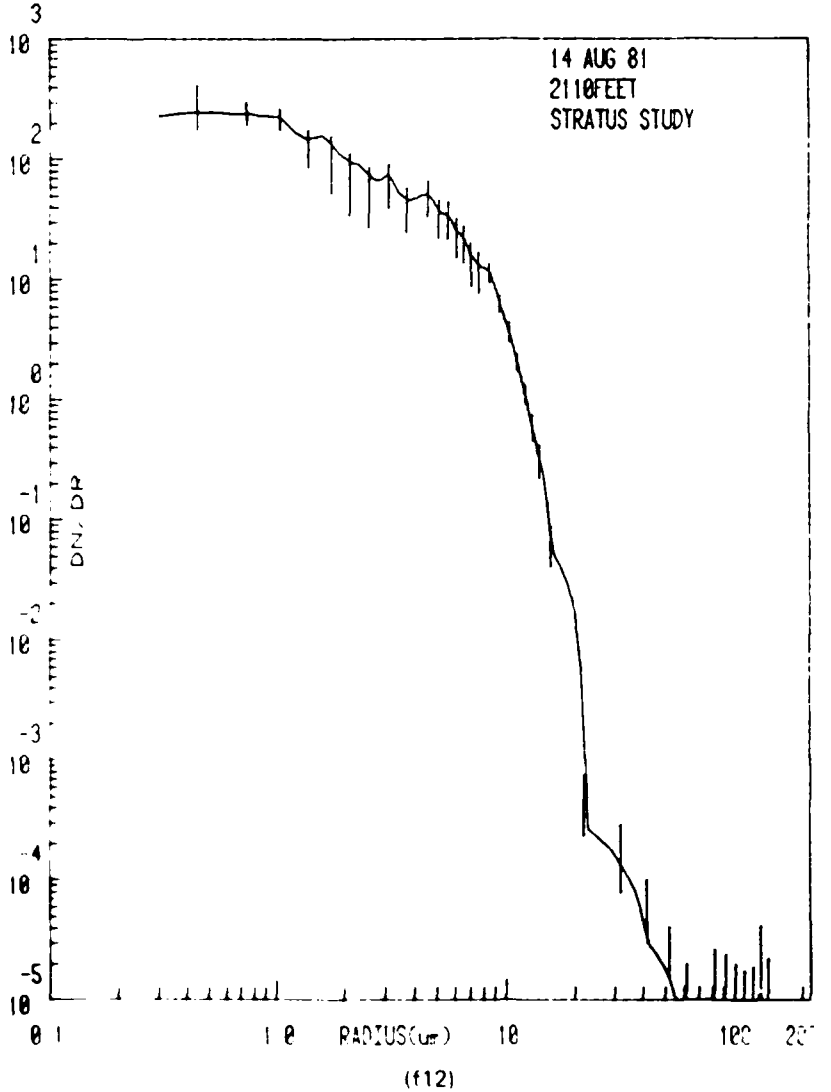

Figure 3. Continued.

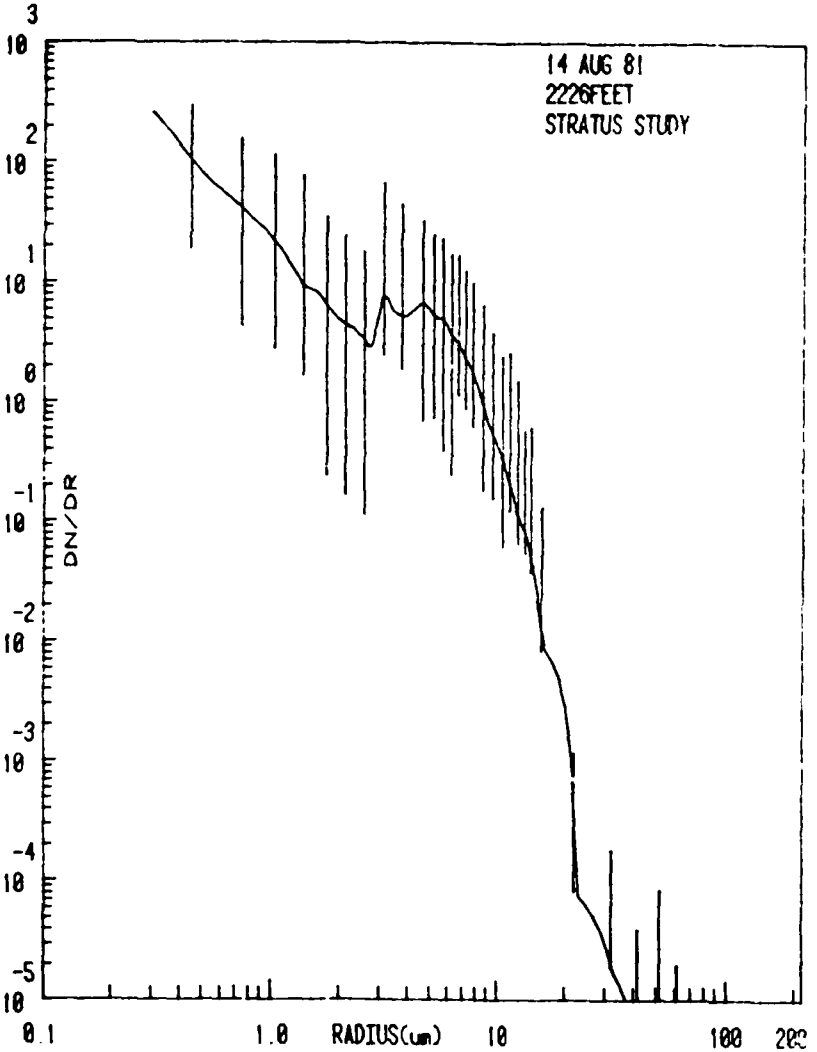

(f13)

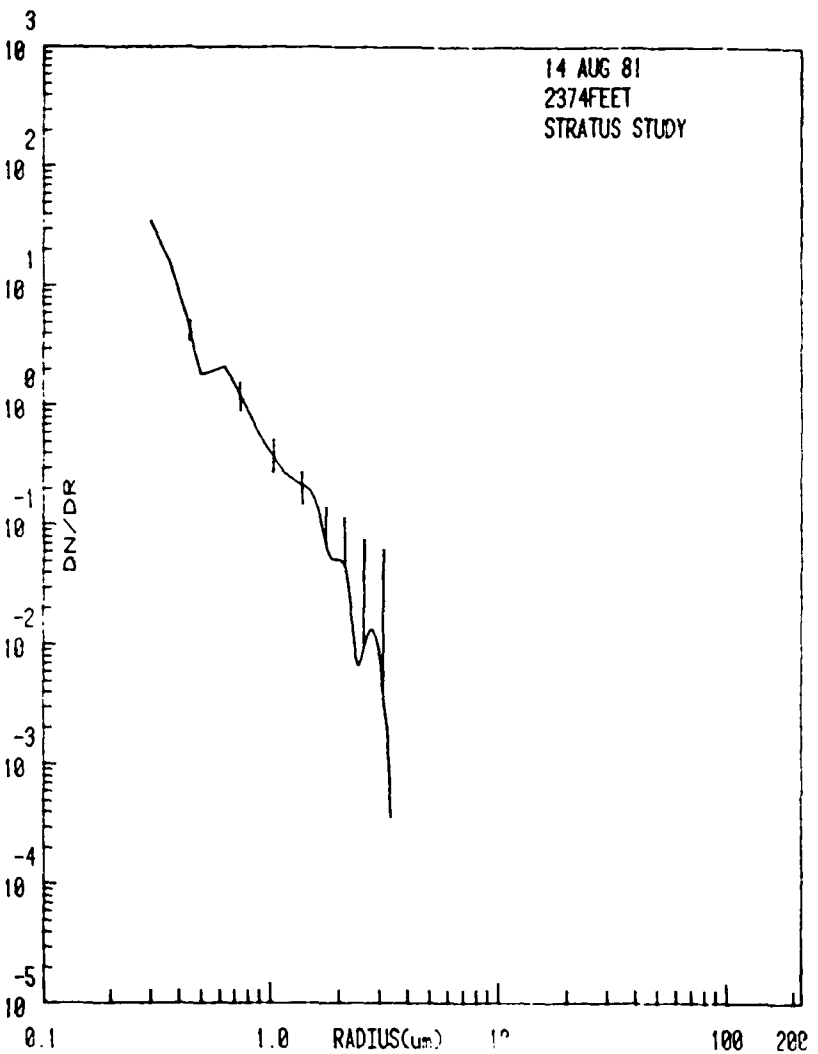

(f14)

Figure 3. Continued.

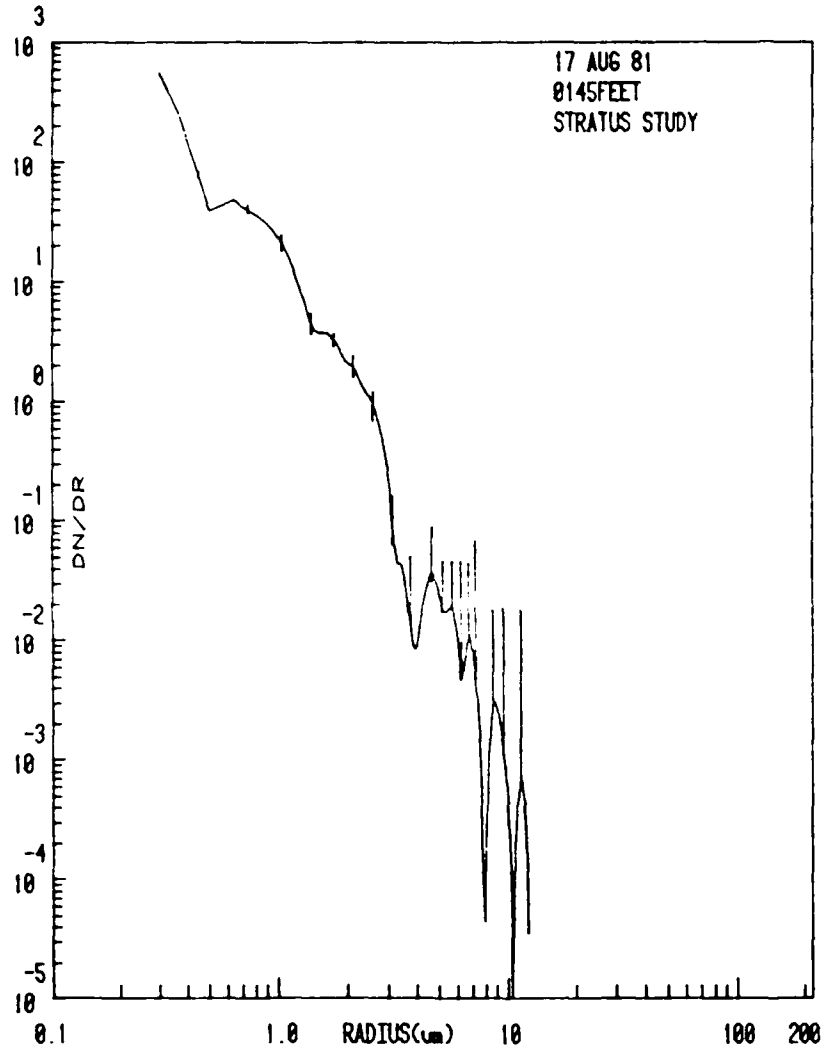

(g1)

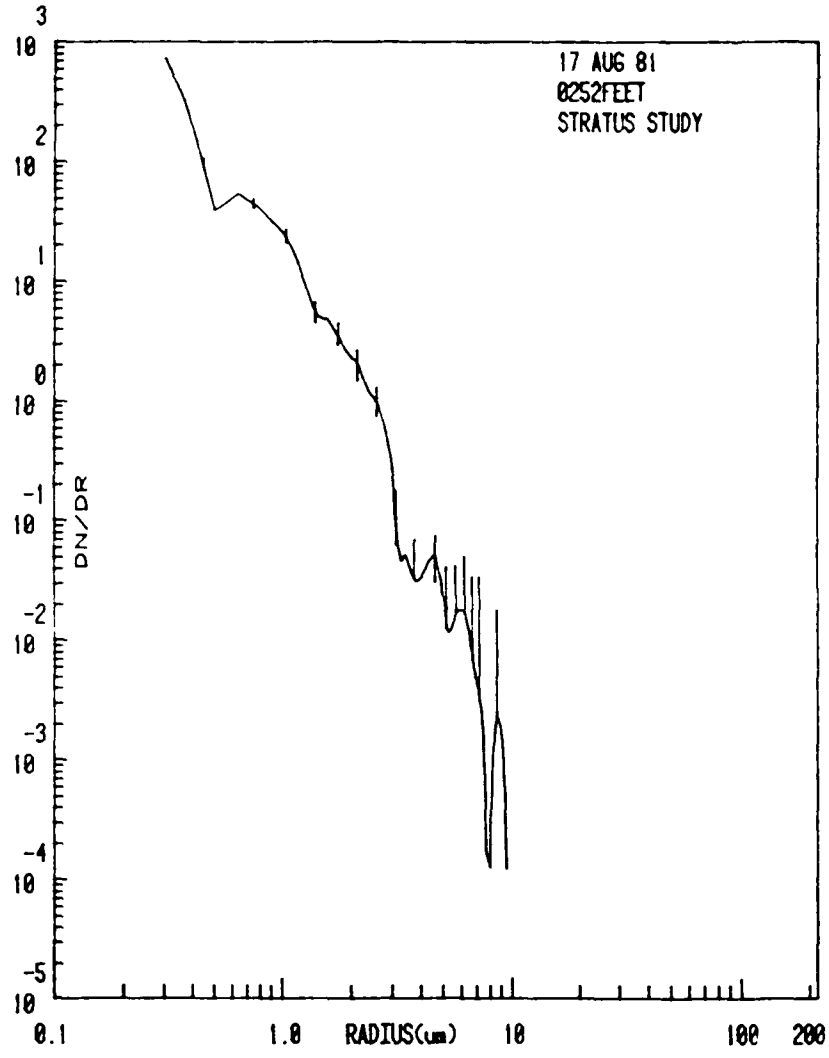

(g2)

Figure 3. Continued.

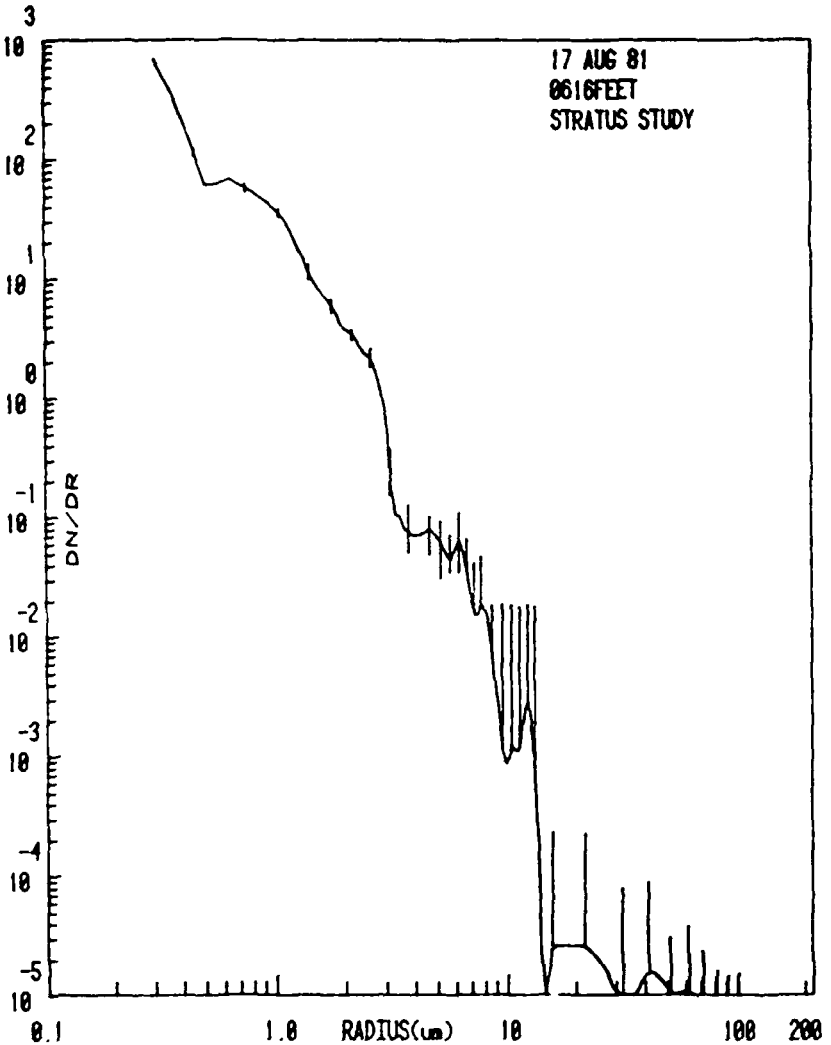

(g3)

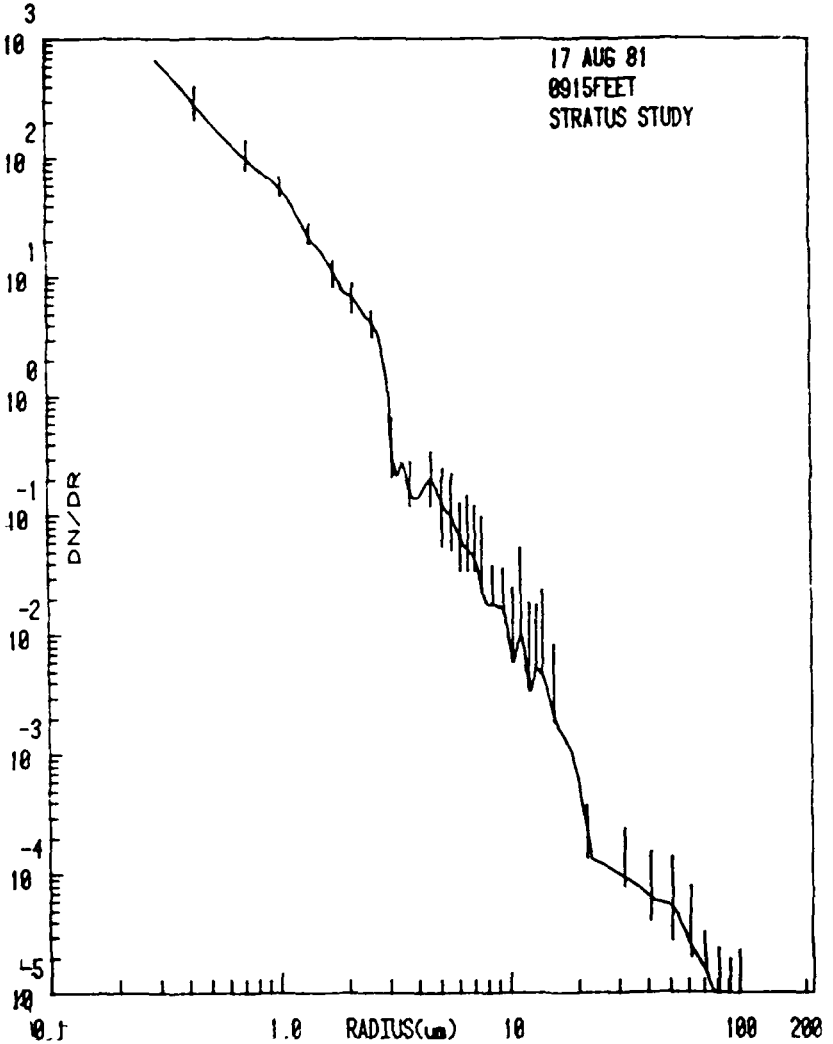

(g4)

Figure 3. Continued.

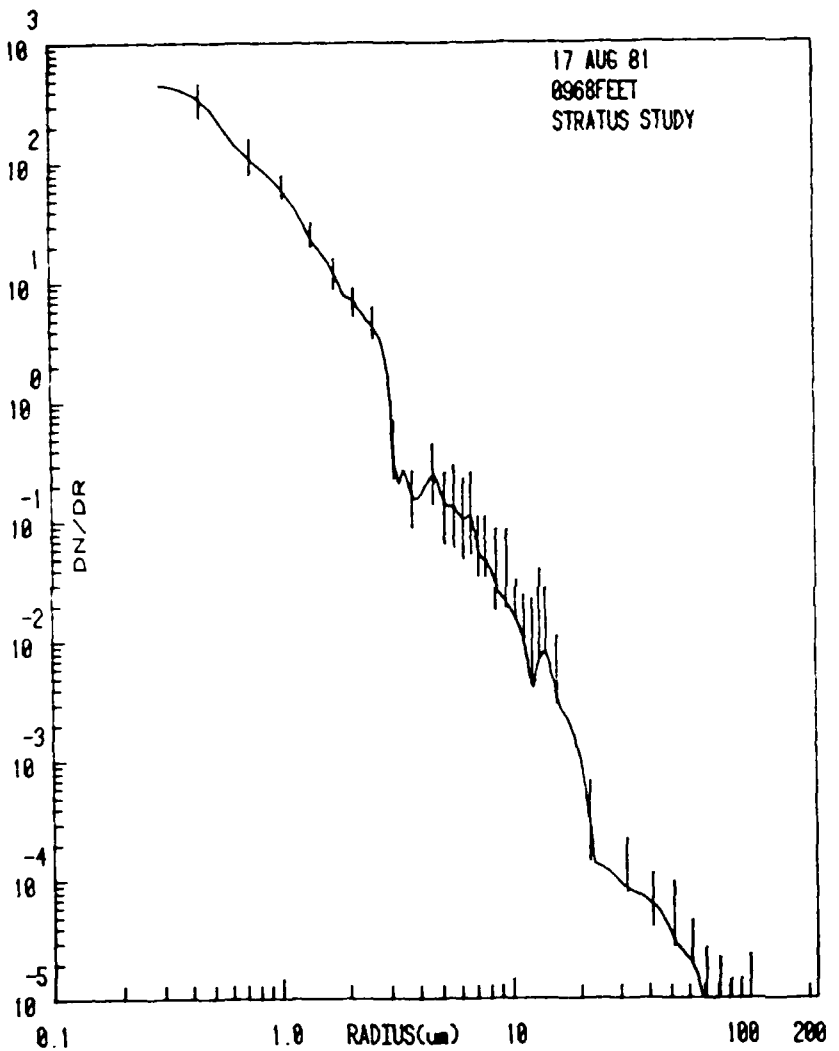

(g5)

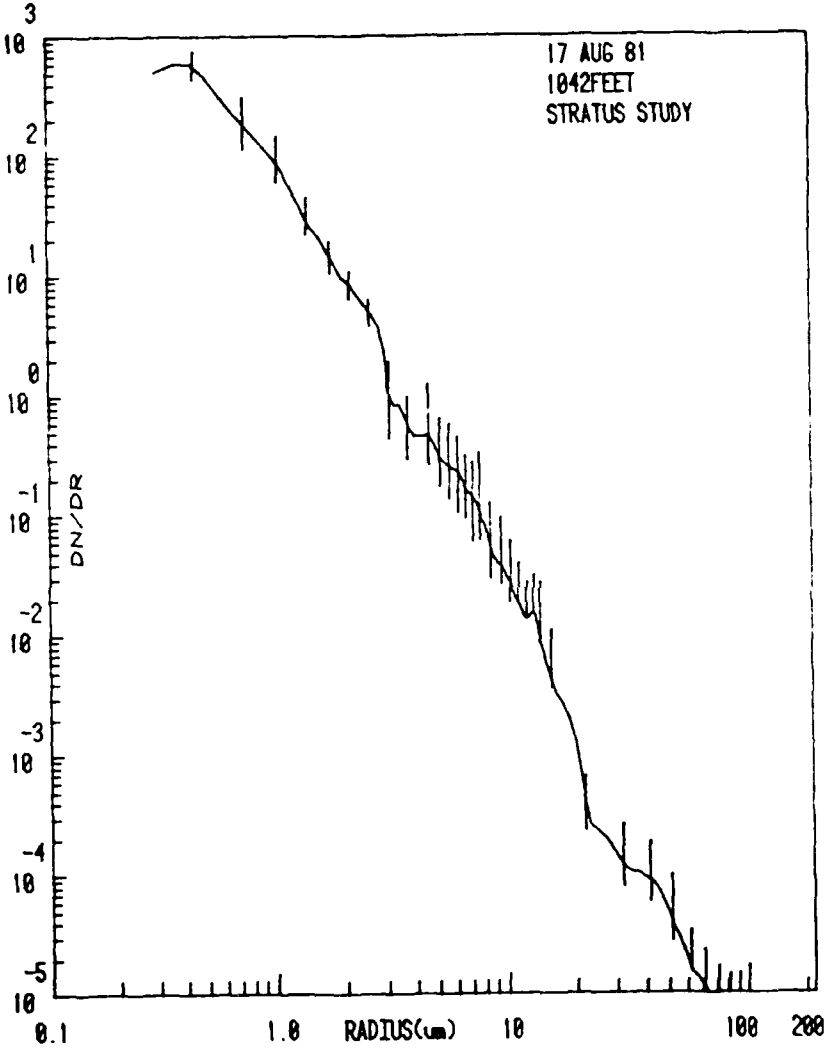

(g6)

Figure 3. Continued.

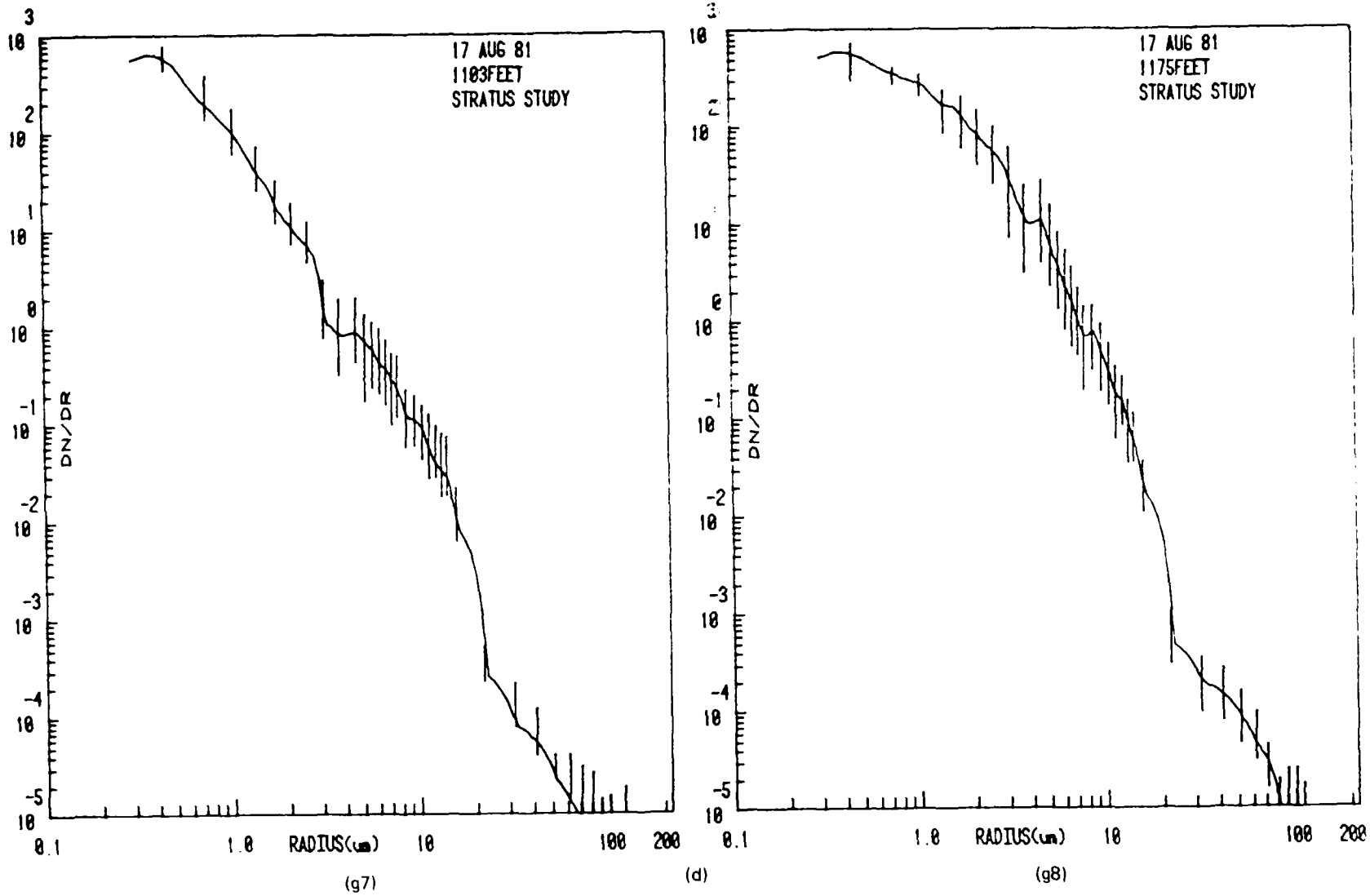

(g7) (d) (g8)

Figure 3. Continued.

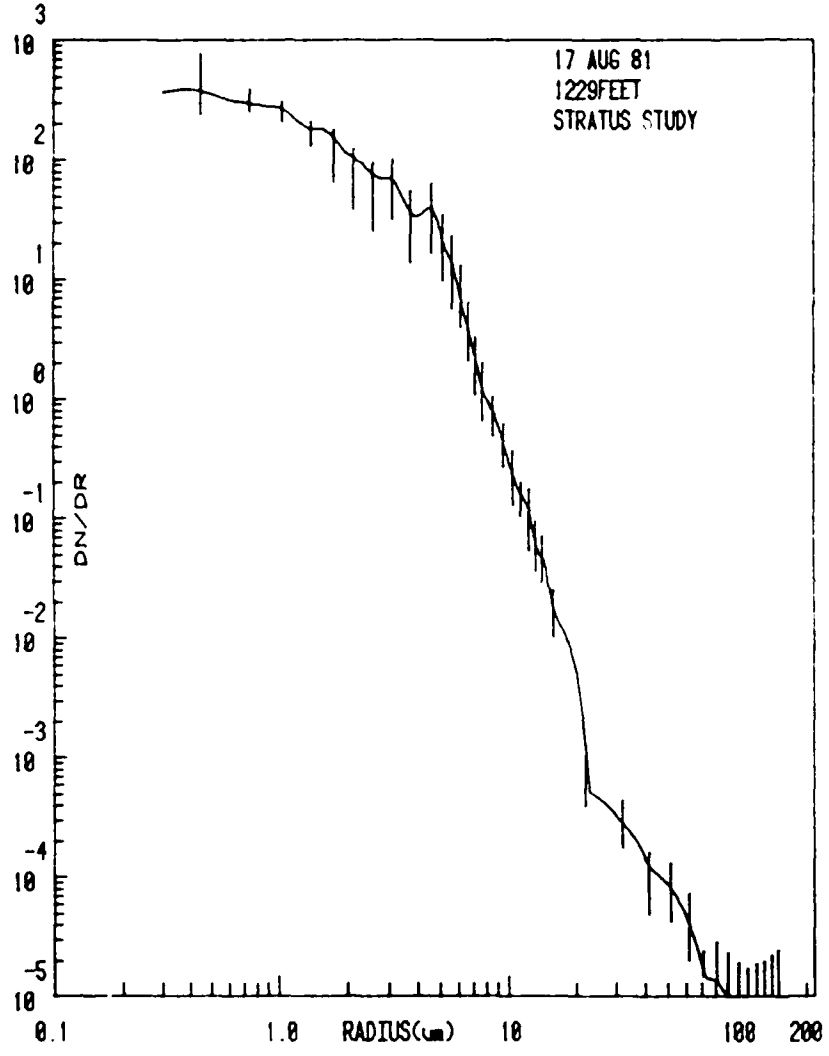

(g9)

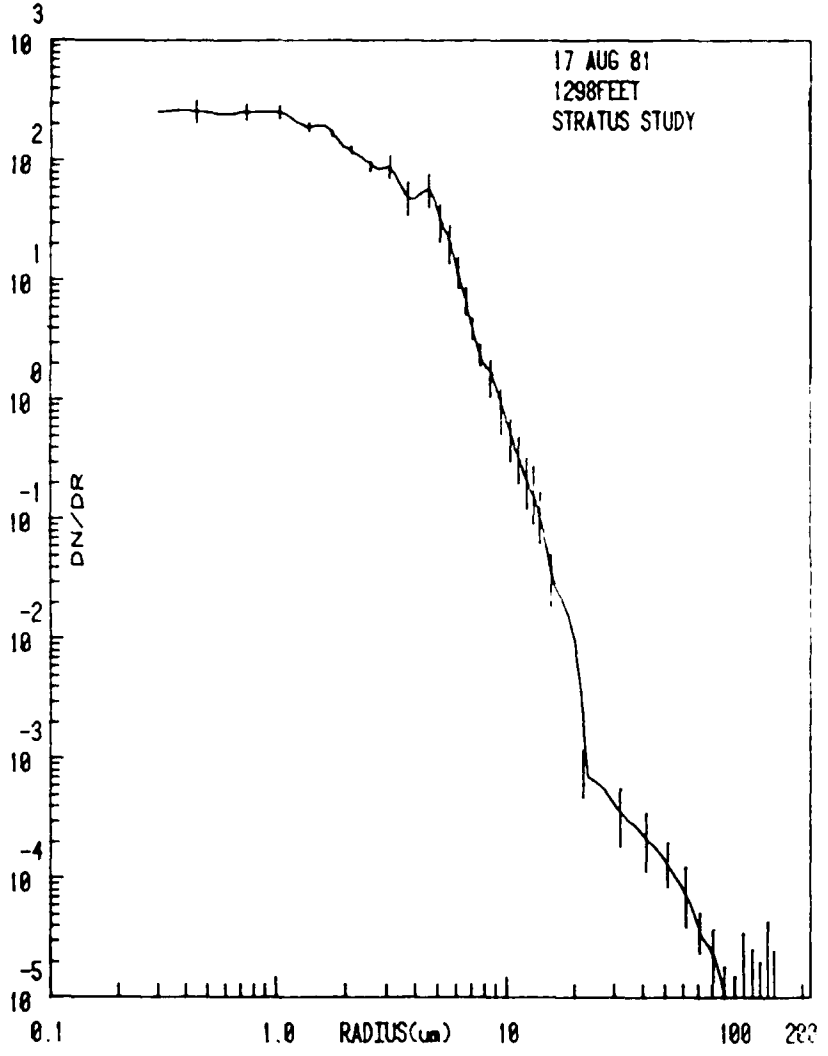

(g10)

Figure 3. Continued.

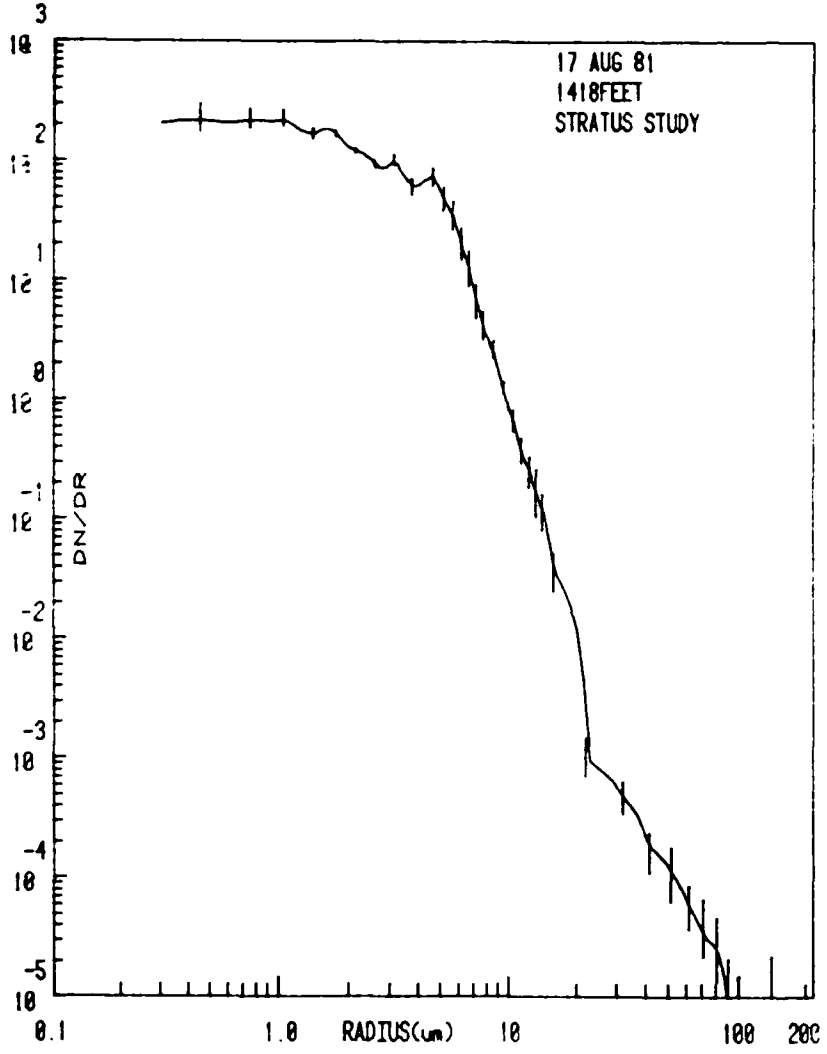

(g11)

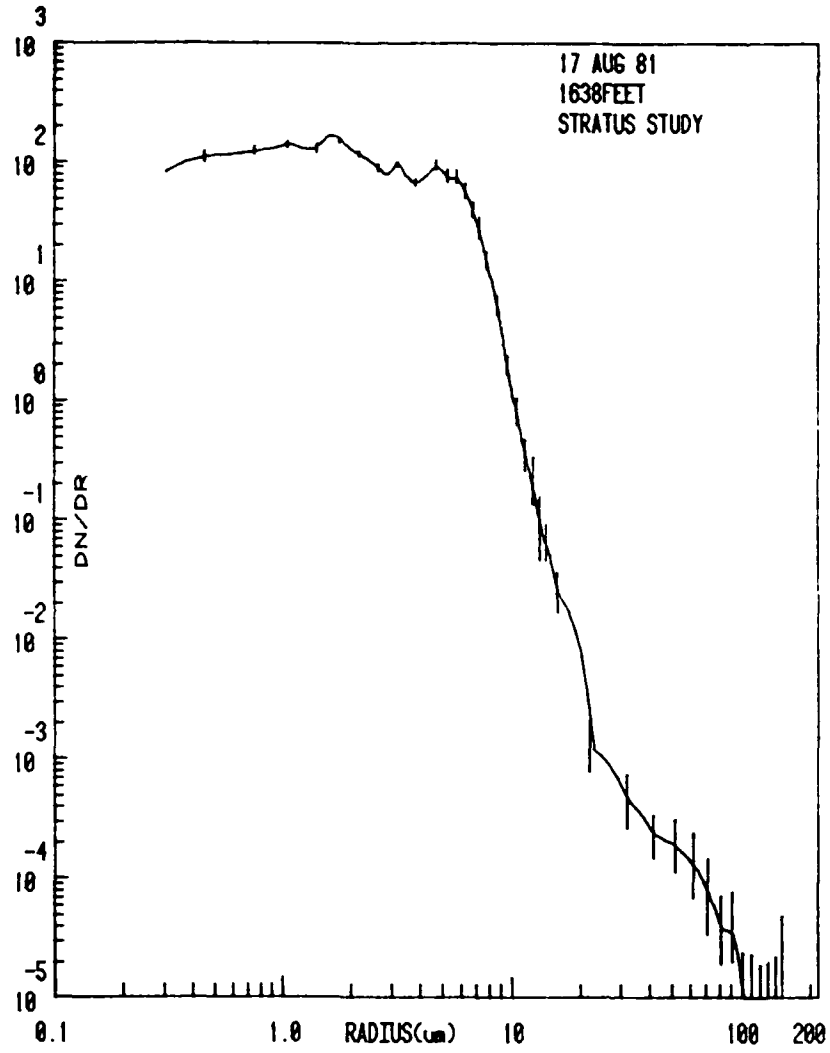

(g12)

Figure 3. Continued.

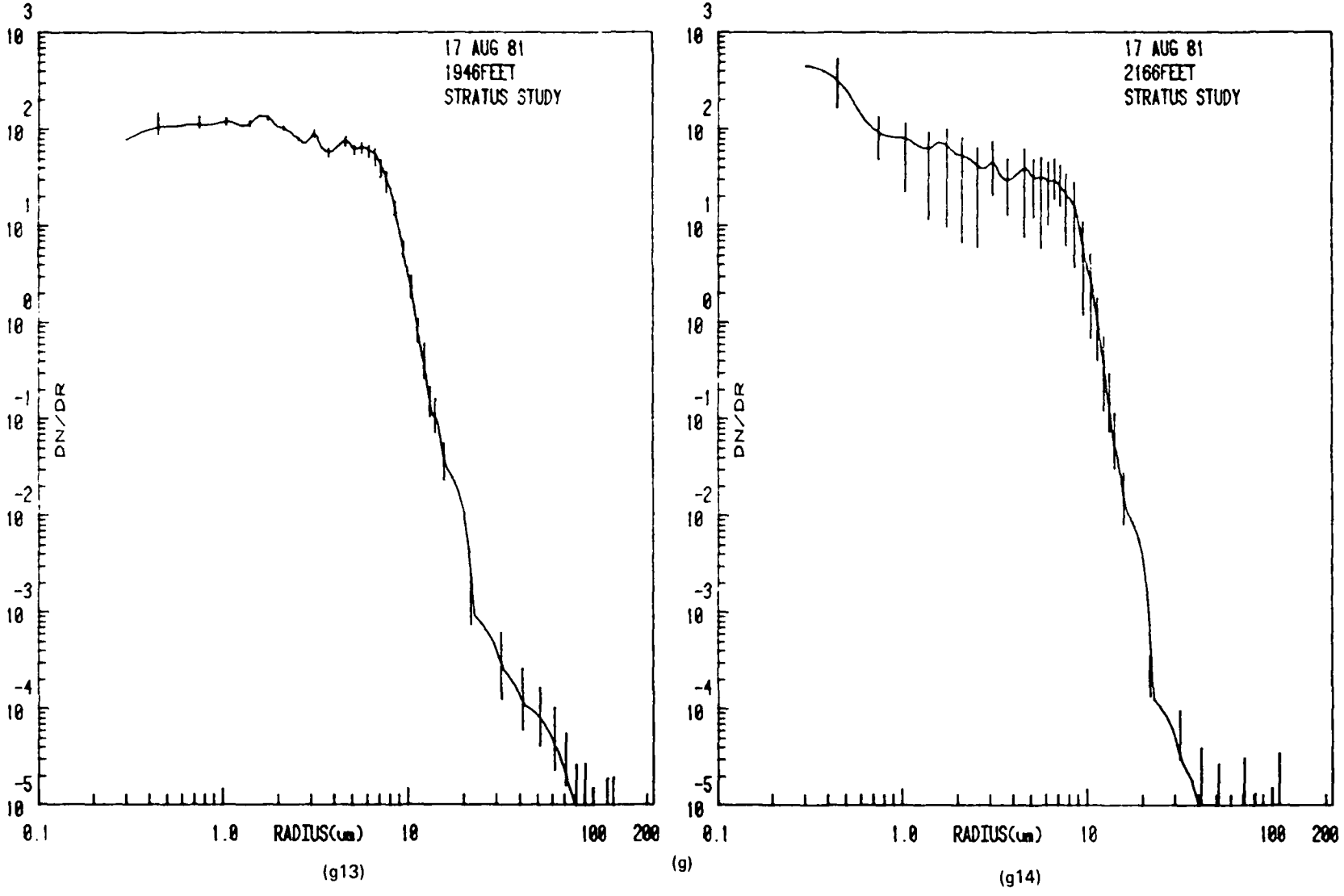

(g)

Figure 3. Continued.

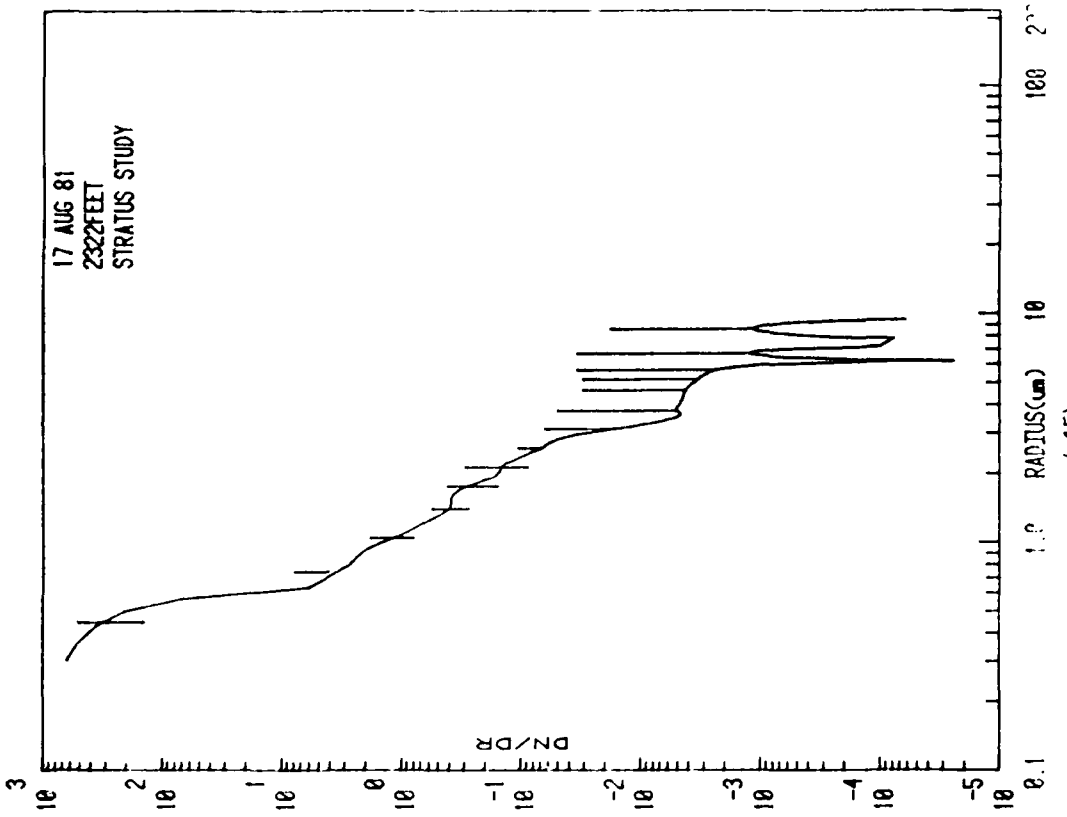

Figure 3. Continued.

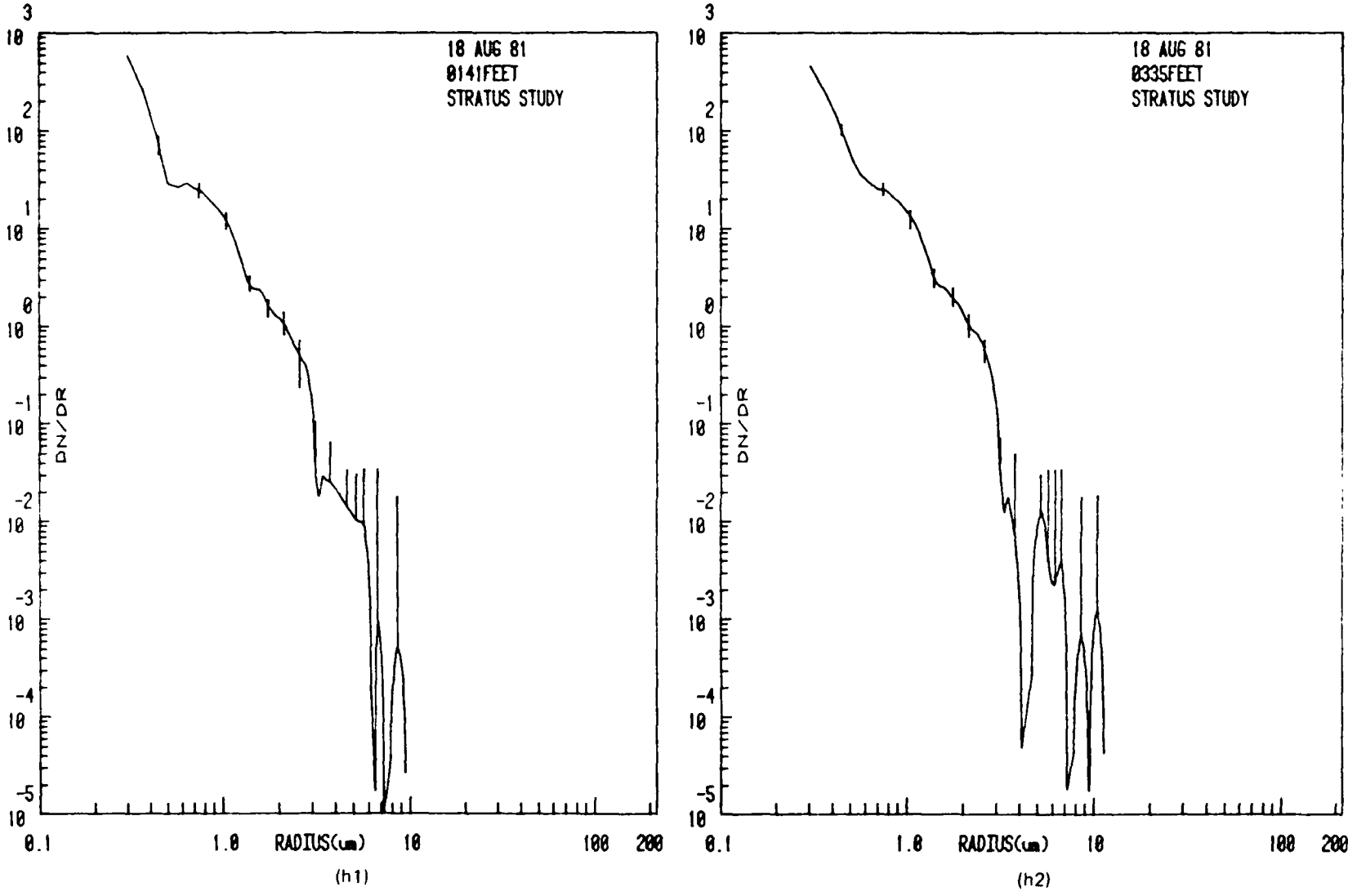

Figure 3. Continued.

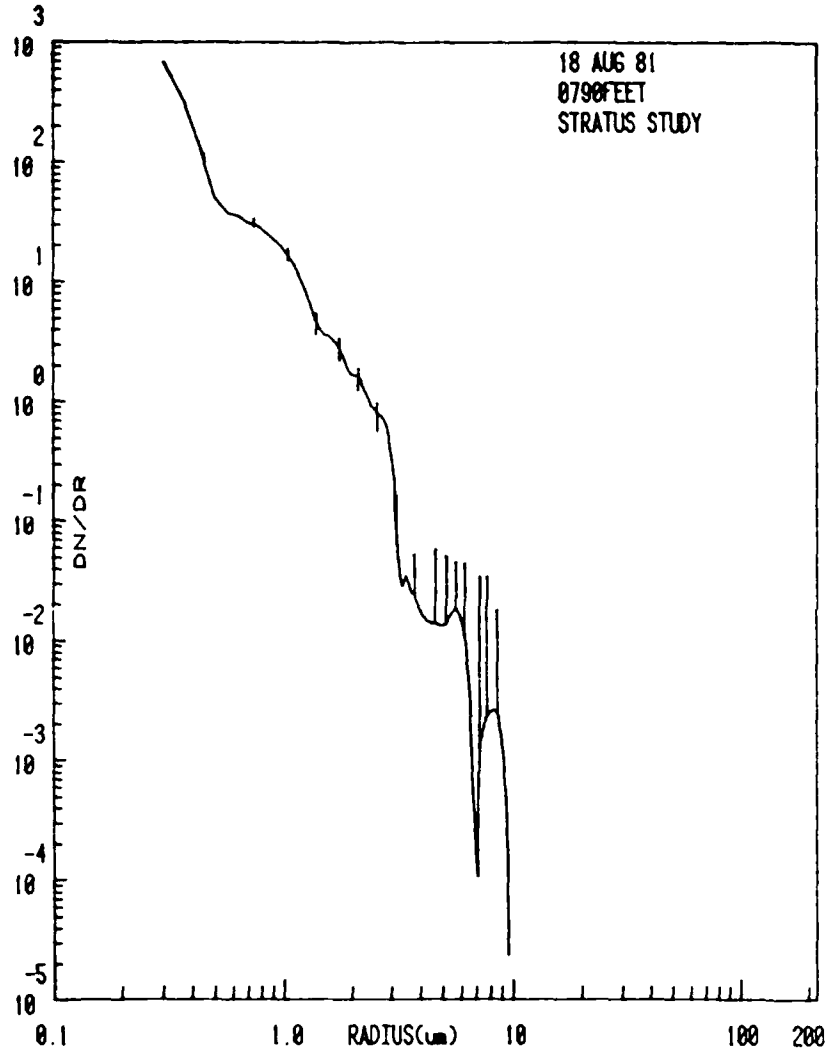

(h3)

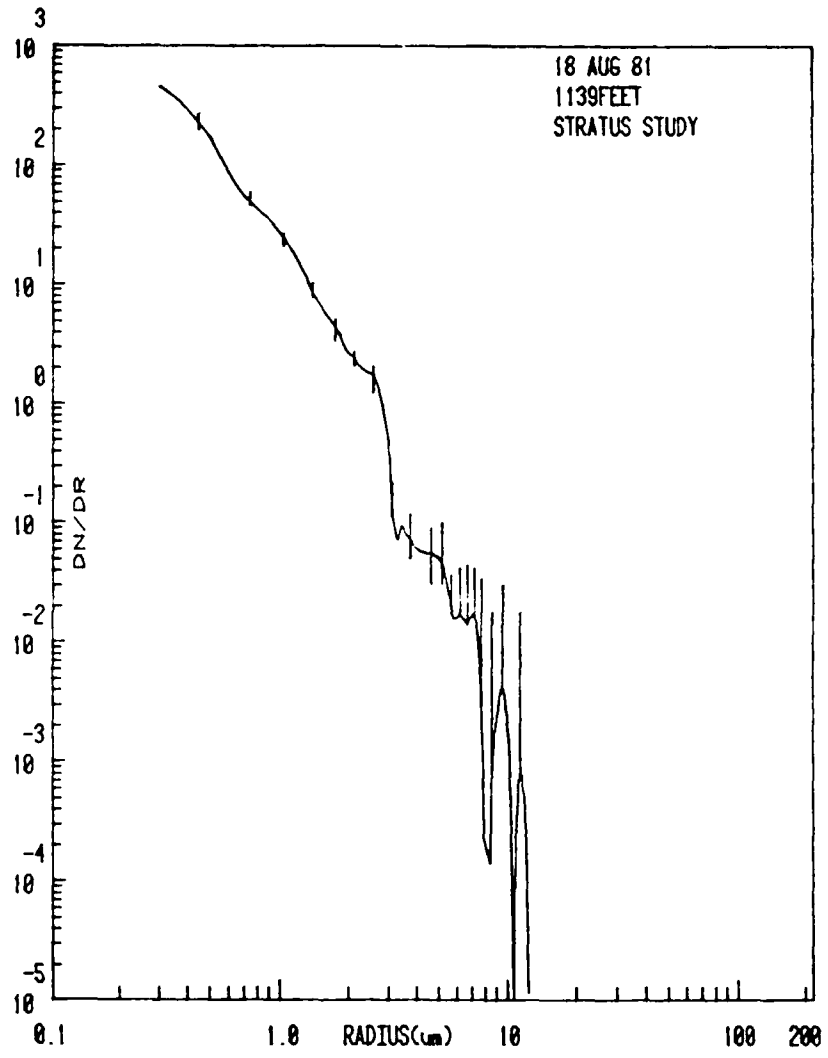

(h4)

Figure 3. Continued.

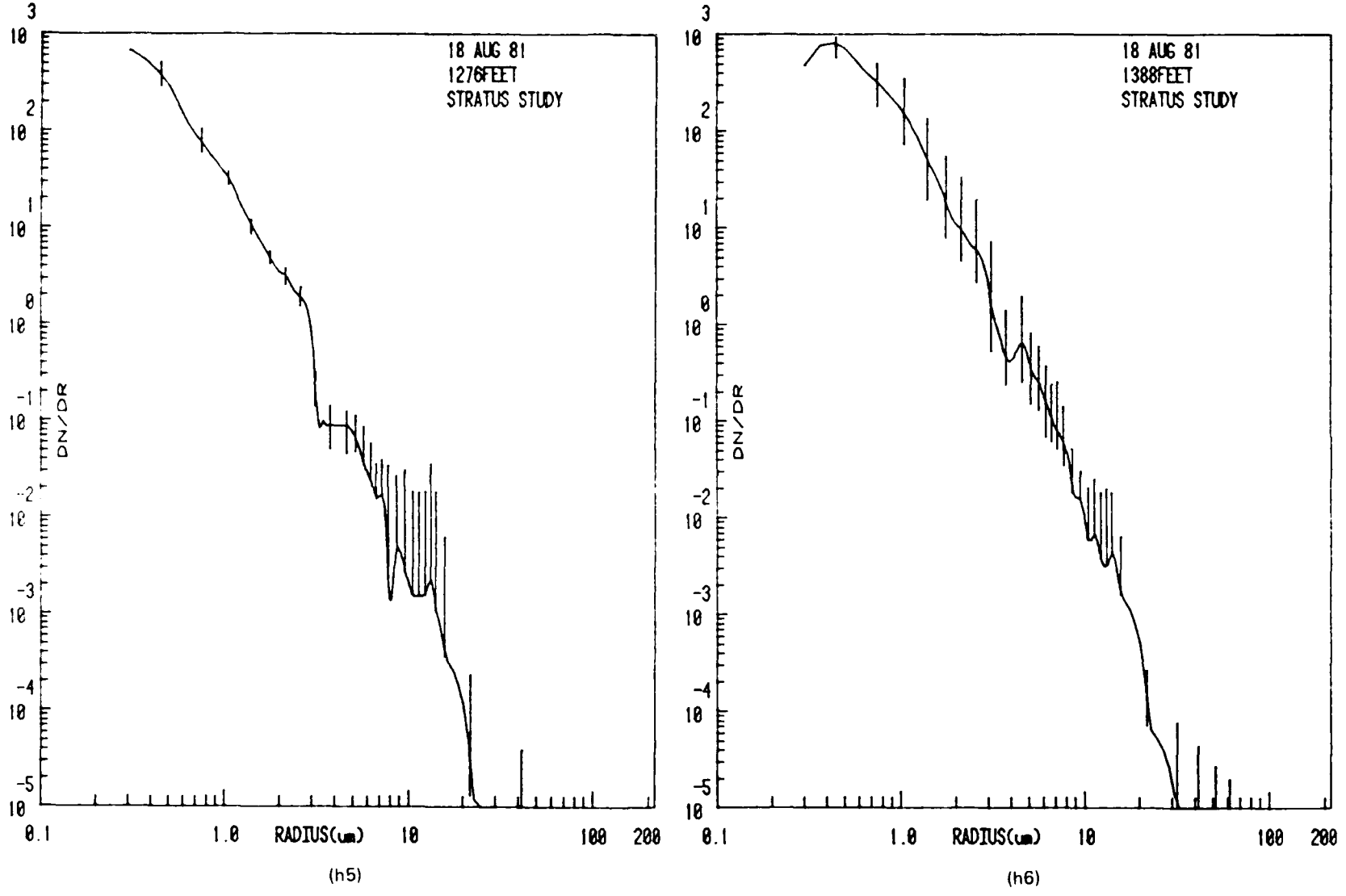

Figure 3. Continued.

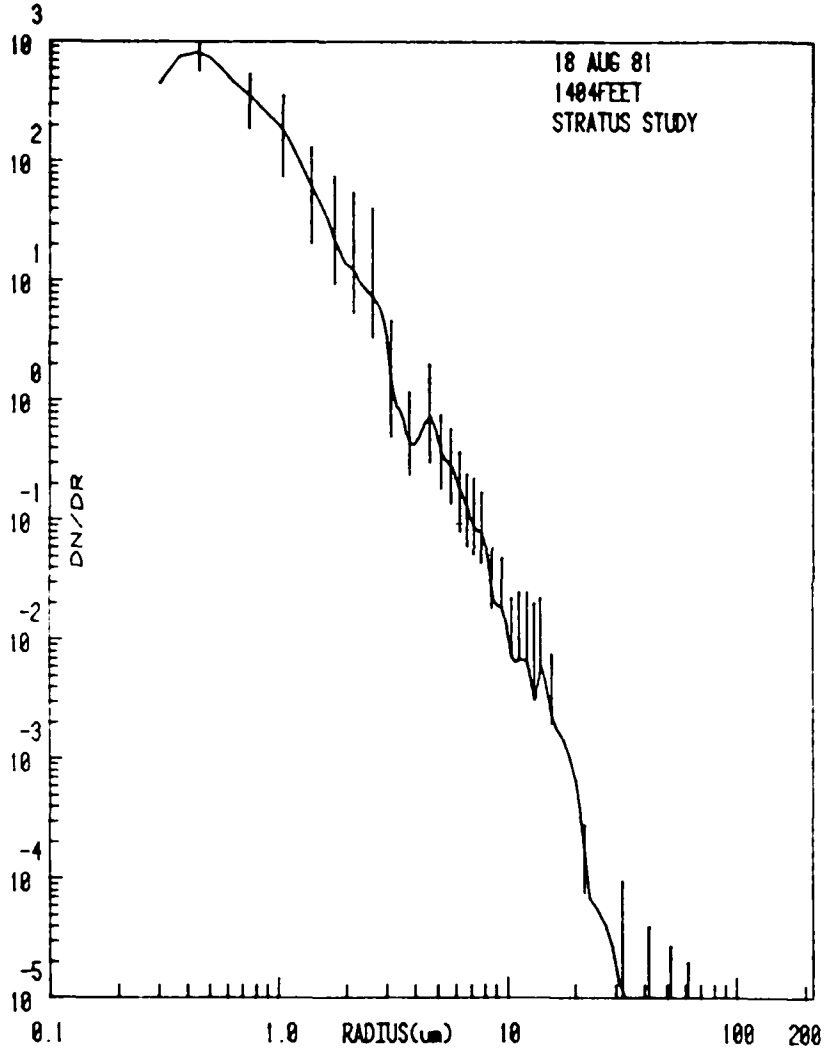

(h7)

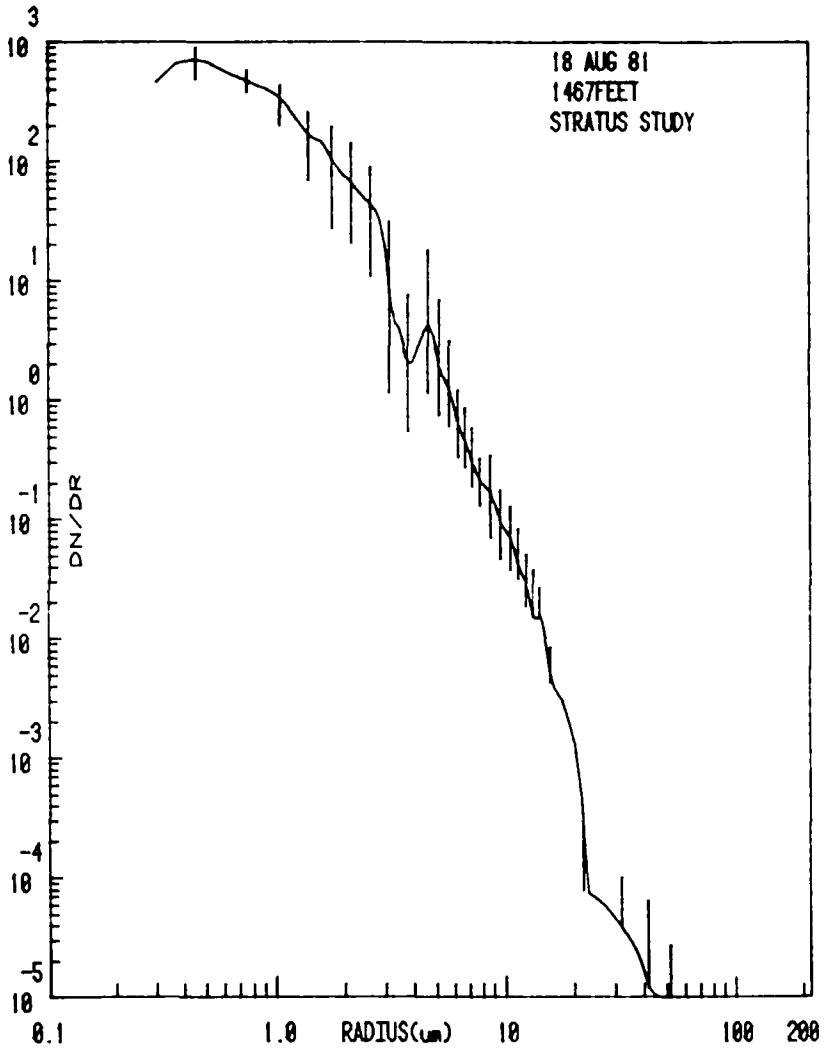

(h8)

Figure 3. Continued.

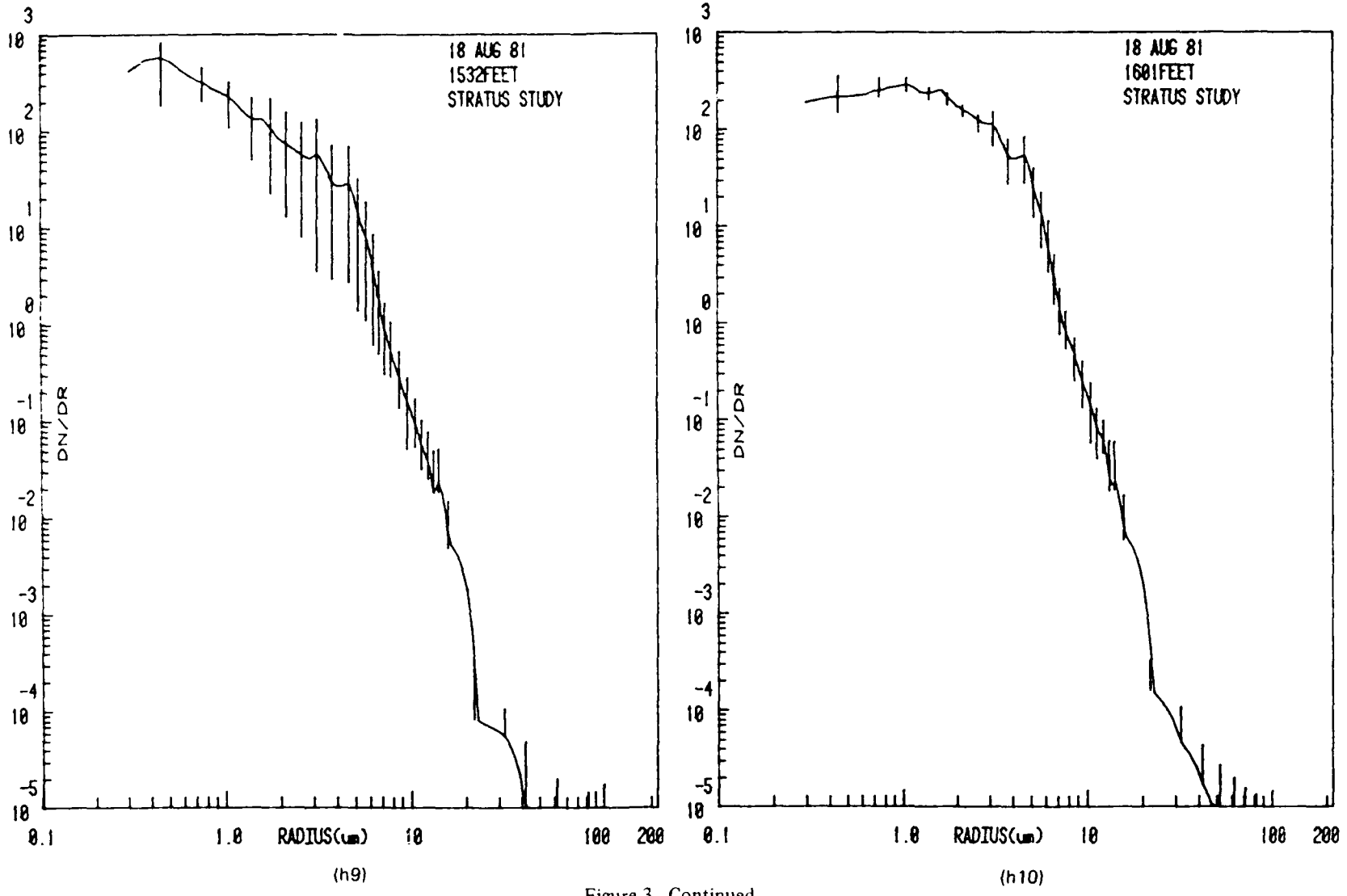

Figure 3. Continued.

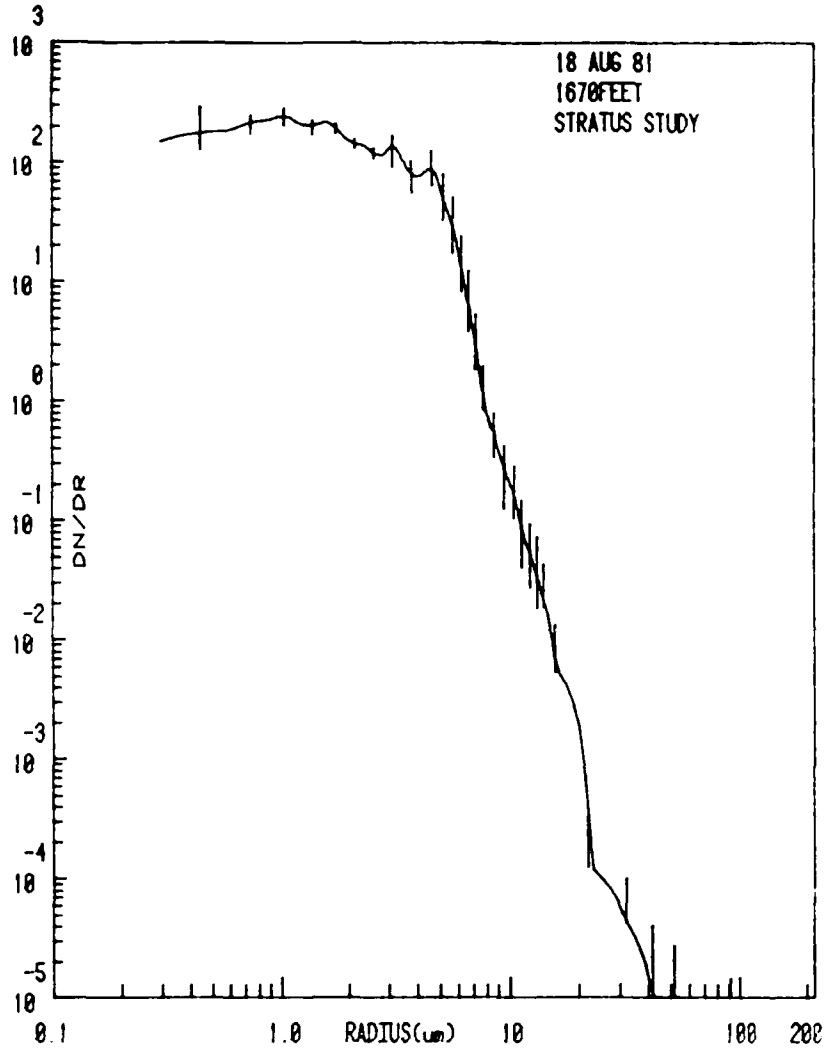

(h11)

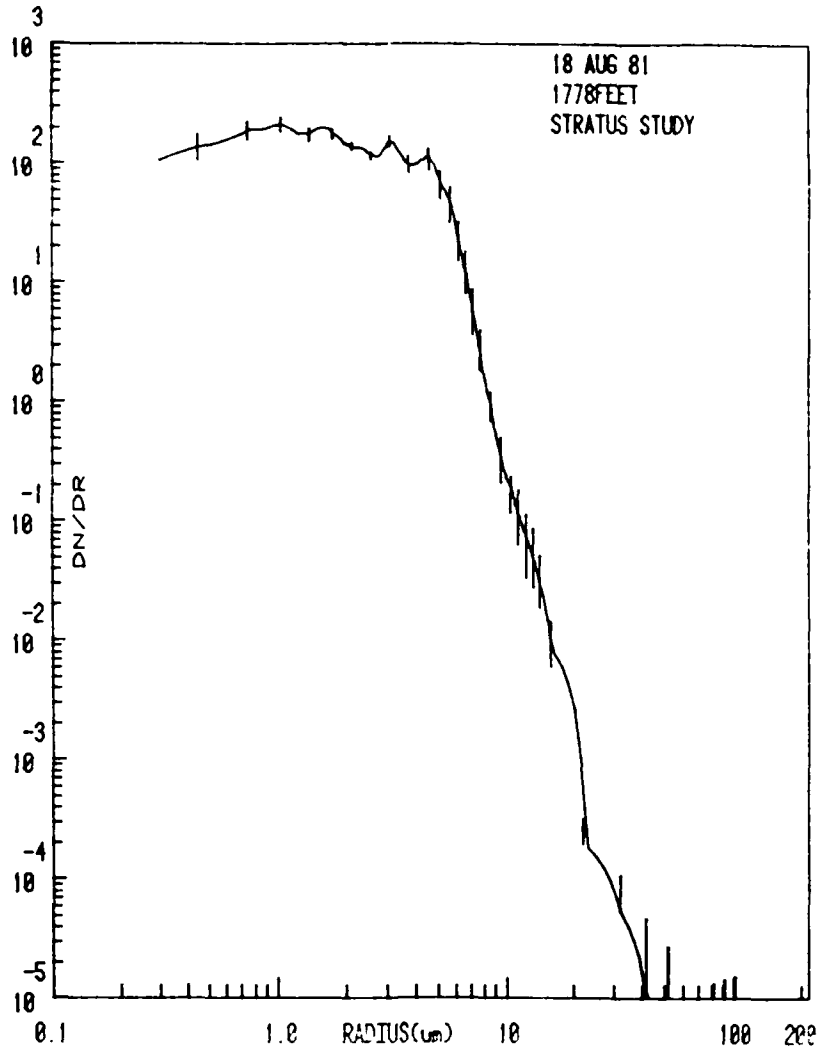

(h12)

Figure 3. Continued.

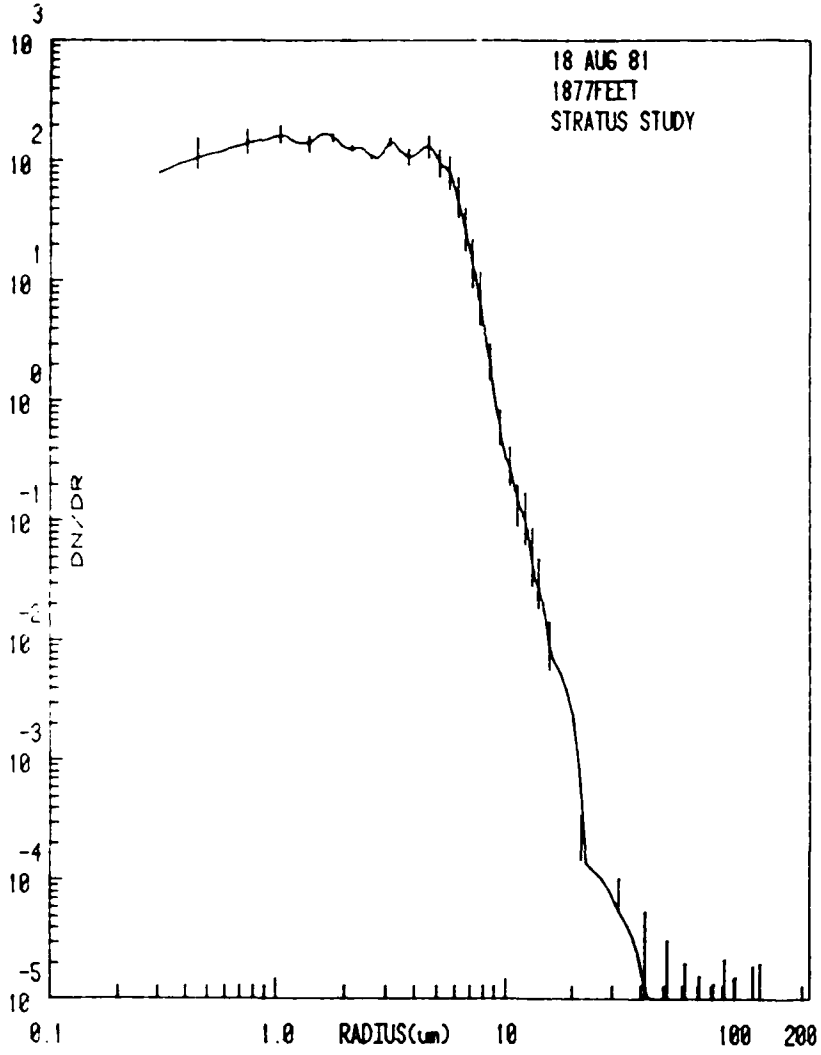

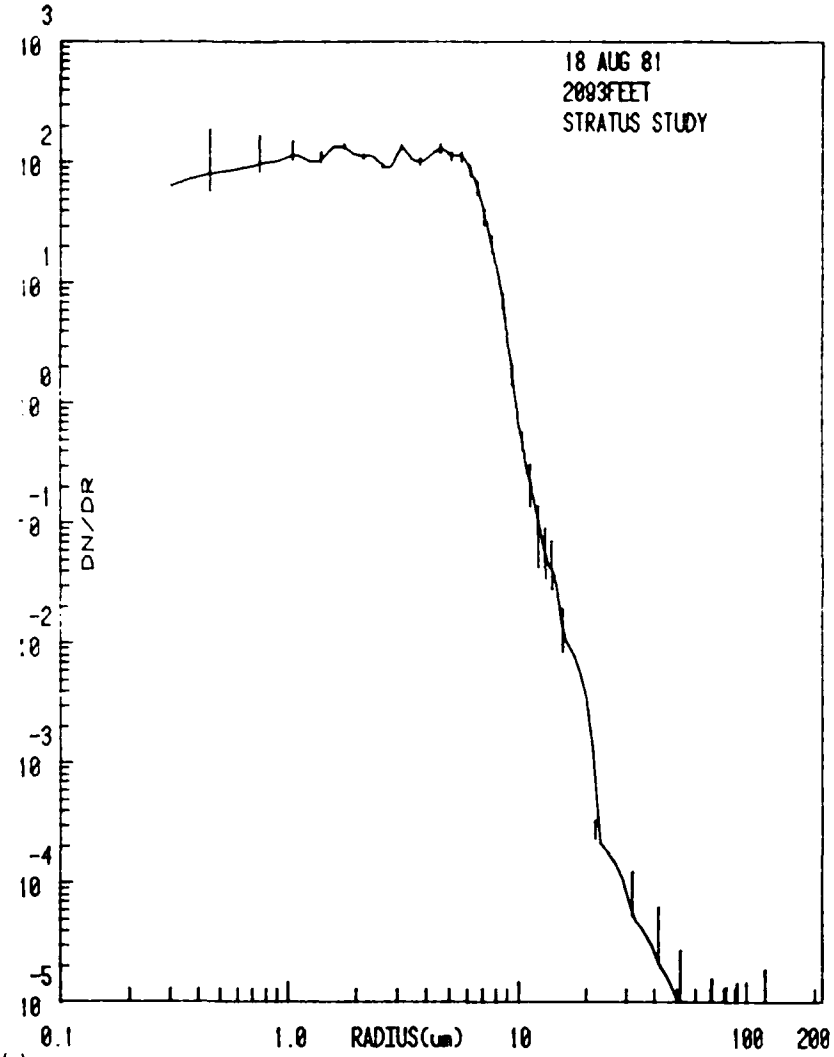

(g)

Figure 3. Continued.

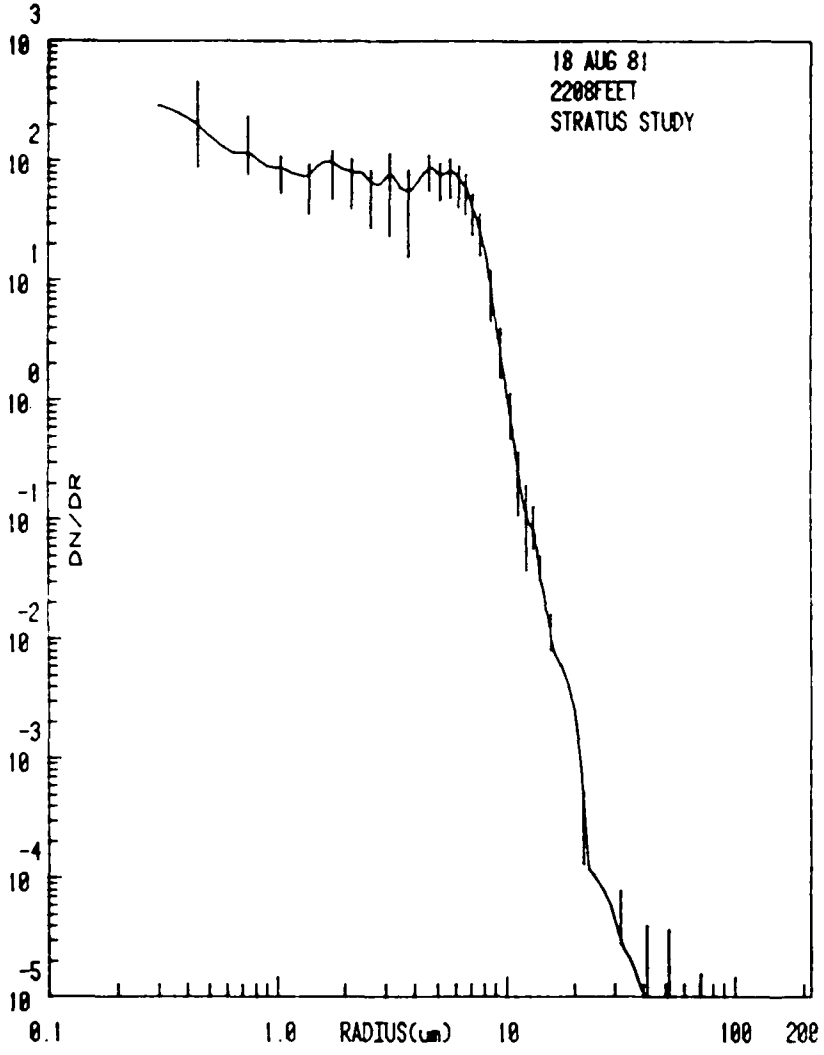

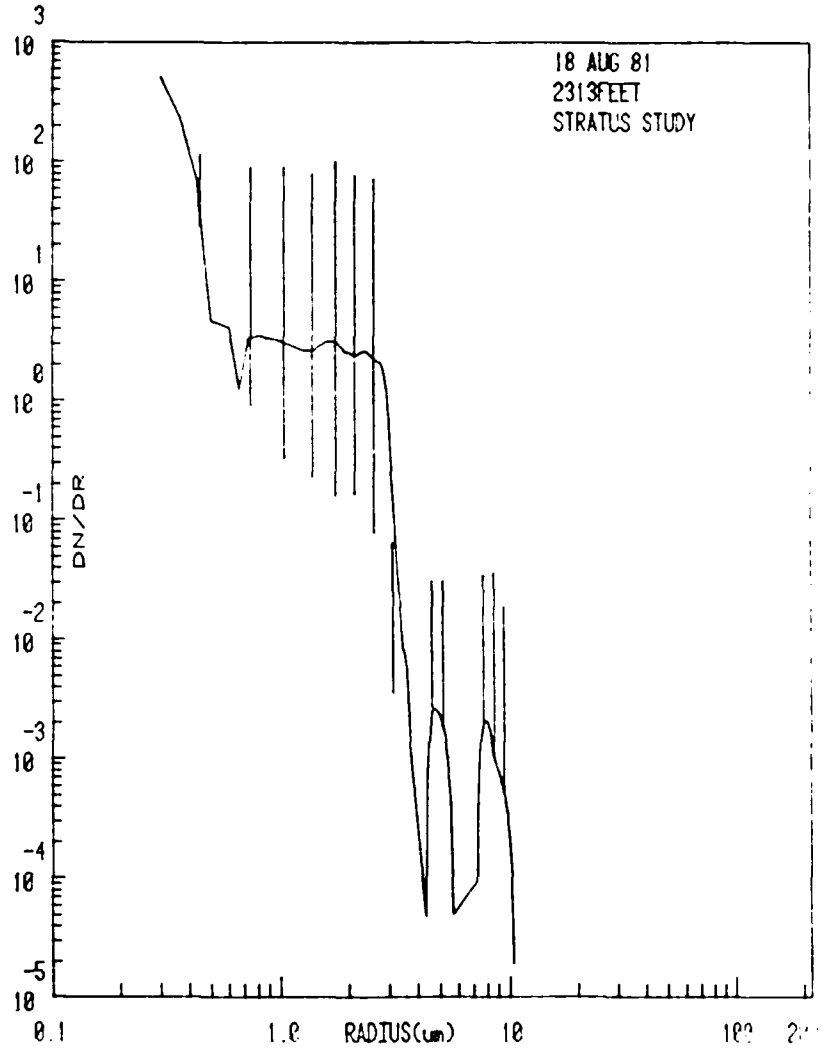

Figure 3. Continued.

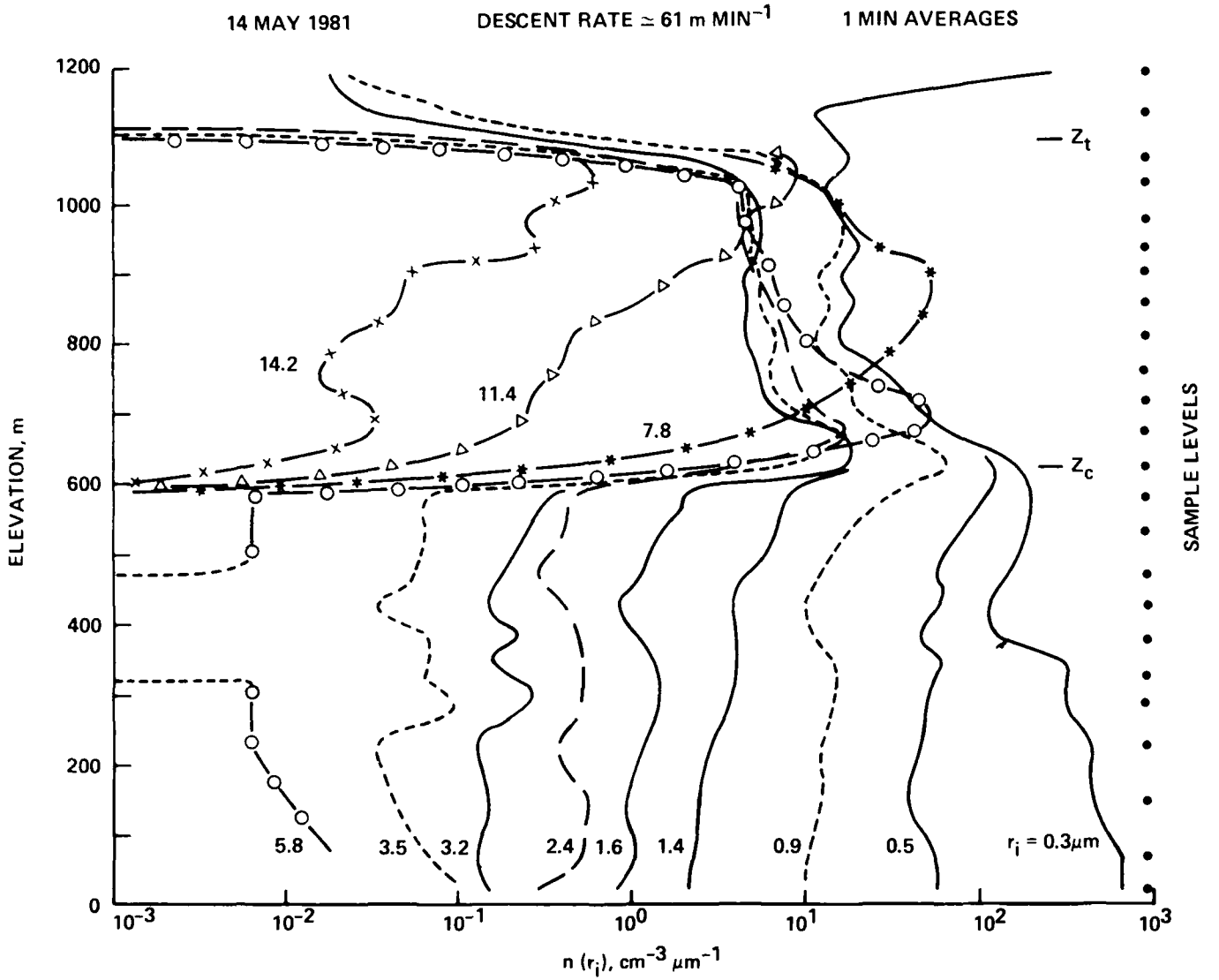

(a)

Figure 4. Aerosol spectral values (DN/DR, cm^{-3} μm^{-1}) for selected radii r_i as a function of elevation.

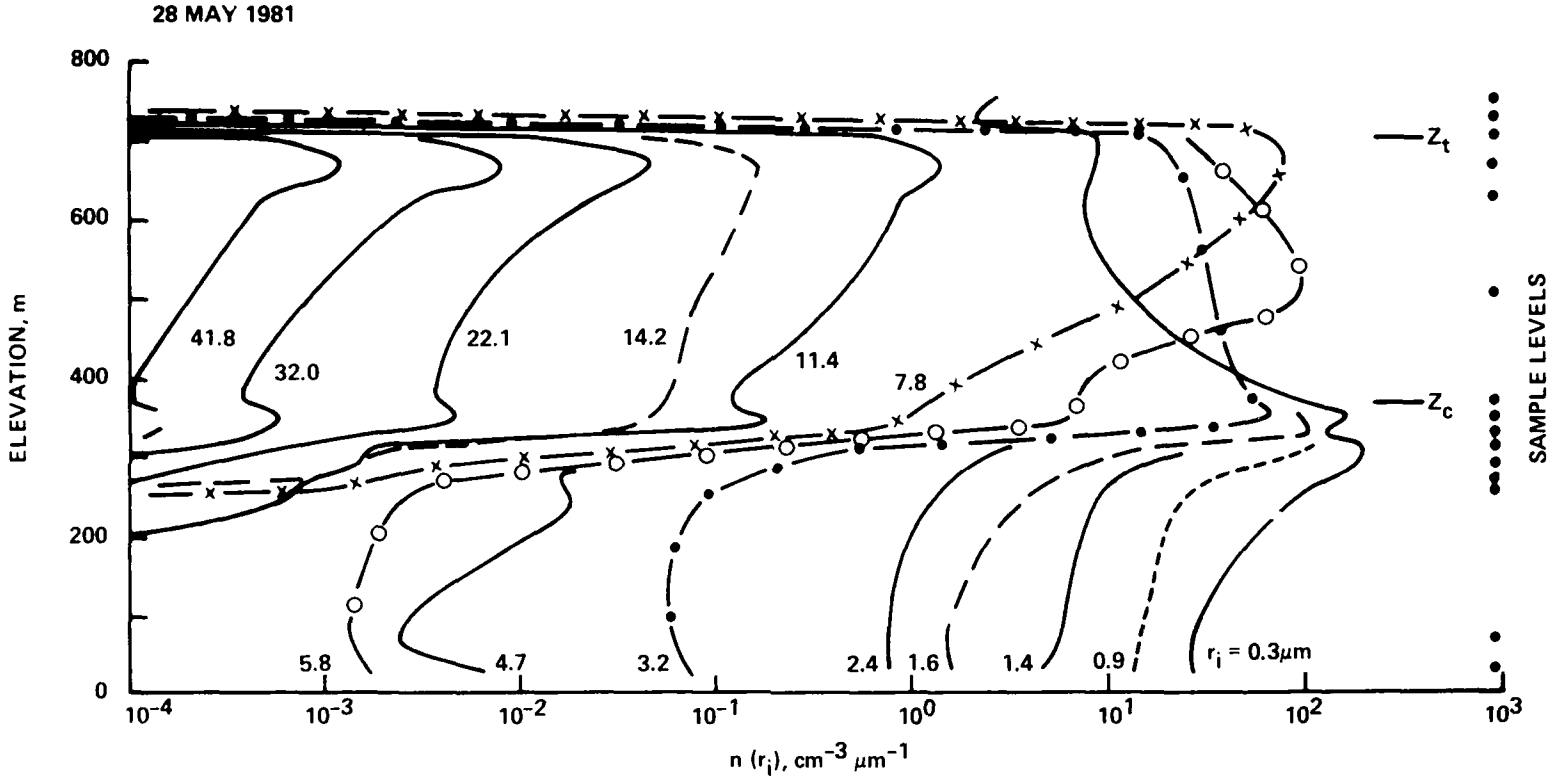

(b)

Figure 4. Continued.

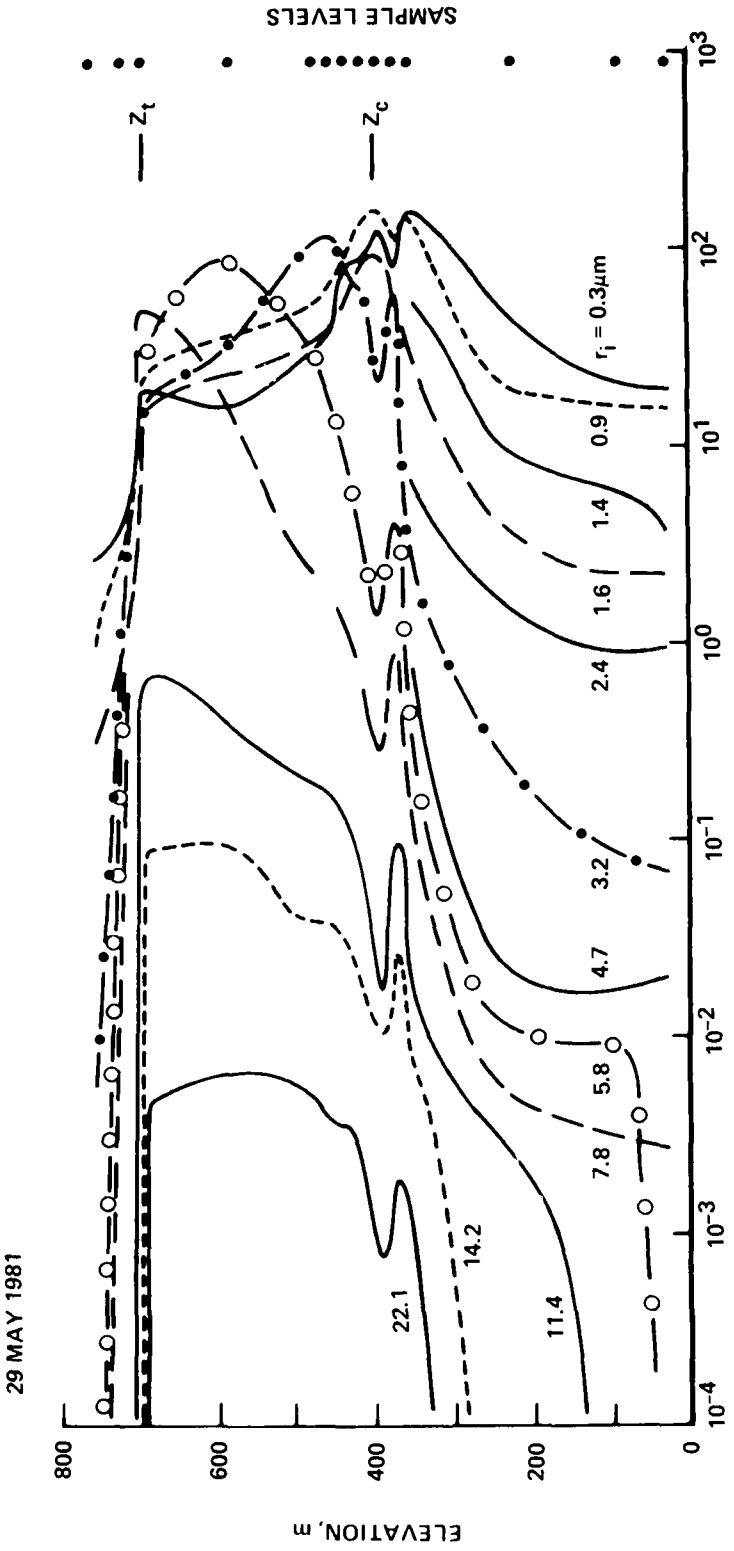

(c)

Figure 4. Continued.

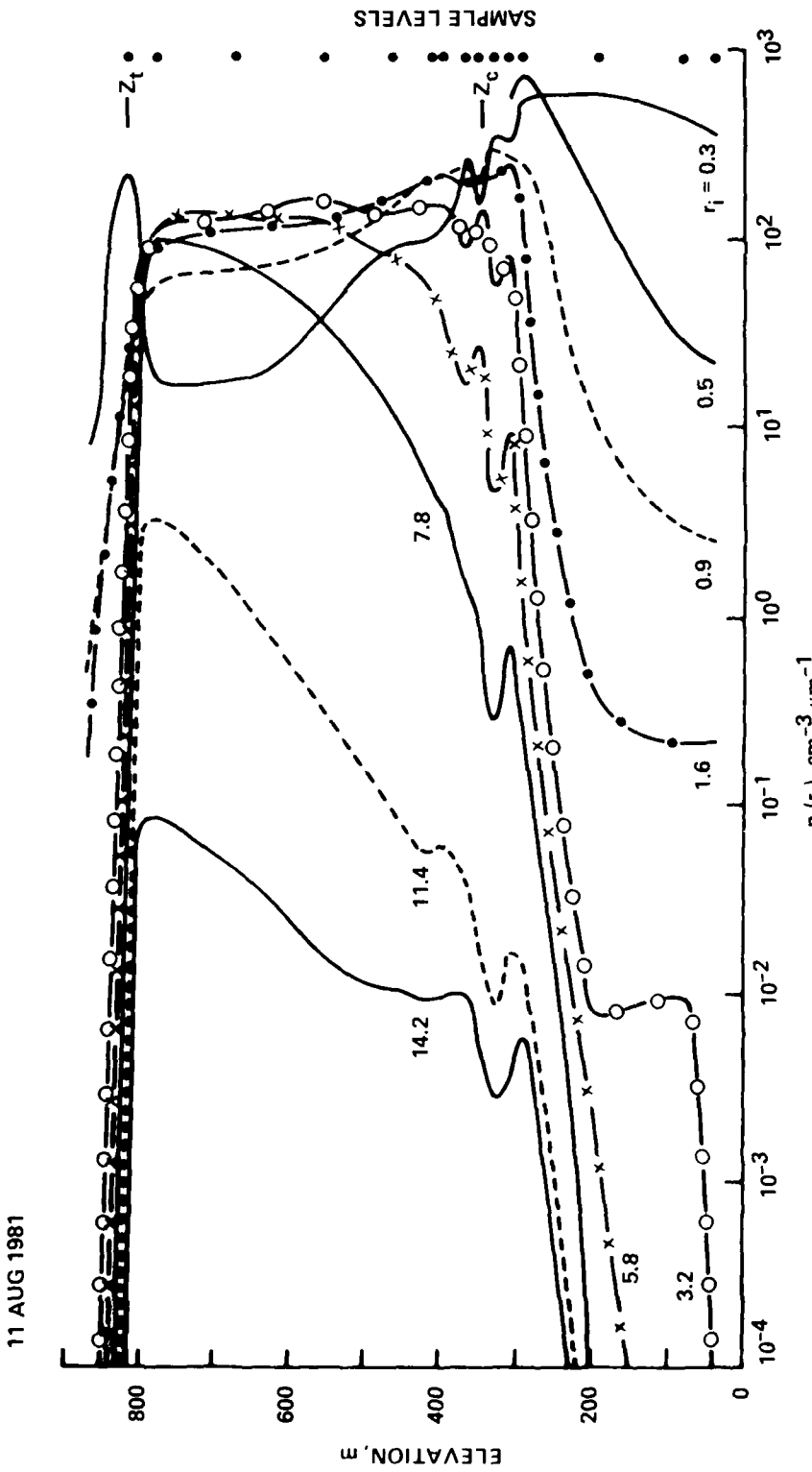

(d)

Figure 4. Continued.

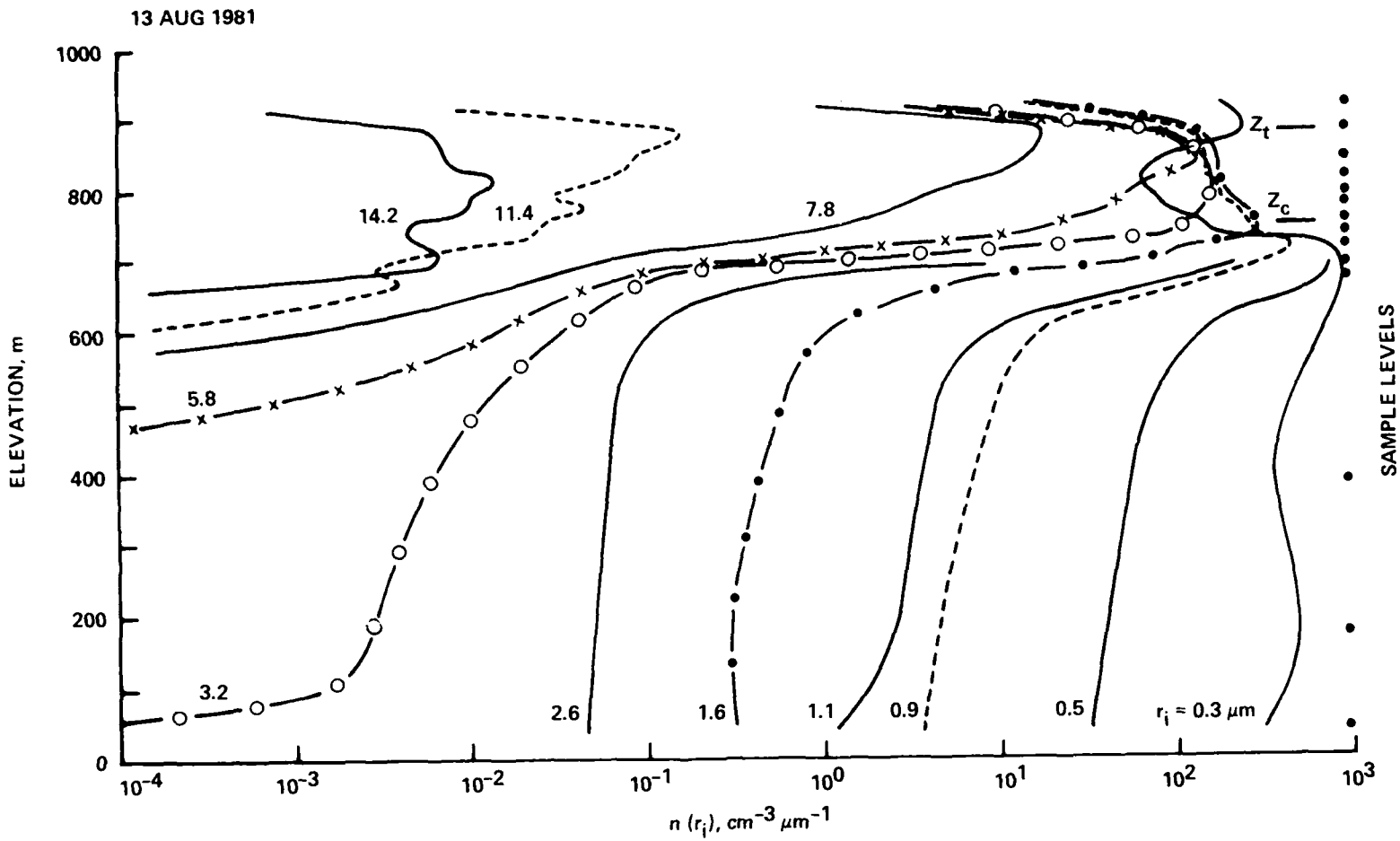

(e)

Figure 4. Continued.

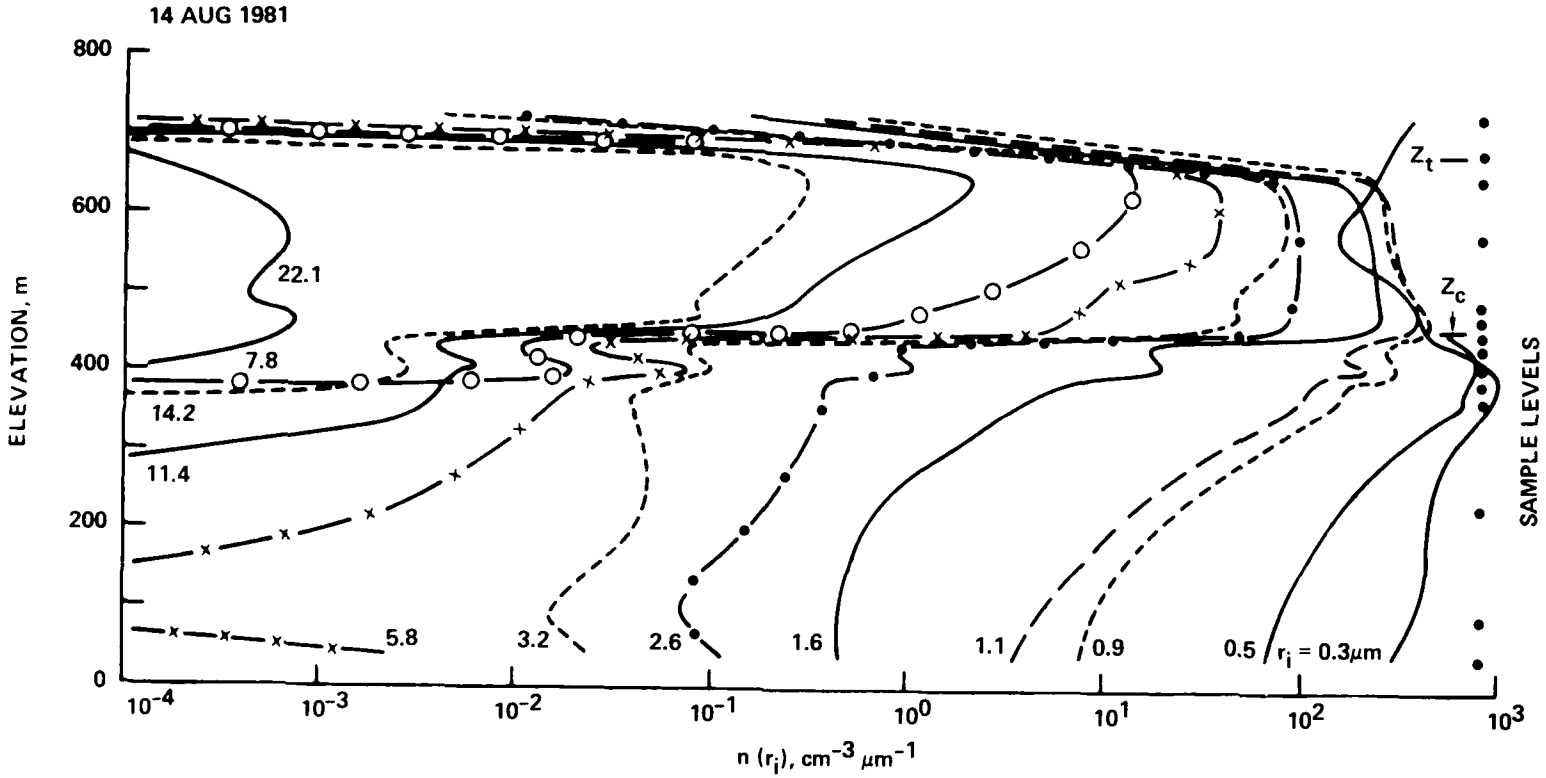

(f)

Figure 4. Continued.

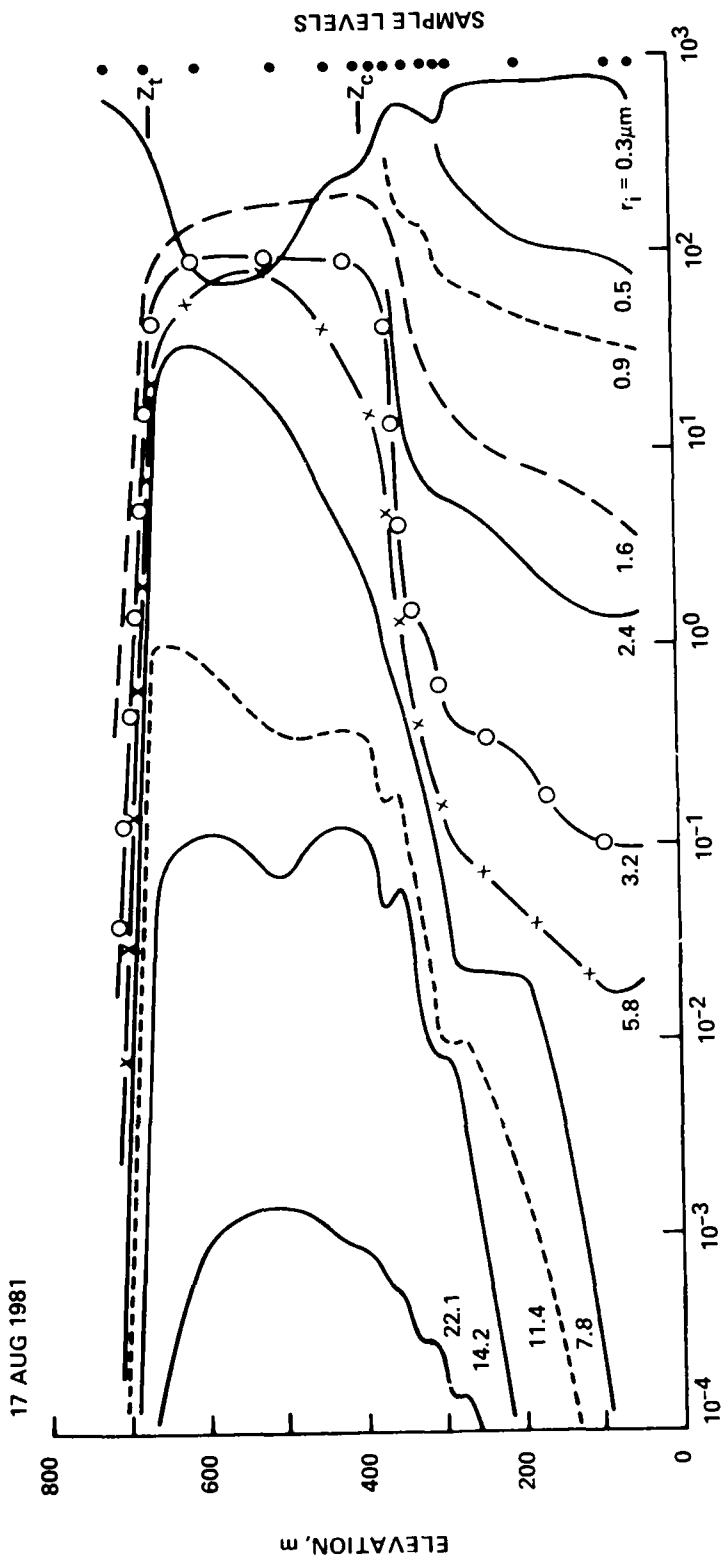

(g)

Figure 4. Continued.

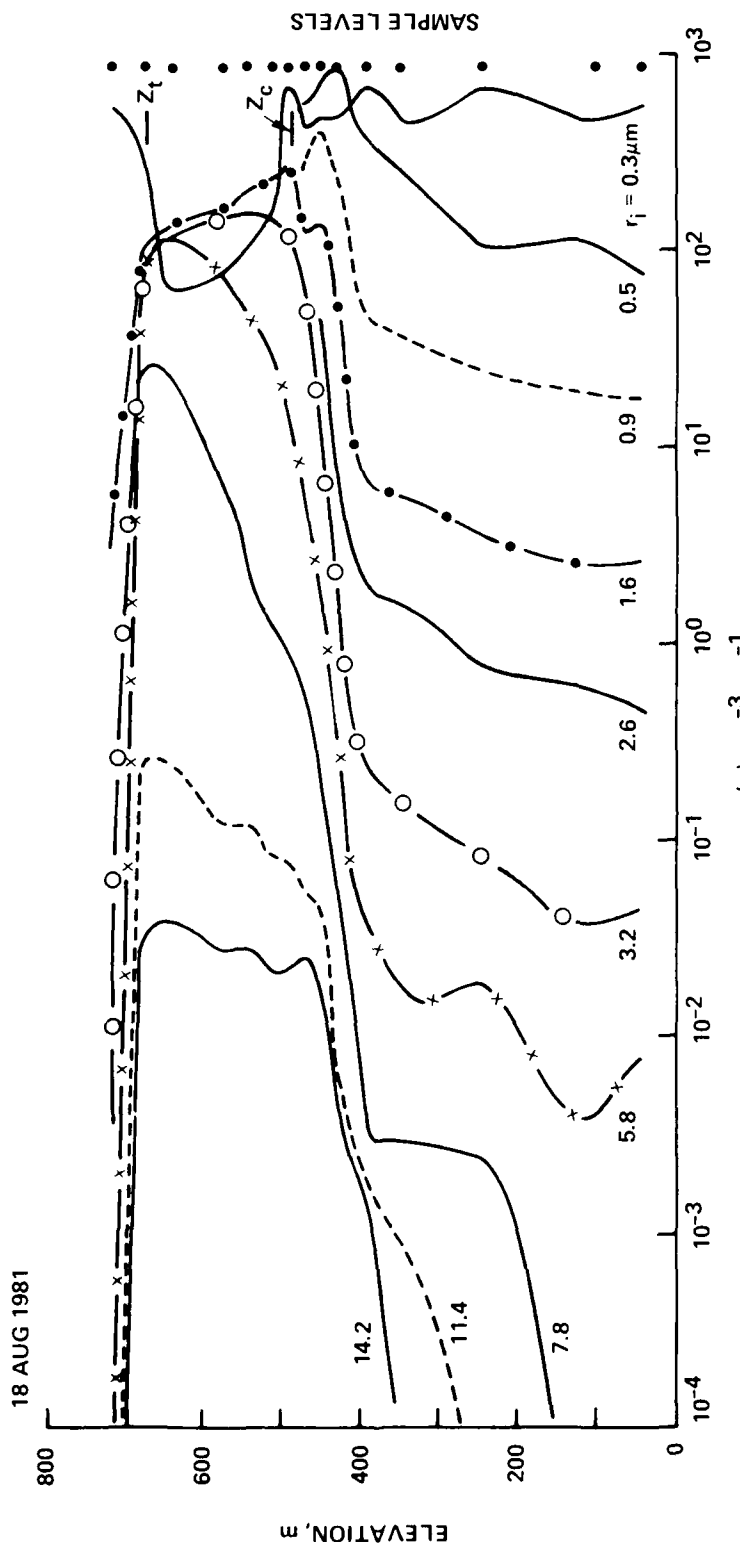

(h)

Figure 4. Continued.

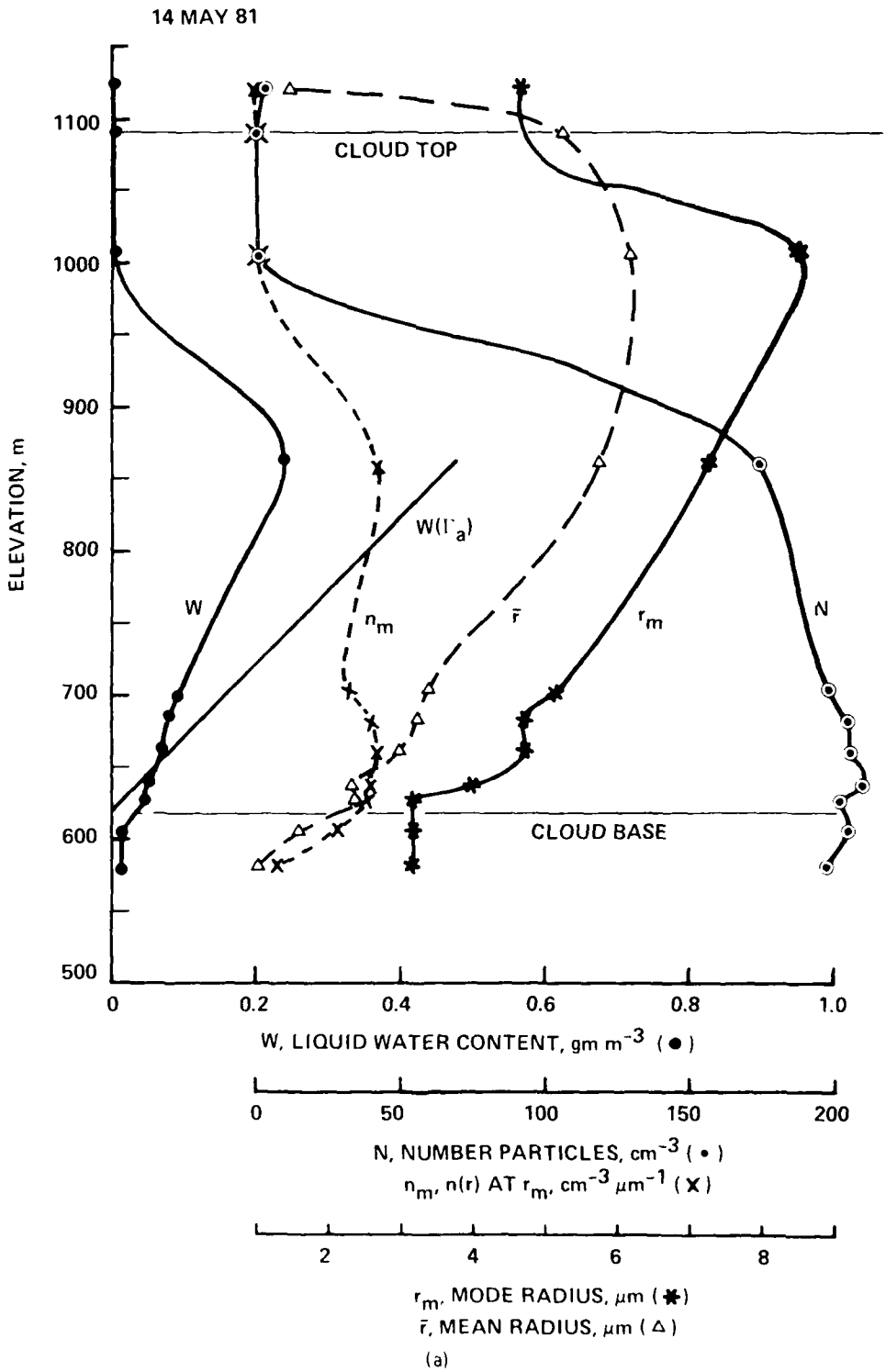

Figure 5. Vertical profile of aerosol spectral parameters. Data points are at sample levels.

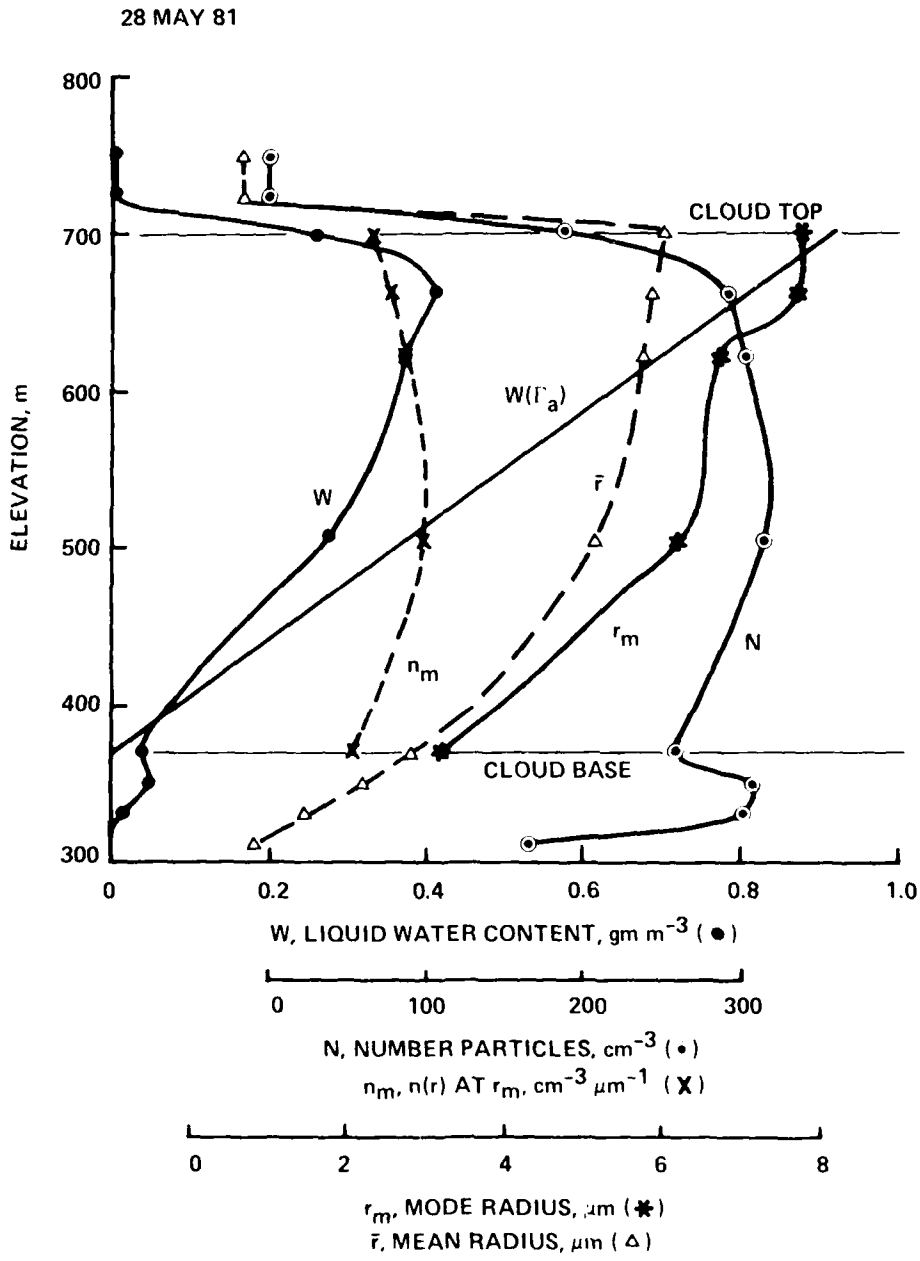

(b)

Figure 5. Continued.

AD-A169 168 AEROSOL AND HUMIDITY STRUCTURE BENEATH MARITIME STRATUS CLOUDS: 1981 DATA(U) NAVAL OCEAN SYSTEMS CENTER SAN DIEGO CA V R NOONKESTER 03 MAY 82 NOSC/TR-783 2/2

UNCLASSIFIED F/G 4/2 NL

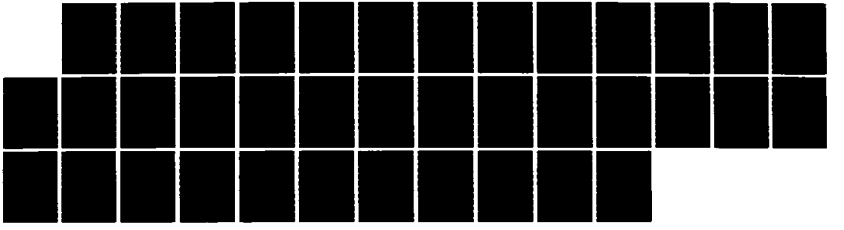

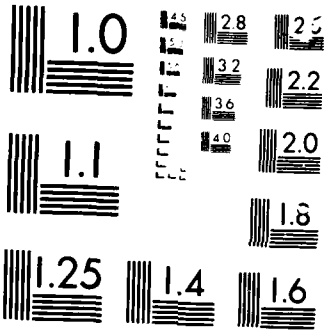
1.0
1.1
1.25
1.4
1.6
1.8
2.0
2.2
2.5
2.8
3.2
3.6
4.0

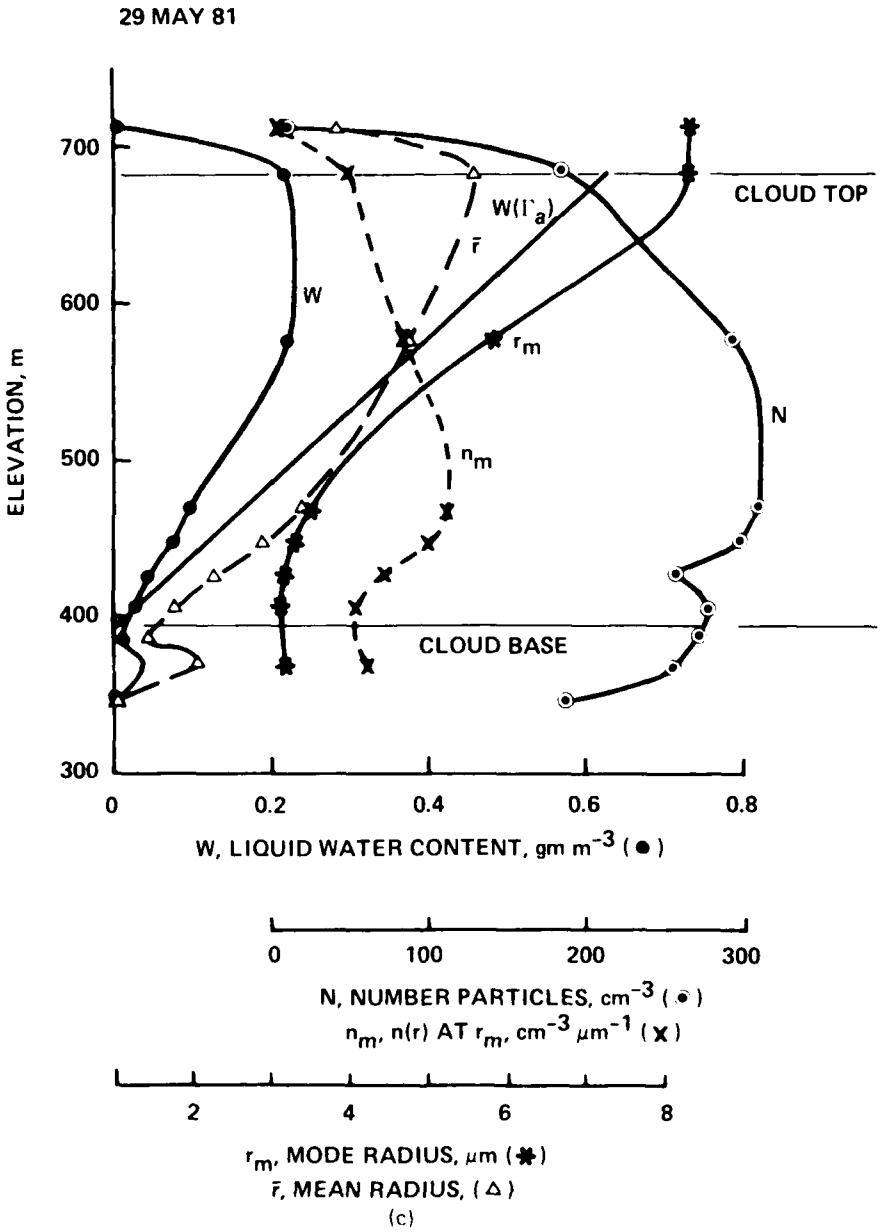

(c)

Figure 5. Continued.

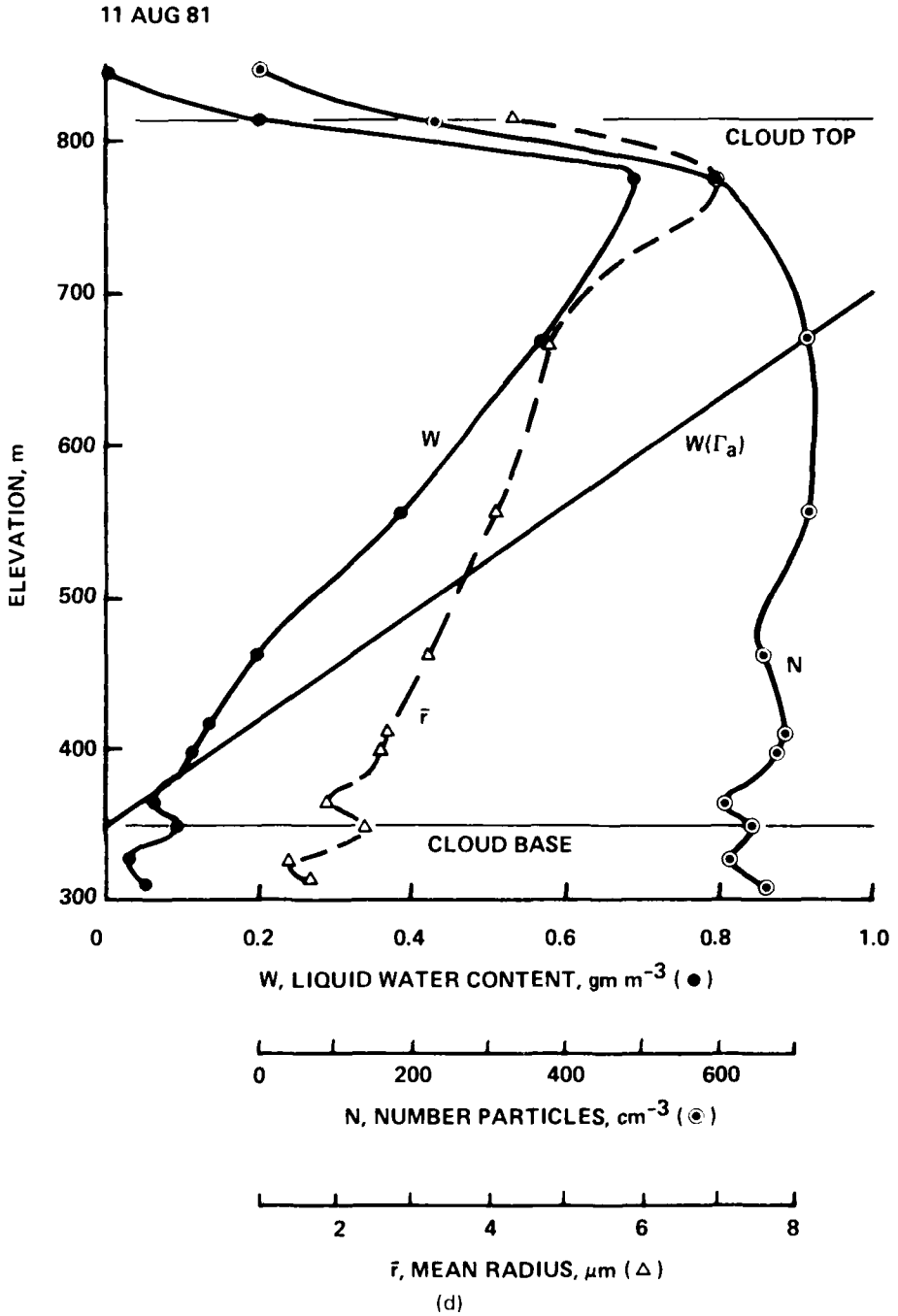

(d)

Figure 5. Continued.

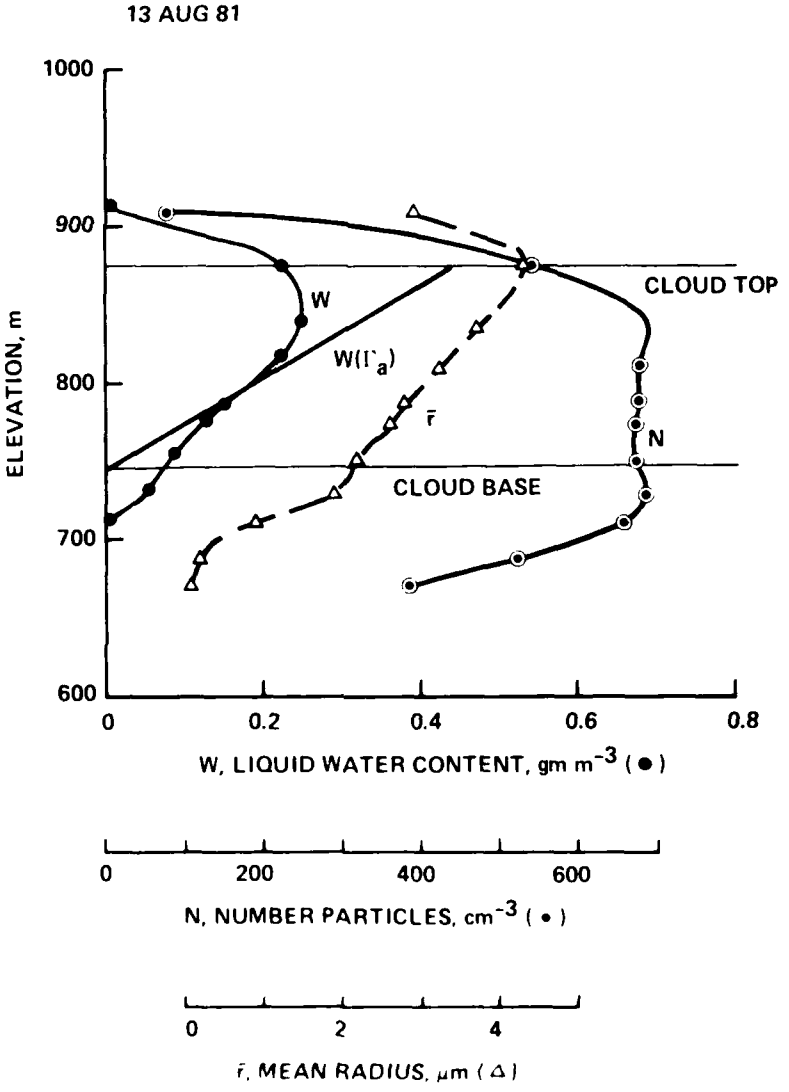

(e)

Figure 5. Continued

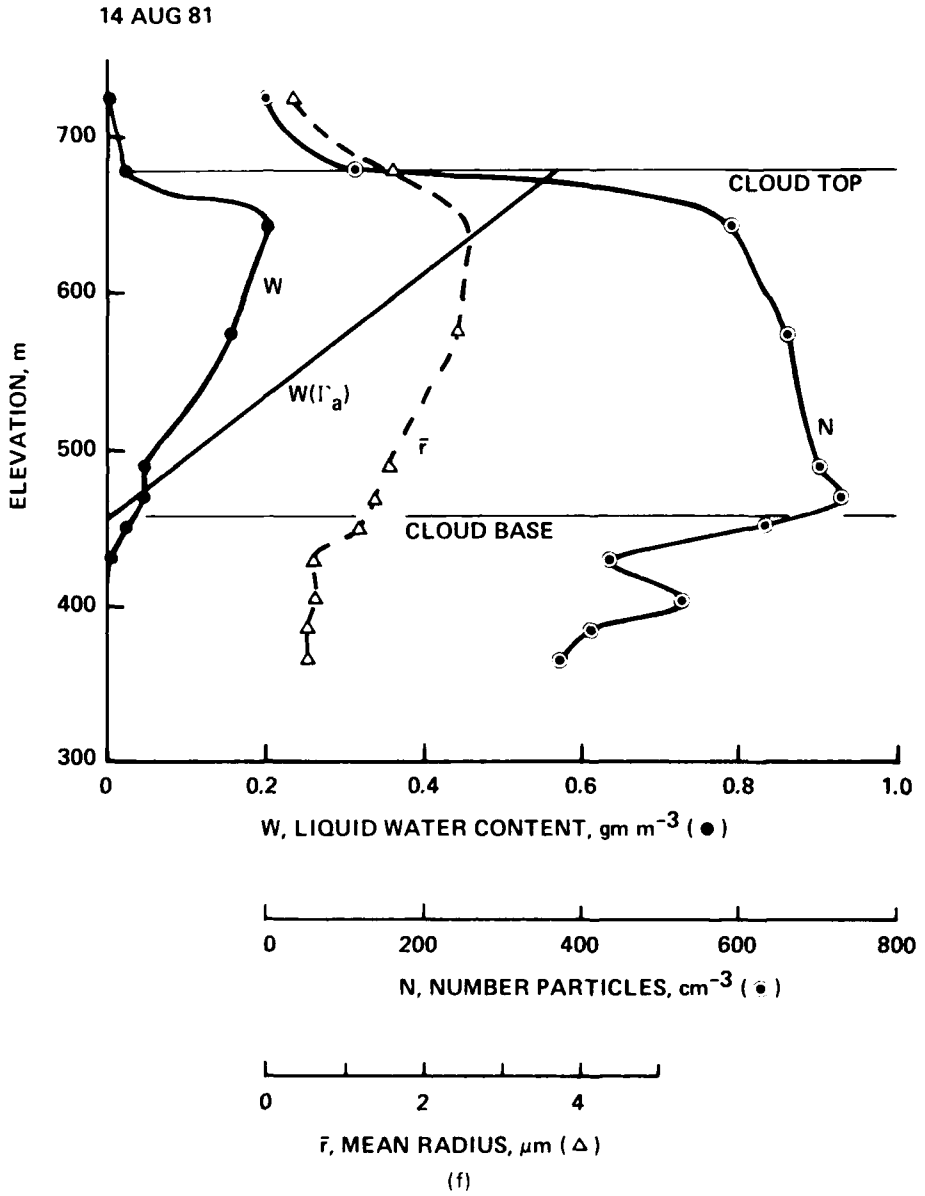

Figure 5. Continued.

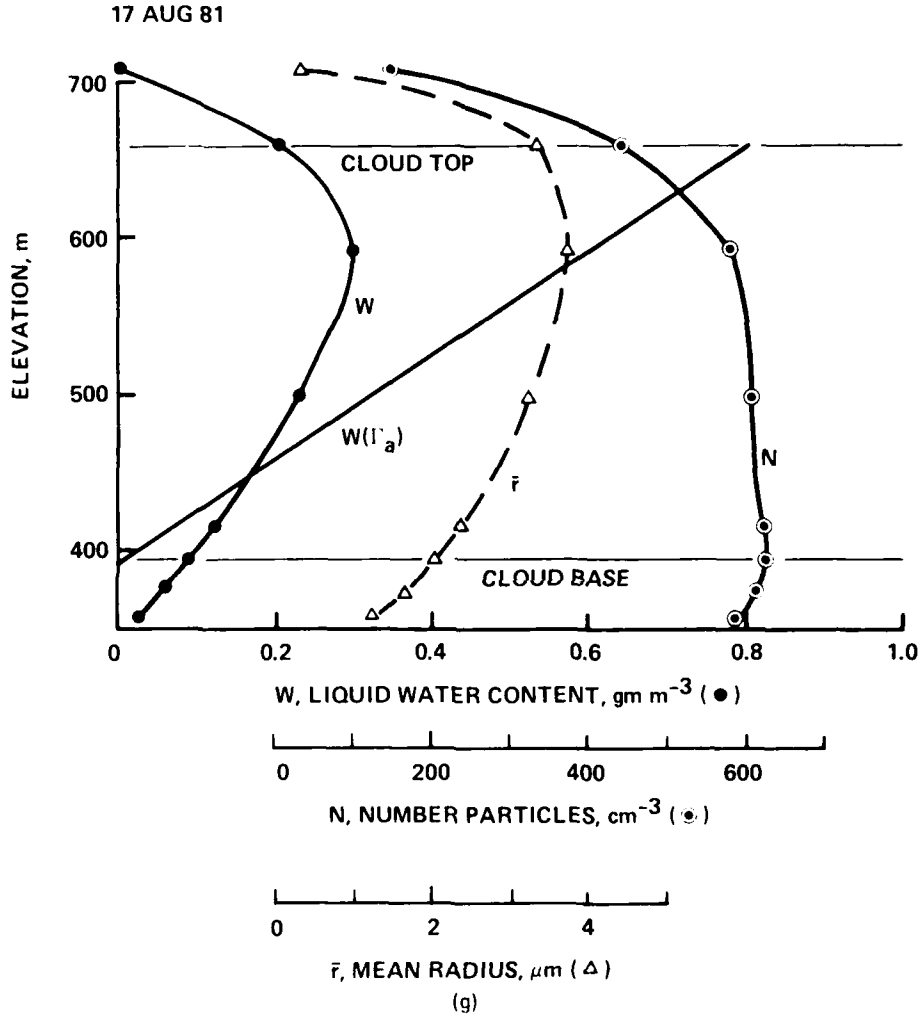

(g)

Figure 5. Continued.

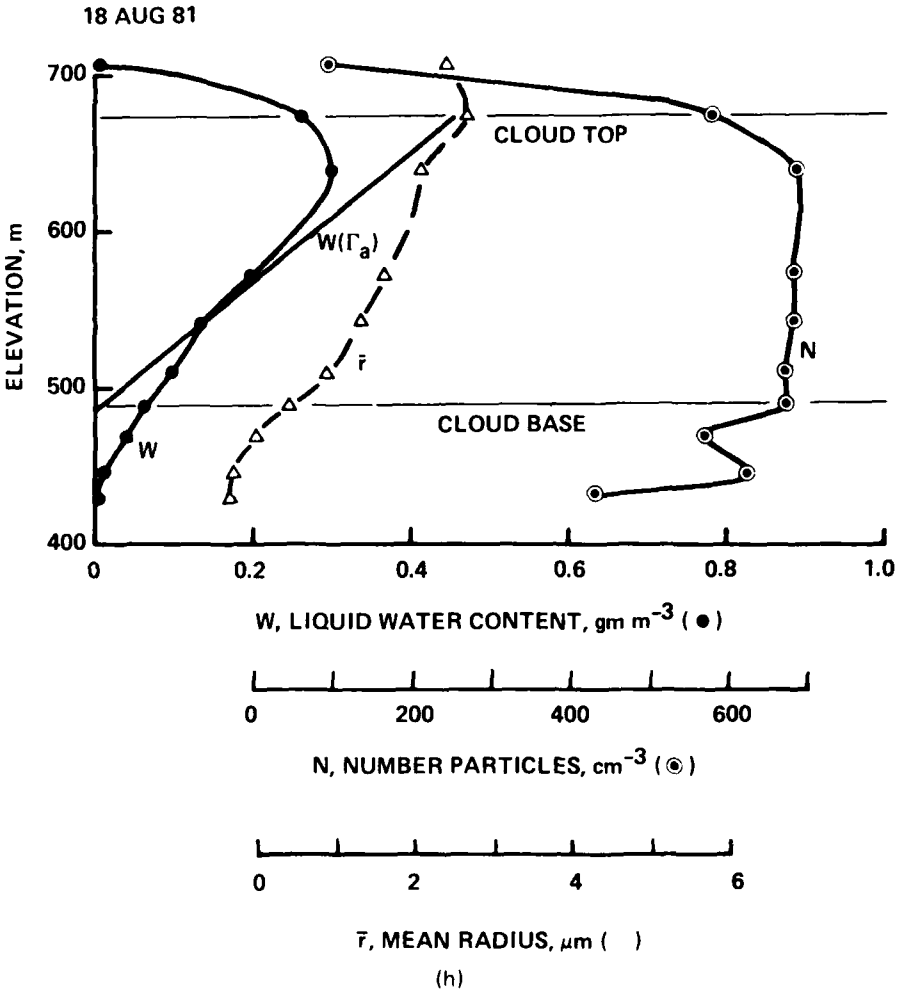

(h)

Figure 5. Continued.

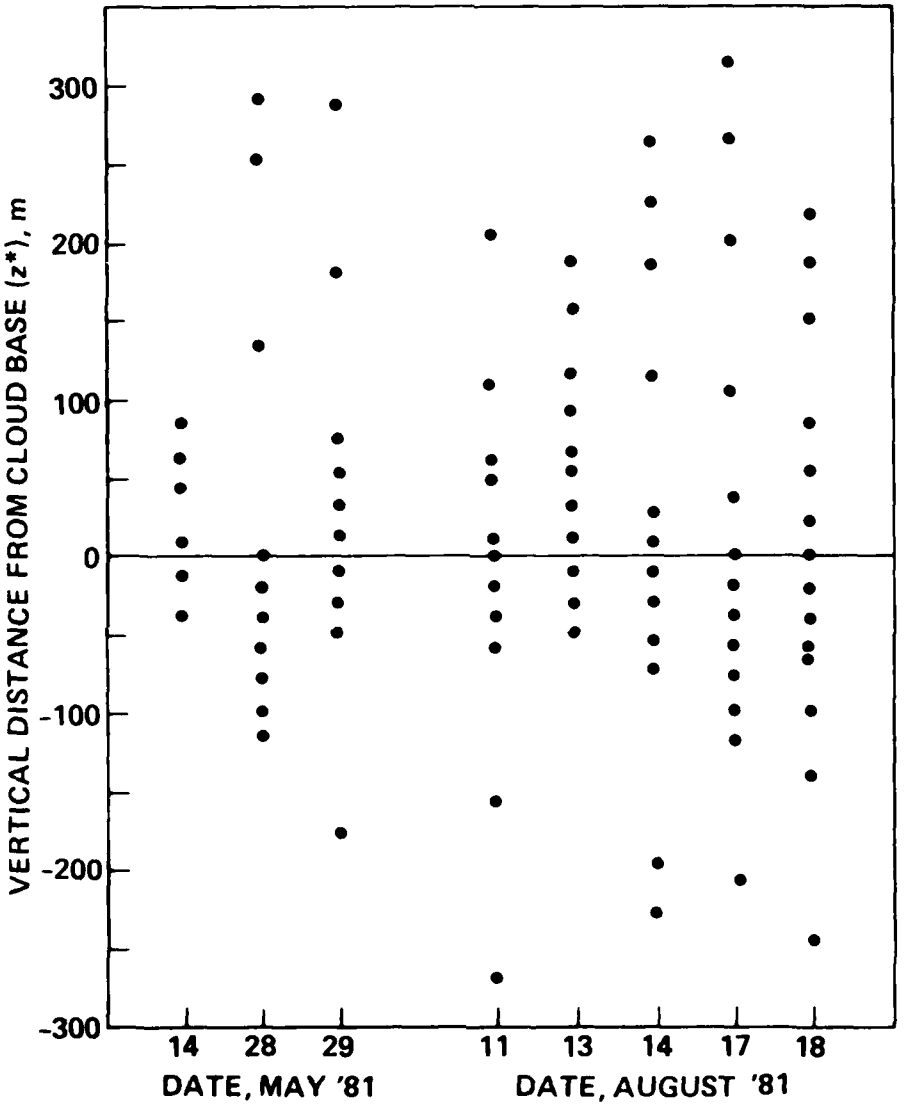

Figure 6. Elevation of horizontal measurement runs relative to the cloud base height.

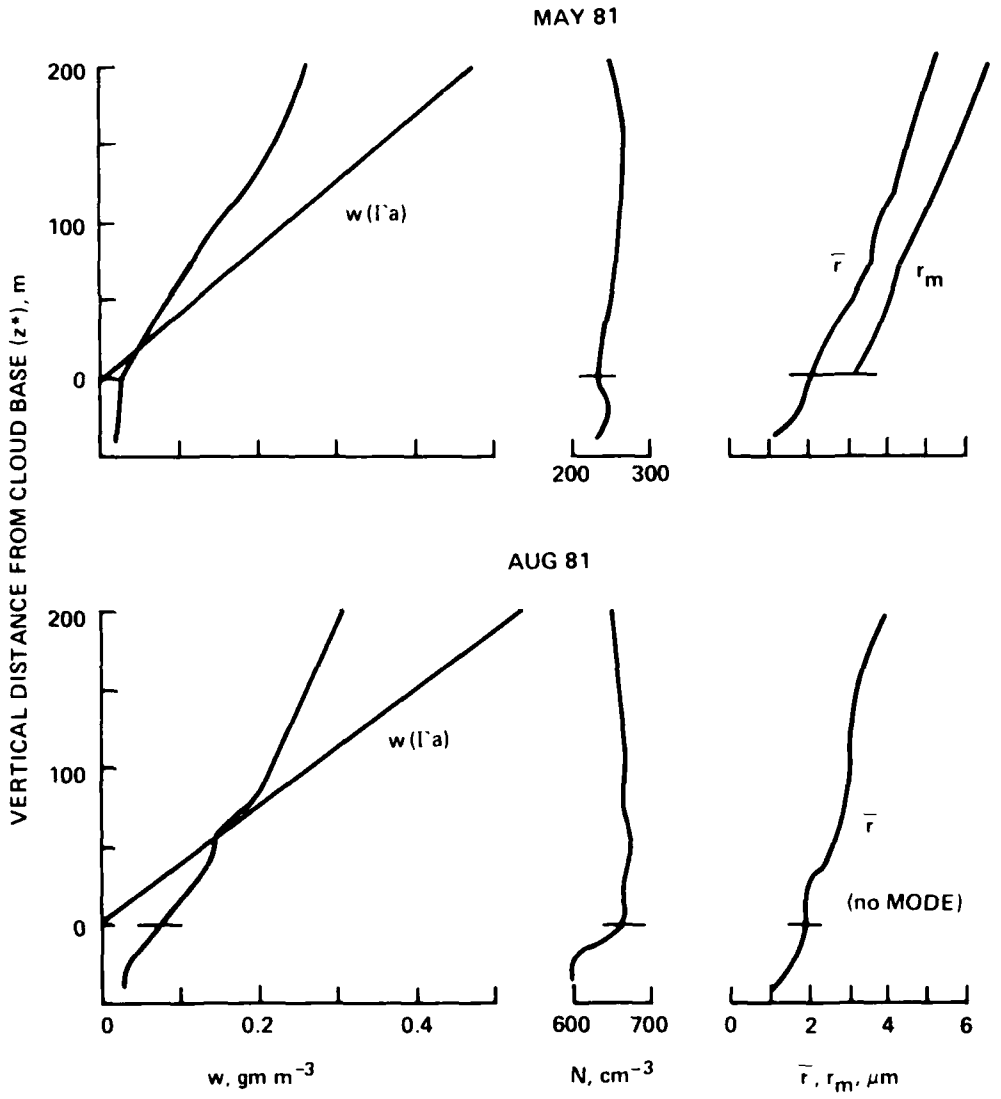

Figure 7. Vertical profile of aerosol spectral parameters in the cloud region averaged for the May and August days. $W(\Gamma_a)$ is for moist adiabatic changes.

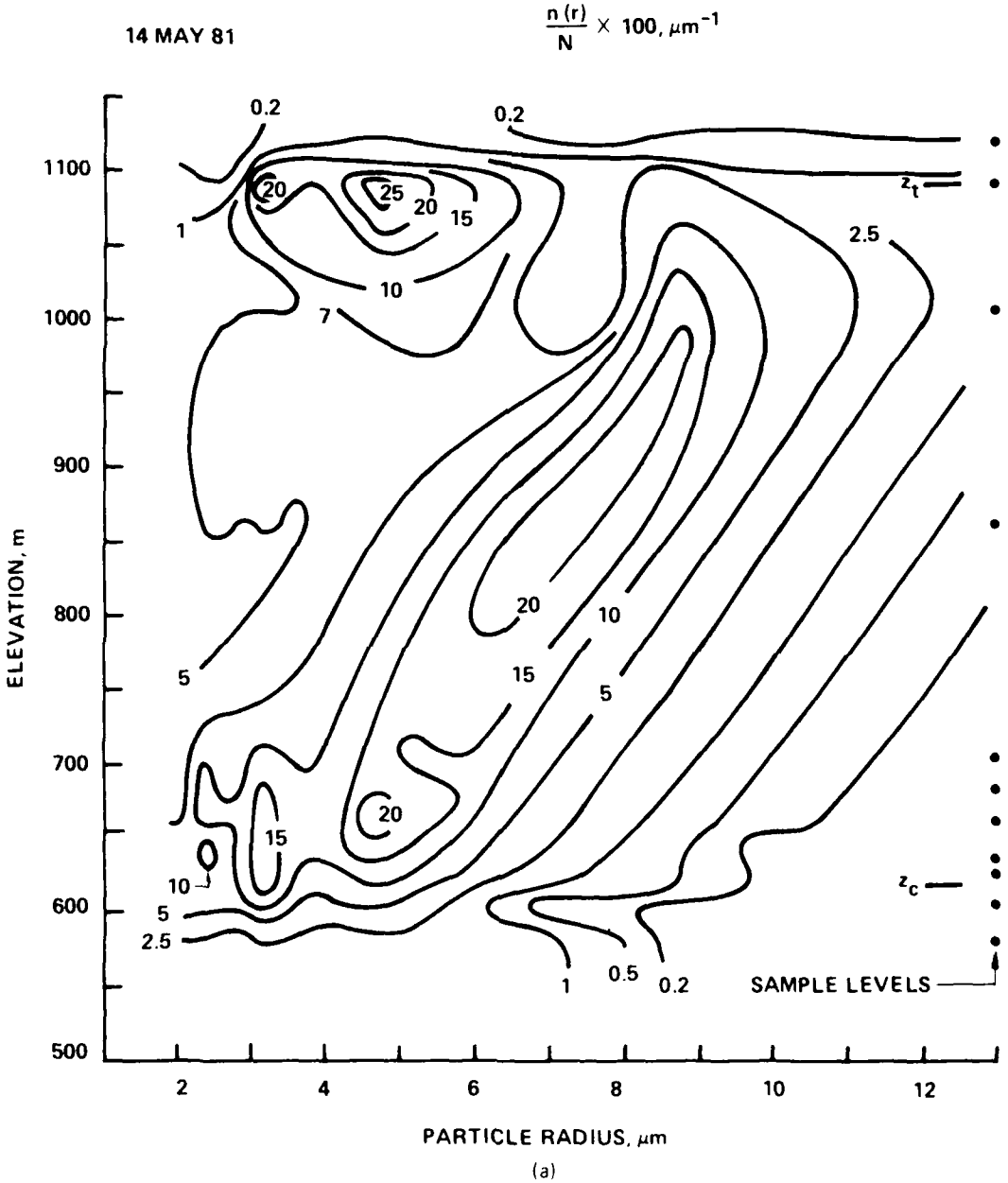

(a)

Figure 8. Isopleths of (n(r) N) x 100 in the cloud region.

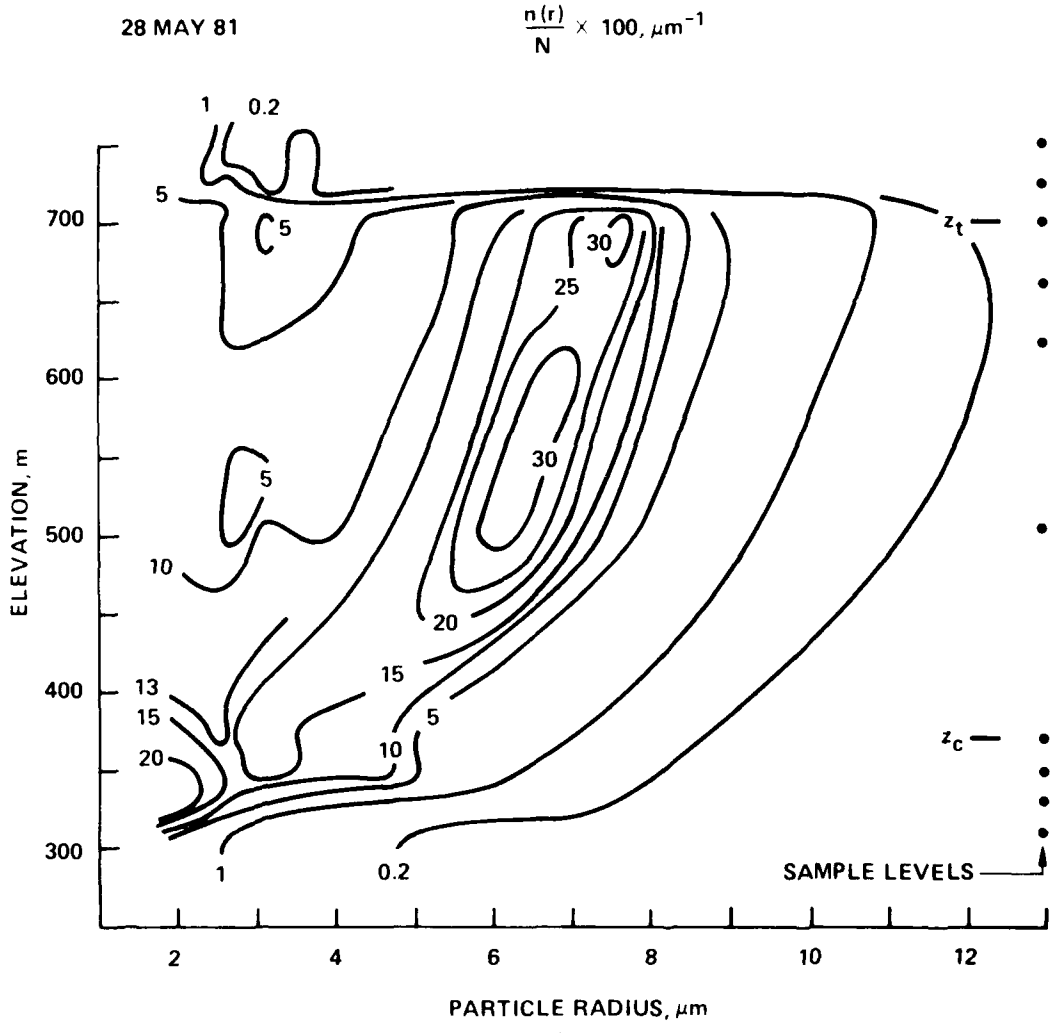

(b)

Figure 8. Continued.

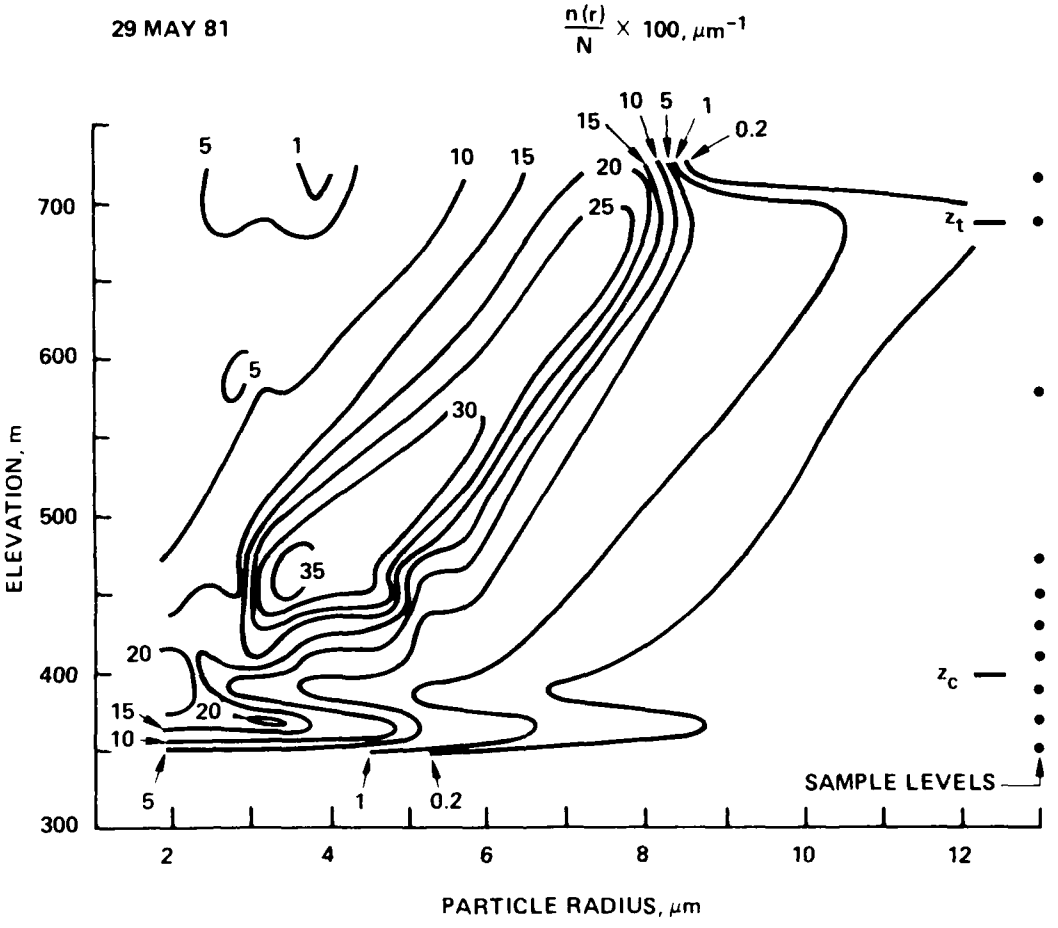

(c)

Figure 8. Continued.

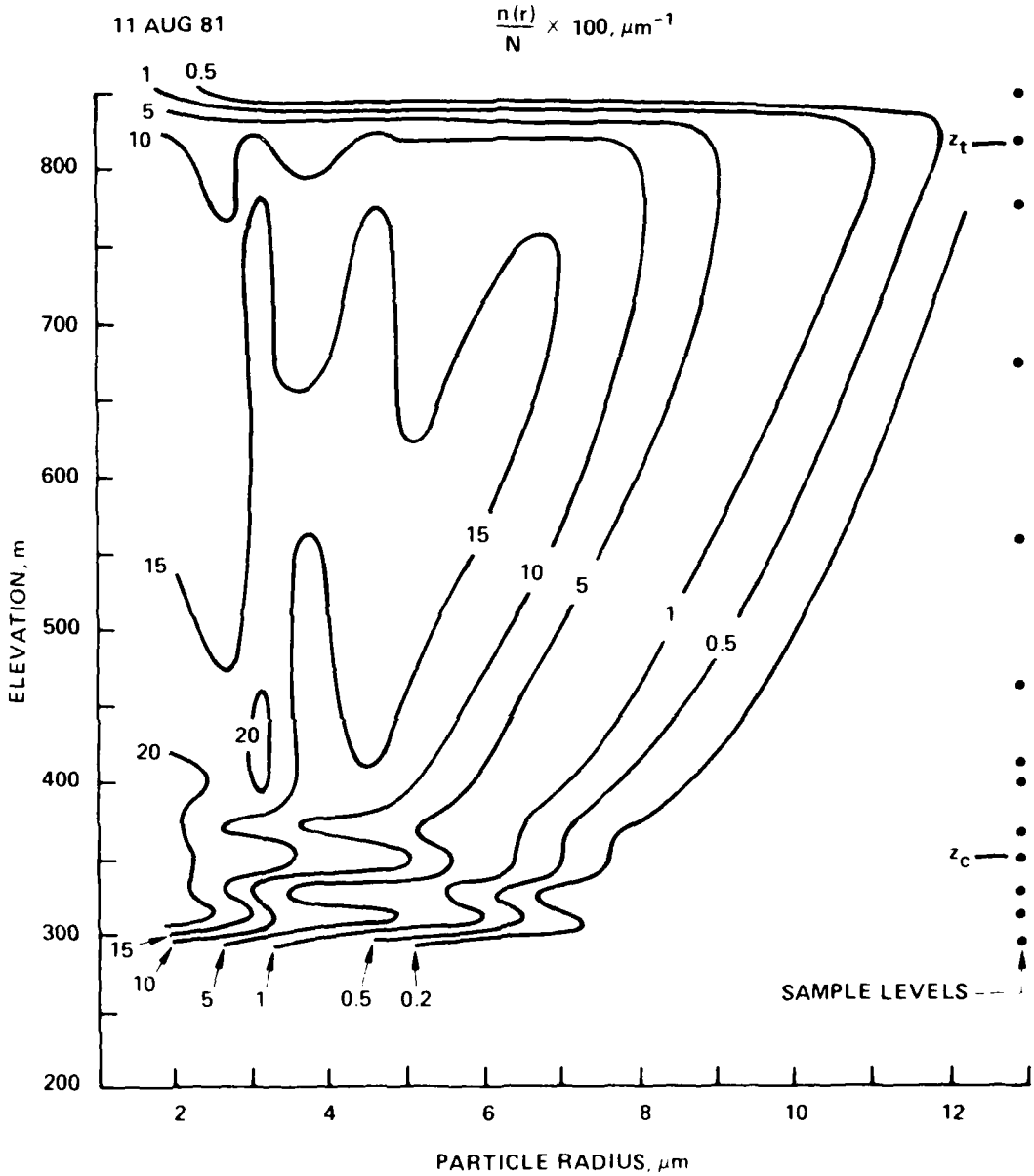

(d)

Figure 5. Continued

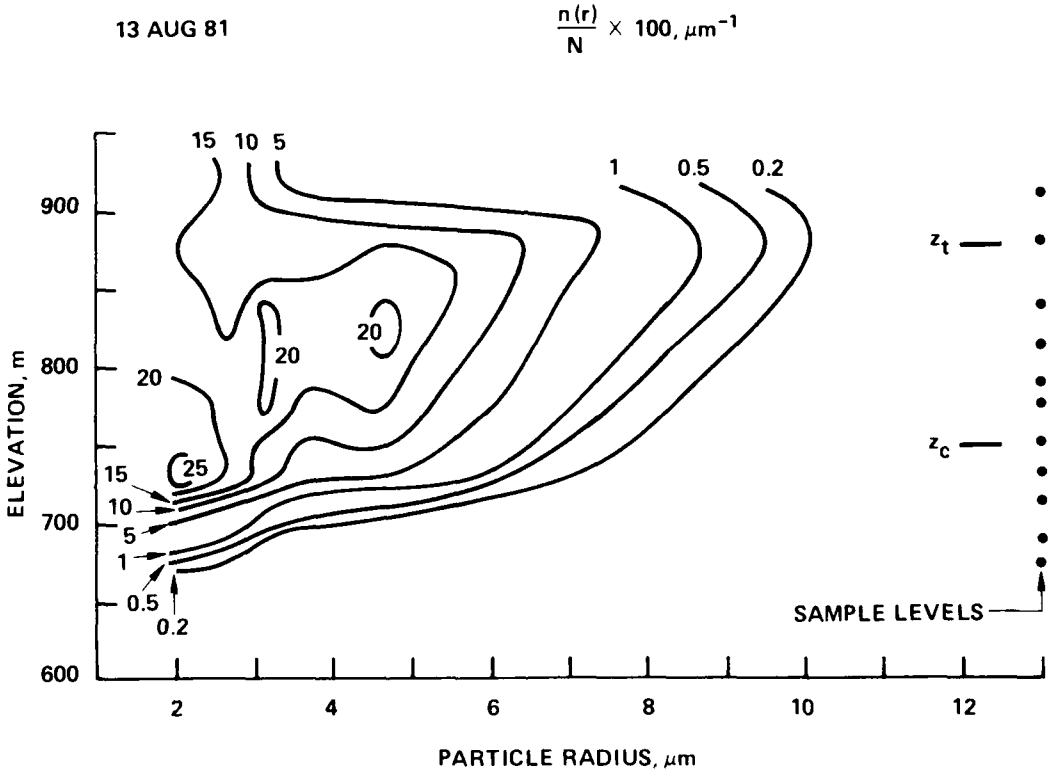

(e)

Figure 8. Continued.

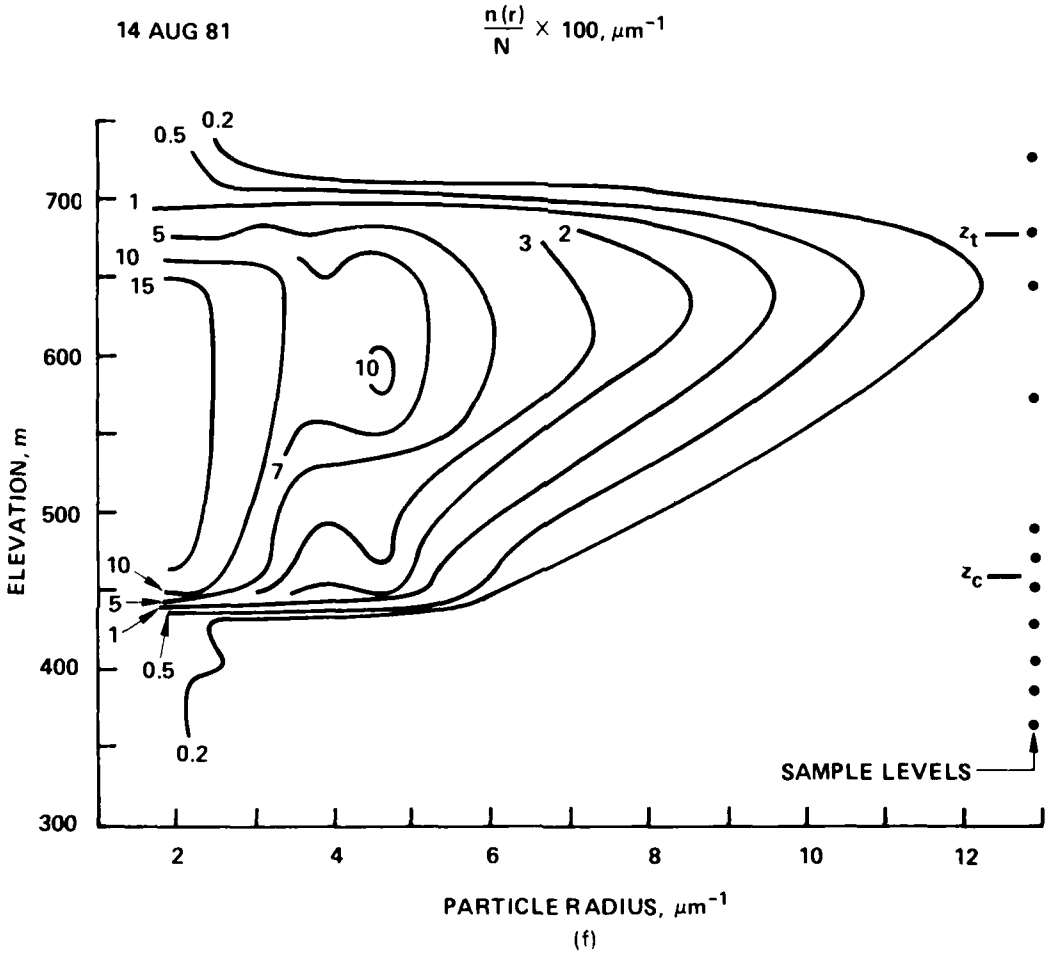

(f)

Figure 8. Continued.

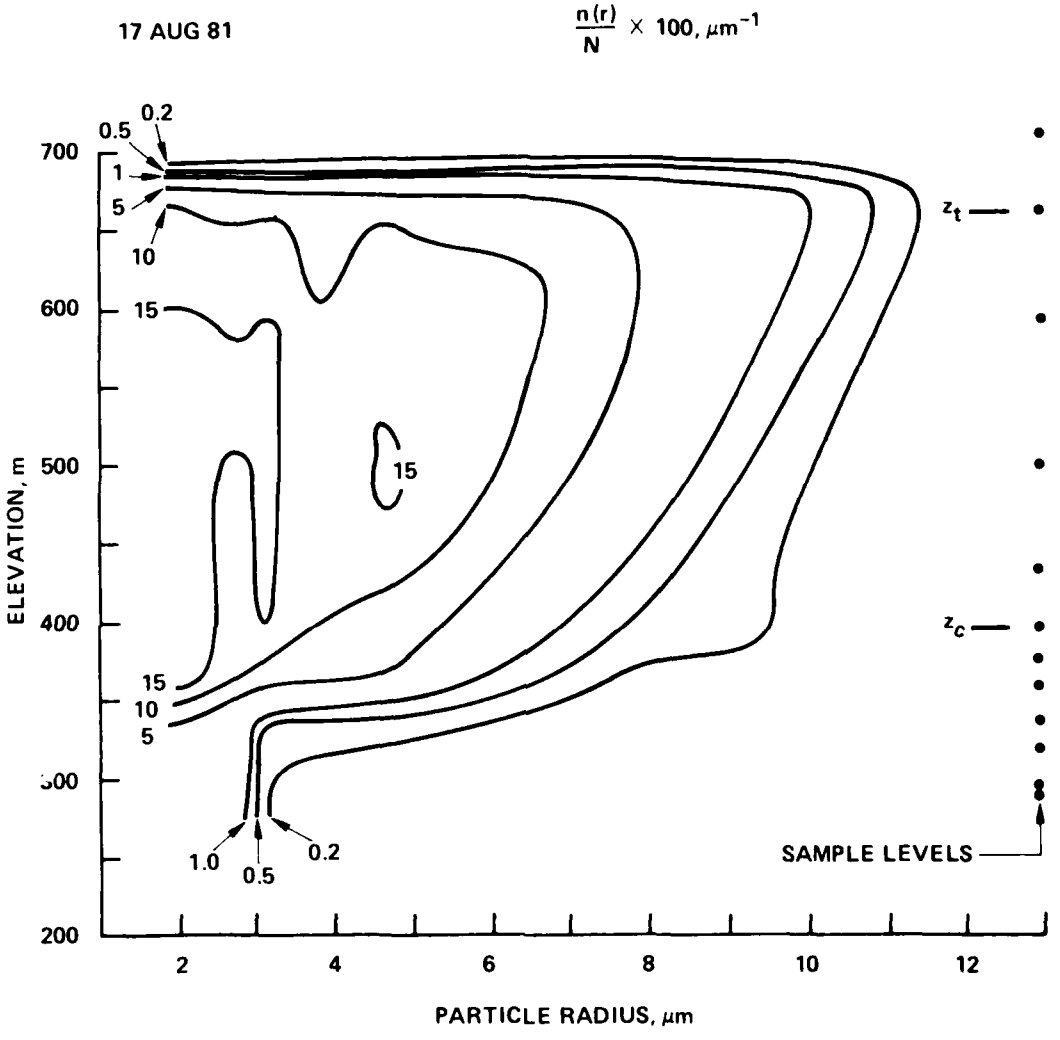

(g)

Figure 8. Continued.

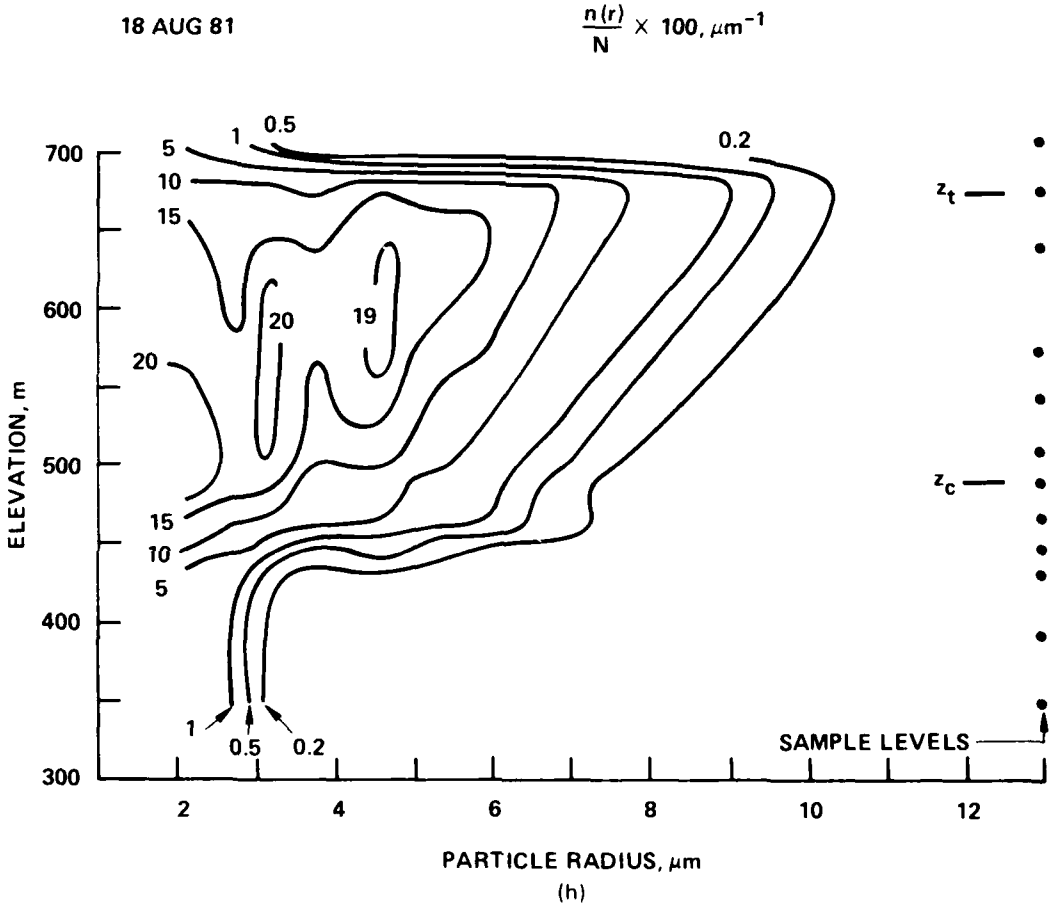

(h)

Figure 8. Continued.

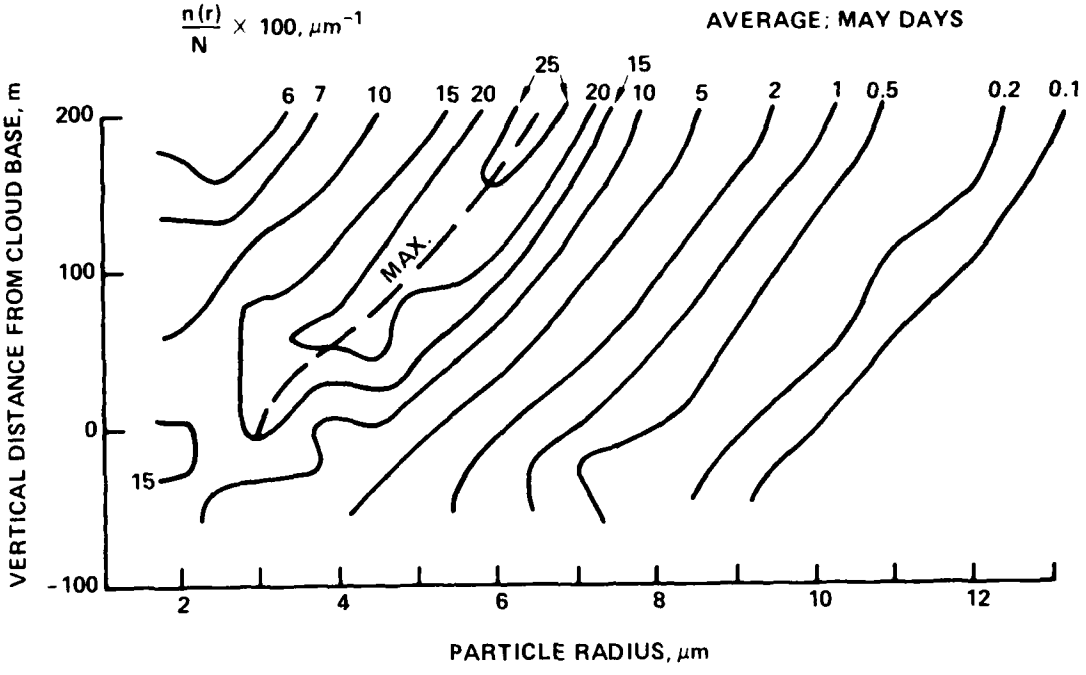

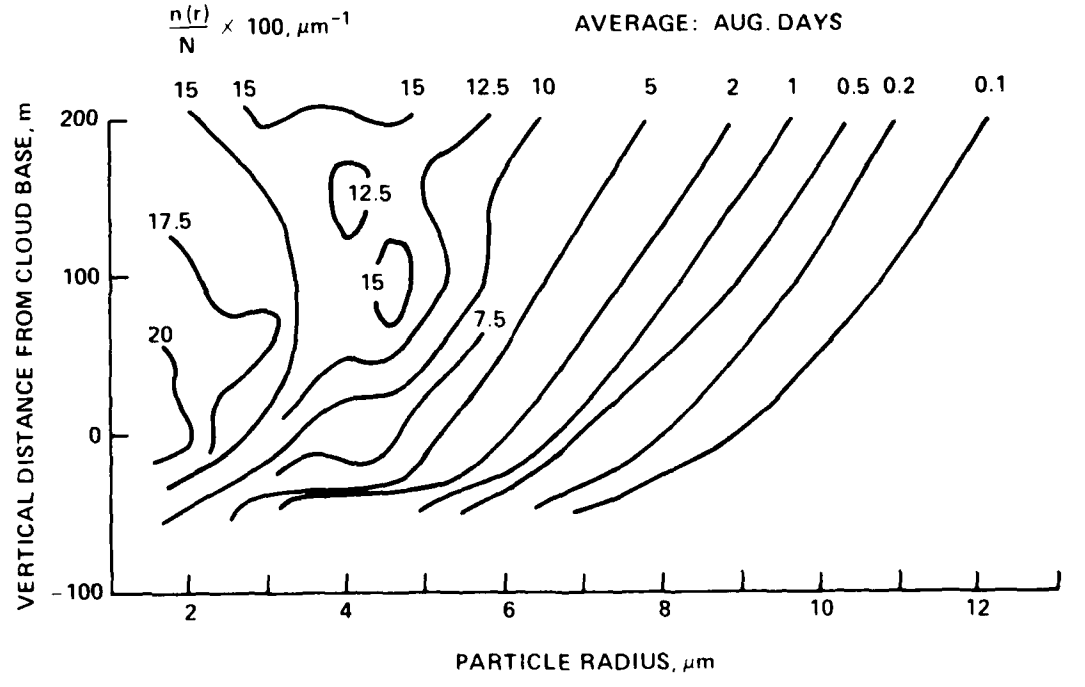

Figure 9. Isopleths of (n(r)/N) x 100 in the cloud region for the May and average days.

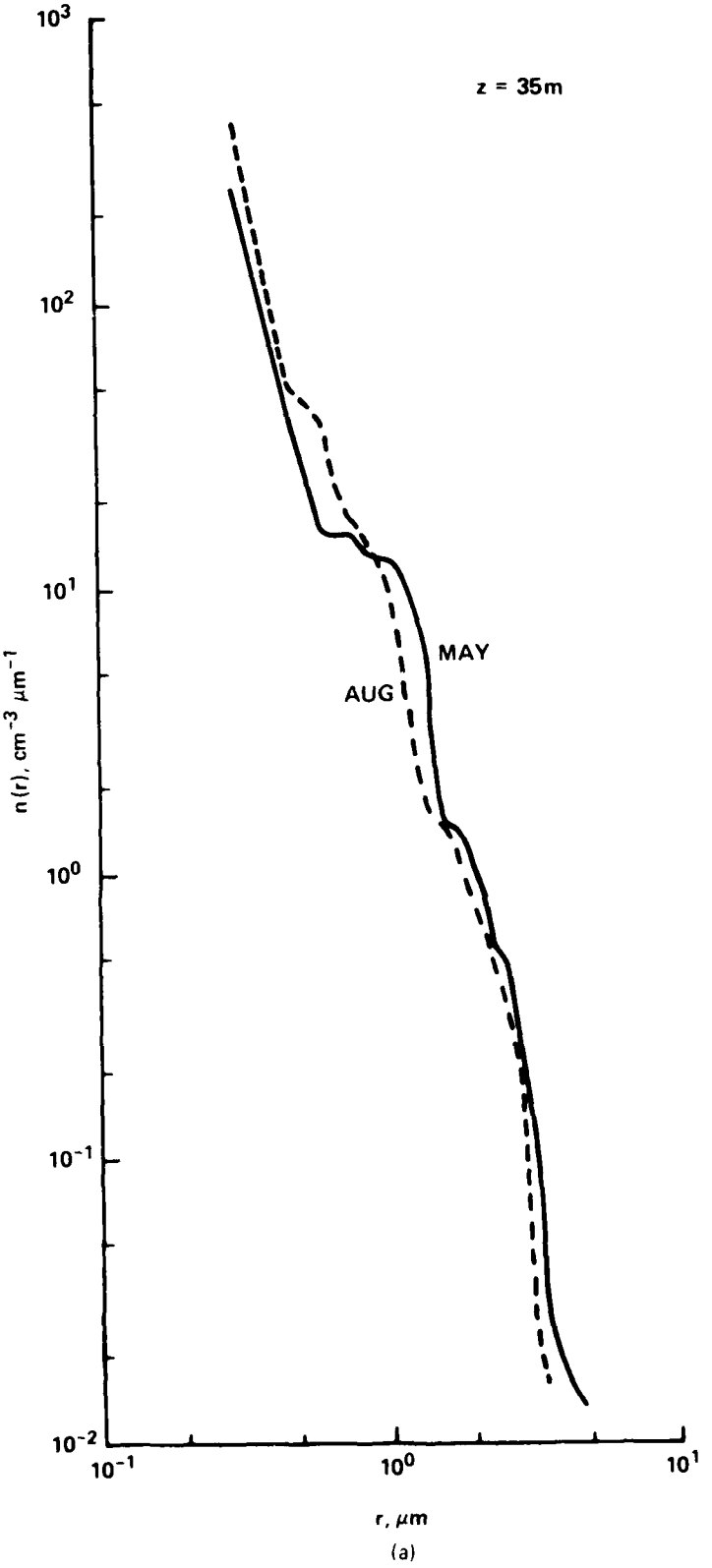

Figure 10. Aerosol spectra averaged for the May and August days for selected elevations.

For 40 m below the cloud base.

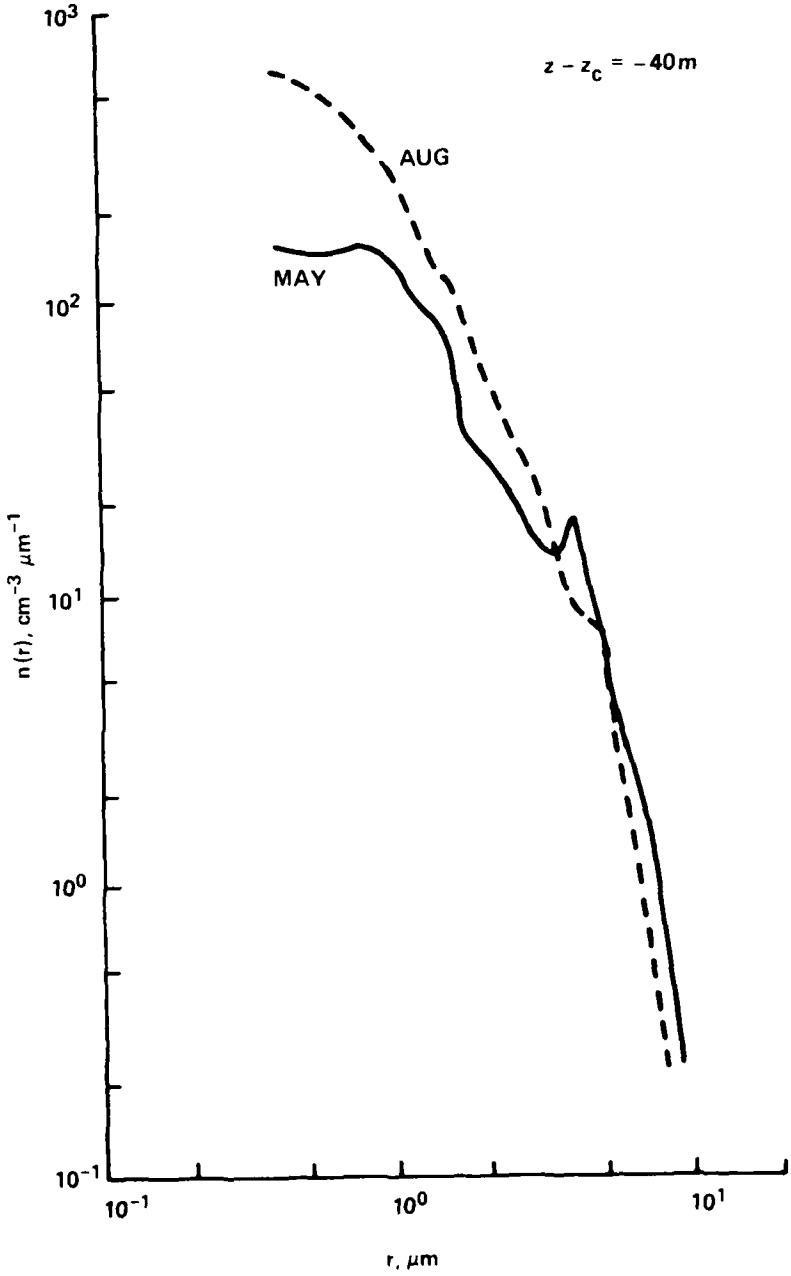

(b)

Figure 10. Continued.

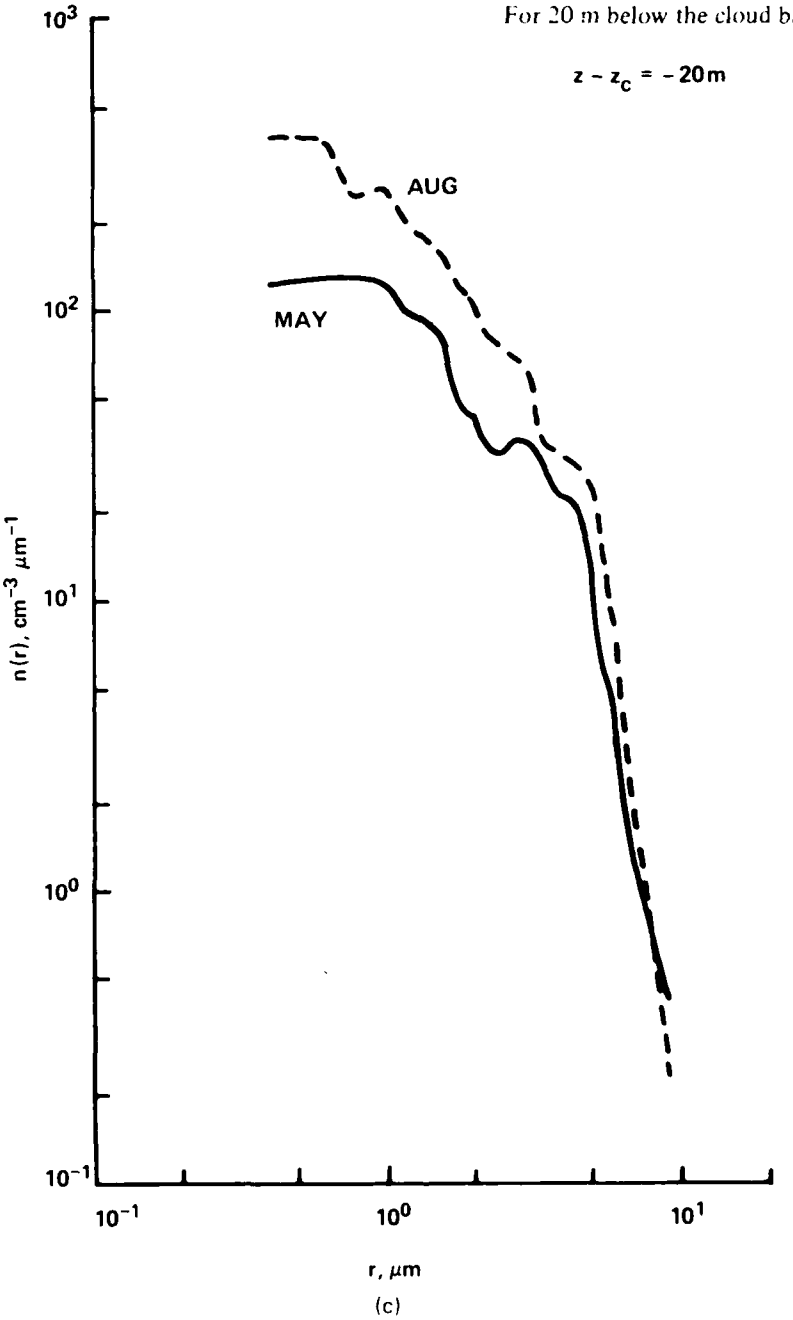

(c)

Figure 10. Continued.

For cloud base.

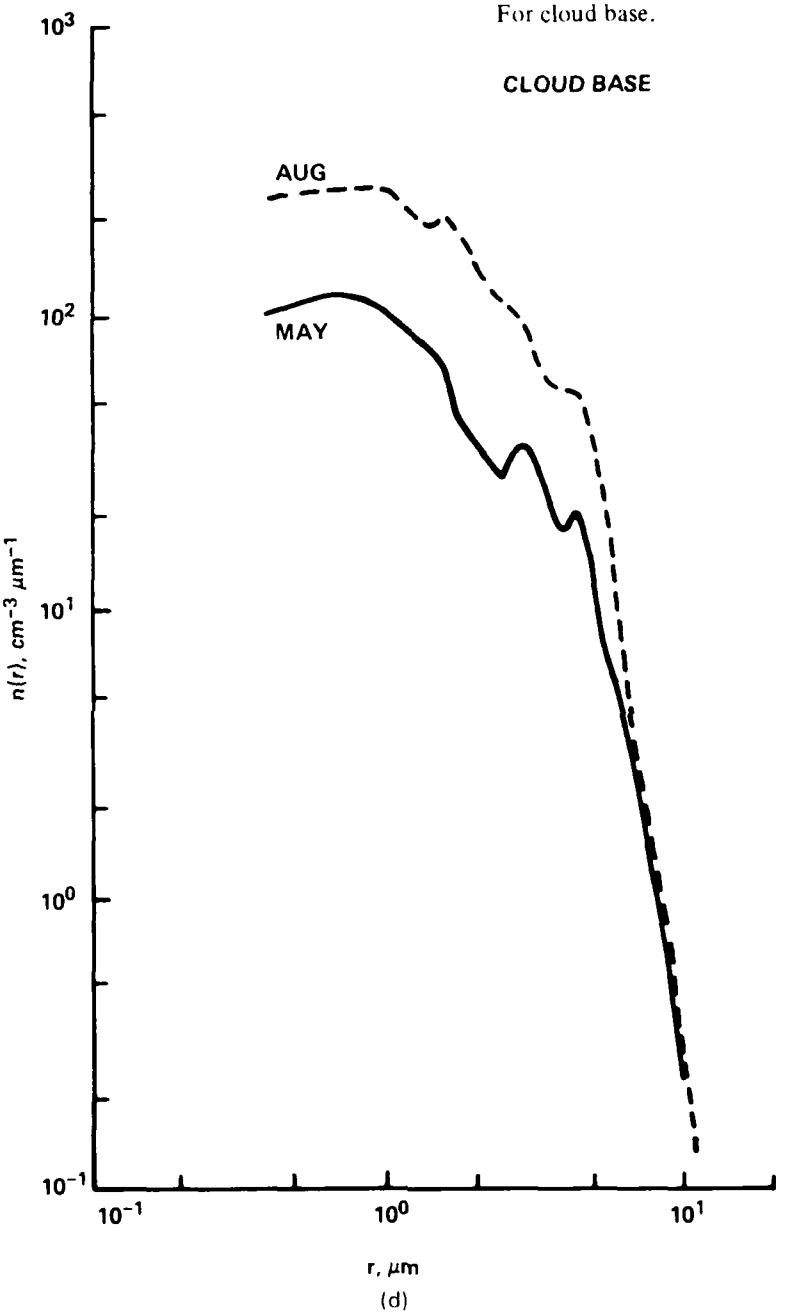

(d)

Figure 10. Continued.

For 20 m above the cloud base.

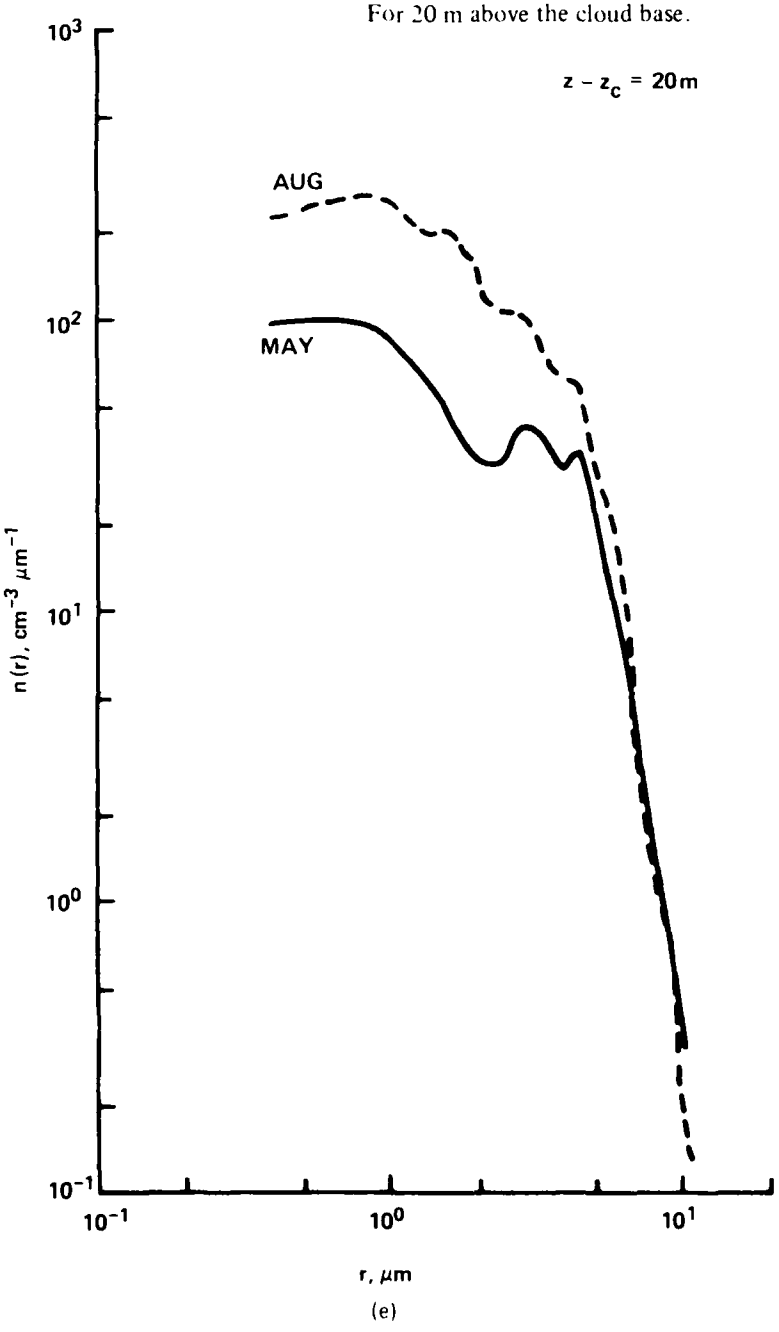

(e)

Figure 10. Continued.

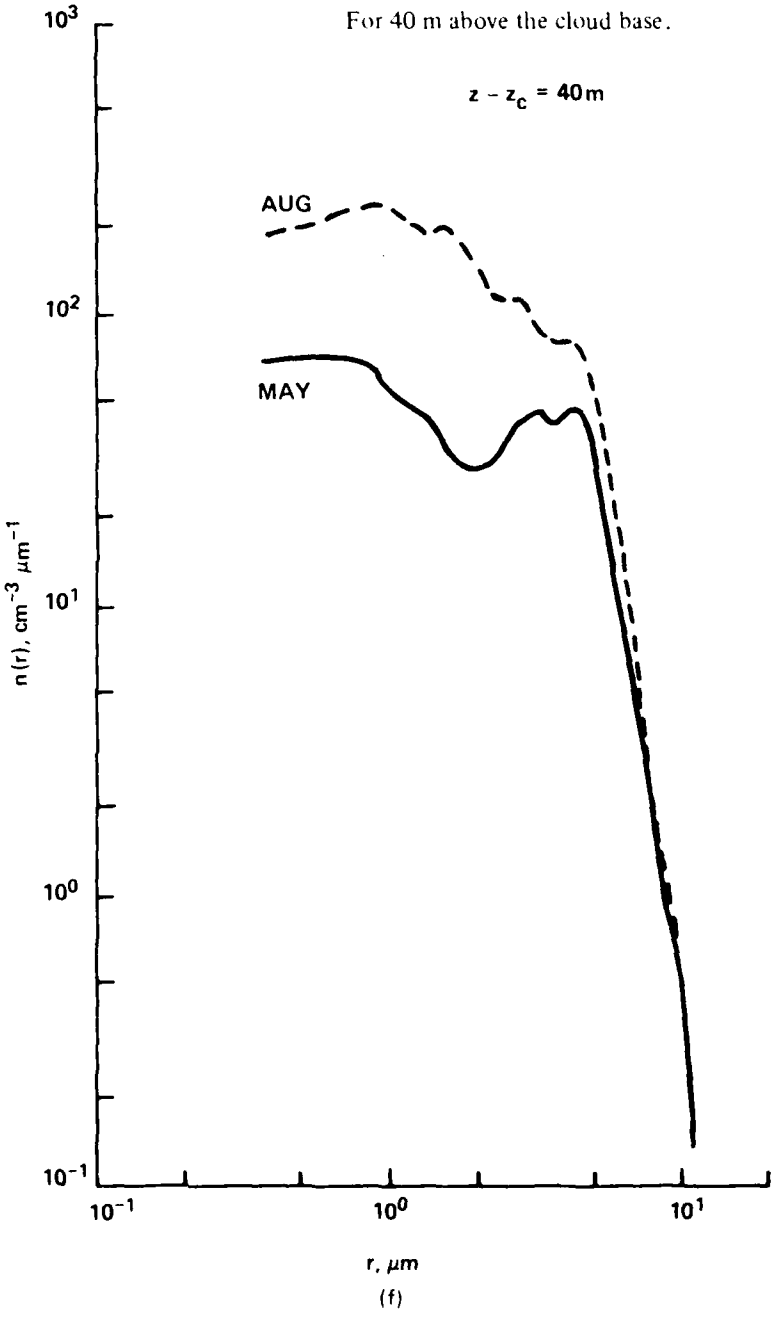

Figure 10. Continued.

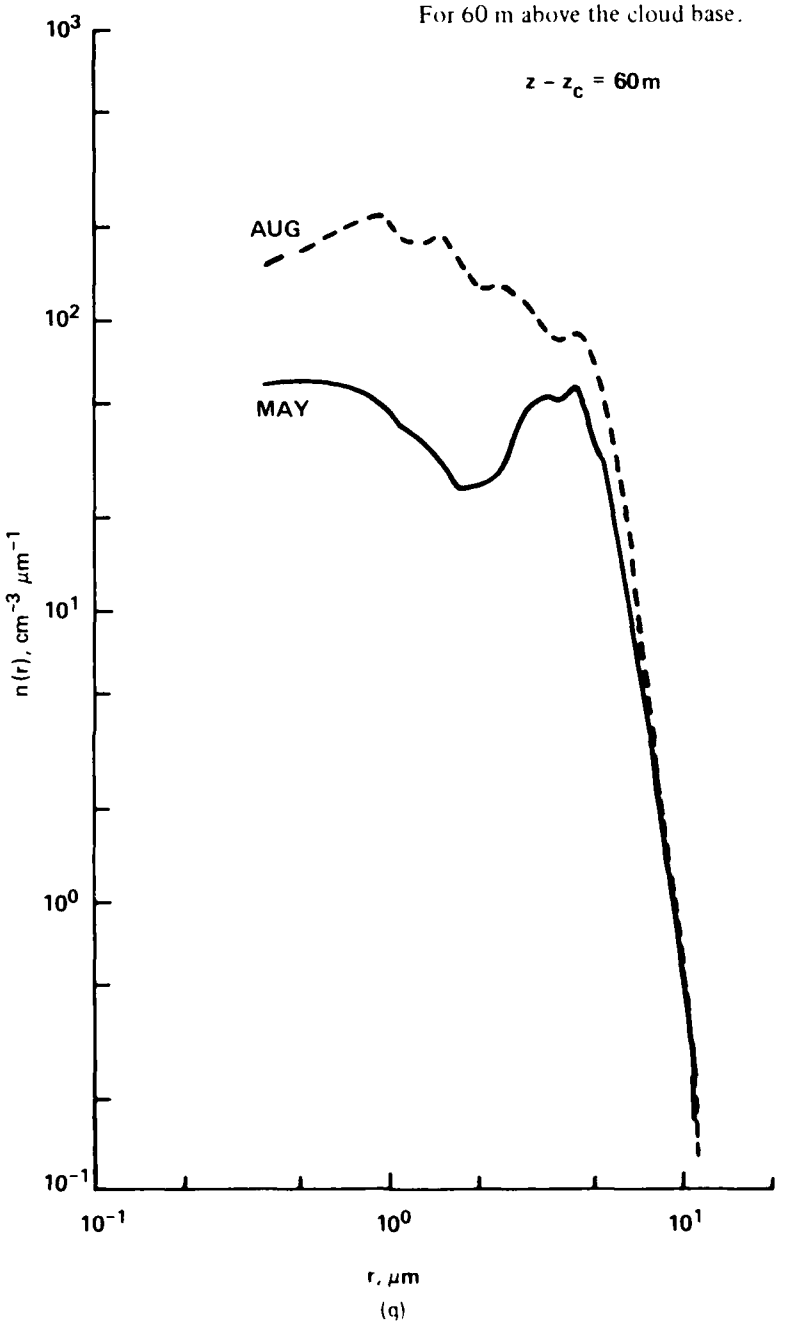

(q)

Figure 10. Continued.

For 80 m above the cloud base.

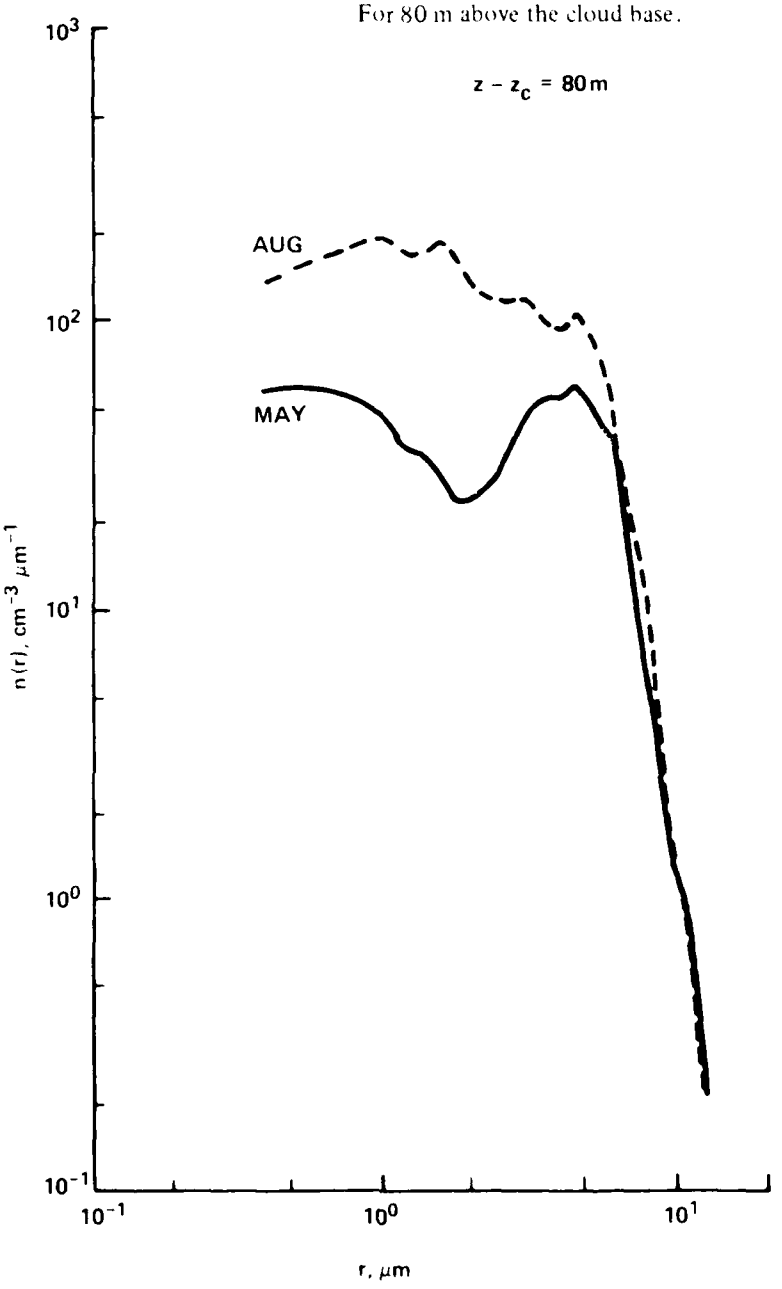

(h)

Figure 10. Continued.

For 100 m above the cloud base.

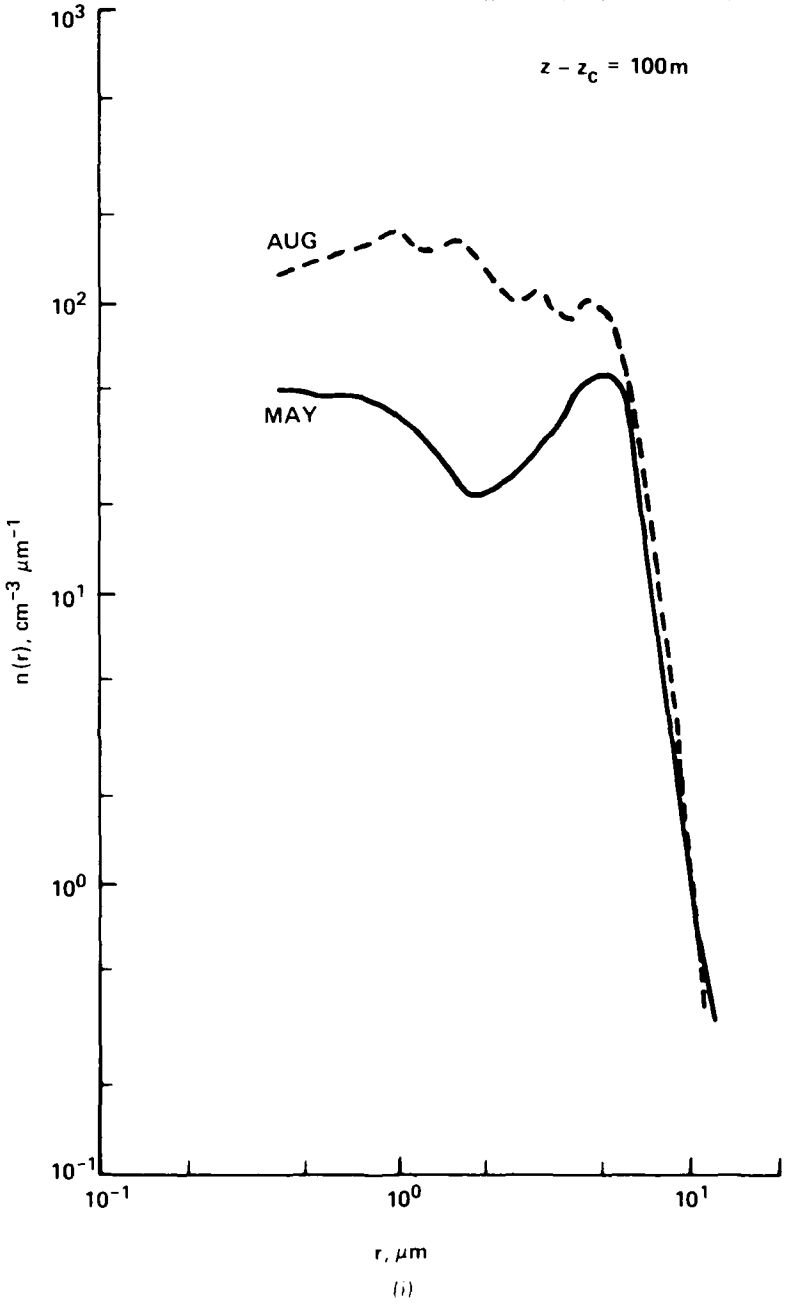

(b)

Figure 10. Continued.

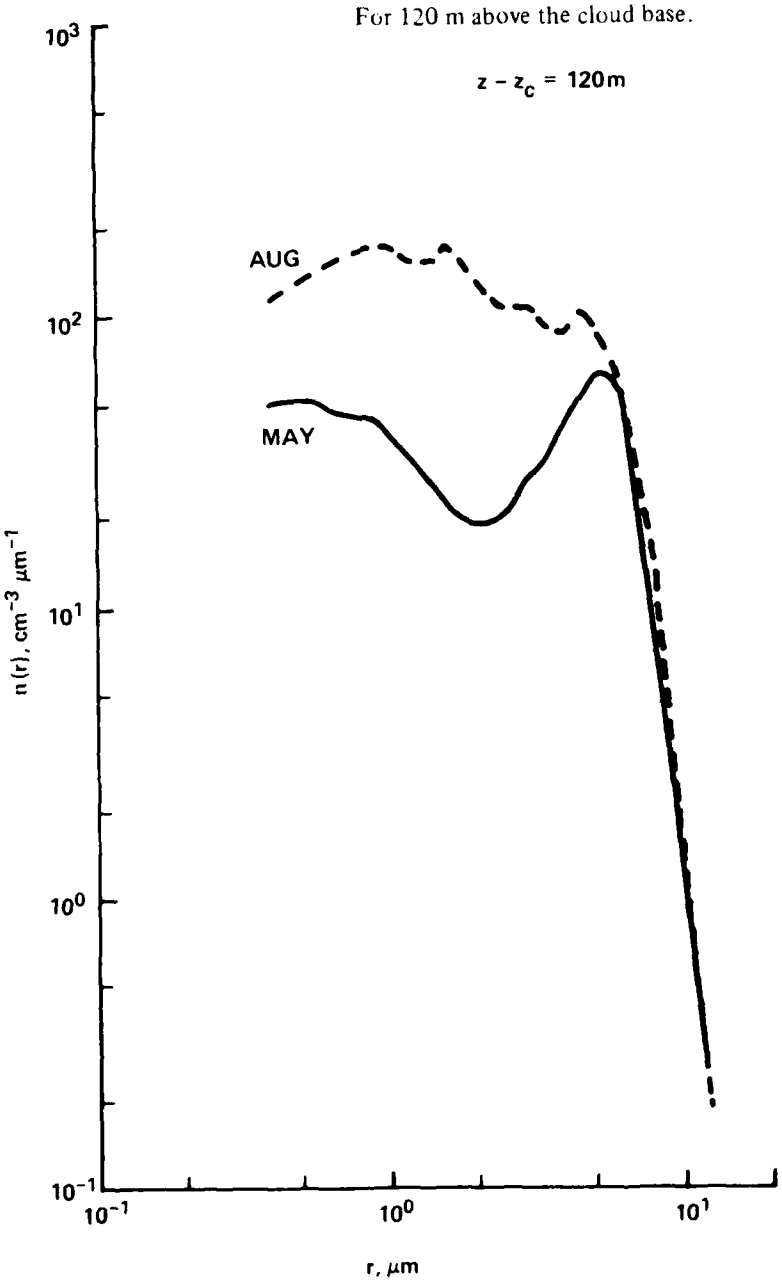

(j)

Figure 10. Continued.

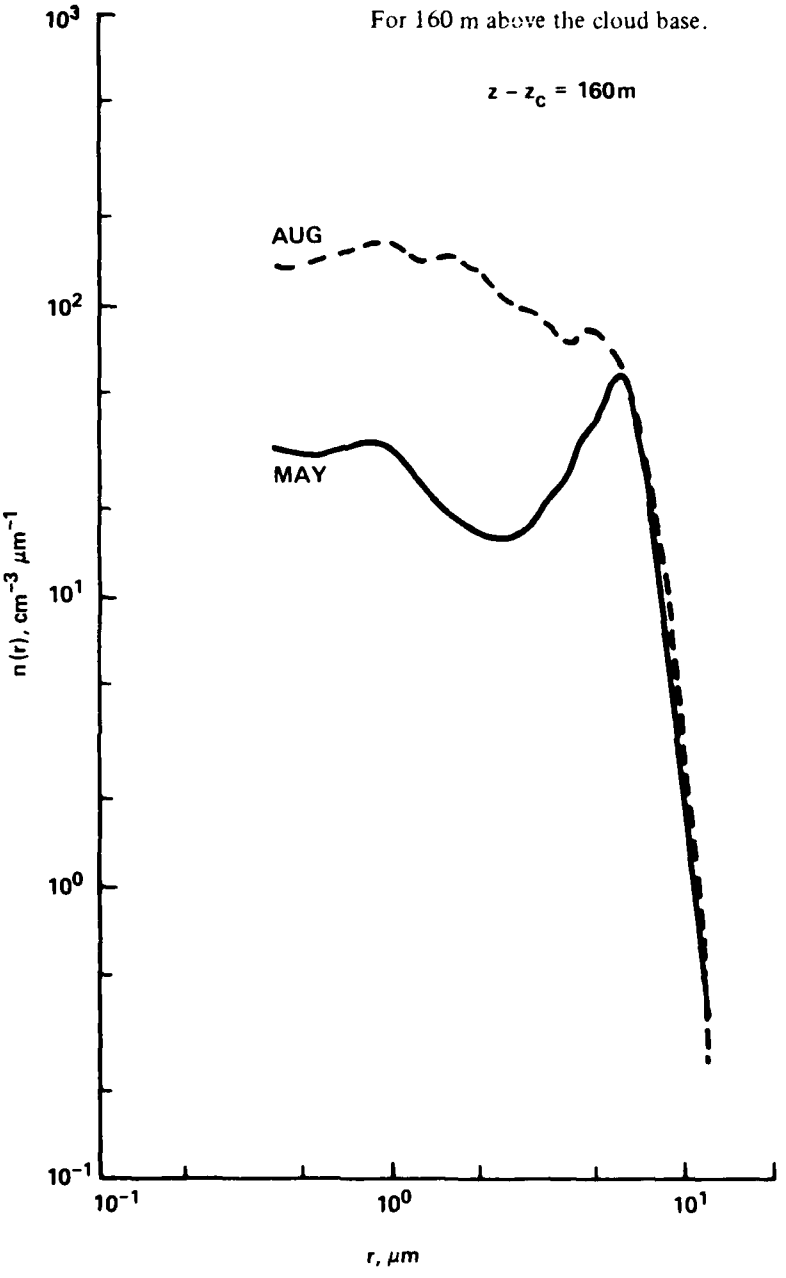

(k)

Figure 10. Continued.

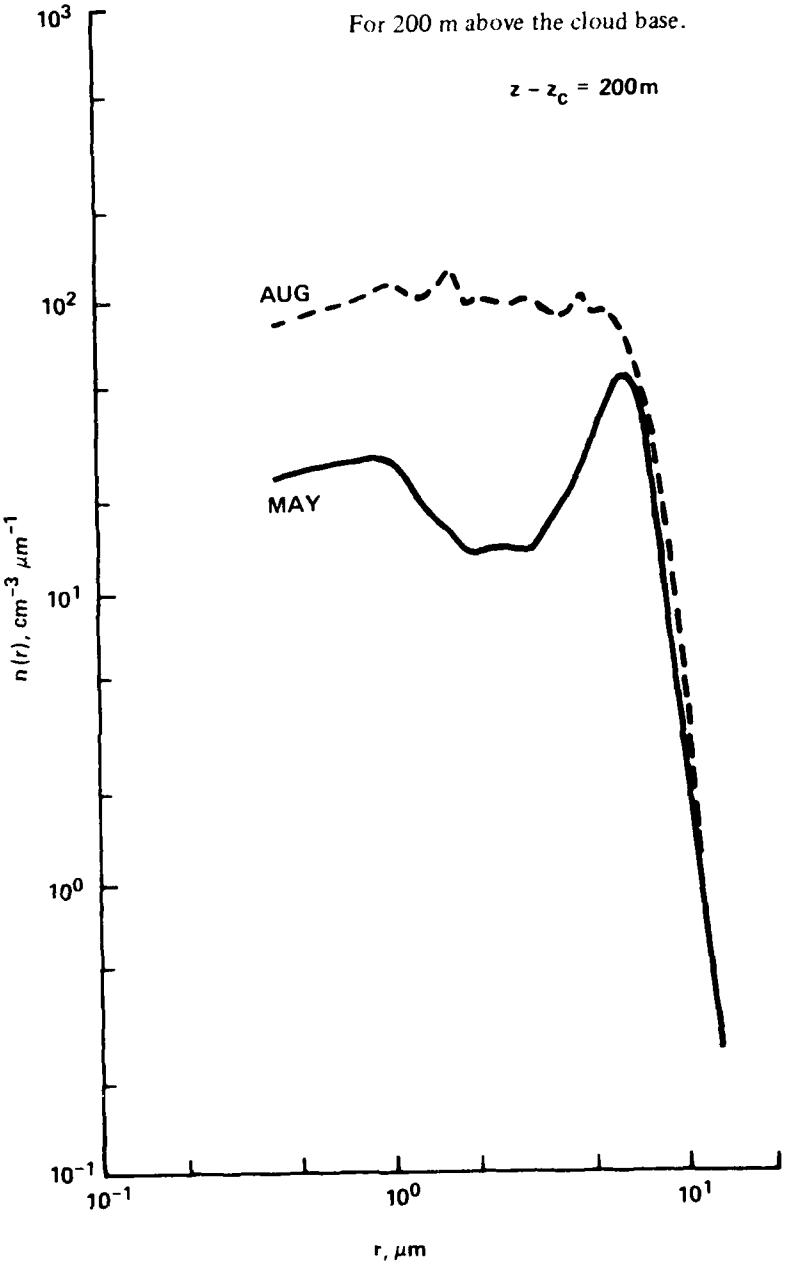

(l)

Figure 10. Continued.

For 14 May 1981.

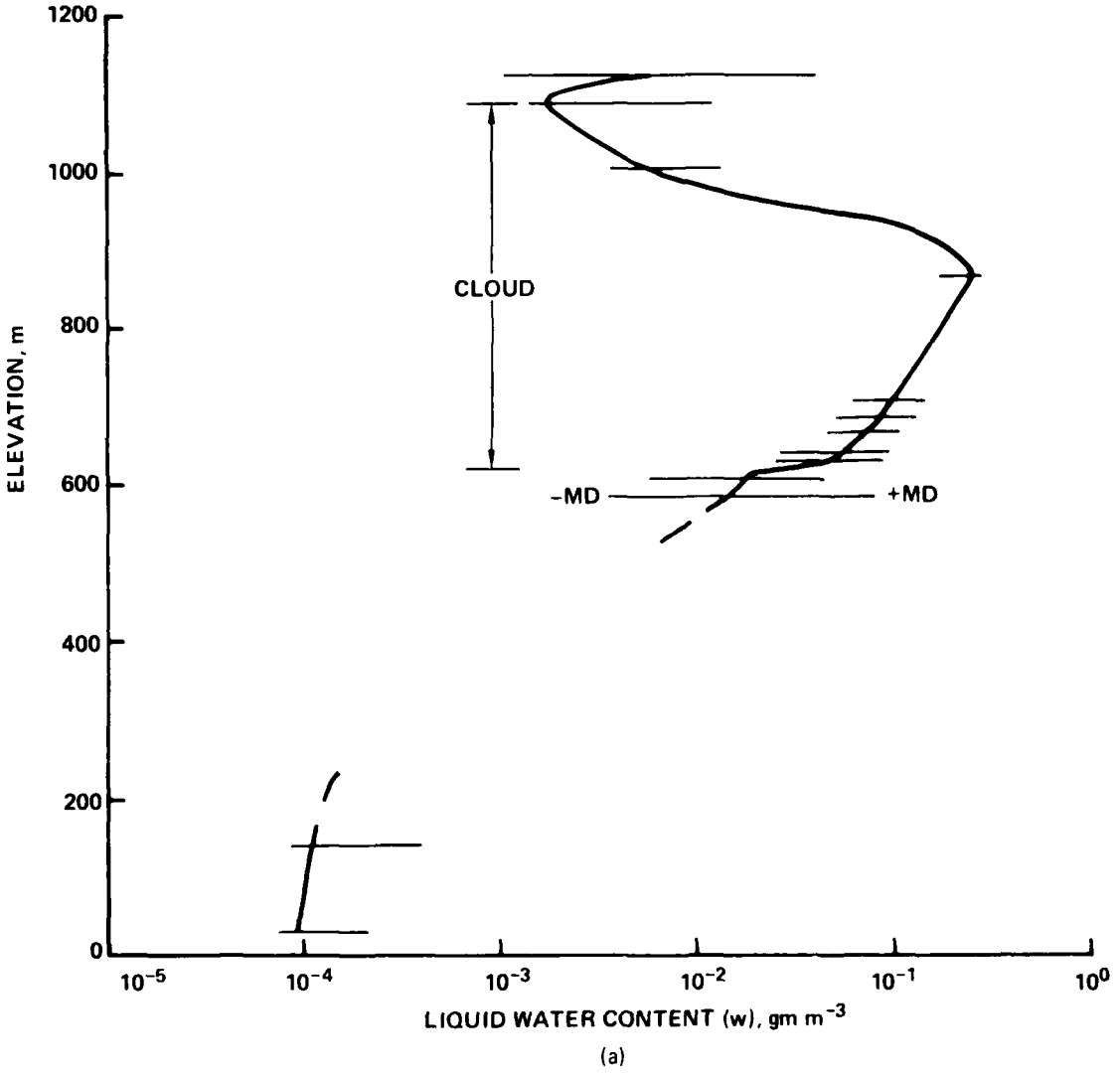

Figure 11. Vertical profile of the liquid water content w computed from the aerosol spectra. The continuous line is the average w. The horizontal lines extend between the mean deviation of w above and below the average w at the sample levels.

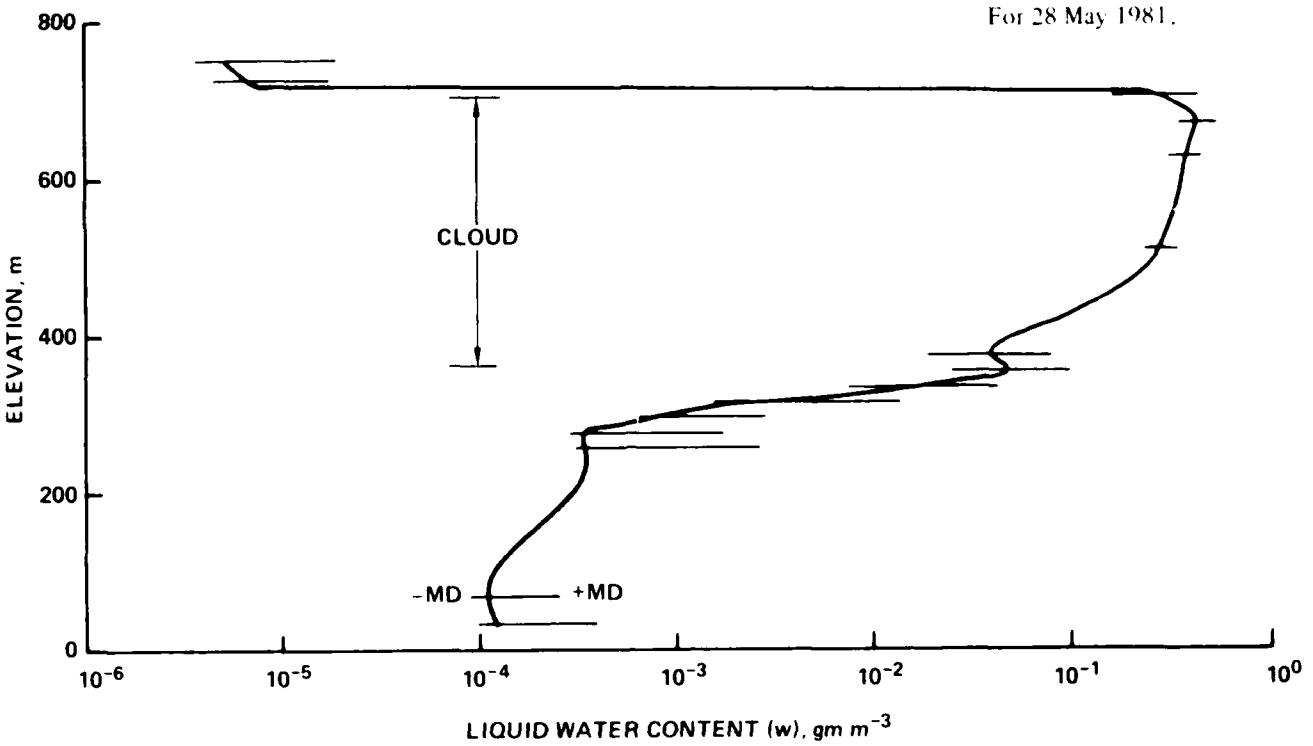

(b)

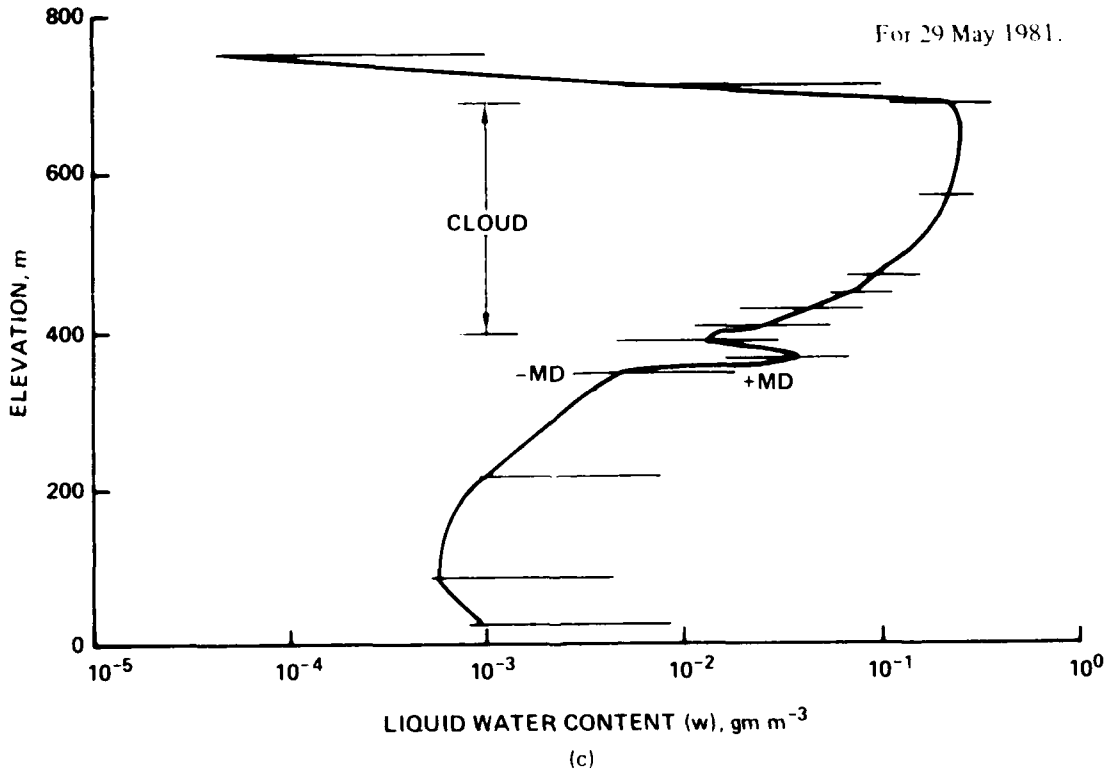

(c)

Figure 11. Continued.

For 11 August 1981.

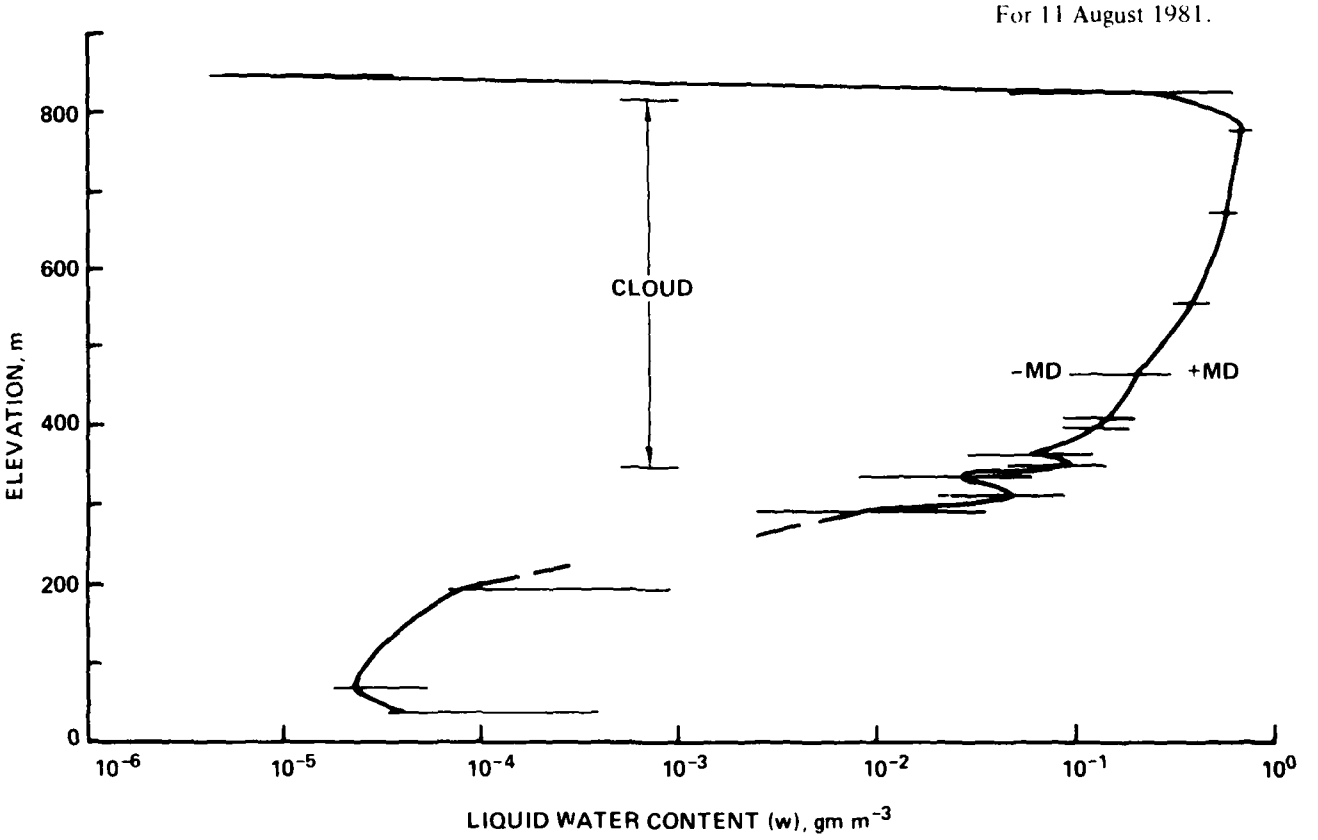

(d)

Figure 11. Continued.

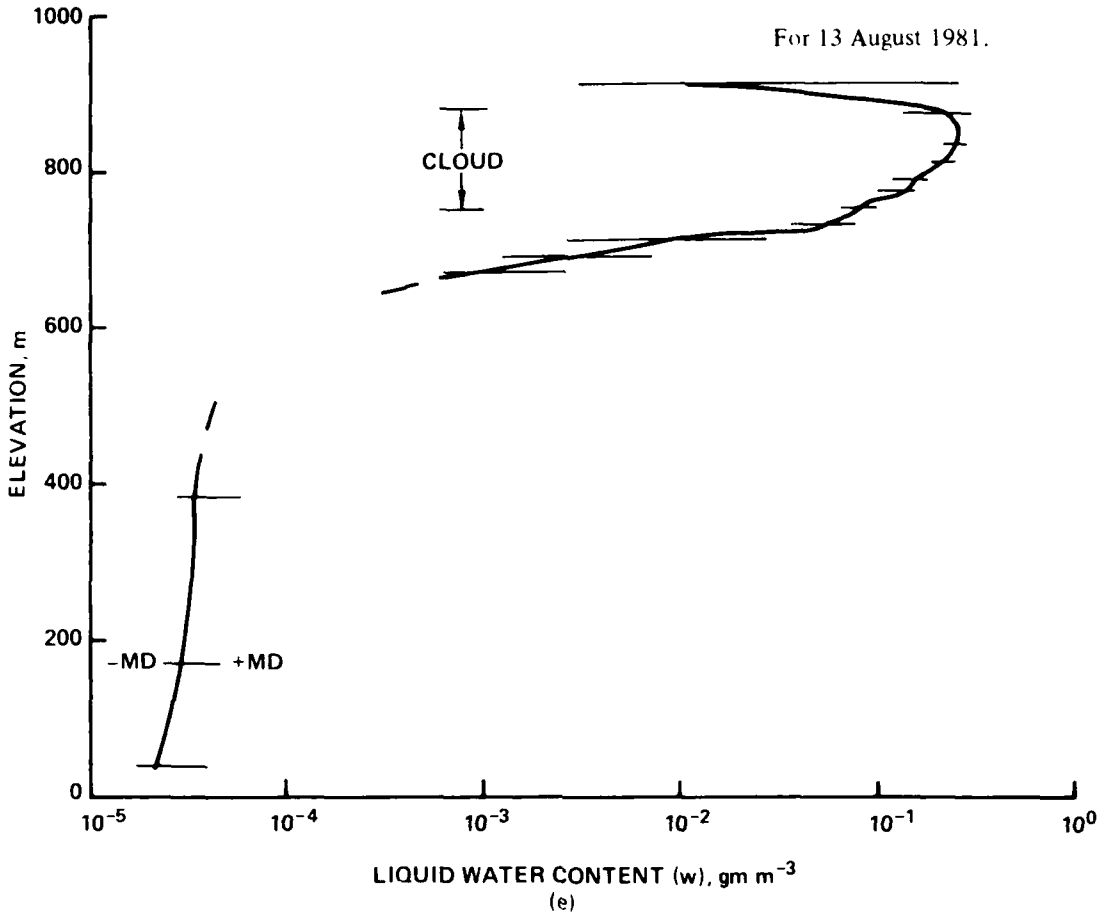

(e)

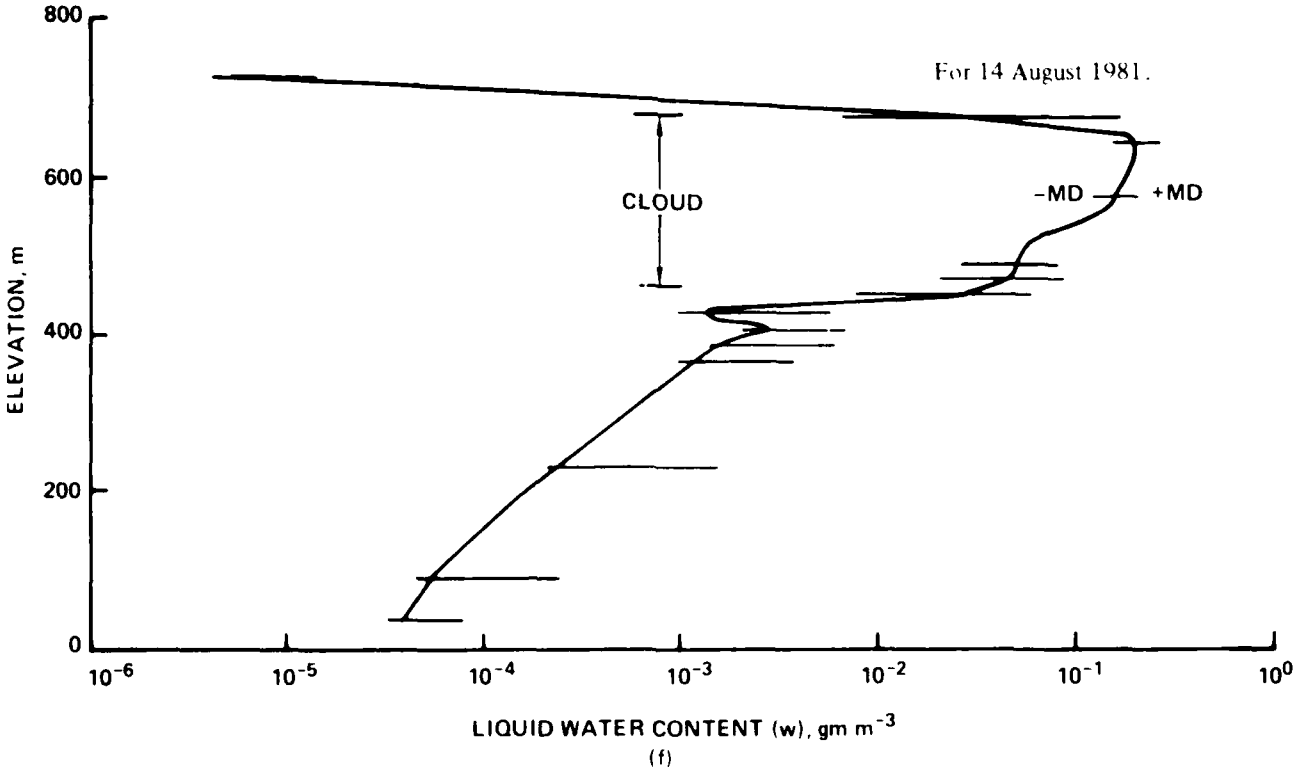

(f)

Figure 11. Continued.

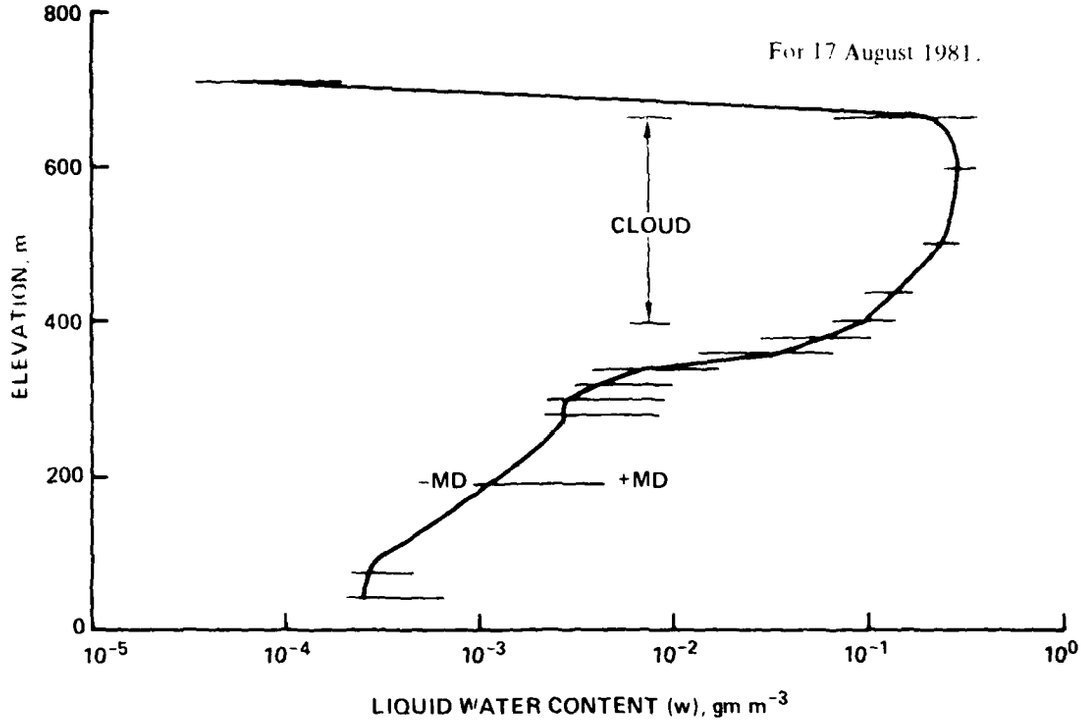

(g)

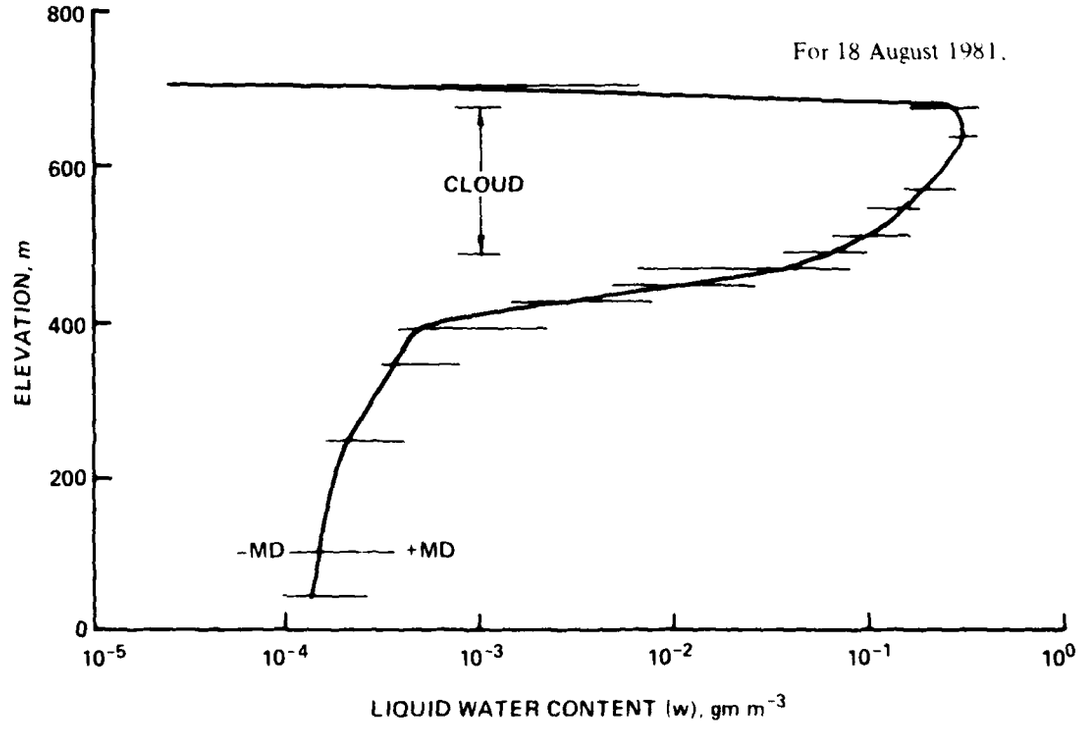

(h)

Figure 11. Continued.

Averaged for the May days (subscript M) and the August days (subscript A).

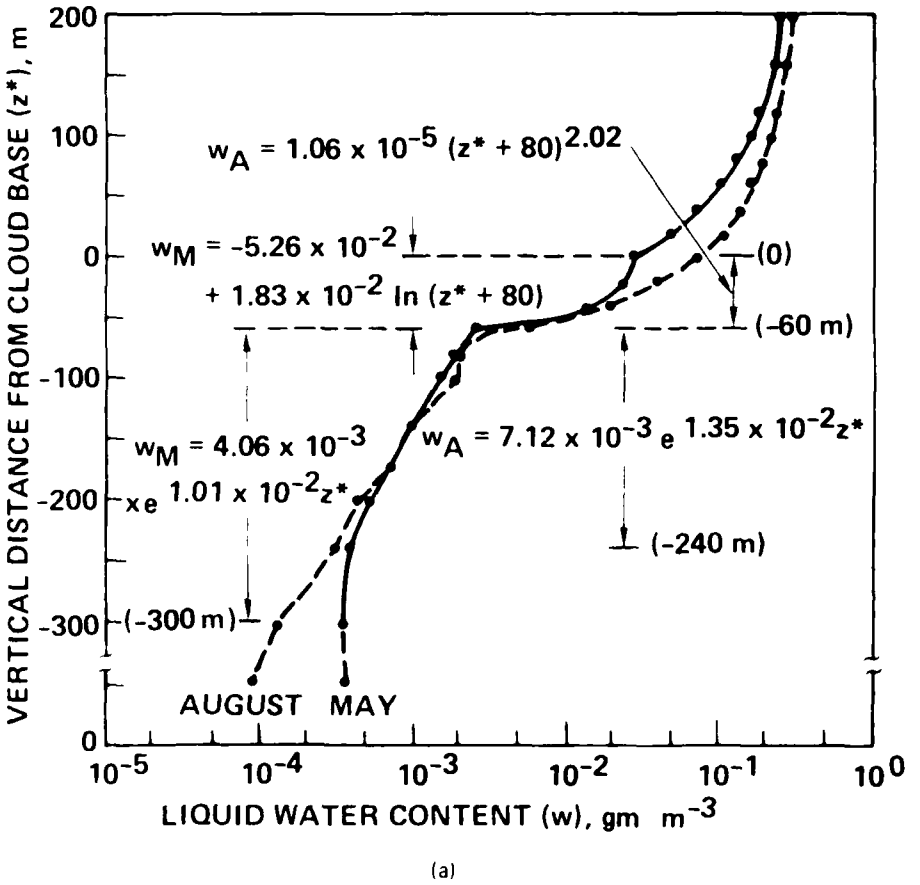

(a)

Figure 12. Vertical profiles of the liquid water content w. The equations were determined by statistical regression analysis for various elevation spans.

Averaged for the May and August days combined.

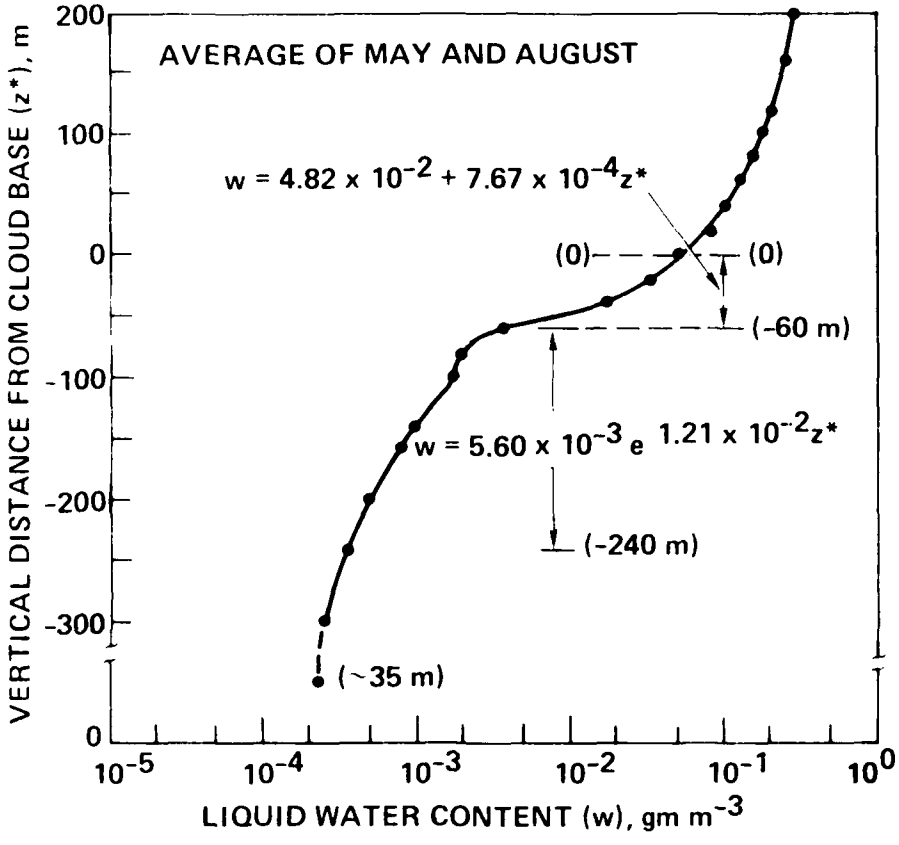

(b)

Figure 12. Continued.

END

DTIC

7-86